ΕΘΝΙΚΟ ΜΕΤΣΟΒΙΟ ΠΟΛΥΤΕΧΝΕΙΟ
ΣΧΟΛΗ ΠΟΛΙΤΙΚΩΝ ΜΗΧΑΝΙΚΩΝ
ΤΟΜΕΑΣ ΓΕΩΤΕΧΝΙΚΗΣ

NATIONAL TECHNICAL UNIVERSITY OF ATHENS
SCHOOL OF CIVIL ENGINEERING
GEOTECHNICAL DIVISION

Διπλωματική Εργασία

Αλέξανδρου Μεντεκίδη

Επιβλέπων:

Καθηγητής Γ. Γκαζέτας

ΣΕΙΣΜΙΚΗ ΑΝΑΛΥΣΗ ΒΑΘΡΩΝ ΓΕΦΥΡΑΣ ΘΕΜΕΛΙΩΜΕΝΗΣ με Συνδεδεμένους και Ασύνδετους Πασσάλους

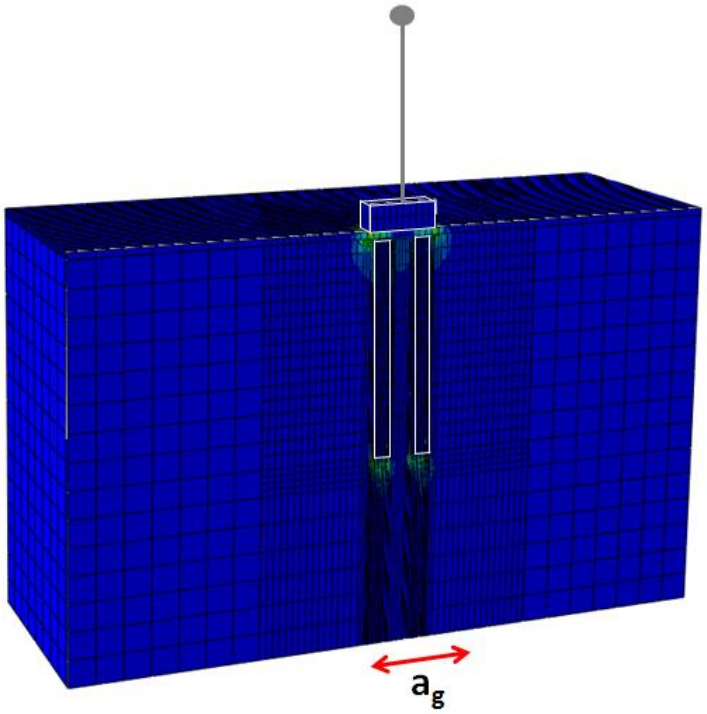

SEISMIC ANALYSIS OF BRIDGE PIER FOUNDED on Connected and Unconnected Piles

Diploma Thesis by

Alexandros Mentekidis

Supervised by

Professor G. Gazetas

Athens, October 2017

Ευχαριστίες

Ολοκληρώνοντας τις προπτυχιακές μου σπουδές και την εκπόνηση της διπλωματικής μου εργασίας θα ήθελα να ευχαριστήσω όλους όσους συνέβαλαν σε αυτό τα τελευταία χρόνια.

Ιδιαίτερα θέλω να ευχαριστήσω τον καθηγητή κ. Γ. Γκαζέτα που μου έδωσε την δυνατότητα να εκπονήσω την παρούσα εργασία υπό την επίβλεψή του και να μελετήσω θέματα που με ενδιαφέρουν. Η διάθεσή του να βοηθήσει οποιαδήποτε στιγμή είχα ανάγκη και η εμπιστοσύνη που μου έδειξε κατά την συνεργασία μας αποτέλεσαν πηγή έμπνευσης για μένα.

Επίσης, θέλω να ευχαριστήσω όλα τα μέλη της ερευνητικής ομάδας του κ. Γκαζέτα για το ευχάριστο κλίμα συνεργασίας και τη βοήθεια που μου πρόσφεραν κατά τη διάρκεια της διπλωματικής μου. Η βοήθεια, ιδιαίτερα στο πρώτο στάδιο της διπλωματικής μου, της υποψήφιας διδάκτορα Ε. Γεωργίου και της Dr. Φ. Γελαγώτη ήταν πολύ σημαντική και τις ευχαριστώ για αυτό.

Σημαντική ήταν η συνεισφορά τα τελευταία χρόνια των συμφοιτητών, των φίλων και της οικογένειας μου μέσα από την στήριξη τους και της πολύωρες συζητήσεις μας για επιστημονικά και μη θέματα.

Abstract

In current pile foundation design practice, overstrength factors are applied on the forces transmitted to the foundation and so piles are assumed to remain elastic during earthquakes. However, in many strong earthquakes, such as Kobe 1995, structural failure of piles has been observed. In addition, recent studies have examined the use of unconnected piles on raft foundations in order to reduce the developed bending moments and shear forces both on the pile heads and on the rafts. Based on these, this diploma thesis examines the static and dynamic response of bridge piers supported on foundations with the piles not connected to the cap. In addition to an unconnected pile foundation that is designed according to the current seismic codes, a new design philosophy is studied. According to it, the mobilization of the foundation's bearing capacity is used as an earthquake hazard mitigation technique, aiming to limit the forces transmitted to the superstructure and increase its safety against collapse. Hence, three different foundations were studied: (1) a conventional pile group designed according to Eurocode 8, (2) a foundation with unconnected piles, for the design of which the Eurocode's overstrength factors were also used, (3) an unconventional foundation with unconnected piles designed with a smaller moment capacity than the supported pier. To compare the response the systems, three-dimensional dynamic finite element simulation was employed and real earthquake timehistories were used. Two piers, a short one and a tall one, were studied in order to examine the effects of slenderness in each foundation. It was found that the pier supported on unconnected pile foundation performed slightly better in most earthquakes, with a significant decrease of forces and moments developed on the piles, compared to the conventional foundation. The rocking foundation was found effective in order to protect the structure from collapsing, even under severe excitations that led to the collapse of the two conventionally designed systems. For both piers the residual deck displacements were decreased compared to the conventionally designed systems, but for the short one the maximum displacements were significantly increased. The main drawback of rocking foundations was found to be the excessive settlements.

Περίληψη

Σύμφωνα με τους ισχύοντες κανονισμούς στον σχεδιασμό θεμελιώσεων με πασσάλους χρησιμοποιούνται συντελεστές υπεραντοχής για τις μεταβιβαζόμενες δυνάμεις στην θεμελίωση και η συμπεριφορά των πασσάλων θεωρείται ελαστική. Παρ' όλα αυτά σε ισχυρούς σεισμούς, όπως στον σεισμό του Kobe το 1995, έχουν παρατηρηθεί δομικές αστοχίες πασσάλων. Επίσης, σε πρόσφατες έρευνες η χρήση ασύνδετων πασσάλων κάτω από πλάκα θεμελίωσης έχει μελετηθεί με σκοπό την μείωση των δυνάμεων και ροπών που εμφανίζονται τόσο στην πλάκα όσο και στην κεφαλή των πασσάλων. Με αφορμή αυτά, η παρούσα διπλωματική εργασία εξετάζει την στατική και δυναμική συμπεριφορά βάθρων γεφυρών θεμελιωμένων με ασύνδετους πασσάλους. Πέρα από την θεμελίωση με ασύνδετους πασσάλους σχεδιασμένη κατά τους ισχύοντες κανονισμούς εξετάζεται η εφαρμογή μιας νέας φιλοσοφίας σχεδιασμού σε τέτοιες θεμελιώσεις. Σύμφωνα με αυτήν ο λικνισμός της κατασκευής, μέσω της κινητοποίηση του μηχανισμού αστοχίας της θεμελίωσες, μπορεί να χρησιμοποιηθεί ως σεισμική μόνωση, στοχεύοντας στην μείωση των αδρανειακών δυνάμεων της ανωδομής και την αύξηση της ασφάλειας της έναντι κατάρρευσης. Τρία διαφορετικά συστήματα θεμελίωσης μελετήθηκαν: (1) συμβατικά σχεδιασμένη θεμελίωση με πασσάλους σύμφωνα με τον Ευρωκώδικα 8, (2) θεμελίωση με ασύνδετους πασσάλους για τον σχεδιασμό της οποίας χρησιμοποιήθηκαν οι συντελεστές υπαραντοχής του Ευρωκώδικα 8, (3) μη-συμβατική θεμελίωση με πασσάλους με αντοχή σε ροπή μικρότερη από αυτή της ανωδομής. Για την σύγκριση της συμπεριφοράς των τριών συστημάτων πραγματοποιήθηκαν 3-D δυναμικές αναλύσεις με χρήση προγράμματος πεπερασμένων στοιχείων και πραγματικές σεισμικές καταγραφές. Η επιρροή του ύψους της κατασκευής διερευνήθηκε με την μελέτη ενός ψηλού και ενός κοντού βάθρου. Από τις δυναμικές αναλύσεις βρέθηκε πως η συμπεριφορά του θεμελιωμένου βάθρου σε ασύνδετους πασσάλους ήταν ελαφρώς βελτιωμένη σε σχέση με το συμβατικό, ενώ οι δυνάμεις και ροπές στους πασσάλους μειώθηκε σημαντικά. Η αντισυμβατική θεμελίωση αποδείχθηκε ικανή να προστατέψει την κατασκευή από αστοχία ακόμα και σε πολύ ισχυρές διεγέρσεις όπου τα δύο συμβατικά συστήματα αστόχησαν. Και για τα δύο βάθρα που μελετήθηκαν οι παραμένουσες μετατοπίσεις του καταστρώματος μειώθηκαν ενώ το κοντό βάθρο ανέπτυξε μεγαλύτερες μέγιστες μετατοπίσεις κατά την διάρκεια των σεισμών. Επίσης, επιβεβαιώθηκε πως το βασικό μειονέκτημα τέτοιων θεμελιώσεων είναι οι αυξημένες καθιζήσεις.

Table of Contents

Chapter 1: Introduction 1

1.1 Literature Review 3
1.1.1 New Design Philosophy – Rocking Isolation 3
1.1.2 Unconnected Pile Foundations 4
1.2 Scope Of This Study 9
Figures of Chapter 1 11

Chapter 2: Numerical Simulation 27

2.1 **Finite Element Model** 29
2.2 **Soil Constitutive Model** 30
Figures of Chapter 2 33

Chapter 3: Numerical Analysis 37

3.1 **Problem Statement** 39
3.2 **Design of the Short Pier** 39
3.2.1 Design of the Superstructure 39
3.2.2 Design of the Conventional Pile Group 41
3.2.2 Ductility Capacity 43
3.3 **Static Push-Over Analyses** 44
3.3.1 Single Pile 44
3.3.2 Full Model 44
Figures of Chapter 3 47

Chapter 4: Design of Unconnected Pile Foundations 59

4.1 **Design Process** 61
4.1.1 Push-Over Analyses 61
4.1.2 Comparison and Selection 67
4.2 **Comparison of Conventional Connected and Unconnected Pile Foundations** 68
4.2.1 Developed Forces and Moments 68
4.2.2 Ductility Capacity 69
4.2.3 Fundamental Period 69
4.3 **Design of Rocking Foundation** 69
4.3.1 Push-Over Analyses for the Rocking Foundation 70
4.4 **Comparison of Rocking and Conventional Foundations** 71

4.4.1 Developed Forces and Moments 71
4.4.2 Ductility Capacity 72
4.4.3 Fundamental Period 72
Figures of Chapter 4 **74**

Chapter 5: Dynamic Analysis of the Short Pier 101

5.1 Selected Earthquakes 103
5.2 Dynamic Analysis of Connected and Unconnected Conventional Pile Foundations 103
5.3 Dynamic Analysis of Unconnected Conventional and Rocking Pile Foundations 106
Figures of Chapter 5 109

Chapter 6: Design of the Tall Pier 123

6.1 Conventional Design 125
6.1.1 Design 125
6.1.2 Comparison with the Short Pier 125
6.2 Unconnected Conventional Pile Foundation 126
6.3 Unconnected Rocking Pile Foundation 126
Figures of Chapter 6 129

Chapter 7: Dynamic Analysis of the Tall Pier 139

7.1 Selected Earthquakes 141
7.2 Dynamic Analysis of Connected and Unconnected Conventional Pile Foundations 141
7.3 Dynamic Analysis of Unconnected Conventional and Rocking Pile Foundation 142
Figures of Chapter 7 145

Chapter 8: Conclusions 157

Appendix A 161

Appendix B 187

References

CHAPTER 1

INTRODUCTION

1.1 Literature Review

1.1.1 New Design Philosophy – Rocking Isolation

According to the current seismic codes, material non-linearity and plastic hinges are allowed to develop on the superstructure during strong earthquakes as long as the stability of the structure is maintained. Plastic deformation of structural members is a way of energy dissipation and reduction of the design forces or accelerations. However, the bearing capacity of the foundations should not be reached at any point. In other words uplifting of the foundations, structural hinging of piles or pile caps, sliding at the soil-footing interface and passive failure along the sides of embedded foundations are restricted. This restriction is based on the fact that inspection and repair at the foundation level is an extremely hard task. To make sure these conditions are satisfied the current seismic codes introduce overstrength factors for the forces transmitted to the foundations.

The mobilization of the bearing capacity or the uplifting of the foundations would be devastating for static loading, leading to collapse of the structure. On the other hand, in the case of dynamic loading exceedance of the available resistance is not associated with failure but with the development of permanent displacements (Newmark 1965). Based on this Pecker (1998) proposed a capacity design methodology according to which failure mechanisms are allowed to develop at the foundation level, but the mode of failure is chosen in order to control the magnitude of the developed permanent displacements. This principle was used in the design of Rion–Antirrion Bridge.

Many recent studies have examined the non–linear behavior of soil–shallow foundation systems. Both geometric (sliding and uplifting of foundation) and material (plastification of soil) non–linearity have been examined using the following methods:

- Winkler spring foundation models have been used in order to study the effects of foundation rocking and uplifting (Psycharis and Jennings 1984, Yim and Chopra 1985).
- Finite element software have been used to simulate the soil-foundation-superstructure response when foundation uplift and rocking were allowed (Anastasopoulos et al. 2010, 2011, 2012, Mergos and Kawashima 2005, Apostolou et al. 2006)
- Centrifuge and shake table tests have been employed in order to calibrate and test numerical and analytical models (Gajan et al. 2004, 2008 and Loli 2015).

These studies concluded that soil-foundation non–linear behavior is not only unavoidable during strong earthquake but it can also be beneficial for the behavior of the structure. In addition this unconventional behavior leads to energy dissipation during shaking and mitigation of the forces transmitted to the structure.

Anastasopoulos et al. (2010) proposed that foundation uplift and rocking could be used as a way of seismic isolation, named *Rocking Isolation*. According to this new design philosophy, the foundation's moment capacity is lower than that of the supported column and so plastic hinging is formed within the soil. **Figure 1.1** compares the response according to the conventional design (left), where plastic deformations are developed only on the superstructure and the soil remains elastic, and the rocking isolated structure (right), where structural deformations are minimal while plastic strains develop within the soil. In that way the inertial forces transmitted to the structure are bounded by the capacity of the foundation. It has been shown that especially in slender structures, like bridge piers, this rocking response leads to great reduction of the structure's ductility demand and has significant margins of safety against collapse.

Through large scale shaking table test experiments Antonellis et al. (2015) examined the behavior of a bridge column supported on rocking shallow foundations. They concluded that even after severe earthquakes the structural damage was negligible.

The main drawback of this design concept is the accumulation of settlements during shaking, especially in poor soil conditions. In order for the settlements to be reduced the rocking response should be dominant, which is achieved when the vertical factor of safety (FS_v) is larger than 2. In contrast when the vertical factor of safety is less than 2, the sinking response is dominant. Loli et al. (2016) explored innovative ways in order to minimize the accumulation of settlements of rocking isolated structures. The use of micro–pile inclusions underneath the rocking footing was found to be very effective.

Rocking and uplifting does not only concern shallow foundation, but piled foundations too. Curras et al. (2001) developed a nonlinear Winkler spring model in order predict the rocking response of a piled supported structure. Their model was validated against centrifuge tests.

1.1.2 Unconnected Pile Foundations

Pile foundations are very commonly used for the support of structures especially in poor soil conditions. Pile foundations are also used in the case of liquefiable shallow soil layers or when soil corrosion is probable. According to the current design codes the load is transmitted to the piles from the structure and the pile cap does not affect the bearing capacity of the foundation. This conservative assumption often leads to the need of a large number of piles, especially in seismic areas. In contrast, in the case of piled raft foundation, where piles are used to reduce raft's settlements, both the piles and the raft are considered in the bearing capacity. However, in piled raft foundations significant bending moments can be developed on the raft if the distance between the piles is large. As it has been observed after strong earthquakes (Kobe 1995) structural failure can occur on pile heads due to the development of large bending moments and shear forces. It is believed that disconnecting the piles from the pile cap, through an improved soil layer, will reduce the inertial forces transmitted to the superstructure as well as the shear forces and

bending moments on pile heads, avoiding their failure. In addition in an unconnected pile foundation the pile cap will have the role of a shallow footing on improved soil, playing an important role on the bearing capacity of the foundation.

There have been studies of unconnected pile foundations, however most of them deal with vertical loading. Fioravante and Giretti (2010) compared the behavior of contact (PR) and non-contact (NC) piled rafts on vertical loading for different piled raft setups (**Figure 1.2**). The load transfer mechanisms of contact and non–contact piles are shown in **Figure 1.3**. In the case of contact piles the settlement at the foundation level are equal for the raft (w_r), the soil (w_s) and the pile (w_p) and the load is directly transmitted to the piles. For non–contact piles the soil layer between the piles and the raft leads to relative settlements between the soil and the piles ($w_s > w_p$). This relative settlement introduces negative skin friction on the pile near its head, which reduces with depth until a neutral plane where the skin friction becomes positive and the pile is providing bearing resistance.

Another important difference is that the contact piled raft has a non-linear force–displacement response while the non–contact piled raft response linearly even for large settlements. This non–linearity comes from the non–linear behavior of piles, which is not observed in non–contact piles. In addition, from the settlement–load graphs it is seen that the yielding load of the connected pile raft increases non–linearly with the number of piles. For example the yielding load of the raft with four piles is almost equal to four times the yielding load on the one piled raft, while the yielding load of the raft with the nine piles is a lot larger than nine times the yielding load on the one piled raft. The increase of the yielding load with the increase of the numbers of piles is due to the compaction of sand. As already mentioned the non–connected piled raft response linearly and so there is no yielding load. However, it is observed that the foundation's stiffness is proportional to the number of piles. It is also noted from **Figure 1.4** that in the contact piled raft most of the load is carried from the piles at small settlements and the subsoil is progressively loaded as the settlement increases. In contrast in non–connected piled raft the subsoil carries most of the weight and the piles carry a small amount. This can explain the linear response of the piles in the latter case.

The differences of foundation stiffness observed in **Figure 1.4** can be explained from the capacity mobilization of the piles. In the case of contact piles, the initial loading is transmitted mainly to the piles, since they are stiffer than the subsoil, and until their capacity is reached they govern the piled raft stiffness. In non–contact piles the load transfer mechanism is depended on the deformation of the interposed soil layer and so is the capacity mobilization of the piles. As a result the initial stiffness of the piled raft depends on the stiffness of the soil layer. It is also important to note that while in the non–contact piles the stiffness is similar for the cases of one and four piles, due to pile–soil–pile interaction the piles of the nine piled raft has decreased stiffness. Fioravante and Giretti analyzing the loading mechanisms observed in their experiments and taking account of group effects, derived the following equations to approximate the stiffness of non–connected piled rafts.

Since the raft stiffness is independent of the number of piles the piles and the raft can be considered independent nonlinear springs. Hence raft settlement (w_r) and the piles settlement (w_p) can be calculated as:

$$w_r = \frac{Q_r}{k_r} \quad \text{and} \quad w_p = \frac{Q_p}{k_p} \tag{1.1}$$

where k_r is the unpiled raft stiffness, k_p is the stiffness of the pile group and Q_r and Q_p the load transmitted by the raft to the subsoil and axial load transmitted to the pile heads respectively. k_p can be calculated as:

$$k_p = n\mu k_{p1} \tag{1.2}$$

k_{p1} is the stiffness of a single pile at small settlements, n takes values between 0.3 and 0.6 and $\mu=n^{-1}$, where n is the number of piles. As the total applied load on the raft is

$$Q_t = Q_r + Q_p \tag{1.3}$$

using the previous equations the piled raft settlements can be found

$$w_r = \frac{Q_t}{k_{pr}} = \frac{(w_r k_r + k_p w_p)}{k_{pr}} \tag{1.4}$$

and so the stiffness of the piled raft can be approximated from the equation:

$$k_{pr} = \frac{k_r w_r}{w_{pr}} + \frac{k_p w_p}{w_{pr}} \tag{1.5}$$

Their results matched very well with the experimental ones.

Liang et al. (2003) devolved an alternative piled raft model (**Figure 1.5**) with short piles made of soil–cement or sand–gravel columns, used to enhance the bearing capacity of shallow soil, long piles, used to minimize settlements, and an improved soil layer between the raft and the piles in order to redistribute the stress between the raft and the piles. They conducted a parametric analysis, using finite element method, in order to examine the role of the elastic modulus and the length of the piles and the elastic modulus and thickness of the interposed soil layer on the vertical stiffness of the piled raft and on the participation of each component on the total resistance.

In the first part of this study the improved soil layer was not included in order for the effects of piles' moduli of elasticity and lengths to be examined. They concluded that, until a certain limit is reached, the increase of the modulus of elasticity of short piles increases the vertical stiffness of the piled raft. In addition for a given modulus of elasticity of piles, the piled raft stiffness increases with the increase of the length of the piles, especially with that of the long piles. If the length of the long piles and short piles are close the modulus of elasticity of short piles plays an important role

on their load–sharing ration. However, this statement does not hold true if the long piles are a lot longer than the short ones. Moreover, it was found that for given length of short piles, as the length of the long piles increases the load transmitted to them also increases, whereas the load transmitted to the short piles and the subsoil decreases.

In the second part of the study the effects of interposed soil layer to the response of the piled raft was studied. It was found that the axial stress was decreased on long piles and increased on short piles, compared to the case of connected piles. As previous studies had also stated, the maximum axial stress moves from the pile heads to a certain depth when the piles are not connected to the raft due to the negative skin friction. The loading of the subsoil was increased and so the shallow bearing capacity can be better used when the piles are not connected to the raft. It was also observed that the decrease of the elastic modulus of the subsoil mobilizes the shallow soil bearing capacity and decreases the stress on the long piles. In addition, the greater the distance between the piles and the raft is the greater the subsoil and short piles stresses and the lesser the long pile stresses are. From these observations it can be concluded the use of a soil layer as a cushion is an effective way to adjust the load-sharing mechanisms in a piled raft.

Gerolymos et al. (2010) studied the unconnected piled raft shown in **Figure 1.6**, where the piles and the interposed well-compacted coarse-grained layer act as soil improvement. The purpose of their study was to determine the ratio of soil impedances before and after the soil improvements, as well as the parameters affecting it. It was found that the most important dimensionless parameters are:

- The thickness of interposed layer to the pile distance ratio (H_{gr}/s)
- The pile distance to the pile diameter ratio (s/d)
- Pile–soil interface strength to soil strength ratio ($r=\tan\phi_{int}/\tan\phi_{soil}$)
- The elastic modulus of grained layer to the elastic modulus of the soil ratio ($E_{gr}/E_{soil)}$
- The length of the piles to the diameter of the piles

From parametric analyses it was shown that the increase of the distance of the piles (s) increases the settlements but decreases the bending moments on the raft. The impedance of the improved soil increases as the modulus of elasticity of the interposed soil layer increases. The strength of the pile–soil interface was also found important for the settlements but does not affect the bending moments on the raft. A very interesting result is shown in **Figure 1.7**, where it can be seen that the increase of the grained layer thickness leads to greater settlements. However, for s/d > 4 this is correct until a certain limit after which the increase of the thickness results in reduction of settlements. This is because initially as the thickness increase the piles get further away of the raft and so the system's stiffness decreases but after a specific value the interposed layer acts as replacement of the initial poor soil and the settlements decrease. Employing statistical analysis of these results the researchers derived equations able to approximate the ratio of soil impedances before and after the soil improvements.

Cao et al. (2004) examined the effect of disconnected piles on a raft supporting a typical high–rise building with a central core. The structure they studied and the simulation of the loading are shown in **Figure 1.8** and **1.9** respectively, where the central load illustrates the core and the outer ones the columns. They parametrically varied the rigidity of the raft, the pile lengths, the piles' number and the arrangements in order to study their effect on the raft's behavior. The tested arrangements are shown in **Figure 1.10**. In **Figure 1.11** the increase of piled raft's stiffness compared to unpiled raft's stiffness is shown for different plate thickness and normalized settlement s/B, where s is the settlement and B the raft's width. The stiffness increase is calculated by the ratio $\frac{Pcr-Pr}{Pr}$, where P_{cr} is the load of the pile raft and P_r the load of the unpiled raft at the same settlements. From this graph it can be concluded that the increase in stiffness decreases with settlements but increases with the rigidity of the plate. In addition Cao et al. found that the differential settlements and so the bending moments of the raft decrease as the pile length increases. Another interesting finding is that even though both in the case of the 35 cm and 50 cm piles the raft carried a large amount of the applied load when the settlements were small, in the latter case the amount was even bigger due to the greater soil improvement provided from the longer piles. As **Figure 1.12** shows, the percentage of the load carried by the piles increased with settlements and then decreased until a steady value of 30–35% for long piles and 20–30% for short piles. Moreover they found that even though when the piles are located in the central 32.5% of the raft the differential settlements and the bending moments greatly reduce, this is not the case when they are located at the central 65% of the raft. In addition the increase of the pile rows in the same area does not lead to reduction of the maximum settlement.

Sawwaf (2010) examined the effects of connected and unconnected piles on an eccentrically loaded raft. The author suggests the use of short piles instead of longer ones, which would provide greater stiffness but also lead to higher shear forces and bending moments of the raft, due to their increased geotechnical bearing capacity. The configuration of the model studied is shown in **Figure 1.13**. A parametric analysis, with a total of 36 experiments, was employed in order to study the effects of pile length, pile number, load eccentricity and pile arrangements (**Figure 1.14**). In order to compare the different set ups, an improvement factor was introduced called Bearing Pressure Improvement (BPI), which is the ration of the applied pressure on the piled raft to the unpiled raft for the same settlement level. As **Figure 1.15** shows, and has also been discussed previously, the use of either connected or unconnected piles increases the stiffness of the raft, while connected piles are even more effective. Furthermore piled raft's improved performance decreases as the settlements increase. As the number of the piles increases the performance of the piled raft increases until a certain point, from which there is no reduction of settlements for a given pressure (**Figure 1.16**). In contrast to Cao et al. (2004) finding Sawwaf found that due to the eccentricity of the applied load, placing the piles at the edges of the raft improves its behavior, while Arrangement 3 (**Figure 1.14**) is the optimum solution. This finding is shown in **Figure 1.17**, where the behavior of the raft in the three different arrangements is compared for a given eccentricity. As Arrangement 3 was proved the most effective it was tested for three different

eccentricity levels. From **Figure 1.18** it is concluded that piles, either connected or unconnected, improve the bearing pressure of the raft, however, the bearing pressure significantly reduces as the eccentricity increases. **Figure 1.19** shows the settlements along the section S–S, it is obvious that the use of connected or unconnected piles greatly reduce the rotation of the raft.

Nakai et al. (2004) studied the dynamic response of a five-storey structure supported on the piled rafts, shown in **Figure 1.20**, using finite element analyses, which was validated through centrifuge testing. As other researchers have also noted, from the centrifuge tests it was concluded that the shear forces and bending moments on the unconnected piles (RU) are significantly reduced (**Figure 1.21**) while the load carried by the raft is quite important. The analysis showed that in the unconnected piled raft case the acceleration on the superstructure was reduced but the base shear forces and over–turning moments were increased. Also the raft without piles developed larger acceleration but the base shear and overturning moment was reduced. In the PF and PR cases a hinged connection between the piles and the raft was tested but did not affect the response of the structure significantly. The addition of short piles was also examined (**Figure 1.22**), which lead to the reduction of shear forces and bending moments on long piles in the PF case. Their size appeared to have great influence on the developed bending moments and shear forces of long piles but did not affect the load sharing ratios of the piles and the raft.

Limniati (2012) studied the monotonic and dynamic behavior of unconnected pile groups on clay with linearly increasing modulus of elasticity, using finite element software. In that the response of a pile group, designed according to the current codes, a group with unconnected piles, designed using push over analyses so that the safety factors of the current codes are maintained, and a group of unconnected piles where the seismic factor of safety was below 1 in order to achieve Rocking Isolation. After dynamic analyses for several earthquakes, even very strong ones exceeding the design specification, the study concluded that the unconnected pile foundations performed better that the connected ones. The developed acceleration on the superstructure, the ductility demand and the residual settlements were smaller for the unconnected pile foundations. It is important to note, that between the two foundation designs with unconnected piles the unconventionally design one performed better, proving that rocking isolation can be used in this type of foundations. Since the reaction forces and moments on the piles were quite important some dynamic analyses were performed with inelastic piles. The results did not change significantly from the previous case, however, pile failure was observed in some of them showing that the design codes' assumption that foundation failure is avoided due to overstrength factors is incorrect.

1.2 Scope Of This Study

From the preceding literature review the need to further study the dynamic response of structures supported on unconnected pile groups is obvious. This study will attempt to confirm or contradict the advantages and disadvantages that this

type of foundation is believed to have, as well as understand the response of this system under seismic loading.

For this purpose, an unconnected pile foundation will be designed according to the design philosophy of the current codes and its dynamic response will be compared to the conventional system. In addition, an unconnected pile foundation with an Earthquake Factor of Safety (FS_E) less than 1 will be designed, in order to examine if Rocking Isolation can be achieved in this type of foundation. All systems will be supporting a bridge pier, whose height will vary in order to study the effect of slenderness.

Figures of Chapter 1

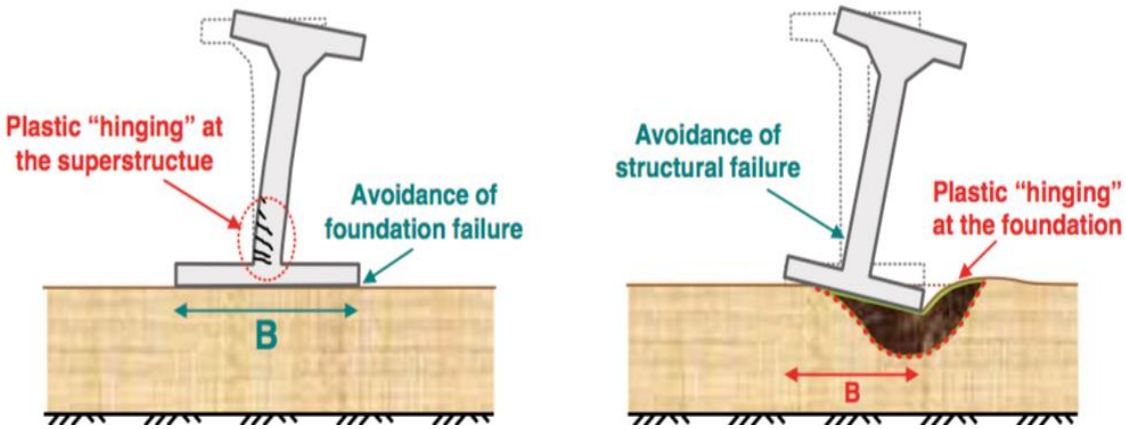

Fig. 1.1: Conventional design – plastic hinge on superstructure (left) compared to new design philosophy – plastic hinge within the soil (right), by Anastasopoulos et al.

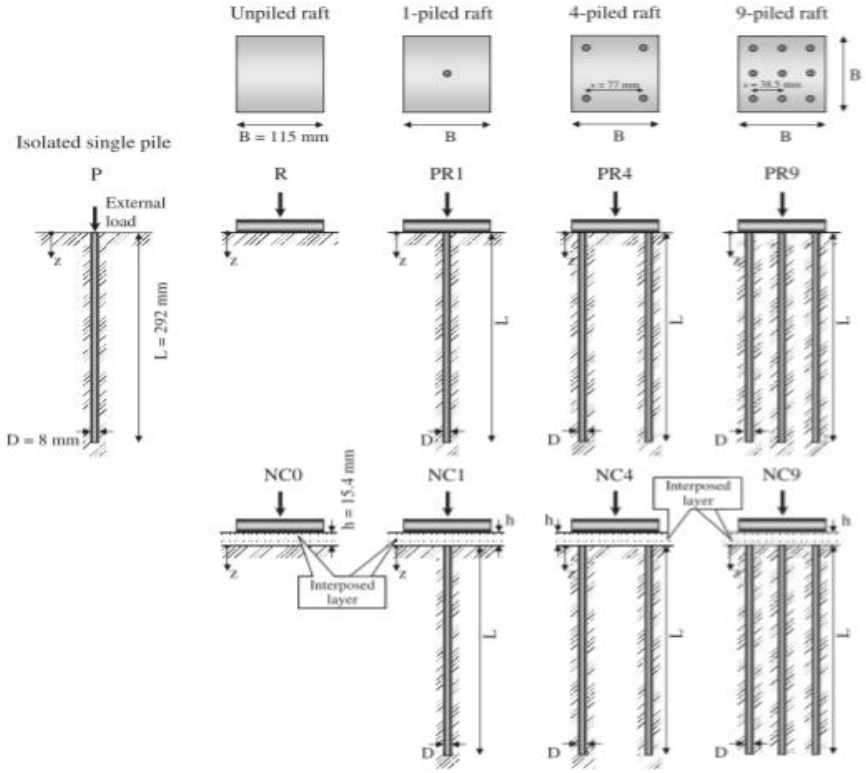

Fig. 1.2: Setups of connected (PR) and non-connected (NC) piled rafts studied by Fioravante and Giretti

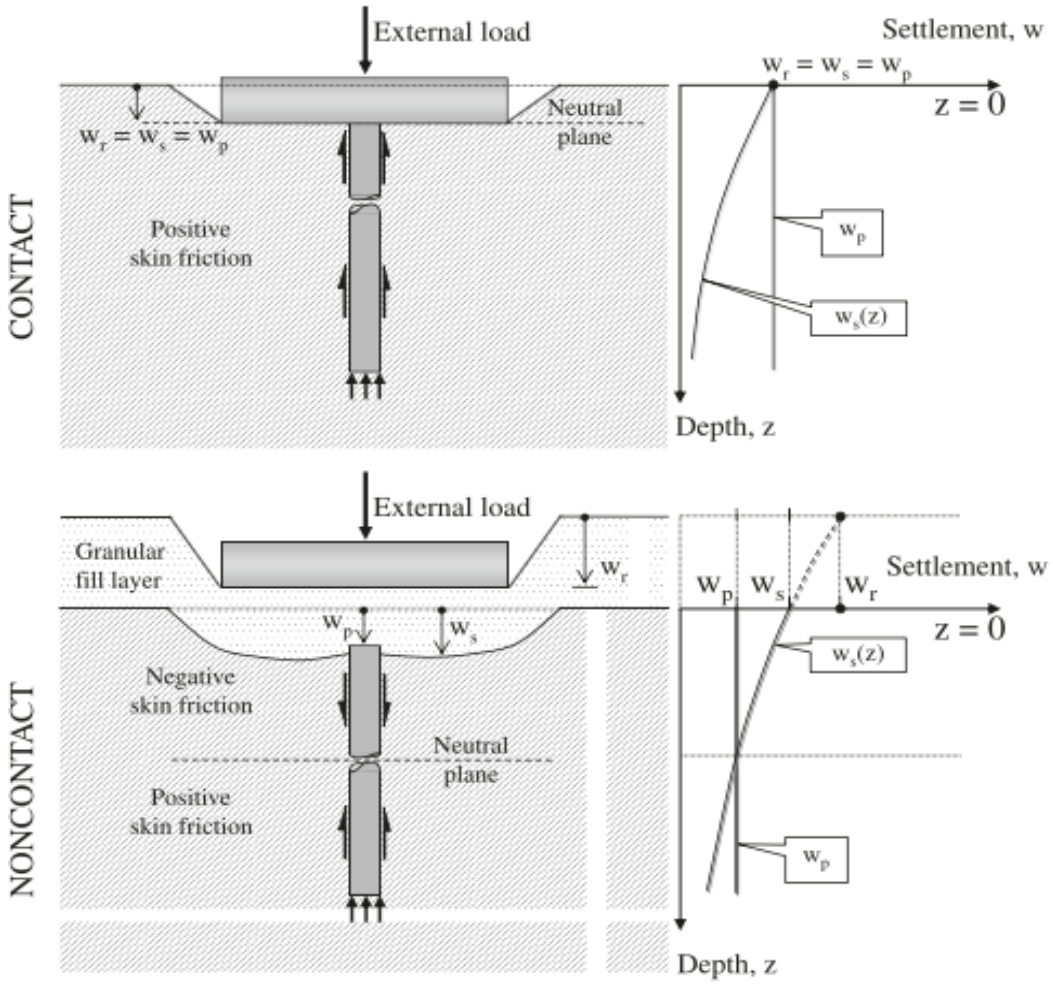

Fig. 1.3: Comparison of loading mechanisms and settlements on connected and unconnected piled rafts (Fioravante and Giretti).

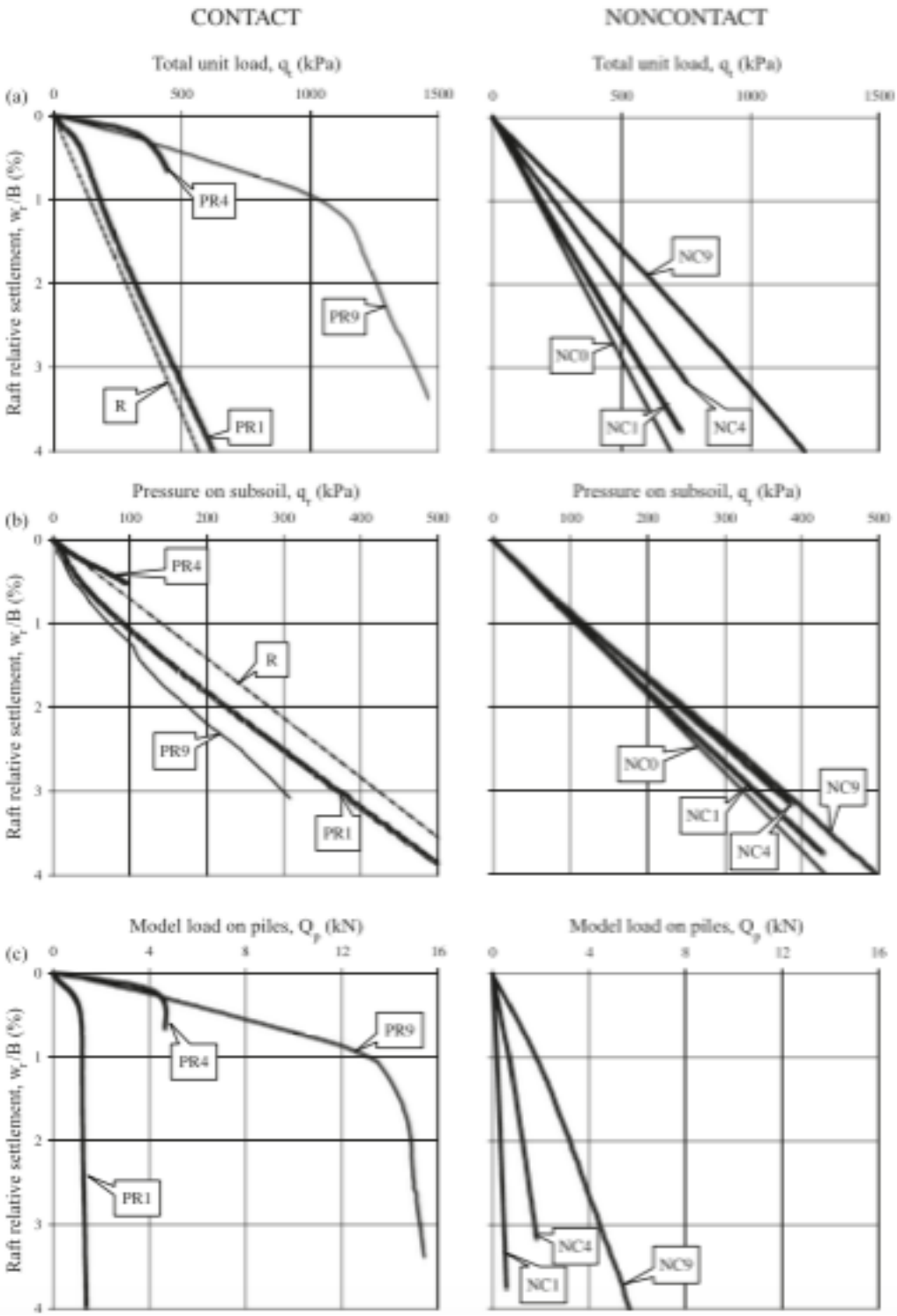

Fig. 1.4: Relation of settlement and (a) total stress of the raft (b) subsoil stress (c) axial load on pile heads for contact (left) and noncontact (right) piled rafts, by Fioravante and Giretti

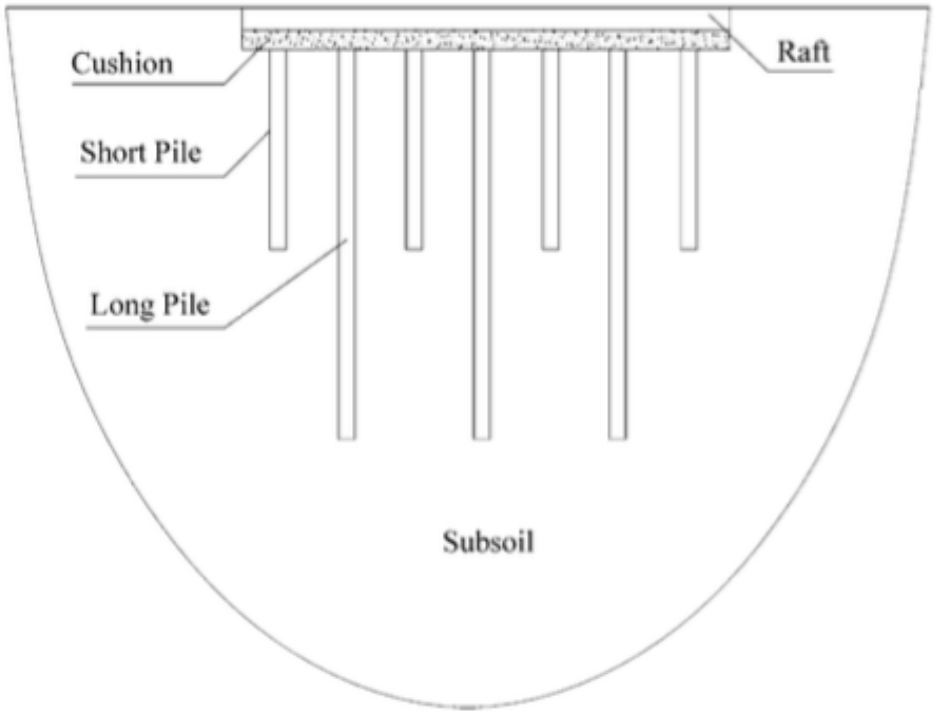

Fig. 1.5: Piled raft model proposed by Liang et al. combining improved soil layer and short and long piles.

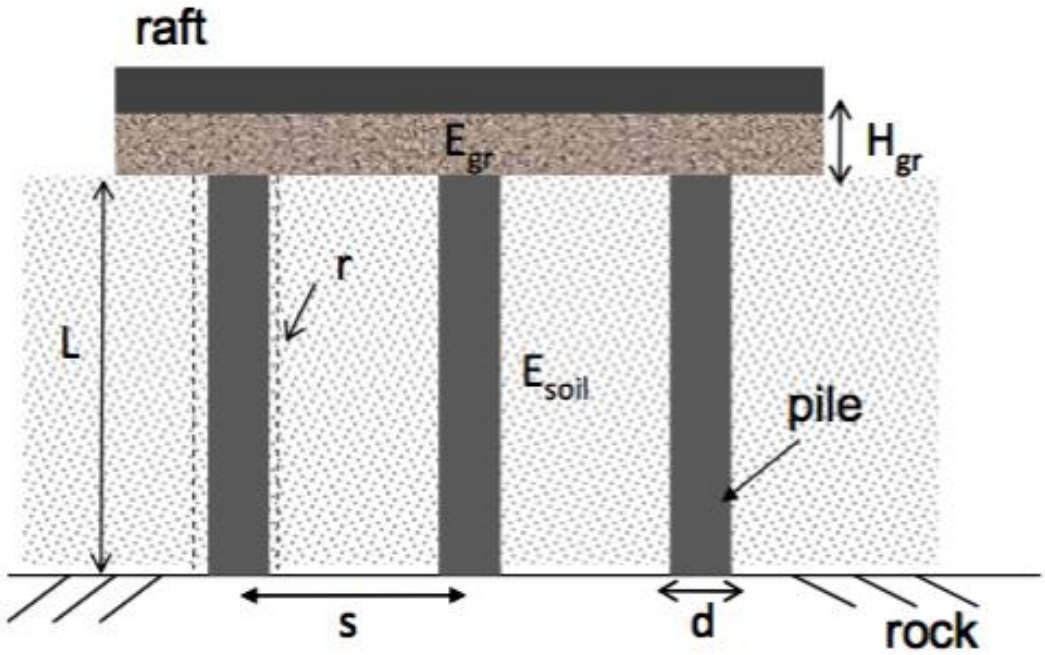

Fig. 1.6: Unconnected piled raft studied by Gerolymos et al. where the effect of five dimensionless parameters was studied.

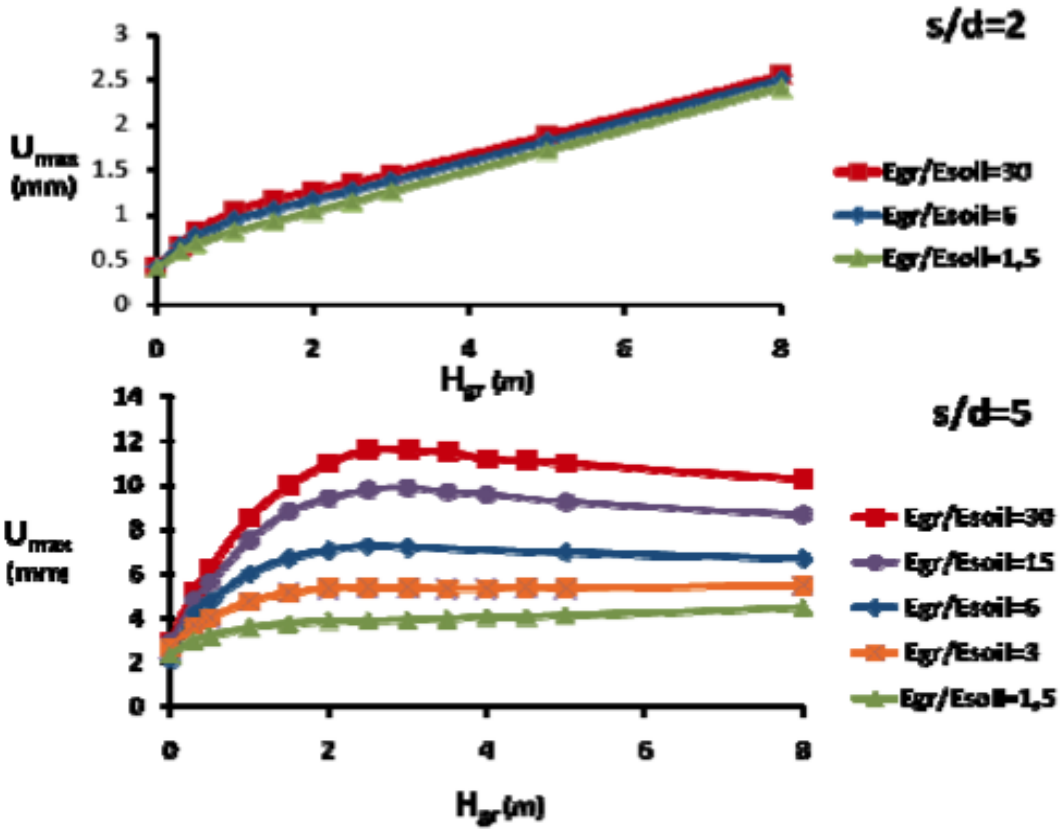

Fig. 1.7: Raft settlement versus Interposed grained layer thickness for different pile distanced and grained layer to soil modulus of elasticity ratios, by Gerolymos et al.

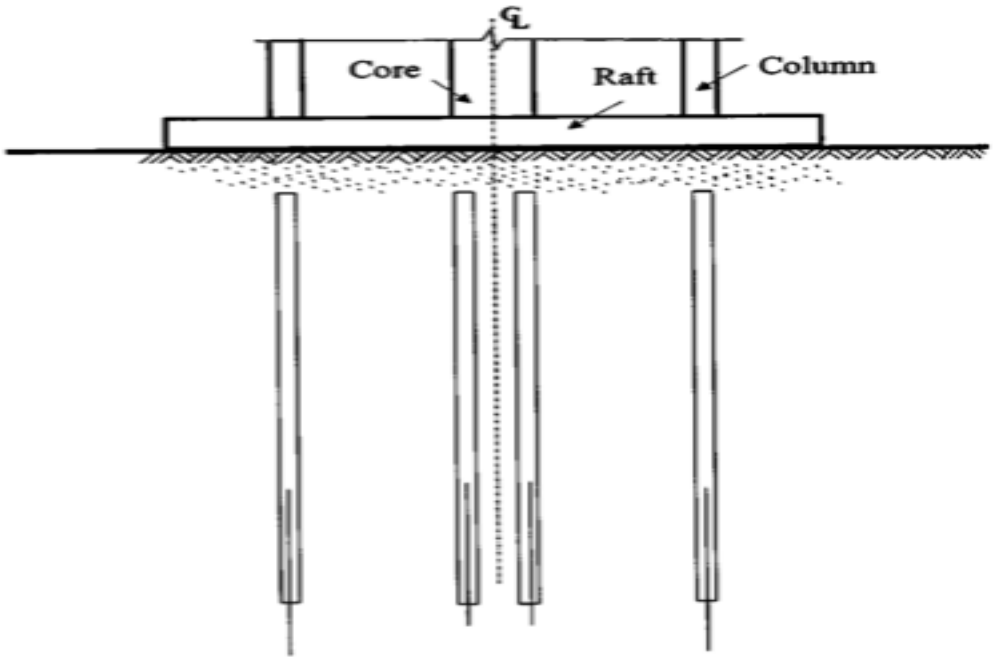

Fig. 1.8: Unconnected piled raft supporting a high-rise structure with central core studied by Cao et al.

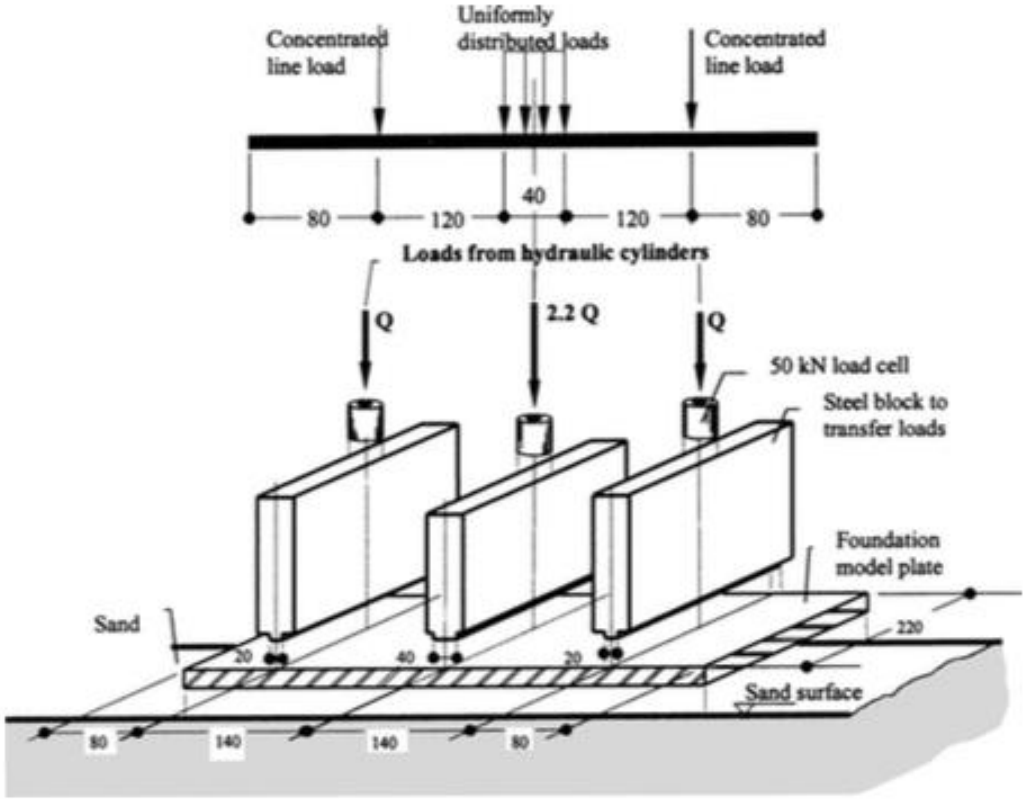

Fig. 1.9: Loading set up where the outer point loads simulate columns and the central load simulates the distributed load form the core (dimensions in mm), by Cao et al.

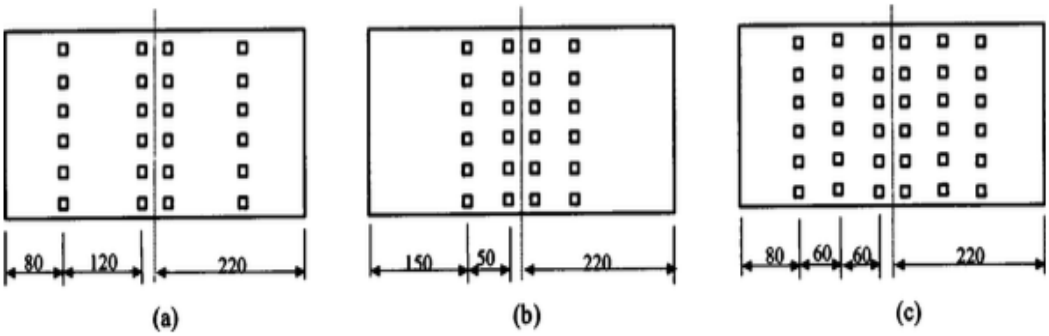

Fig. 1.10: Studied pile arrangements: (a) four rows of 6 piles at the central 65% of the raft (b) four rows of 6 piles at the central 32.5% raft area (c) three rows of 6 piles at the central 65% of the raft. (Cao et al.)

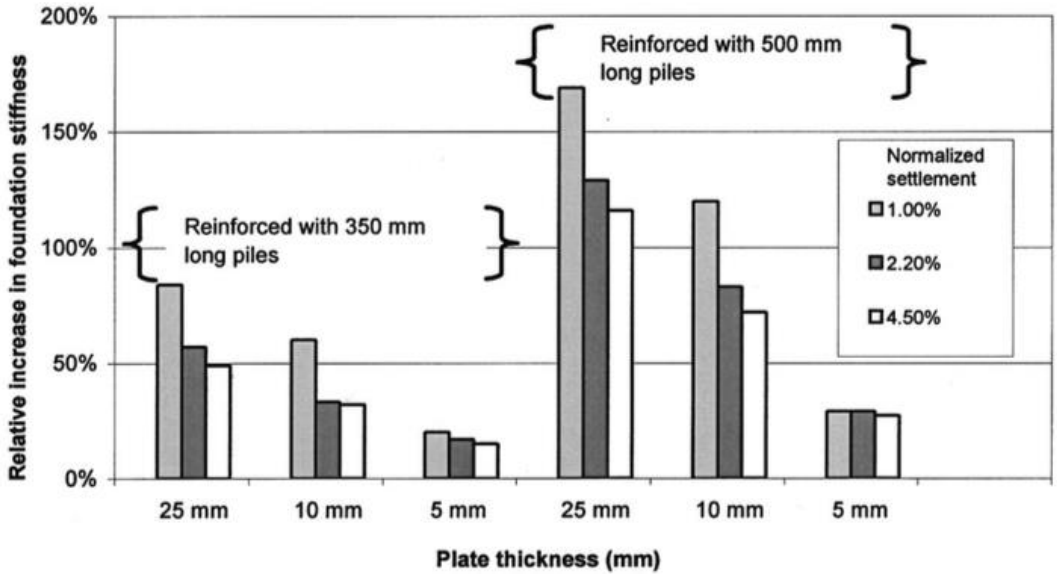

Fig. 1.11: Relative increase in foundation stiffness when unconnected piles 350mm and 500mm long are used for different values of plate thickness. (Cao et al.)

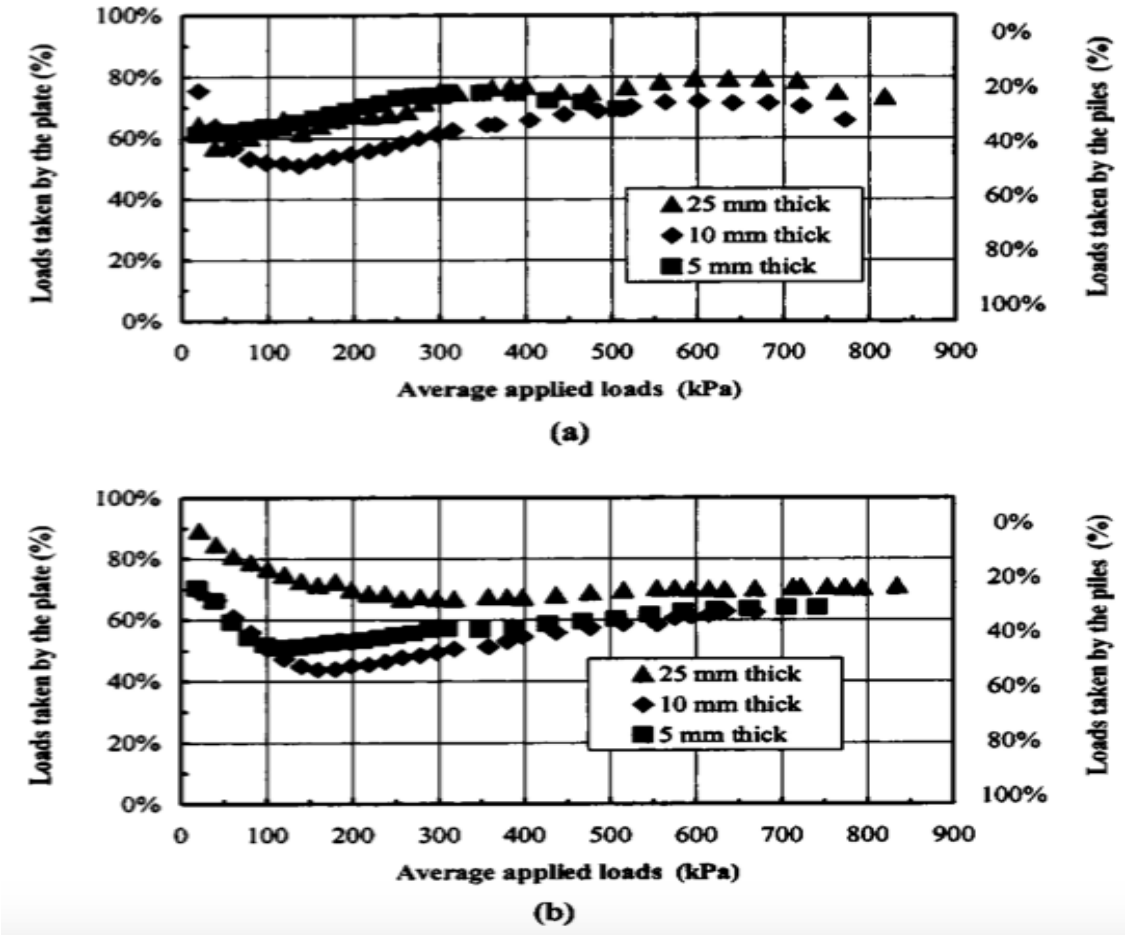

Fig. 1.12: Percentage of load taken by the raft compared to the applied load for different plate thickness and for (a) 350mm long piles (b) 500mm long piles, by Cao et al.

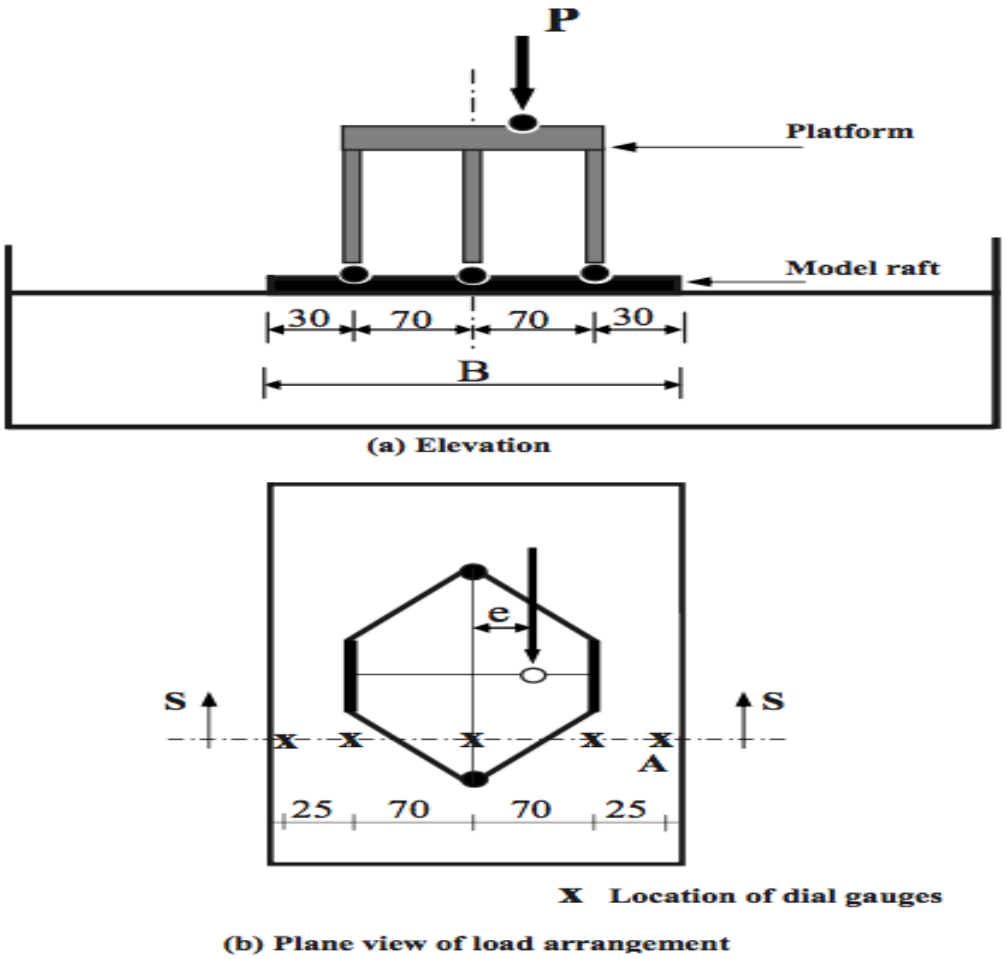

Fig. 1.13: Configuration of the eccentrically loaded raft studied by Sawwaf. (a) elevation (b) plan view of the experimental set up.

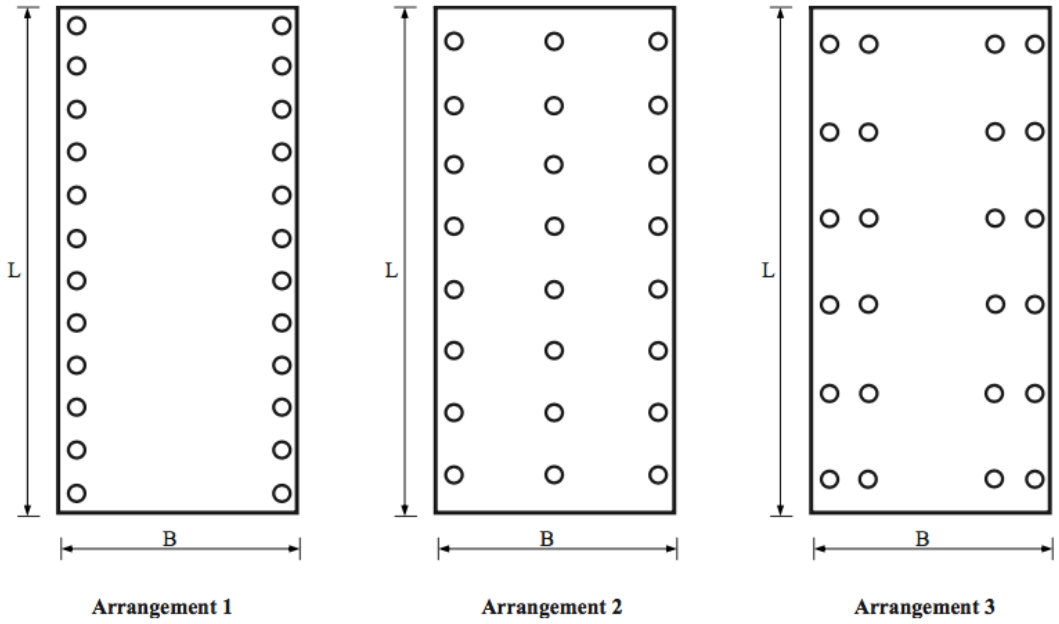

Fig. 1.14: Different arrangements of the 24 piles studied by Sawwaf.

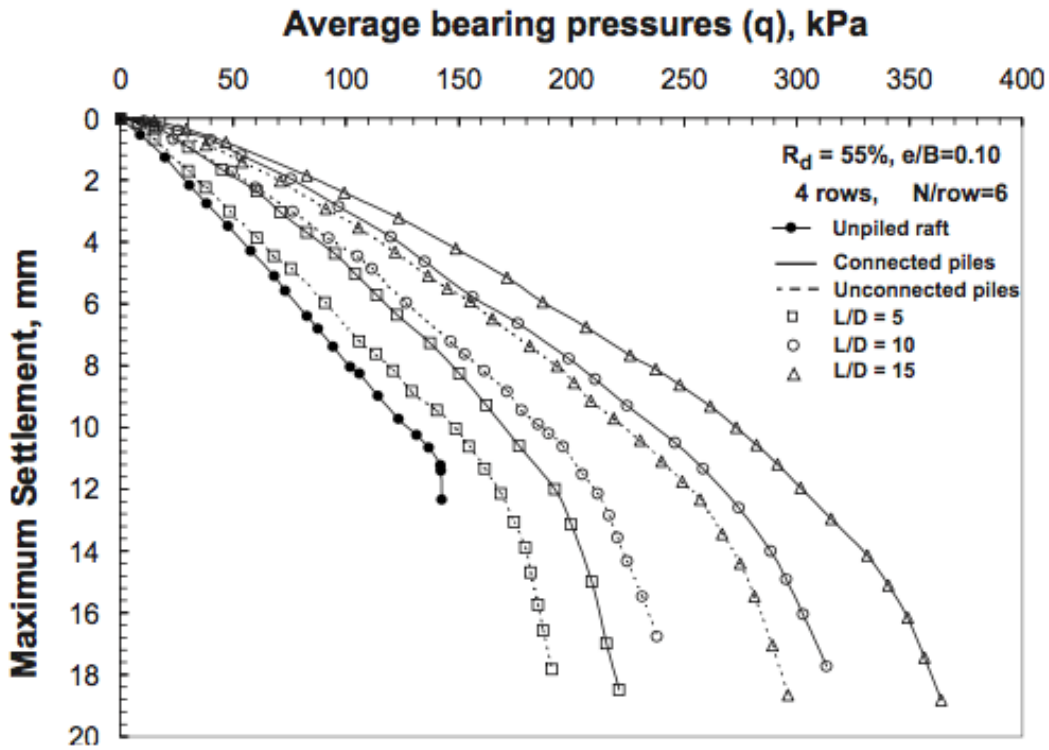

Fig. 1.15: Variation of average bearing pressure with settlements for different pile lengths in the cases of unpiled raft and piled raft with connected and unconnected piles. (Sawwaf)

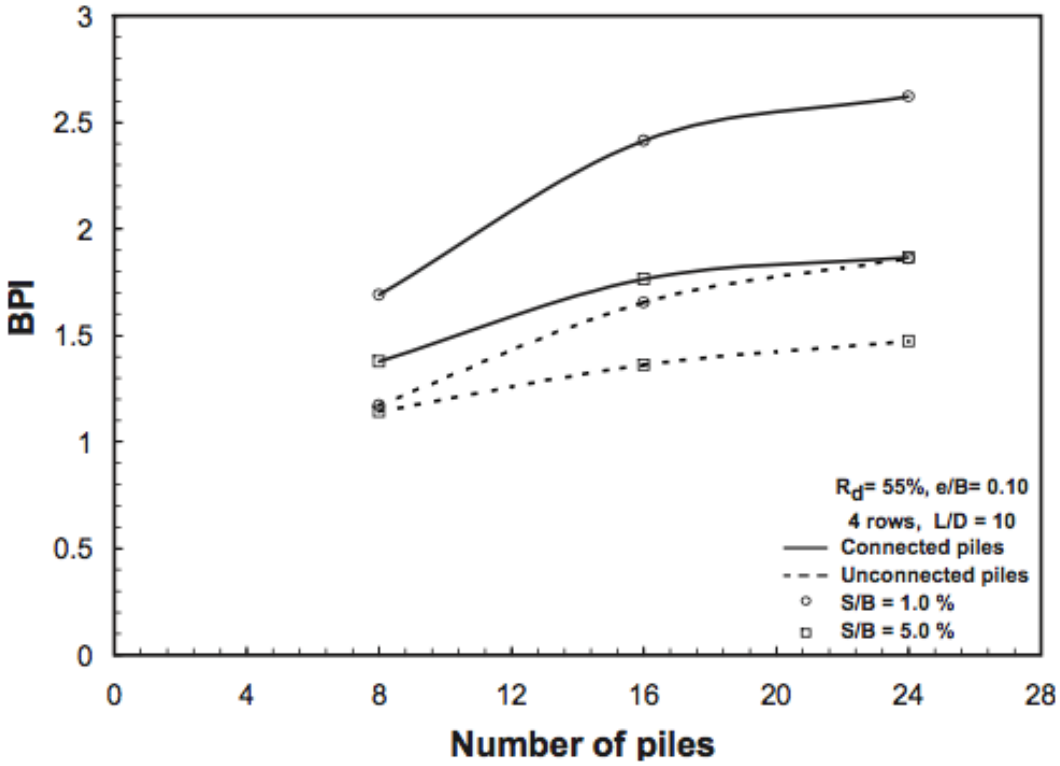

Fig. 1.16: Variation of BPI with the number of piles for connected and unconnected piled rafts. (Sawwaf)

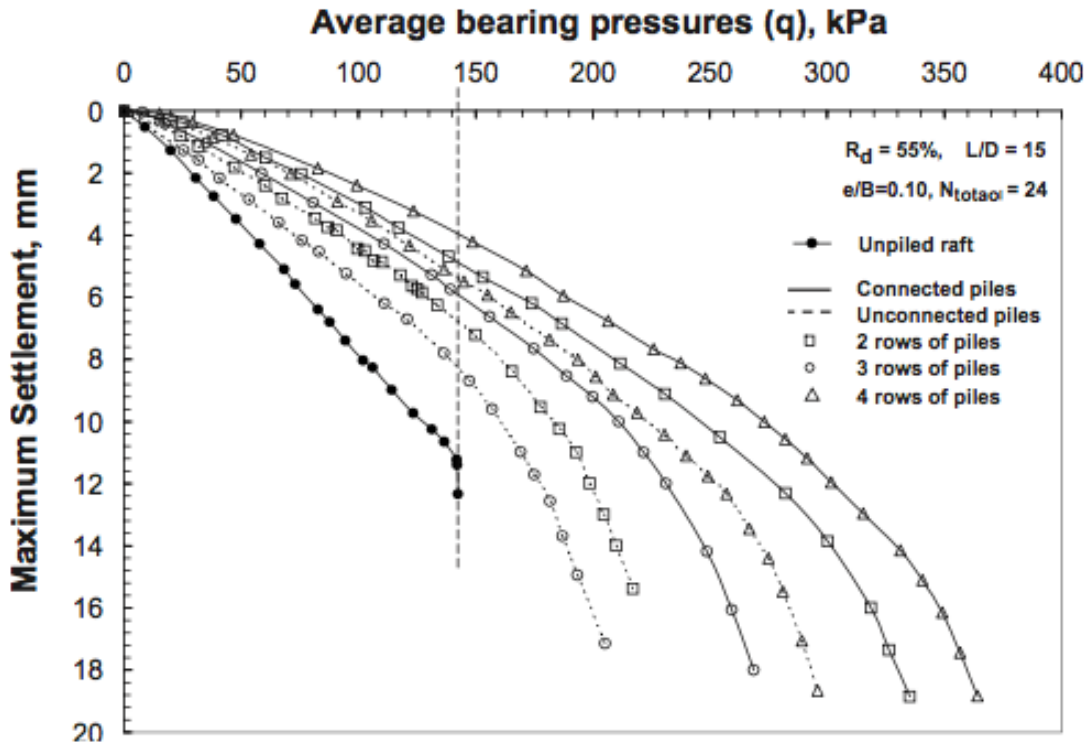

Fig. 1.17: Variation of average bearing pressure with settlements for different pile arrangements in the cases of unpiled raft and piled raft with connected and unconnected piles. (Sawwaf)

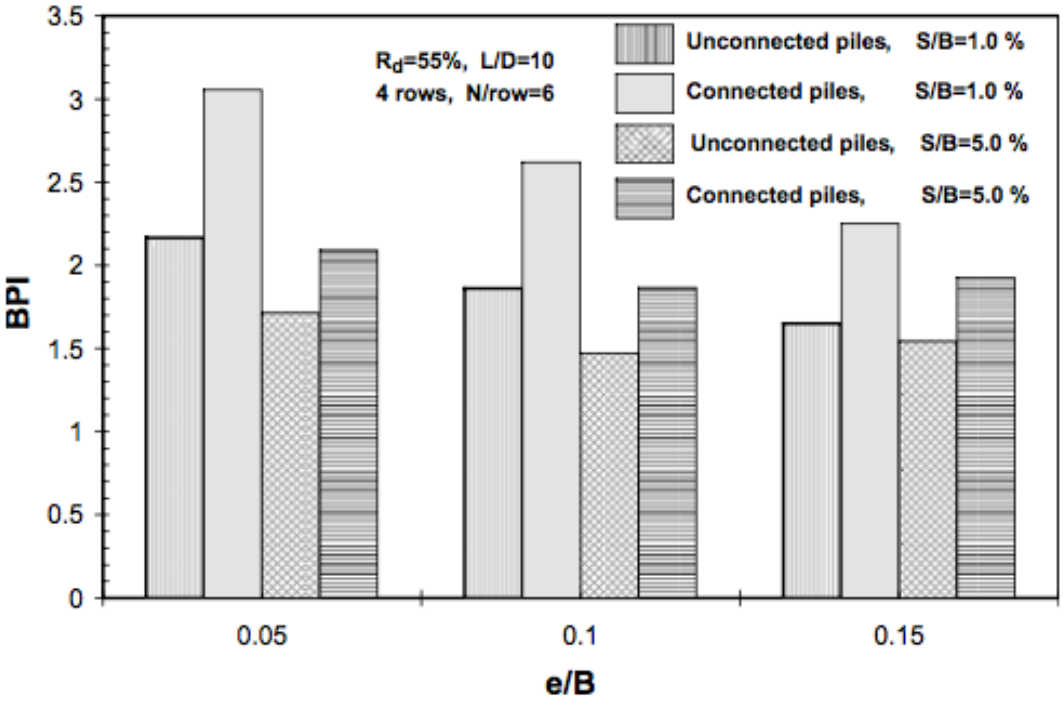

Fig. 1.18: Variation of BPI with loading eccentricity e/B for different settlement ratios S/B=1.0% and 5.0%. (Sawwaf)

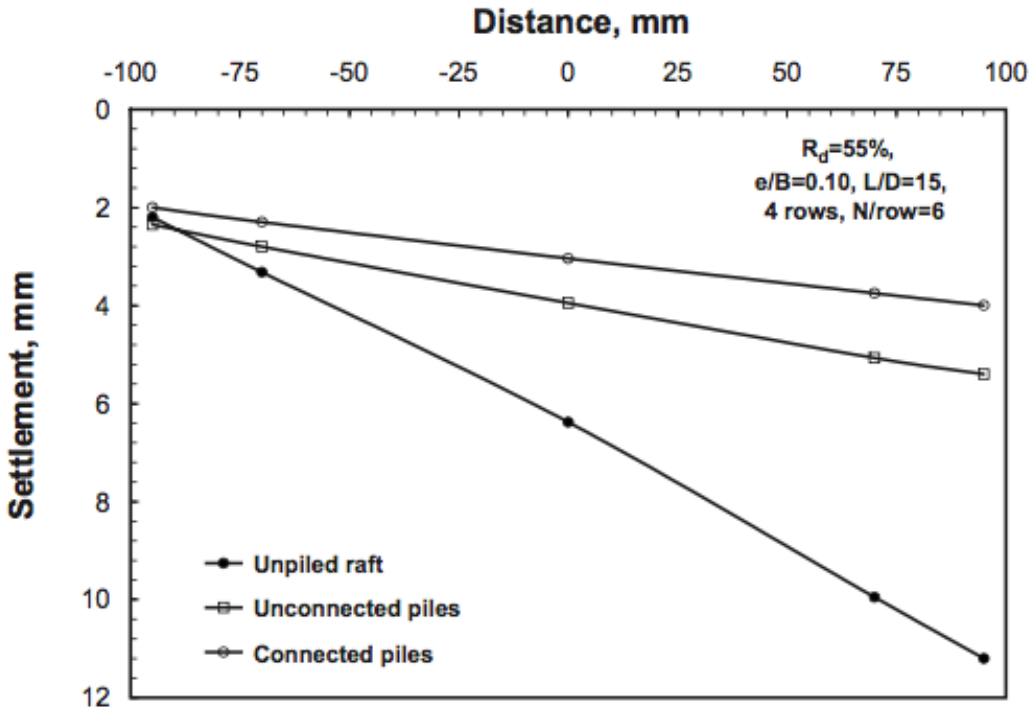

Fig. 1.19: Settlements along section S-S in the three studied raft cases. (Sawwaf)

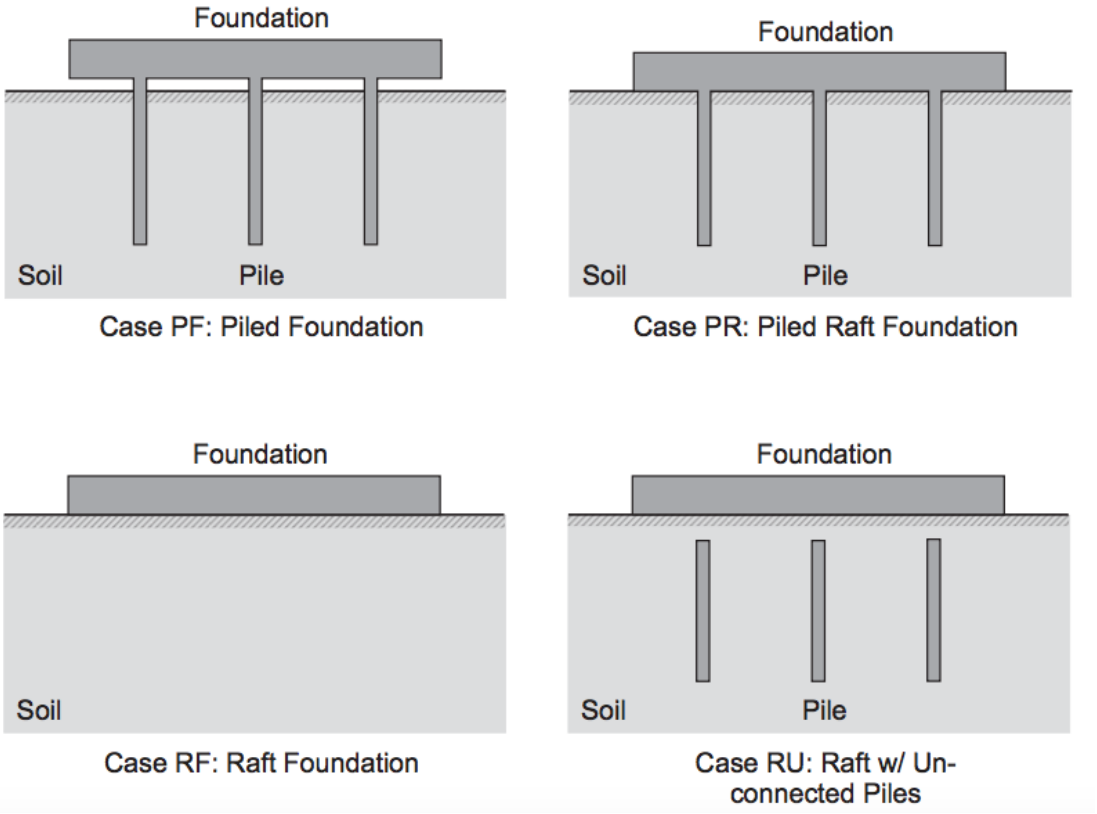

Fig. 1.20: Piled raft configurations studied by Nakai et al. using centrifuge testing and finite element analyses.

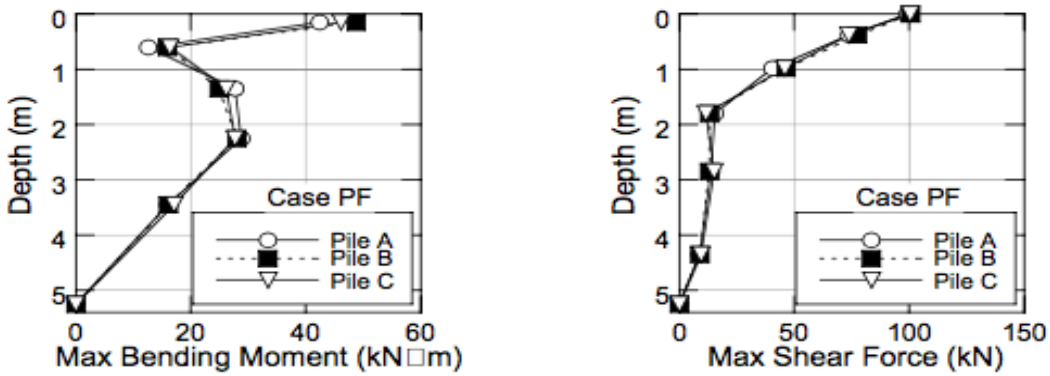

(a) Case PF

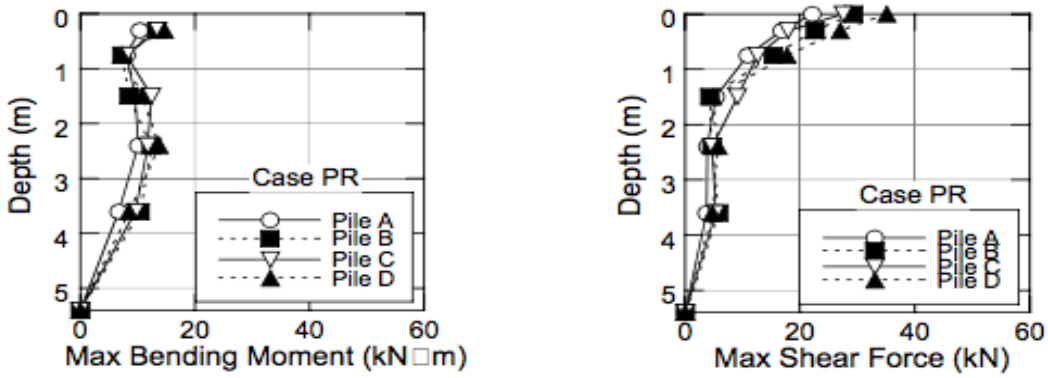

(b) Case PR

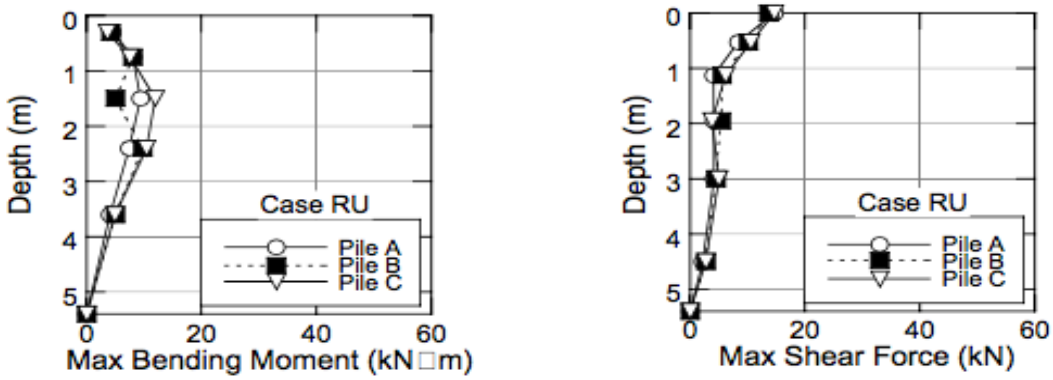

(c) Case RU

Fig. 1.21: Comparison of bending moments (left) and shear forces (right) on the different piled raft configurations studied by Nakai et al.

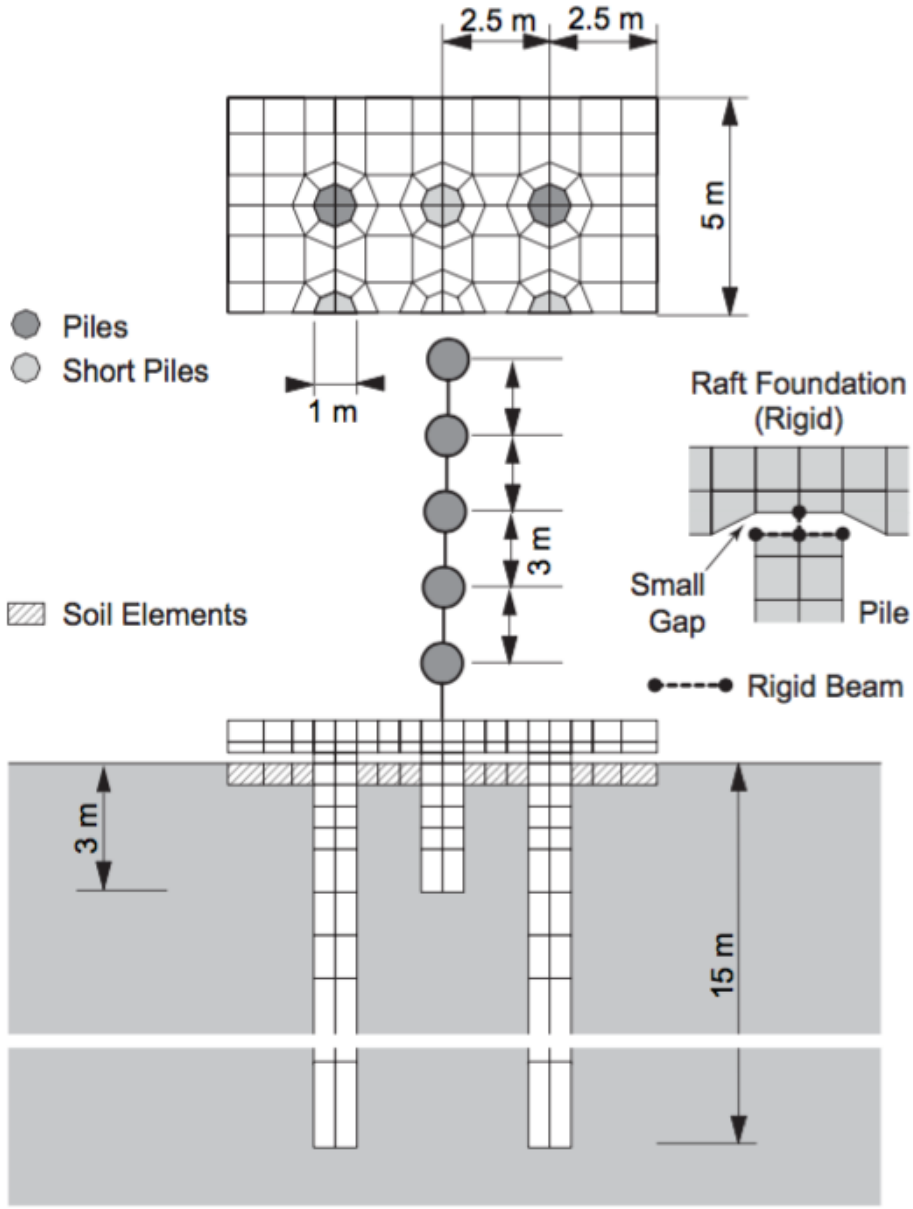

Fig. 1.22: Finite element model of five-story structure supported on piled raft with long and short piles, by Nakai et al.

Chapter 2

Numerical Simulation

2.1 Finite Element Model

As stated in the previous chapter, in this thesis the static and dynamic response and behavior of two different bridge piers, a tall and a short one, supported on three different foundations will be studied. All three systems are founded on homogenous saturated clay. For this purpose three dimensional models were developed in the finite element software Abaqus. Sketches of the tested configurations are shown in **Figure 2.1**.

Since, the dynamic response of bridge piers excited on their transverse direction can be simulated by a single degree of freedom oscillator, the pier is modeled as circular beam elements (B31) and the deck as a concentrated mass on top of the pier. The pile cap, in both cases of connected and unconnected pile groups, is simulated by elastic three-dimensional octagonal elements (C3D8) with concrete's modulus of elasticity. The soil is also simulated by the same type of elements (C3D8) and its nonlinear behavior is described by the constitutive model of the following chapter.

For the piles, zero weight and stiffness, three-dimensional elastic octagonal elements (C3D8) are used, which simulate the soil–pile interaction. Their stiffness and Poisson's ratio is introduced by circular elastic beam elements (B31), that run across the solid elements' centerline. To simulate correctly the behavior of the piles, the solid elements should follow the movement of the beam elements. This is done by connecting with rigid beam elements (MPC), in every level, each node of the solid element with the corresponding node of the beam element. This way a disc is formed on every level, which follows the movement of the beam and is able to rotate, always remaining perpendicular to the beam element. A schematic illustration of this is given, along with its undeformed and deformed shape, in **Figure 2.2**.

The interaction between the soil and the structural elements is introduced by interface elements, allowing sliding and uplifting to be developed. The tangential interaction is described by a coefficient of friction. While for the interfaces between the soil and the pile cap, the piles' base and the piles' head (in case of unconnected piles), a very common friction coefficient, equal to 0.7, is used, for the interface between the soil and the piles' perimeter an extremely large friction coefficient, equal to 5.0, is used. It is noted that this unrealistically large, lacking of physical meaning, friction coefficient does not affect the soil–pile interaction, and hence the behavior of the system, but helps the development of soil's saturated strength (aS_u) along the pile–soil interface, as Eurocode suggests.

The normal behavior of all interfaces is described by an exponential pressure – overclosure relationship, which, in order to avoid numerical instability, allows minimal tension stresses to be developed. As shown in **Figure 2.3**, to define this exponential relationship, two parameters are needed. The first one, p_0, describes the interface pressure when no relative movement has been developed and the second one, c_0, the relative movement for which tension is allowed. Herein p_0 and c_0 were

given the values 10 and 0.001 respectively, which are commonly used in the literature.

To realistically simulate the behavior of a structure using finite element software, the boundaries of the model should be sufficiently remote from it, in order not to affect its behavior. This is especially true in case of earthquake loading, where seismic waves can be reflected from the boundaries. Hence, according to the literature, in the case of a pile cap with length B parallel to the earthquake loading (x-direction), the boundaries were set at a distance of 3B to the right and to the left of the cap. In the other direction (y–direction), where there is no excitation and the width of the pile cap is C, the boundaries were set at a distance of 2C. The height of the model was taken equal to 1.5 L, where L = 20 m, the length of the piles of the conventional foundation. Despite the piles being shorter in the case of the unconnected foundation, the height of the model is kept equal in all cases. This ensures that all models have the same soil amplification. In addition, to reduce the computational cost and given the symmetry of the system, only half of it was modeled. In the plane of symmetry, the movement in the y–direction was restricted. For the further reduction of the computational cost, the soil was modeled as an "internal soil", with an area 3B χ 1.5C and dense mesh, and an "external soil" area with elements of greater size. Using data from the literature as well as a few sensitivity analyses, the optimal size of the elements for each area was decided in order to both accurately predict the behavior of the system and reduce the total amount of elements. All these features are shown in **Figure 2.4** for the case of the conventionally designed pile group.

The boundary conditions at the base of the model restricted the movements in all three directions, except in the cases of earthquake loading, where acceleration was applied in the x–direction. Furthermore, the nodes on the two opposite boundaries of the model in the direction of earthquake loading with the same y and z coordinates, were rigidly connected together in order to simulate the actual soil behavior as well as the behavior of a laminar box.

2.2 Soil Constitutive Model

In this study the nonlinear soil behavior is described by the simplified constitutive model developed by Anastasopoulos et al. (2011), which is able to accurately model saturated clay's behavior, in the problem of interest. According to it, soil's elastoplastic response follows Von Mises failure criterion combined with nonlinear kinematic hardening and an associated flow rule.

The evolution of stresses is defined as:

$$\sigma = \sigma_0 + \alpha \tag{2.1}$$

where σ_0 is the stress at zero plastic strain and α is the "backstress", which describes the kinematic evolution of the yield surface in the stress space. The yield surface is defined by a function F:

$$F = f(\sigma - \alpha) - \sigma_0 \tag{2.2}$$

where $f(\sigma - \alpha)$ is the equivalent Mises stress with respect to the backstress α. Since an associated plastic flow rule is used, the plastic flow rate is given by:

$$\dot{\varepsilon}^{pl} = \dot{\bar{\varepsilon}}^{pl} \frac{\partial F}{\partial \sigma} \tag{2.3}$$

where $\dot{\bar{\varepsilon}}^{pl}$ is the equivalent plastic strain rate.

The evolution of stress is composed by two components:

1. An isotropic hardening component, which describes the change in the equivalent stress σ_0, defining the size of the yield surface as a function of the equivalent plastic strain $\bar{\varepsilon}^{pl}$:

$$\sigma_0 = \sigma_0 + Q_\infty(1 - e^{-b\bar{\varepsilon}^{pl}}) \tag{2.4}$$

   where Q_∞ and b are model parameters, defining the maximum change of the size and the rate of change of the yield surface respectively. For $Q_\infty = 0$ the size of the yield surface remains constant and the isotropic hardening component is eliminated.

2. A nonlinear kinematic hardening component, defined by a superposition of a purely kinematic term and a relaxation term that introduces the nonlinear behavior. This component describes the translation of the yield surface in the stress space by the equation:

$$\dot{\alpha} = C\frac{1}{\sigma_0}(\sigma - \alpha)\dot{\bar{\varepsilon}}^{pl} - \gamma\alpha\dot{\bar{\varepsilon}}^{pl} \tag{2.5}$$

   where C is the kinematic hardening modulus ($C = \sigma_y e_y = E = 2(1+\nu)G_0$) and γ is a parameter that determines the rate that kinematic hardening decreases with increasing plastic deformation.

The two hardening components, for unidirectional and multiaxial loading, are shown in **Figure 2.5 (a)** and **(b)** respectively**.** From the evolution law that governs the kinematic hardening component, the backstress α must be contained within a cylinder of radius $\sqrt{2/3}\,{}^{C}/_{\gamma}$. Given the bounded yield surface, all stress points lie within a cylinder of radius $\sqrt{2/3}\sigma_y$, where σ_y is the maximum yield stress. At large plastic strains, that σ approaches σ_y, the magnitude of α becomes equal to $\alpha_s = {}^{C}/_{\gamma}$ and $(\sigma - \alpha)$ tends to σ_0, hence, $\dot{\alpha}$ tends to zero. Combining those and equation (2.5), the maximum yield stress can be defined as:

$$\sigma_y = \sigma_0 + \frac{C}{\gamma} \tag{2.6}$$

For the case of saturated clays, studied in the present thesis, the ultimate yield stress is given by:

$$\sigma_y = \sqrt{3} S_u \tag{2.7}$$

From (2.6) and (2.7) γ can be calculated by:

$$\gamma = \frac{C}{\sqrt{3} S_u - \sigma_0} \tag{2.8}$$

The model was calibrated using: (1) The undrained shear soil strength, Su; (2) The small strain stiffness, E_0; and (3) the G – γ curves of Vucetic & Dorby (1991).

Figures of Chapter 2

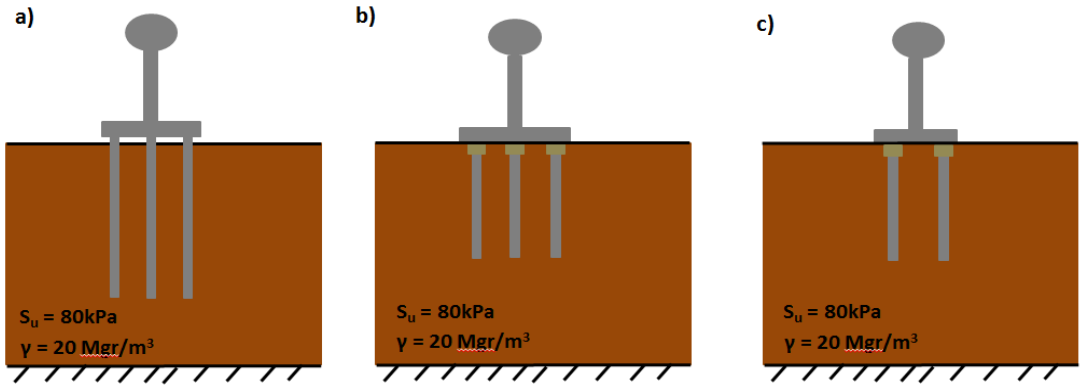

Fig. 2.1: Sketches of the three studied systems (a) Conventional pile foundation (b) unconnected pile foundation, according to current code's factors of safety (c) rocking foundation on top of unconnected piles.

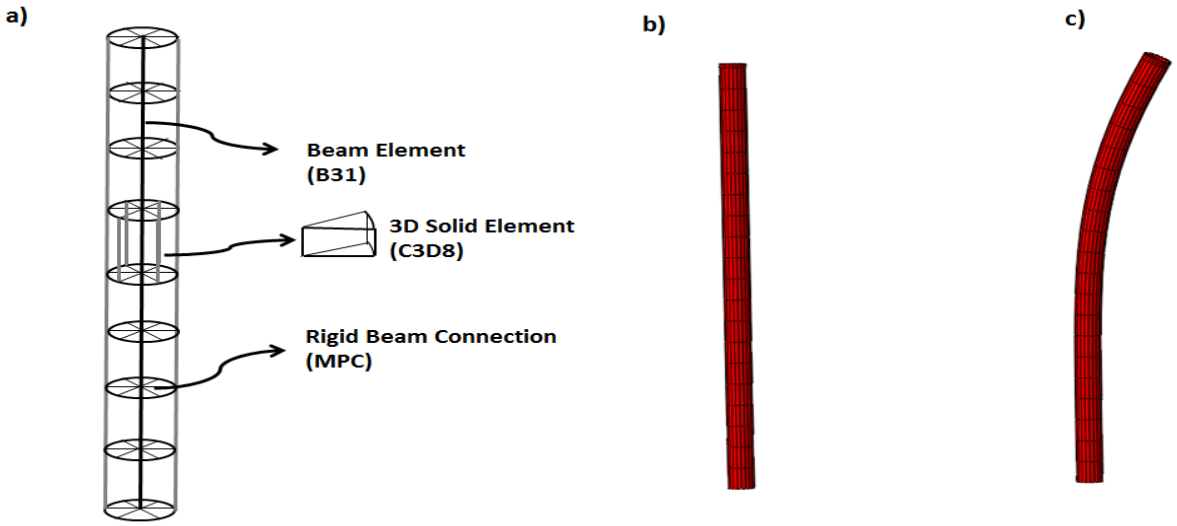

Fig. 2.2: (a) Schematic illustration of piles' simulation with beam elements, solid elements and rigid links (b) undeformed and (c) deformed shape of the pile.

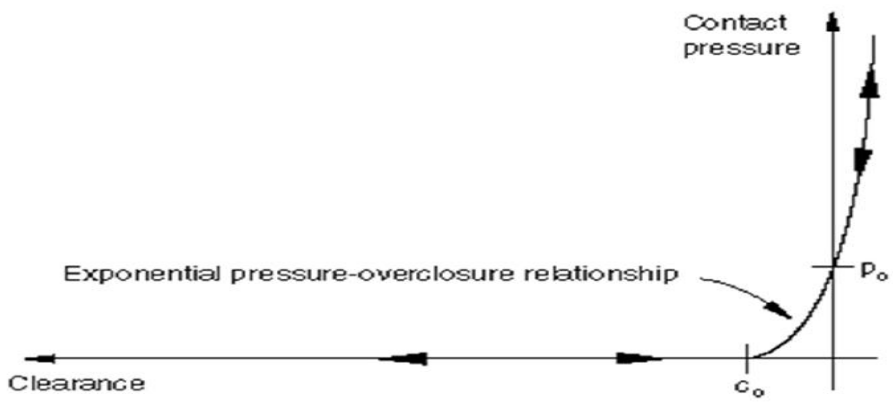

Fig. 2.3: Exponential pressure–overclosure relationship of the soil–pile cap and soil–pile interfaces.

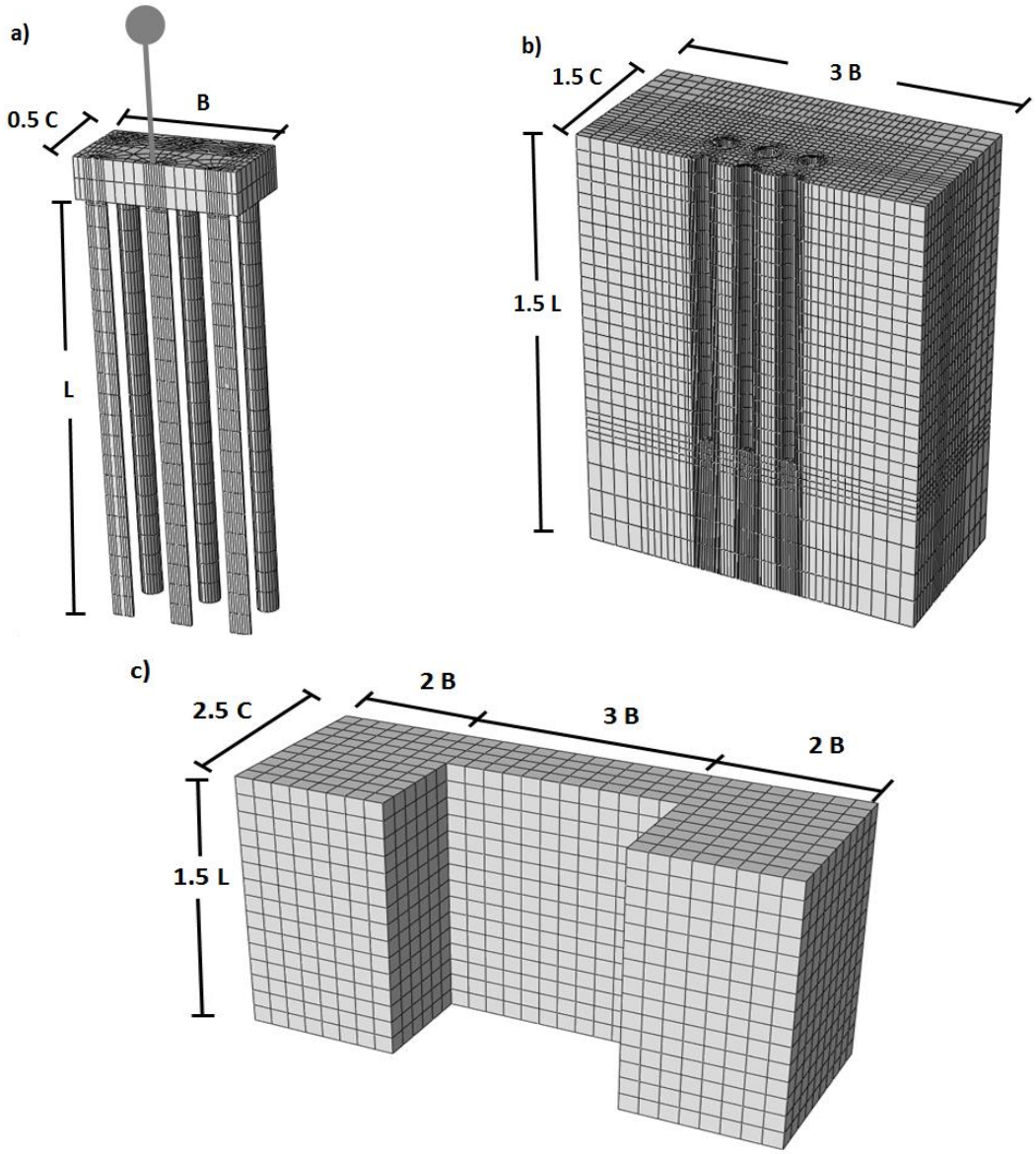

Fig. 2.4: Parts, in different scales, of the three-dimensional finite element model on Abaqus (a) Conventional foundation with connected piles (b) “internal soil” (c) “external soil”.

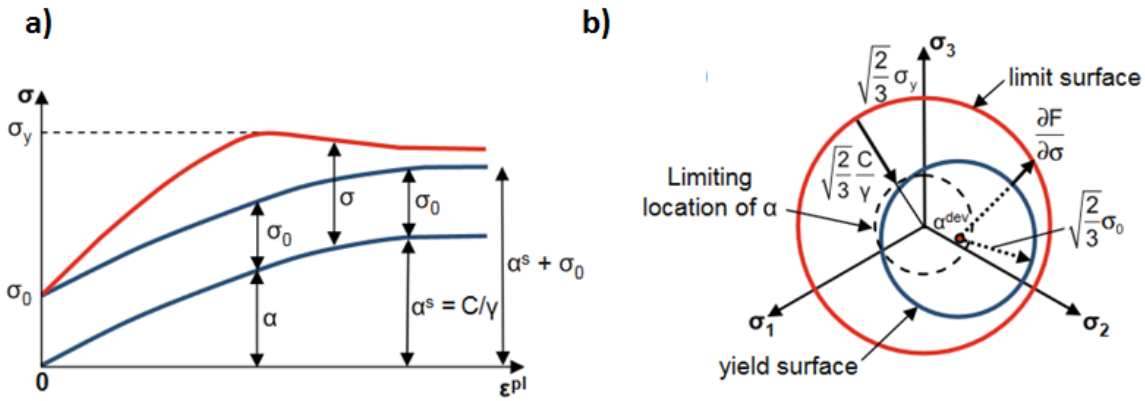

Fig. 2.5: Simplified constitutive model (a) one–dimensional representation of the hardening components (b) three–dimensional representation of hardening in the nonlinear model. (by Anastasopoulos et al. 2011)

CHAPTER 3

Conventional System Design

3.1 Problem Statement

The dynamic response of bridge piers founded on three different foundation systems will be examined in the following chapters. The first system is a conventionally designed pile group, according to the current seismic codes. The second one is also designed using the codes' philosophy, with a capacity design leading to the failure of the superstructure, but this time the piles are not connected on the pile cap and there is a soil layer between them. The third is also a foundation with unconnected piles designed according to the Rocking Isolation philosophy, where the moment capacity of the foundation is smaller than that of the bridge pier. To compare the three systems push–over analyses and real earthquake timehistories are used.

Two bridge piers with characteristics of typical motorway bridges were tested. Both of them had a circular cross section with diameters D_{pier} = 2.0 m and supported a deck mass m_{deck} = 500Mgr. In order to understand the effects of slenderness on the response of structures supported on unconnected pile foundations, especially in the case that the foundation is designed according to the new philosophy, two piers were analyzed, a short one, h = 5.0 m, and a tall one, h = 12.5 m. In both cases the deck mass was assumed to be 1.5 m above the pier top. Sketches of the piers are shown in **Figure 3.1** for the case of the conventional pile foundation.

In all cases, the piers were founded on a homogenous saturated clay, with undrained strength S_u = 80 kPa, density ρ = 2.0 Mgr/m^3 and a small–strain modulus of elasticity $E_0 = 1200S_u$.

The design and analysis of the short pier are presented first, while the presentation of the tall pier follows in later chapters.

3.2 Design of the Short Pier

3.2.1 Design of the Superstructure

Concrete C45/55 and steel reinforcement S400 was used for the bridge pier, designed according to Eurocode 8 (EC8) and the Greek Seismic Code (EAK 2000). The elastic spectrum of the EC8 is shown in **Figure 3.2**. The soil class in the studied problem is B, the structure is assumed to be in Seismic Zone II, with a peak ground acceleration a_{gR} = 0.24 (g), and the importance factor of the bridge is 1.3. The behavior coefficient (q factor) is taken equal to 3. The design response spectrum is also shown in the figure.

As already stated, the bridge pier is assumed to be a single degree of freedom oscillator with its mass concentrated on top, so its stiffness and fixed base period are:

$$k = \frac{3EI_{eff}}{h^3} \tag{3.1}$$

$$T_F = 2\pi\sqrt{\frac{m}{k}} \tag{3.2}$$

where effective moment of inertia, I_{eff}, is taken as 50% of the pier's geometric value ($I = \frac{\pi D^4}{64}$) due to cracking and the mass, m, is assumed to be the deck mass m_d = 500 Mgr and 50% of the pier's mass m_{pier} = 39 Mgr, which is negligible. The height was taken equal to h = 5.0 + 1.5 = 6.5 m, since the deck mass is 1.5 m above the pier's top. So, T_F = 0.36 (s).

The fundamental period of the system, accounting for soil–structure interaction, was calculated as:

$$T_{SSI} = T_F\sqrt{1 + \frac{k}{k_H} + \frac{k}{k_R}h^2} \tag{3.3}$$

where k_h and k_R the horizontal and rotational stiffness of the foundation respectively (**Figure 3.3 (a)**). The horizontal loading of the pile leads to large shear strain at the soil surface continuously reducing until the critical length of the pile, where they are zero. Hence, to calculate the horizontal stiffness of the piles, the soil was assumed to have a linearly increasing modulus of elasticity, since it is dependent on the magnitude of the shear strain (**Figure 3.3 (b)**). The following equations were used:

$$L_c = 1.5d\left(\frac{E_p}{E_S{}^*}\right)^{0.22} \tag{3.4}$$

$$E_S{}^* = \frac{E_0}{L_c}d \tag{3.5}$$

$$k_H = 0.6E_S{}^*d\left(\frac{E_p}{E_S{}^*}\right)^{0.35} \tag{3.6}$$

where L_c the critical length of the pile, d the pile's diameter, E_p pile's modulus of elasticity and $E_S{}^*$ soil's modulus of elasticity at depth equal to pile's diameter.

The rotation of the pile cap induces significantly smaller shear strains to the soil and so the assumption that the soil is homogeneous with constant modulus of elasticity, equal to E_0, is valid. The rotational stiffness of the pile group is calculated as the sum of the axial stiffness of the peripheral piles and their bending stiffness, as shown in **Figure 3.3 (c)**. Where the axial and bending stiffness of each pile are given by equations (3.7) and (3.8) respectively:

$$k_v = \frac{2\pi LG}{\ln\left(\frac{4L}{d}\right)} \tag{3.7}$$

$$k_M = 0.15E_sd^3\left(\frac{E_p}{E_s}\right)^{0.75} \tag{3.8}$$

So:

$$k_R = \sum x_i{}^2k_v + 9Km \tag{3.9}$$

where L is the length of the pile, G is soil's shear modulus and x_i is the distance each pile, in from the center of the pile cap the direction of loading.

From this analysis T_{SSI} was found equal to 0.56 s and so the design acceleration $S_d = \frac{S_{el}}{q} = 0.24(g)$. Consequently, the loads applied on the pier according to EC8 are shown in **Figure 3.4**.

To find the required longitudinal reinforcement it was taken into account that:

- The pier should withstand the combination of the axial force and the bending moment shown in **Figure 3.4**
- According to EC8, the area of the reinforcement should be at least 1% of the area of the pier

So, 40Φ32 (320cm^2) are required, which for the applied axial force, lead to a design moment capacity M_{Rd}=12200 kNm.

The transverse reinforcement is calculated according to the capacity design specifications, which state that the shear capacity of the pier should be 1.4 times greater than its moment capacity, in order to avoid shear failure, which is bristle as opposed to the ductile bending failure. So, the required shear capacity is:

$$V_{CD} = 1.4\frac{(M_{R,1}+M_{R,2})}{h} \quad (3.10)$$

where h is the height of the pier, $M_{R,1}$ and $M_{R,2}$ is the moment capacity of each of the two ends of the pier. Of course, since this is designed as a cantilever pier, $M_{R,2} = 0$. In addition it was verified that the transverse reinforcement satisfies the confinement requirements and bars of diameter d_{bw} = 12 mm with 8 mm spacing were used.

In **Figure 3.5** the cross section and the Moment–Curvature diagram, computed with USC_RC software, of the pier are shown. It is noted that for the Moment–Curvature relationship no material safety factors were used in order for it to describe the real behavior of the pier and not the design one.

3.2.2 Design of the Conventional Pile Group

The conventionally designed pile group, which satisfies the requirements of EC8, should:

- Have a vertical factor of safety, FS_v, greater than 2
- Follow the capacity design principle that states that the ratio of the moment capacity of the foundation to that of the pier should be equal or greater to 1.4

In all the studied cases the height of the pile cap was selected equal to h_{pc} = 2.0 m, in order for it to behave as a rigid body. For the conventional pile group, a total of n = 9

piles of diameter d = 1.0 m were selected. The distance between the piles was selected equal to $S = 3d = 3.0\ m$ and the distance between the perimeter of the outer piles and the edge of the pile cap equal to 0.5 m (d/2). The width and the length of the pile cap were found equal to 8.0 m. The final length of the piles was selected from an iterative procedure in order to satisfy the specifications mentioned earlier.

The vertical capacity of each pile was calculated as the sum of its base and shaft resistance:

$$Q_{ult} = Q_b + Q_s = N_c S_u A_b + L\pi d(aS_u) \tag{3.11}$$

where $N_c = 9$ according to Meyerhof, A_b the area of the pile's cross section, L the length of the pile, d the diameter of the pile, and aS_u is the shaft friction that can be developed along the perimeter of the pile, according to Tomlinson (1971). The reductive coefficient a depends on the undrained shear strength, S_u, as shown in **Figure 3.6**.

To calculate the ultimate capacity of the pile group an interaction coefficient is introduced, since due to pile–to–pile interaction there is a reduction of the developed shaft resistance. Given that the distance between the piles is $S = 3d$ this coefficient, E_f, is taken equal to 0.7. Additionally, instead of a single vertical factor of safety, FS_V =2, two distinct ones are applied. The first one, $\gamma_b = 2$, is applied on the base resistance, and the second one, $\gamma_s = 2.5$, is applied on the shaft resistance. Accordingly, the ultimate vertical capacity of the pile group is given by:

$$Q_{PG} = 9\left[\frac{N_c S_u A_b}{\gamma_b} + E_f \frac{L\pi d(aS_u)}{\gamma_s}\right] \tag{3.12}$$

, which should be larger than the applied vertical load.

The loads transmitted to the foundation by each component of the system are given in **Table 3.1**. It is clarified that the acceleration of the deck is taken equal to the design spectral acceleration, while the acceleration of the pile cap equal to the design peak ground acceleration. The acceleration of the pier is taken as the average of the two.

The vertical load is equally divided on the nine piles due to the rigidity of the pile cap. The moment is received as axial load of the peripheral piles while the central ones remain unloaded. Hence, the axial load of each pile due to the combination of the vertical loads and moments are given:

$$Q_i = \frac{N_{Ed}}{9} \pm \frac{M_{Ed} x_i}{\sum {x_i}^2} \tag{3.13}$$

where x_i is the distance of each pile from the center of the pile cap in the direction of loading, N_{Ed} and M_{Ed} the design vertical force and moment on the pile group respectively. M_{Ed} is not the value given in **Table 3.1**, but the one that results from

the capacity design of the foundation. The acting loads on the foundation and its design loads are shown in **Figure 3.7**. In order for the foundation to be able to withstand the combination of the design loads the following equations should hold true in case of pile compression and tension respectively:

$$Q_i < Q_b + Q_s \tag{3.14}$$

$$Q_i < Q_s \tag{3.15}$$

Table 3.1: Foundation's static and seismic loading from each component of the system.

	DECK	PIER	PILE CAP	SUM
m (Mgr)	500	39	320	859
N (kN)	5000	390	3200	8590
V (kN)	1200	95	789	2084
M (kNm)	10200	428	1578	12206

In order to satisfy the above specification the length of the piles was selected to be 20.0 m, as shown in **Figure 3.8**. In this case, of the short pier, the vertical loading was found to be the critical parameter for the design.

3.2.3 Ductility Capacity

The plastic design of structures demands that their structural elements are able to sufficiently deform in their plastic region before they collapse. This characteristic is called ductility capacity and is given, in terms of curvature, by:

$$\mu_k = \frac{k_{collapse}}{k_y} \tag{3.14}$$

where $k_{collapse}$ is the curvature at which collapse is unavoidable and k_y is the yield curvature. In order to compare the conventionally designed system with the ones proposed in this thesis, both ductility capacity and ductility demand, for a given earthquake, will be key parameters.

In this conventionally designed system, plastic deformations should only developed on the superstructure and so the capacity demand requirements are satisfied by proper confinement of the concrete, as stated by EC8. In terms of curvature, the ductility capacity of the pier is found from the moment–curvature diagram and is equal to 8.30.

The displacement ductility capacity of the system was computed equal to 3.70 according to the following procedure (Priestley et al. 1996):

$$\mu_\Delta = \frac{M_u}{M_n} + 3(\mu_r - 1)\frac{L_p}{h}(1 - 0.5\frac{L_p}{h}) \tag{3.15}$$

where M_u and M_n is the ultimate and the yield bending moment pier's base cross section, h the high for the pier and L_p the length of the plastic hinge, which can be calculated:

$$L_p = 0.08 + 0.022 f_{ye} d_{bl} \quad (3.16)$$

where f_{ye} the design yield strength of the longitudinal reinforcement and d_{bl} its diameter.

3.3 Static Push Over Analyses

3.3.1 Single Pile

In order to test the model of the piles that will be used in the following analyses, a single pile was first simulated on Abaqus. Horizontal and vertical push–over analyses were performed and their results were compared with the ones from analytical solutions.

Figure 3.9 shows the deformed mesh and the settlement–resistance curve for the vertical push over. The ultimate resistance of the pile was found $Q_{ult} = 3260\ kN$ and so the deviation from the analytical solution was equal to 5%. This was considered acceptable and proved the accuracy of the Finite Element model.

The deformed geometry and the force–displacement relationship of the pile under horizontal loading are presented in **Figure 3.10**. In addition the distribution of shear forces and bending moments along the piles are presented in **Figure 3.11** showing that as displacement increases the stresses on the pile also increase. In addition with increasing displacement the depth of the maximum positive moment increases.

3.3.2 Full Model

Vertical Push Over

After it was verified that the single pile model works well, the whole system was simulated on Abaqus. Vertical push over analysis was employed to find the vertical factor of safety and compare it with the analytically calculated one. It is noted here that in the simulation there is a 20 cm gap between the pile cap and the soil in order to simulate the actual response of a pile group. The settlement–resistance curve of the model, along with the deformed mesh, is shown in **Figure 3.12**. It is interesting to note that while the pile group reaches its capacity and a plateau appears at about 25000 kN, there is a sudden increase in stiffness when the settlement approaches 20cm. This happens when the pile cap touches the soil and starts providing resistance. However, this settlement is unrealistically large and the resistance of the pile cap is not considered in the ultimate bearing capacity of the system. The ultimate capacity of the pile group is $Q_{PG} = 28427\ kN$. As it was expected, this value is less than $9Q_{ult} = 29340\ kN$, where Q_{ult} the capacity of each pile, due to pile–soil–pile interaction but the interaction coefficient, E_f, used for the designed

proved to be quite conservative. The vertical factor of safety is equal to $F_{SV} = 3.31$, which satisfied the code requirements.

Figure 3.13 shows the axial load–settlement curve of the piles. It can be seen that when the settlements are small, the outer row of piles (1, 2, 3) have greater stiffness than the inner row (4, 5, 6). This is due to interaction between the piles. Because the piles of the inner row have more neighboring piles, they have more induced settlement for a given load. Hence, for a given settlement, their reaction is smaller. For the same reason the stiffness of the central pile of each row is smaller than that of the other two piles. On the contrary, piles 4, 5 and 6 have greater bearing capacity than piles 1, 2 and 3. This can be explained from the restriction of the volumetric deformation and the outward movement of the soil, induced by the loading of a pile, provided by the surrounding piles. Consequently, piles 4, 5 and 6 are located in enhanced soil and their bearing capacity is increased.

The axial load distributions along the piles are shown in **Figure 3.14 (a) and (b)** for settlements 3 cm and 18 cm respectively. As expected, from the preceding analysis, piles 1 and 3 develop greater axial loads than the rest of the piles, while pile 5 has the smallest one for the case that the response of the piles is almost elastic (w = 3 cm). Interestingly, the compression of pile 5 increases with depth taking its maximum value at z = 7 m. This can be explained from the negative skin friction induced to pile 5 from the neighboring piles due to the settlement of the surrounding soil. At settlement w = 18 cm the piles have reached their capacity and it can be seen that piles 4, 5 and 6 have greater axial load than piles 1, 2 and 3. In addition, since the shaft friction has reached its ultimate value, aS_u, the compression of the piles linearly decreases with depth. However, in the latter case, the differences between the loads of the piles are not as great as in the first case, proving that pile-to-pile interaction is more prominent when the piles respond elastically.

Horizontal Push Over

For the horizontal push over analysis horizontal displacement was applied on the top of the pier, which was simulated as a rigid element. P–δ effects were taken into account. The deformed mesh and the developed plastic deformations are shown in **Figure 3.15** and the horizontal force–deck displacement and moment–rotation curves of the foundation are shown in **Figure 3.16**. The deck displacement is the sum of the horizontal displacement of the pile cap and the displacement at the deck due to the rotation of the pile cap, which is equal to hθ. From the graphs it can be concluded that when the pier reaches its moment capacity, corresponding to a shear force equal to 1877 kN, the response of the foundation remains approximately elastic. In this case, of piles being elastic elements, the applied load reaches extremely large values. Its actual limit is determined by the failure of the piles. A sudden increase of foundation stiffness, which was also observed in the vertical push over analysis, steams from the fact that at some point the pile cap reaches the soil and provides additional resistance. **Figure 3.17** shows the settlement–rotation curve, which shows a sinking response despite the large vertical factor of safety.

Figure 3.18 (a) shows the shear force–displacement relationship of all the piles. The shear forces on the front piles (3 and 6) are greater than on the rest of the piles. Respectively, piles 2 and 5 have greater shear forces than piles 1 and 4. This pile–to–pile interaction that causes the front piles to receive greater loads than the rear piles is related to the distance between the piles and is called *shadow effect*. This effect is especially important on pile 4, which reaches an ultimate shear force that remains constant for increasing displacement. The shadow effects can be seen from the distribution of soil stresses in the direction of loading (**Figure 3.18 (b)**). The distribution of shear forces and bending moments along the depth of the piles are shown in **Figure 3.19** for displacements of the pile heads equal to 3.6 cm and 6.5 cm, which correspond to displacements of the pier top equal to 10 and 20 cm respectively. The interaction between the piles is again obvious. The front piles (3 and 6) develop greater shear forces and bending moments compared to the rest. This is also true for the outer row of piles (1, 2 and 3) compared to the inner row (4, 5 and 6) since they have less neighboring piles and so the shadow effects are not so important on them. The shear force on the front piles takes its maximum negative value higher than on the rest of the piles. This is explained from the higher soil reactions acting on the front piles. From the distribution of the axial forces it is obvious that the differences between the inner and the outer rows are not so prominent. As expected piles 3 and 6 are in compression and piles 1 and 4 are in tension. Due to the highly inelastic response of the soil, pile–soil–pile interaction is not important for the axial loads, while the enhancement of the soil leads to slightly greater forces on the piles of the inner row. Moreover the shear forces and bending moments on pile heads are decreased compared to the single pile for a given displacements. This can be explained from the complete restriction of rotations at the head of the single pile, while pile cap is able to develop small rotations, which alleviates the forces and moments on the piles.

The horizontal push over analysis was repeated but this time the pier was described by the moment–curvature relationship of **Figure 3.5**. The evolution of the fundamental period of the system was extracted and is shown in **Figure 3.20**. Its initial value is equal to 0.56 s that is identical with the analytically calculated one.

Figures of Chapter 3

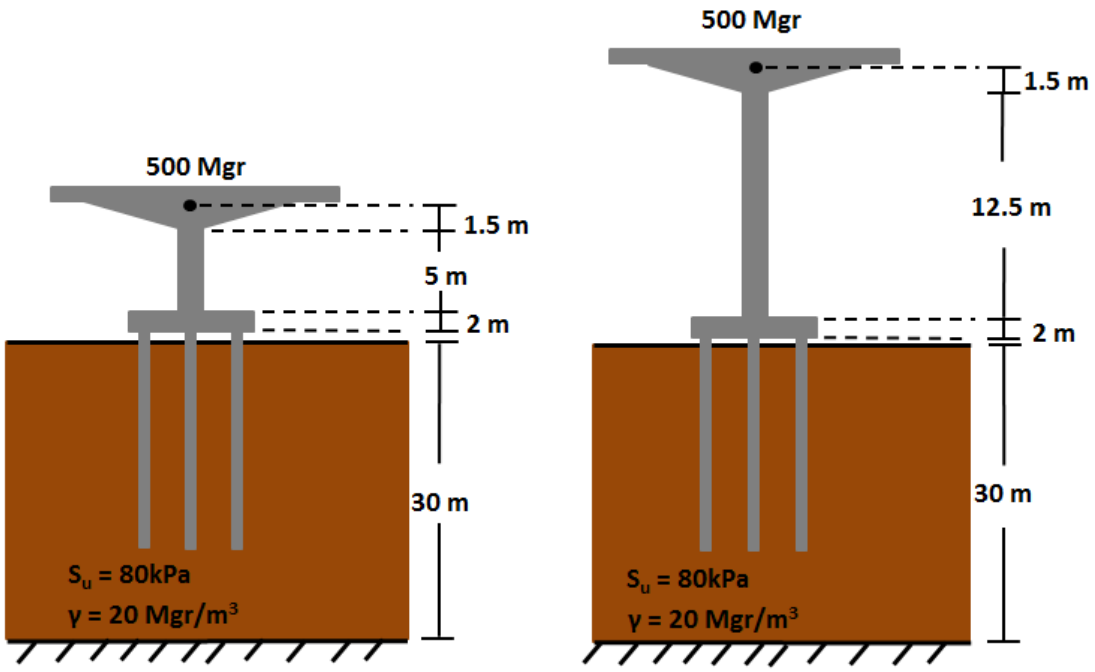

Fig. 3.1: Sketches of the two studied piers with geometric and soil properties supported on conventional pile groups.

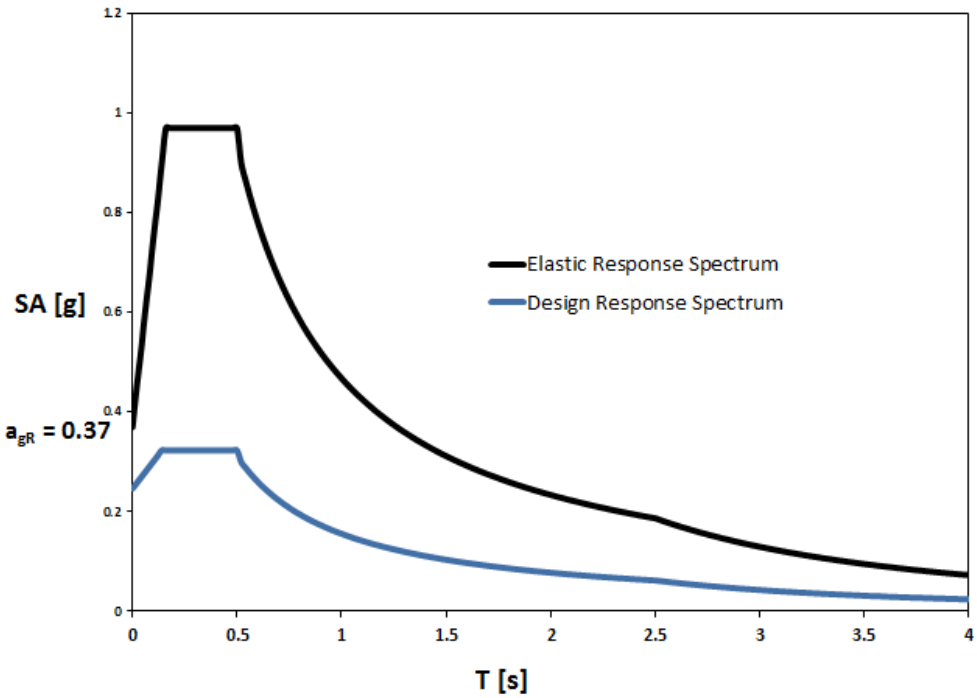

Fig. 3.2: Elastic and design response spectra according to EC8 and EAK 2000.

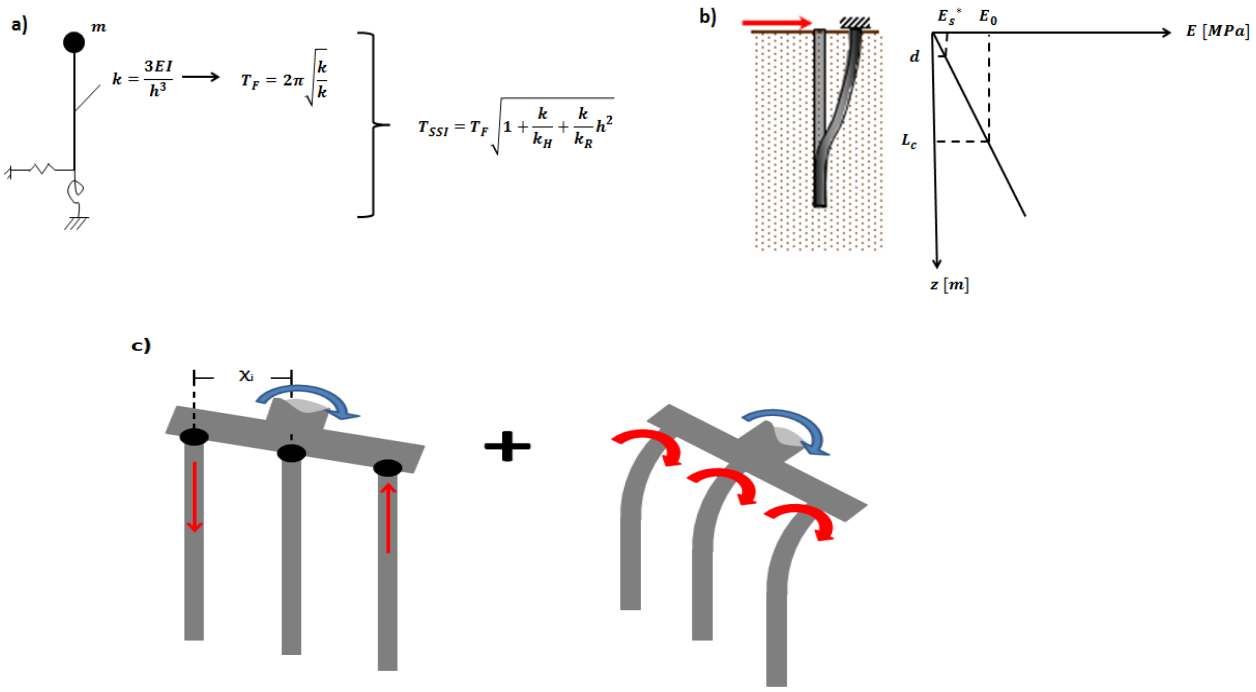

Fig. 3.3: (a) Single degree of freedom oscillator and effects of soil – structure interaction (b) soil's modulus of elasticity for horizontal loading of a pile (c) components of the rotational stiffness of a pile group.

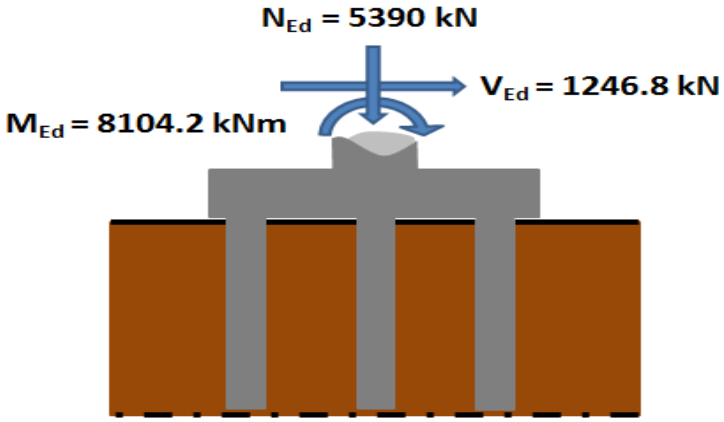

Fig. 3.4: Seismic loads on the pier base according to EC8.

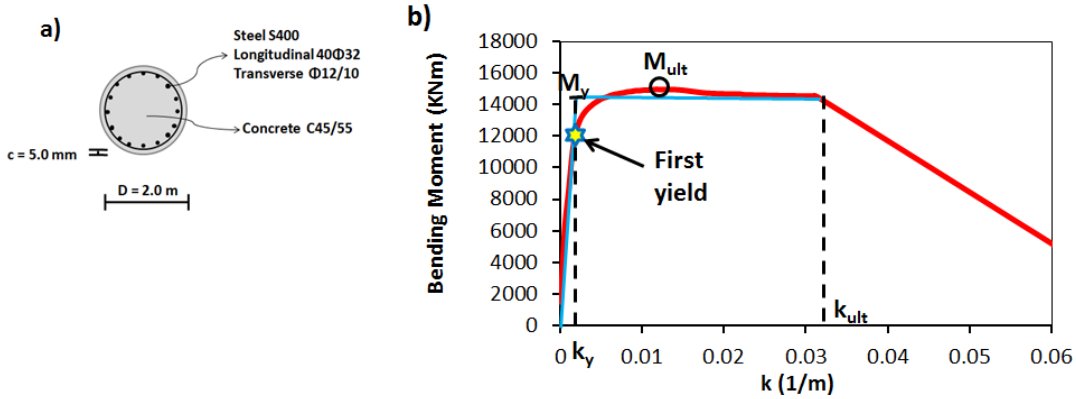

Fig. 3.5: (a) Geometry and reinforcement of the reinforced concrete sections (b) moment – curvature relationship at the pier base

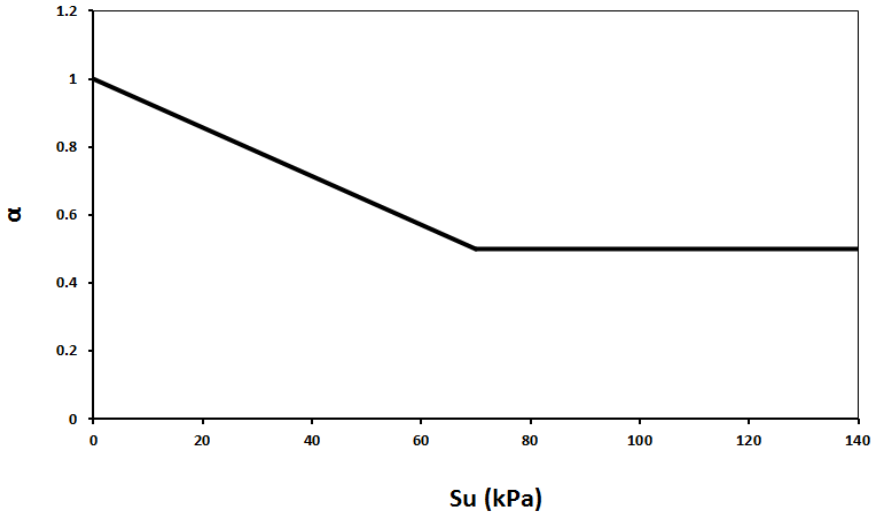

Fig. 3.6: Variation of reductive coefficient, α, of the stress developed on the shaft of the pile with the undrained shear strength. (by Semple & Ridgen 1984)

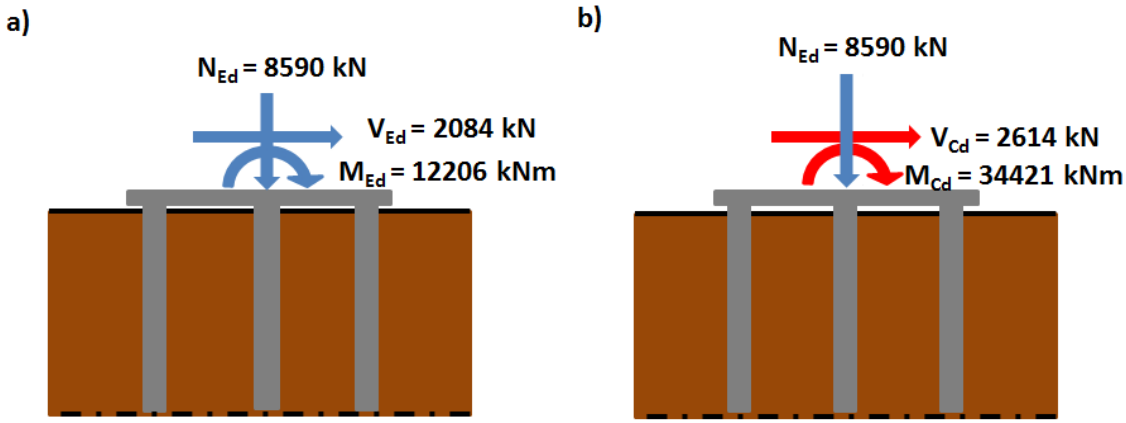

Fig. 3.7: (a) Static and seismic loads acting on the foundation level (b) Static and seismic design loads according to the capacity design.

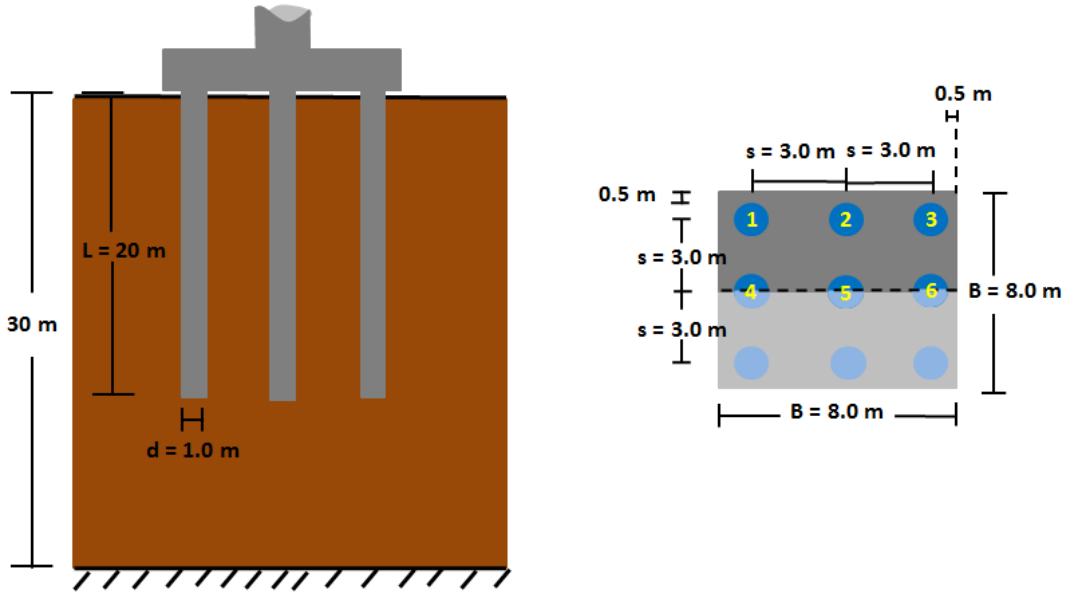

Fig. 3.8: Final configuration of the conventional pile foundation. Section and plan view.

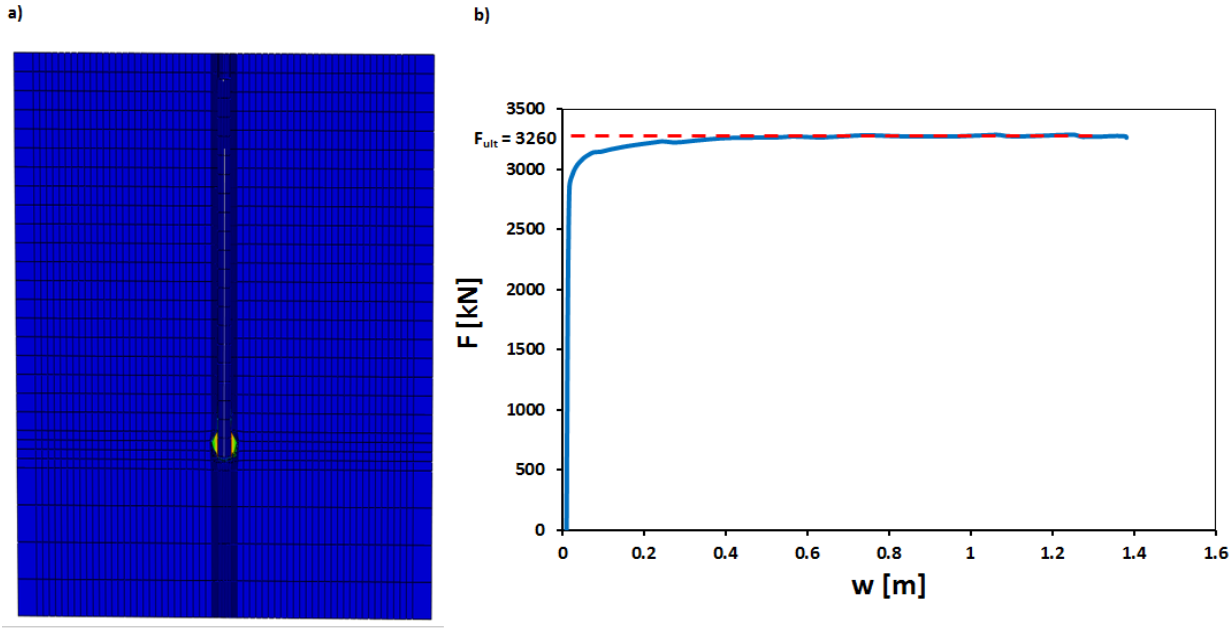

Fig. 3.9: (a) Deformed mesh with plastic strains at the base of the pile (b) force–settlement relationship of the pile.

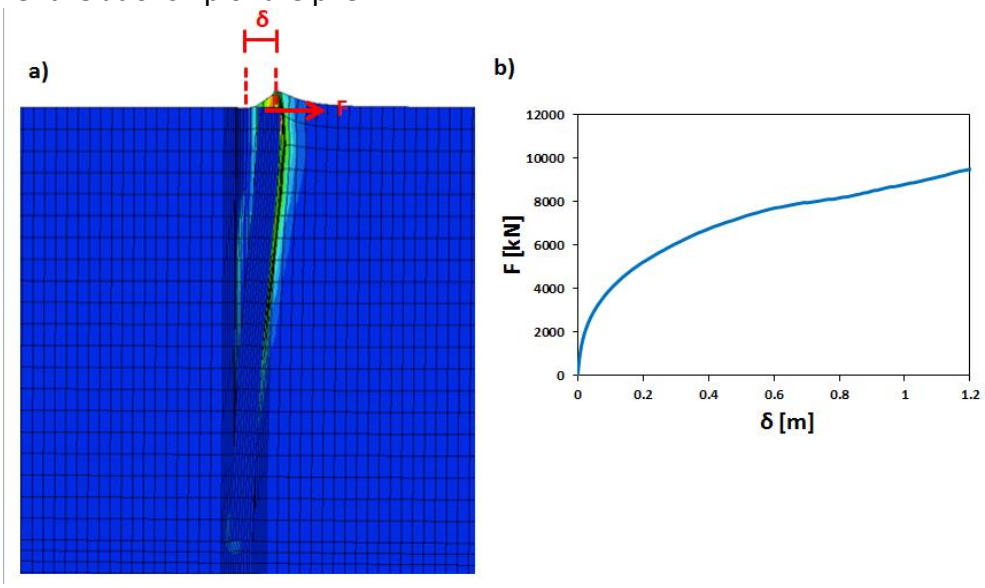

Fig. 3.10: (a) Deformed mesh with plastic strains b) force – displacement relationship of the pile.

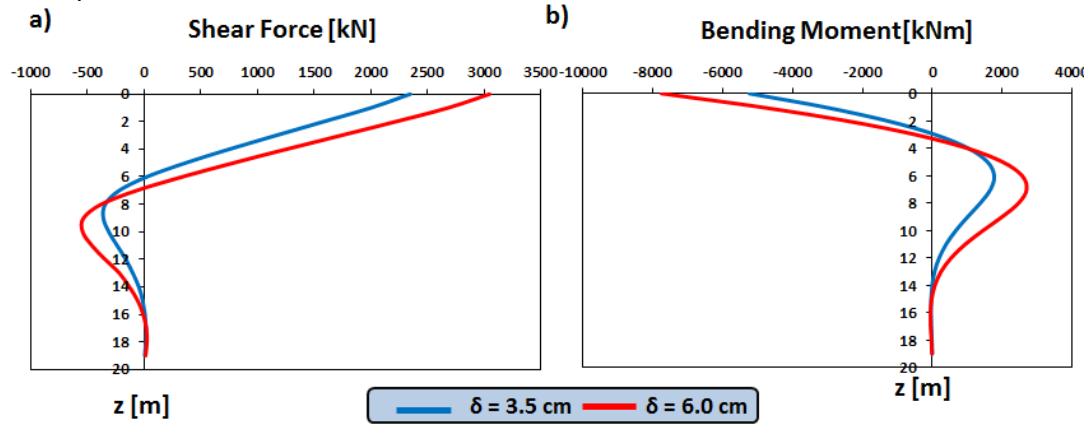

Fig. 3.11: Distribution of (a) shear forces and (b) bending moments along the pile for displacements 3.5 and 6.0 cm.

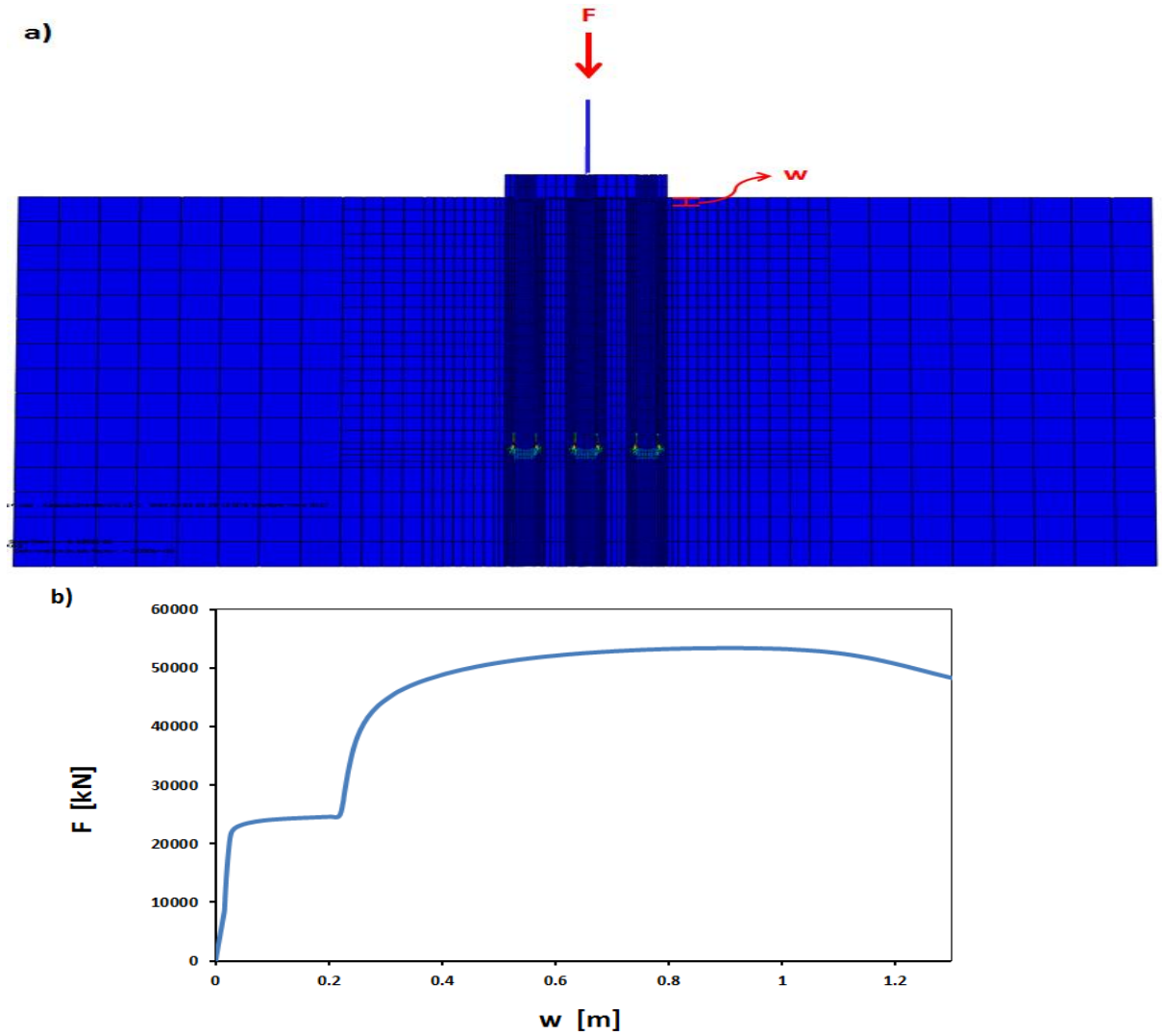

Fig. 3.12: (a) deformed mesh and plastic strains contours (b) force – settlement relationship from the vertical push-over analysis.

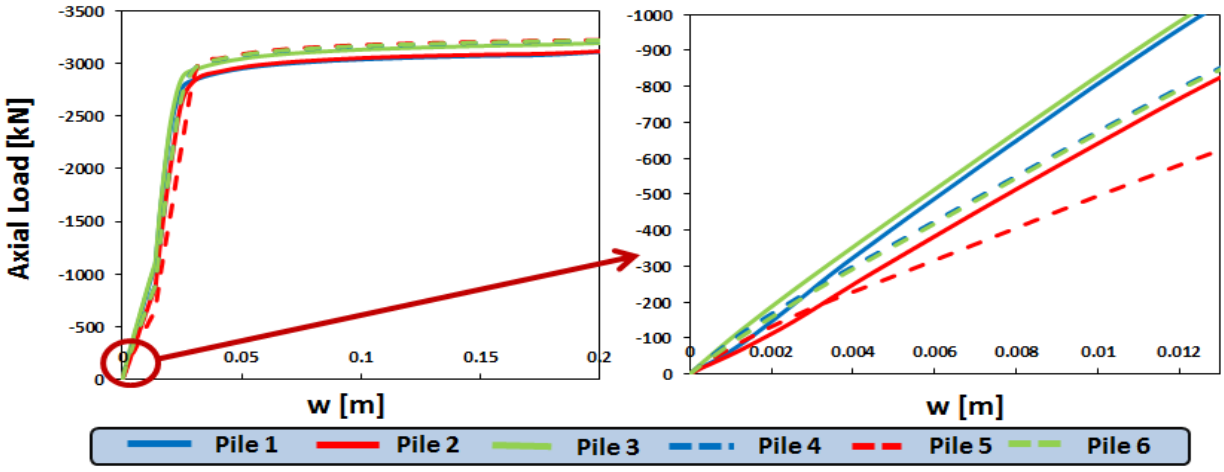

Fig. 3.13: Axial force – settlement relationship of the piles until ultimate capacity (left) and for elastic response (right).

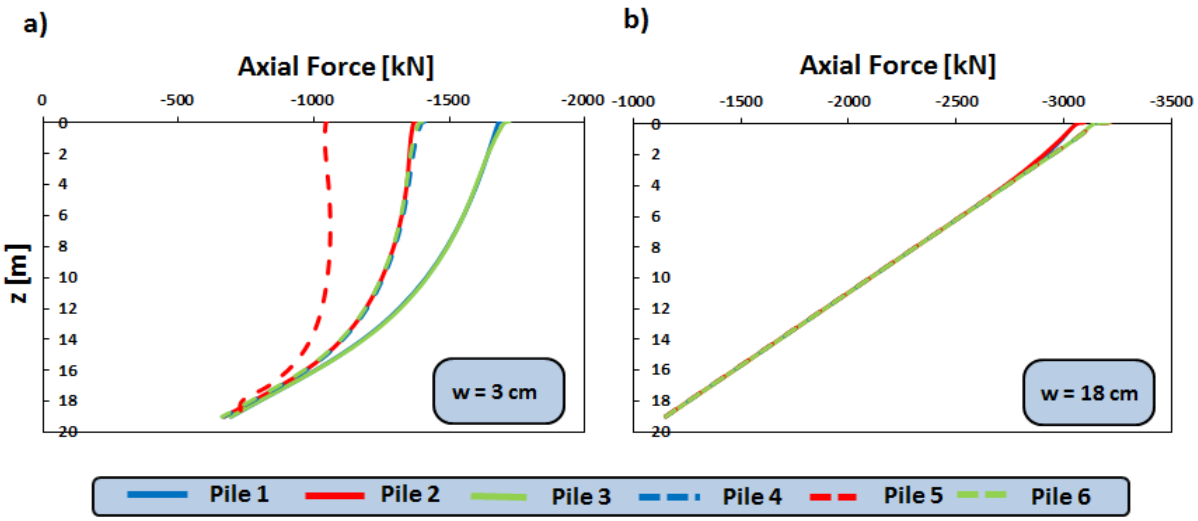

Fig. 3.14: Distribution of axial load along the piles for (a) w = 3 cm (b) w = 18 cm subjected to vertical loading

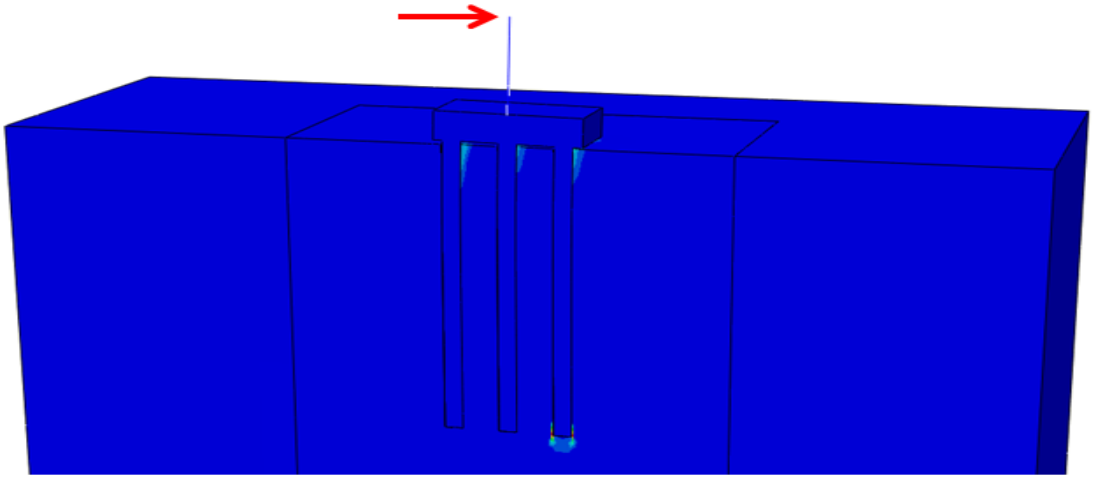

Fig. 3.15: Deformed mesh and plastic deformation for horizontal loading.

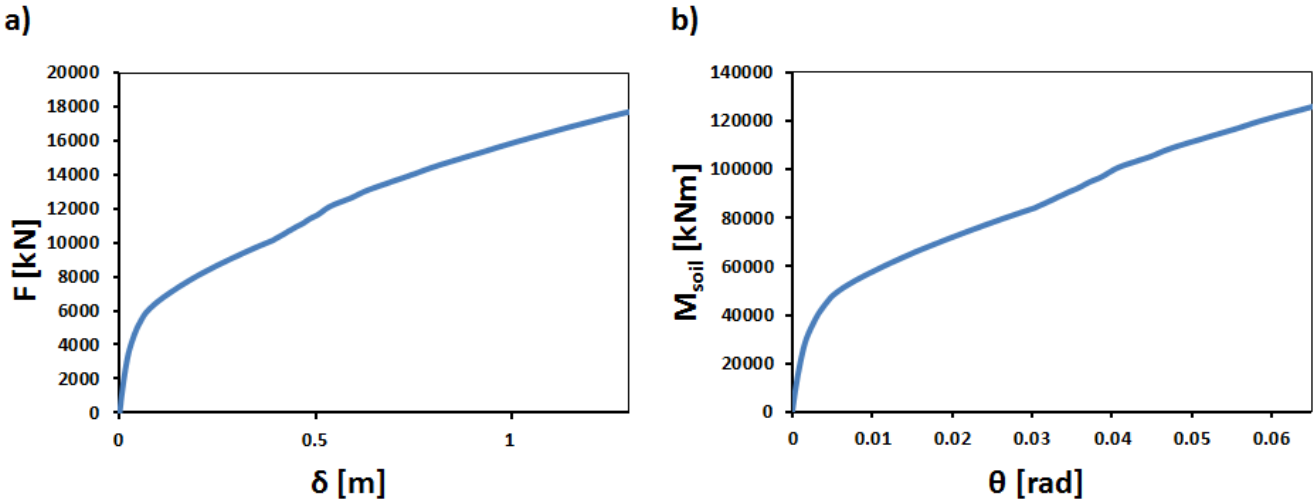

Fig. 3.16: (a) Force – deck displacement (b) Moment transferred to the soil – rotation relationships for horizontal loading.

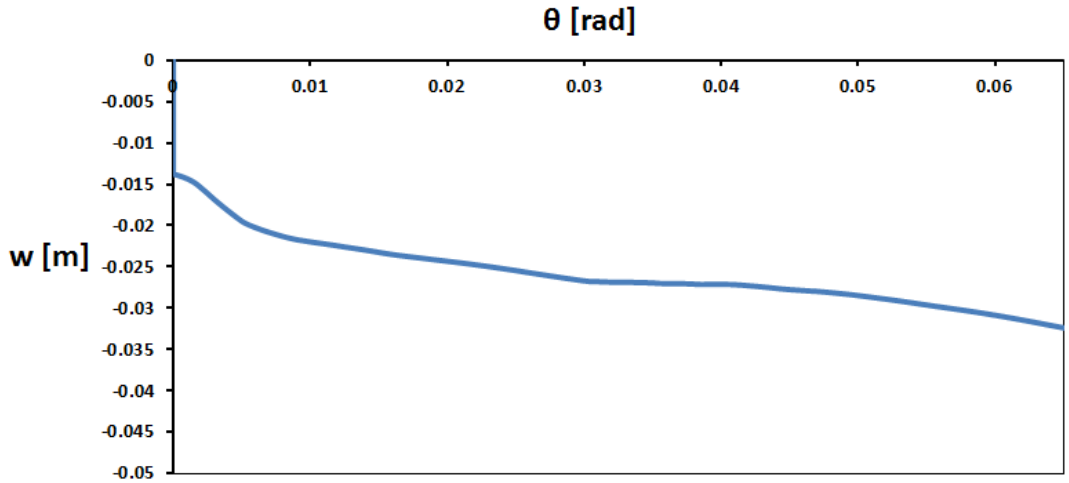

Fig. 3.17: Settlement – rotation curve showing sinking response of the foundation.

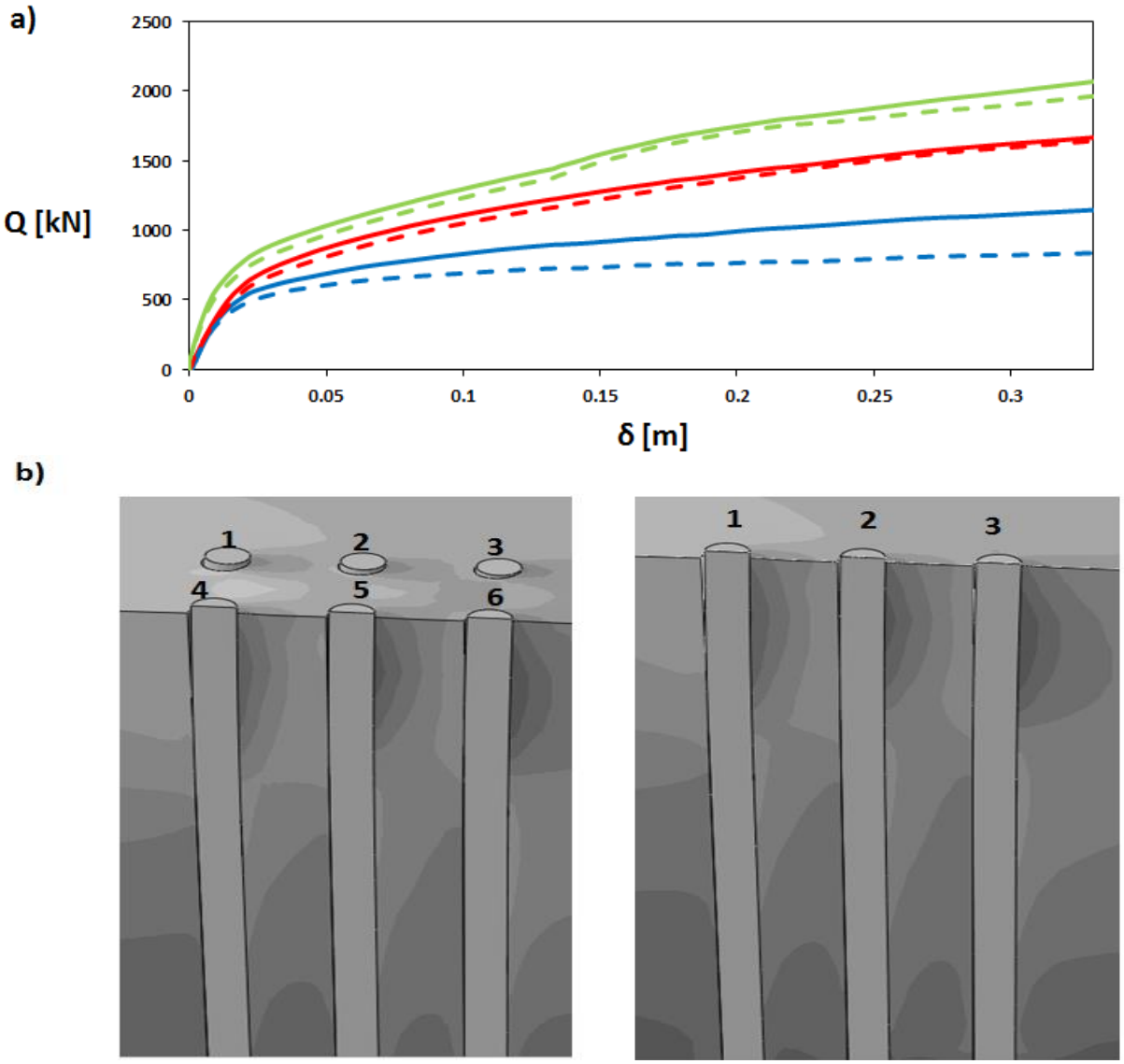

Fig. 3.18: (a) shear force–displacement relationship for the pile heads; (b) contours of stresses in the direction of loading showing the shadow effects.

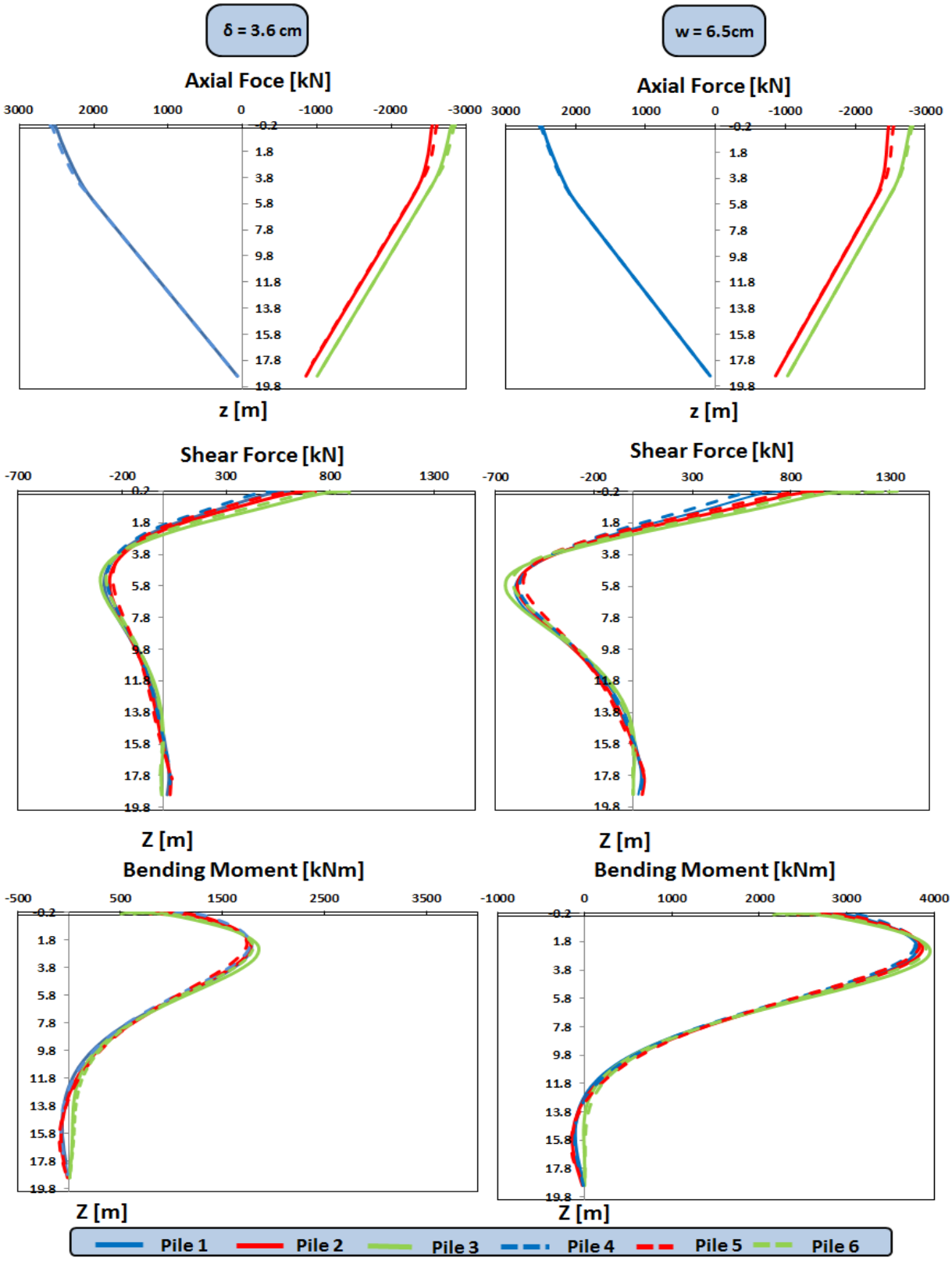

Fig. 3.19: Distribution of axial forces, shear forces and bending moments along the piles for horizontal displacements 3.6 cm and 6.5 cm at the pile heads.

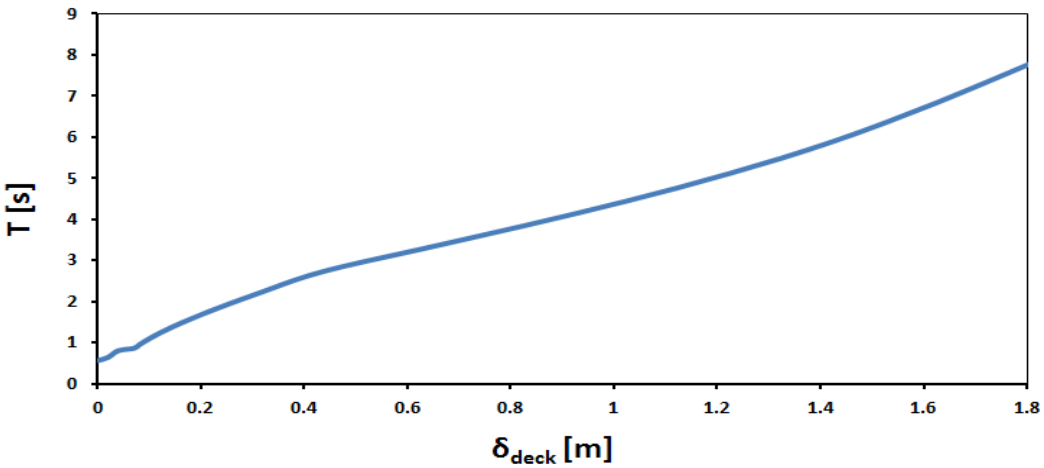

Fig. 3.20: Evolution of fundamental period with deck displacement.

CHAPTER 4

Design of Unconnected Pile Foundations

4.1 Design Process

The main objective of unconnecting the piles from the cap is to reduce their shear forces and bending moments in order to avoid failure during strong earthquakes. In addition it is believed that this can lead to reduction of the accelerations transmitted to the superstructure. In order to test this claims an unconnected pile foundation is designed, which follows the current codes' requirements. Hence, the foundation should:

- Have a vertical factor of safety, FS_V, greater than 2
- Follow the capacity design principle, which states that the ratio of the moment capacity of the foundation to that of the pier should be equal or greater to 1.4

In addition to these requirements stated by seismic codes there is a desire that the foundation has an uplifting and not a sinking response, which is mainly controlled by the vertical factor of safety. A sinking response would lead to accumulation of settlements during shaking.

No analytical tools for the design of such systems exist, so horizontal and vertical push–over analyses were used. In order to find the final design and examine the parameters affecting its response, 5 different system configurations were tested. The thickness of the layer between the piles and the cap was taken equal to α = d and d/2, where d the diameter of the piles. After it was understood how each parameter affects the response of the system, three more configurations were designed, analyzed and tested. Based on the design requirements and the results the final design was selected.

4.1.1 Push-Over Analyses

All of the five initial designs have four piles, instead of 9 that were used in the connected pile group, with distance between them $s = 4d$. Furthermore, since resistance is provided by the cap too and it was believed that the piles would not reach their capacity, the length of the piles was chosen equal to 16 m. The distance between the piles and the edge of the cap was maintained 0.5 m. The descriptions of the tested configurations and the most interesting and important results are presented below.

System 1

As shown in **Figure 4.1** in the first system there is a soil cushion of high α between the piles and the cap, but the initial soil remains the same. First a vertical push over analysis was done in order to find the vertical factor of safety and the influence of the piles. The force–settlement relationship for α = d is given in **Figure 4.2 (a)**. From that it can be concluded that the vertical factor of safety is FS_v = 2.77, which is sufficiently large. In the same graph the total axial load of the piles is shown. It is interesting to note that the piles reach a maximum load, which is significantly lower than their capacity, and then their load reduces. In **Figure 4.2 (b)** the distribution of

the axial load along the depth of pile 1 (pile 2 has exactly the same response due to symmetry) is shown. As explained by Fioravante and Giretti (2010), the relative settlement between the soil and the piles induces negative skin frictions to the piles and so its load increases until a neutral depth. The reduction of pile load with increasing settlement is observed in this graph too. In contrast the depth at which the negative skin friction stops increases with increasing settlements. The explanation is that the increased settlements lead to plastification of the soil and so the friction that leads to axial loading of the pile reduces. In addition, the increased settlements lead to relative slippage between soil and pile at greater depths. This is why the depth of the negative skin friction increases. The maximum load of the four piles is equal to 16% of the ultimate load of the system. This ratio will be called hereafter participation ratio despite the fact that the ultimate load of the piles and the system might not occur at the same displacement. For the case that the distance between the piles and the cap is α = d/2 the force–displacement curve is shown in **Figure 4.3**. Both the vertical factor of safety and the participation of the piles slightly increase to 2.87 and 19% respectively.

The horizontal force–displacement and the moment–rotation curves for the horizontal push over analyses, where the force was applied on top of the rigid pier, are shown in **Figure 4.4** for α = d. This system does not satisfy the capacity design since its moment capacity is less than $1.4M_{Rd} = 17080\ kNm$. The axial forces on the heads of the two piles are shown in **Figure 4.5** with respect to the displacement of the deck. As expected the load on pile 1 monotonically decreases due to the rotation of the pile cap. As the piles are not connected to the cap, tension force cannot be developed on pile 1. On the other hand the response of pile 2 can be divided in four different phases. At first the load of the pile increases due to the compression induced on the soil by the applied moment. However, the pile cap does not only rotate but slides as well. The sliding reduces the lever arm between the pile and the center of the pile cap and so the pile's load decreases. Despite the sliding, the loading increases again, in the third phase of the response, due to the extensive rotation of the cap which leads to greater compression of the soil and to the reduction of the vertical distance between the cap and the pile. In the last part of the loading the sliding is too large and the load is constantly reducing. A schematic illustration of this response is shown in **Figure 4.6**. The settlement–rotation curve of **Figure 4.7** shows a sinking dominated response, which is not desirable.

The response of system 1 when α = 0.5 m is shown in **Figures 4.8** and **4.09**. It can be seen that the ultimate moment capacity is slightly increased though it is still not sufficient. In addition the third phase of the pile's response has a longer duration of displacements and the load increase during that phase is greater. The settlement rotation curves shows that there is an uplifting trend after 0.1 rad of rotation. An explanation for this is that as the settlement increases the pile cap comes closer to the pile and so the resistance on it increases. This forces the center of rotation to move making the pier to uplift. This can be seen in **Figure 4.10 (a) and (b)** where the displacement vectors are shown when the response is sinking and uplifting dominated respectively.

System 2

This system is same with system 1 but this time, in order to improve the participation of the piles, improved soil is used in a square with sides equal to 1.5 m above the pile. This configuration is shown in **Figure 4.11**. The undrained shear strength and the small–strain modulus of elasticity of the improved soil are three times greater of the initial soil's. Hence, $S_u{}^* = 3S_u$ and $E_0{}^* = 3E_0$. A vertical push over analysis was done for α = d and the force–settlement relationship and the distribution of axial load along the pile for settlement equal to 5 and 75 cm are shown in **Figure 4.12**. The behavior of this system is similar with the previous one and neither the vertical factor of safety nor the participation of the piles increased.

A horizontal push over analysis was employed to understand the effect of the improved soil on this type of loading. **Figure 4.13** and **4.14** show the horizontal force –displacement, the moment–rotation and the settlement–rotation relationships of the foundations. In addition **Figure 4.15** shows the axial load on the head of each pile and the distribution of the axial load along the compressed pile. From the latter the reduction of the axial load on the pile with displacement is obvious. However, this reduction is only due to the sliding of the pile cap unlike the case of the vertical loading, where the plastification of the soil led to it. Here only the load transmitted on the pile head is diminished while the negative skin friction remains the same. The moment capacity of the foundation and the overall behavior is similar with system 1. From these two analyses it can be concluded that either the improvement of the soil on top of the pile does not improve the behavior of the system, or that the distance between the cap and the soil is too large for this improvement to be important.

In order to answer this question the system was imposed to two more analyses but this time with α = d/2. The force–settlement relationship of the vertical push over analysis is shown in **Figure 4.16**. At settlement equal to approximately 55 cm a sudden increase of stiffness and capacity appears, which is when the pile cap touches the piles and their ultimate vertical capacity is reached. This does not happen at settlement equal to 50 cm since the pile has also settled. The vertical factor of safety has significantly increased in this case to FS_v = 3.42 before the cap touches the piles or equal to 4.12 after that. The participation of the piles also increased to 38%.

From the horizontal push over analysis the horizontal force–displacement and the moment–rotation curves shown in **Figure 4.17** were extracted. In the second curve the response of system 1 for the case that α = 0.5 m is also shown for comparison. It can be seen that the ultimate moment capacity of system 2 is slightly deceased, however the response is considered improved since for smaller angles the moment is greater. System 1 reaches its capacity at an extremely large displacement of the pier. From **Figure 4.18** it can be seen that system 2 has the desired uplifting dominated response.

The last two analyses showed that the improvement of the soil above the piles can lead to the improvement of the response of an unconnected pile foundation as long as the distance between the piles and the cap is not too large.

System 3

In this configuration an improved soil layer, with $S_u{}^* = 3S_u$ and $E_0{}^* = 3E_0$, between the piles and the cap is introduced. Again the system was tested for a pile–pile cap distance equal to 0.5 and 1.0 m (**Figure 4.19**). From the vertical push–over analysis and **Figure 4.20** the significant increase of the vertical factor of safety, to FS_v = 4.87, and the participation of the piles, to 22%, are observed for α = d. From the distribution of the axial force along the piles it is seen that compared to systems 1 and 2 there is a reduction of the depth that negative skin friction develops but an increase to the load transmitted directly to the pile head. The first can be explained by the localization of stresses, and hence settlements, within the improved layer. The latter leads to the increased participation of the piles. However, the reason for the increased capacity of the system is mainly due to the improved behavior of the pile cap as a shallow foundation and not to the participation of the piles.

Figure 4.21 shows the response of the system in horizontal loading. The moment capacity is greater than in previous cases with a ratio $\frac{M_{ult}}{1.4M_{Rd}} = 0.81$ and uplifting dominates in the response. It is interesting to note in **Figure 4.21 (d)** the different mode of pile loading with displacement of the pier. This time there is smoother monotonic decrease of the compression. The reason for that is the uplifting of the pile cap, which makes its distance from the pile greater. The deformed mesh with the plastic deformation of the soil and the displacement vectors, which imply the uplifting, are shown in **Figure 4.22**.

Vertical and horizontal push-over analyses were performed for α = 0.5 m and their results are shown in **Figure 4.23** and **4.24** respectively. From them it can be concluded that in both cases the behavior is worse than previously, since FS_v = 3.82 and $\frac{M_{ult}}{1.4M_{Rd}} = 0.75$, proving that System 3 performs better than Systems 1 and 2 due to the better behavior of the pile cap as a shallow foundation. Here, that the thickness of the improved soil is decreased, the pile cap's behavior worsens. To further examine the effect of the piles in this specific foundation, a horizontal push over analysis was performed only for the pile cap, without underlying piles. **Figure 4.25** shows the deformed mesh, the force–displacement, moment–rotation and settlement–rotation of the pile cap proving that it is almost the same as when the piles existed, with the moment capacity only 6% smaller.

System 4

This system (**Figure 4.26)** is identical with system 2 but instead of the original soil, between the improved areas clay with S_u = 5 kPa and E_0 = 3000 kPa is used. In this case the participation of the piles is greatly increased to 41%. However, as shown in **Figure 4.27** the ultimate capacity of the system has decreased to unacceptable levels with a vertical factor of safety equal to 1.48. The force–displacement and moment–rotation relationships from the horizontal push–over analysis are shown in **Figure 4.28**. From **Figure 4.29** a different pattern in the loading of the piles is observed. Here, as the shallow soil cannot provide almost any resistance, the compressed pile receives greater load which increases with increasing displacement of the pier.

When the piles are closer to the pile cap, α = 0.5 m, the response is slightly better but still not satisfying. **Figure 4.30** shows the force–settlement relationship and the response of the system under horizontal loading. An increase in the stiffness can be observed at about 0.5 m displacement or 0.03 rad rotation. This is a result of the increased resistance that the pile provides as the pile cap comes closer to it.

System 5

In order to understand how the further improvement of piles' participation would affect the foundation's response, System 5 is identical to 4 but the improved soil has $S_u{}^* = 10S_u$ and $E_0{}^* = 10E_0$ (**Figure 4.31**). As **Figures 4.32** and **4.33** show the response was slightly improved, however, it still did not satisfy the requirements. The most important improvement is that this time the foundation uplifted proving that even in poor soil conditions, if the load transfer between the cap and the underlying piles is sufficient, uplifting is possible. **Figures 4.34** and **4.35** show that for α = 0.5 m the response is slightly improved but not impressively.

From these five systems important conclusions can be made. The first, and most important, is that the distance between the piles and the pile cap greatly affects the response of the system. The closer the distance the greater the vertical and moment capacities of the foundation are. In addition this distance determines whether the response will be uplifting or sinking dominated. Another important remark is that improving the soil in a small area above the pile can enhance the behavior of the unconnected pile foundation, as long as the intermediate soil layer is sufficiently thin. The analyses showed that adding an improved soil cushion between the cap and the piles leads to a better behavior. However, this is mainly due to the improved behavior of the cap as a shallow foundation. In poor shallow soil conditions the piles have an important role in the moment capacity and vertical capacity of the foundation and improving the soil above them can lead to a better behavior.

With the experience gained from these five configurations three more systems were designed. All of them had a soil layer between the pile cap and the piles of thickness 0.5 m, since this proved to be more efficient. In addition, inspired by Allmond and Kutter (2012) who tested a shallow foundation enhanced with unconnected piles and it slipped off the piles, the distance between the piles and the edge of the pile cap was selected equal to d.

System 6

This configuration, shown in **Figure 4.36**, is identical with the second one but instead of $S_u{}^* = 3S_u$ and $E_0{}^* = 3E_0$ the improved soil had properties 10 times better than the initial one. From the vertical push over analysis the force–displacement relationship of the system and of the piles are extracted and presented in **Figure 4.37**. In contrast with system 2, in this case the piles reach their capacity at much smaller settlements without the cap touching the piles, which never happens due to the very hard improved soil between them. While the participation of the piles slightly decreases from 37%, that system 2 had, to 36% the vertical factor of safety increases to FS_v = 4.02. This is due to the overall enhancement of the soil from the improved soil patches.

Figure 4.38 shows the force–displacement and moment–rotation curves from the horizontal push over analysis. The ultimate horizontal force and moment capacity of the foundation are increased but still are not sufficient for a conventional design. **Figure 4.39** shows the significant uplifting that takes place on the foundation and the smooth reduction of compression load on pile 2 due to it.

System 7

This is similar to system 3 but an improved soil layer with $S_u{}^* = 5S_u$ and $E_0{}^* = 5E_0$ that also extends 0.5 m under the pile heads was used, as shown in **Figure 4.40**. The vertical factor of safety is 5.33 and the participation of the piles 27% (**Figure 4.41**). Hence, not only its response as a shallow foundation is improved but the cap–pile load transmission mechanism is improved. Additionally, the mobilization of the piles leads them to sink and so the pile cap touches the piles at settlement about 1.0 m and not 0.5 m, which was their initial distance. The distributions of the axial force along the depth of the piles, as well as the plastic deformations of the soil, are shown for settlement equal to 10cm and 90cm at **Figure 4.42**. From them, it is observed that a large portion of the piles' loads is transmitted directly to their heads. Again, due to localization of the stresses the neutral plain is in shallow depth. It is interesting to note that at small settlement the palstification of the soil is mainly concentrated on the heads and bases of the piles. As the system reaches its ultimate capacity, extensive plastifications develop around the cap and the bases of the piles.

From the force–displacement and moment–rotation curves, in **Figure 4.43**, of the horizontal push–over it is obvious that this system does not satisfy the aforementioned requirements. The large vertical factor of safety and the resistance of the piles lead to an uplifting dominated response as shown in **Figure 4.44** from the settlement–rotation relationship and the displacement vectors at the beginning of the loading.

System 8

Seven systems with 4 piles, unconnected from the cap, were tested but none of them satisfied the required moment capacity. In this case 6 piles were used with a distance between them equal to 3d. A greater distance would lead to a huge pile cap probably able to satisfy the requirements without the piles, which is not the subject of this study. The length and diameter of the piles did not change from the previous cases and are equal to 16 m and 1.0 m respectively.

As shown in **Figure 4.45** improved soil patches are used above the pile heads with $S_u{}^* = 5S_u$ and $E_0{}^* = 5E_0$. **Figure 4.46 (a)** shows the response of the system in the vertical push over. The factor of safety was found equal to FS_v = 5.31 and the piles' participation 37%, greater than most of the previous cases. In the same graph the response of a shallow foundation without the piles is shown. Its capacity is less the capacity of system 8 minus the resistance of the piles, proving that the piles not only add resistance to the system but also enhance the soil. Furthermore, from **Figure 4.46 (b)** the interaction between the piles is similar with the connected pile group case. At small settlement the stiffness of piles 1 and 3 is greater than pile 2 due to its increased settlement from the neighboring piles. In contrast pile 2 reaches a slightly

greater capacity due to enhancement of the soil from the neighboring piles. This can also be observed from **Figure 4.47**, which shows the axial load distribution along the piles from settlements equal to 5 and 100 cm. At small settlement piles 1 and 3 receive greater loads on their heads. In addition the depth of negative skin friction is smaller than for pile 2 because its surrounding soil settles more from the rest of the piles. When settlements increase, pile 2 can receive greater loads since it is in an enchased soil are, as discussed in chapter 3.

A horizontal push over analysis was performed to test the foundation behavior in that type of loading. Its force–displacement and moment–rotation relationships are shown in **Figure 4.48**. In this case $\frac{M_{ult}}{1.4M_{Rd}} = 1.19$. For comparison the moment capacity demand and the moment–rotation relationship of a shallow foundation with same dimensions are also shown. The shallow foundation also has sufficient moment capacity however it is developed at an unacceptably large rotation. In the same figure the settlement–rotation and the axial load on the piles with horizontal displacement of the pier are shown. From the first the uplifting dominated response of the system can be seen, while the shallow foundation has a sinking response.

4.1.2 Comparison and Selection

From the systems tested the one that best satisfies the requirements will be selected to be the final design. As discussed in 4.1, in addition to the EC specifications it is desirable that the system has an uplifting response. The construction and installation of the piles is an expensive procedure and so their participation in the load carrying mechanisms, both in vertical and horizontal loading, is important. **Table 4.1** summarizes the response of the systems and the final design is selected.

Table 4.1 Comparison of the alternative unconnected pile designs.

System	α	FS_v	$M_f/1.4M_{Rd}$	Uplifting	Piles Participation
1	d	2.77	0.65	NO	16%
	d/2	2.87	0.68	NO	19%
2	d	2.75	0.44	NO	16%
	d/2	3.42	0.65	YES	38%
3	d	4.87	0.81	YES	22%
	d/2	3.82	0.75	YES	33%
4	d	1.48	0.46	NO	42%
	d/2	1.92	0.65	NO	48%
5	d	3.22	0.67	YES	50%
	d/2	3.12	0.68	YES	50%
6	d/2	4.00	0.72	YES	36%
7	d/2	5.33	0.92	YES	27%
8	d/2	5.31	1.19	YES	37%

From the tested configurations, System 8 has the optimum response since it satisfies all the requirements, has an uplifting response and the participation of the piles to

load carrying is important. Hence, this is selected as the final design. Hereafter, the unconnected pile foundation that satisfied the conventional capacity design will be called UC.

4.2 Comparison of Conventional Connected and Unconnected Pile Foundations

This chapter will study the static response of the two conventionally designed foundations, CC and UC. A first remark is that in order to achieve the required moment capacity of the unconnected pile foundation the vertical factor of safety is quite larger than the one of the connected system and uplifting response dominates. This will probably be significant in the cyclic loading of the system. The settlement due to self–load remains the same in this system as in the conventionally design one, and equal to about 1.5 cm.

4.2.1 Developed Forces and Moments

As already stated, the main reason to design unconnected pile foundations is to reduce the forces developed on the piles in the case of horizontal loading. Thus it is important to compare them for different horizontal displacements. **Figure 4.49** shows the distribution of axial, shear and moment loading on the piles for deck displacements equal to 5.9 cm, corresponding to the maximum axial force on the compressed pile, and 10 cm, corresponding to 3.0 cm displacement at the base of the pile cap. It is reminded that the distribution of forces and moments along the piles were presented for connected piles for 10 cm deck displacement, which corresponds to pile head displacement equal to 3.6 cm. From the distribution of axial loads it can be noted that not only Pile 3, which is compressed by the overlaying soil, develops forces but Piles 1 and 2 also. This behavior was expected and can be explained by the interaction between the piles. Pile 3 induces settlements to the soil and so negative skin friction is introduced to Piles 1 and 2. Pile 2 develops greater forces with maximum value on lower depth since it is closer to the loaded pile. As the load on pile 3 reduces the loads on the rest of the piles also reduce.

Despite the reduction of axial loads after a specific displacement the shear forces and bending moments keep increasing on Pile 3 and decreasing on Piles 1 and 2. In order to explain this behavior the shear development mechanism should be explained. **Figure 4.50** shows the horizontal displacements on the foundation and the soil for the CC and the UC. In the first system the superstructures induces displacements on the piles, the soil resists this deformation and so stresses are developed. On the other hand in the unconnected pile system the pile cap induces displacements on the soil and not on the piles. The stiffer pile, compared to the surrounding soil, resists on this deformation reducing the soil's displacement in front of the pile. This resistance is what makes the pile develop shear forces and bending moments. As it can be seen from the figure, despite the axial load relief of the Pile 3 the displacements induced in the soil increases and so does the shear. However, as the pile cap uplifts, it loses contact with the soil overlaying Piles 1 and 2. Hence, the

displacement of the soil reduces and the developed shear forces and bending moments also reduce. It is also important to note that due to the rotation of the pile cap, eccentric loading is applied on the head of the compressed pile by the overlaying soil, explaining the bending moment developed there.

Overall it can be concluded that when the piles are not connected on the pile cap, the shear forces, axial forces and bending moments are reduced for a given displacement of the pier.

4.2.2 Ductility Capacity

As UC is design according to the capacity design of the EC, its plastic deformation will be developed on the base of the pier and so its ductility capacity is the same with the connected pile foundation. This can also be seen from the moment–curvature relationship (**Figure 4.51**) extracted from a push over analysis with the pier having the characteristics of the reinforced concrete section designed in the previous chapter. In the same figure the moment transmitted to the soil in respect of rotation is shown. For comparison the same diagram of the connected pile system is presented. From them it can be concluded that the moment–rotation stiffness of UC is less than CC.

4.2.3 Fundamental Period

Despite the greater rotational stiffness of CC, the two systems have the same fundamental periods for small displacements. Their Fundamental periods–deck displacement relationships are shown in **Figure 4.52**. In both systems the period at the beginning of the loading is equal to 0.58 s.

4.3 Design of Rocking Foundation

The concept of Rocking Isolation will be applied herein in an unconnected pile foundation in order to test whether this concept can be efficiently applied to such systems and its response will be evaluated with real earthquake accelerograms. Rocking Foundations should:

- Have a Vertical Factor of Safety, FS_v, greater than 2
- Have a ratio $\frac{M_f}{M_{Rd}} = 0.7 \div 0.8$

where, M_f and M_{Rd} the moment capacity and design moment capacity of the foundation and the pier respectively. The first requirement ensures small settlements due to self–weight and aims that the foundation responds in uplifting manner, meaning it does not accumulate settlements over earthquake cycles. The latter leads to plastic hinging developing within the soil, therefore margins of safety against collapse and energy dissipation increase.

The design of this system will also be decided using push–over analyses. In order to find the optimum design that satisfies the requirements of this philosophy and given the results of unconnected system design according to the capacity principles, two more systems were designed and tested.

4.3.1 Push-Over Analyses for the Rocking Foundation

In both systems the length of the piles was kept 16.0 m, as it was in the previous case. However, since there is a need for moment reduction, only four piles are used in this case with a distance between them equal to 3.0 m. From the two tested distances between the piles and the pile cap, α = d/2 was selected and tested for the rocking system, as it was found that this enhances the uplifting and the participation of the piles. Improved soil was used above the piles since it was proven that this greatly improves the behavior of the system.

Rocking System 1

Figure 4.53 shows configuration of this system along with its response on vertical and horizontal push over analyses. It can be seen that the vertical factor of safety, FS_v = 4.19, is sufficient and the participation of the piles, which reach their ultimate capacity, is 38%. As expected from this large factor of safety, the foundation responds in an uplifting way. From the moment–rotation curve it can be seen that compared to the similar design that the distance between the piles was 4d, the ultimate moment capacity has decreased but $\frac{M_f}{M_{Rd}} = 0.87$, which is greater than the desired limits. It is noted here, that had the design been according to the actual moment capacity and not the design moment capacity of the pier, this system would be acceptable.

Rocking System 2

The dynamic analyses of the UC system, which are presented in Chapter 5, showed that the sliding of the pile cap is significantly smaller than 0.5 m and so there is no fear that it will dismount the piles. Thus, in order to reduce the ultimate moment capacity of the system, the distance between the piles and the edge of the cap can be reduced. This reduction led to the system shown in **Figure 4.54**. In the same figure the response of the system on vertical loading is presented. The vertical factor of safety is equal to 4.05 and the participation of the piles 43%, greater than in the UC case. From the distribution of axial force along the piles it can be seen that as the settlement increases more load is directly applied on the head of the piles, the relative settlements decrease and so the neutral plane is in lower depth. Due to symmetry both piles have the same loads and response. In order to compare the response of this system with CC and UC, that have 3 piles in each row, the piles will be called Pile 1 and Pile 3 instead of Pile 1 and 2.

The results of the horizontal push over analyses, along with the deformed mesh, are presented in **Figure 4.55**. Compared to the previous system, the moment capacity has reduced and now $\frac{M_f}{M_{Rd}} = 0.75$ satisfying the Rocking Isolation requirements. Additionally, uplifting dominates the response of this system, something especially

important for rocking foundations as discussed previously. From the pile axial load–displacement relationship it can be seen that there are three phases in the loading of Pile 3. On the first phase, due to the increase of the moment the load on its head increases. However, this stops as the foundation uplifts and the pile is slightly unloaded. For further increase of the moment and hence the settlement of the compressed side of the pile cap, the distance between the pile and the pile cap decreases again and so its load increases.

The response of this system is satisfying and it is selected as the final design of the rocking foundation, called UR hereafter.

4.4 Comparison of Rocking and Conventional Foundations

The response of UR is compared with the other two systems for static loading. In this system the settlement due to self-weight is slightly increased to 2.0 cm, which is not important and can be taken into account in the design of the bridge.

4.4.1 Developed Forces and Moments

Figure 4.56 shows the distribution of axial forces, shear forces and bending moment along the piles for horizontal displacements at the top of the pier equal to 10cm and 24cm. The first displacement corresponds to 3.5 cm displacement at the base of the pile cap and the second to the maximum axial load on the head of the pile. So a comparison between the developed stresses for the three systems will be attempted.

First of all, as it was expected from the vertical push–over, it can be seen that the length of the piles along which negative skin friction develops, decreases for increasing axial load on the pile's head. In addition the development of the axial load on Pile 1 due to pile–to–pile interaction is also observed, as in the case of the UC system. The most important conclusion is that axial force on the compressed pile of UR is greater than in UC system, since the participation of the piles is greater and so it receives great amount form the moment transmitted to the soil. However, it is reduced compared to the conventional system with connected piles.

Shear forces and bending moments are developed on the piles according to the same mechanism as in the unconnected conventionally designed system. Again, due to the eccentricity of the normal stresses on top of the compressed pile, bending moment and rotation is developed on its head. The horizontal displacements of the system and the soil are shown in **Figure 4.57**. From this, it is concluded that the stresses developed on Pile 1 are due to pile–to–pile interaction and not due to the deformation of the soil. This conclusion has been based on the fact that the displacements of the soil around Pile 1 have been reduced while the shear forces and bending moments on it are essentially the same. The developed forces on the compressed pile are significantly reduced compared to the connected piles but only slightly compared to the piles of the unconnected conventionally designed pile group.

4.4.2 Ductility Capacity

As this foundation is designed according to the new philosophy, plastic deformations will be developed within the soil and not on the pier. Hence, the ductility capacity of this system is not determined by the failure of the pier but from the overturning rotation of the foundation, θ_u. As the deck's displacement due to the rotation of the foundation is hθ, where h the height of the pier and θ the rotation of the foundation, an equivalent ductility capacity is defined for this system as:

$$\mu_{\Delta} = \frac{\delta_{ult}}{\delta_y} = \frac{h\theta_u}{h\theta_y} = \frac{\theta_u}{\theta_y} \tag{4.1}$$

where, θ_y the yield rotation of the foundation. From a horizontal push over analysis, simulating this time the pier with the properties of the concrete cross-section, the ductility capacity was calculated equal to 47.7, which is more than 10 times greater than the ductility of the conventional systems. The Force–hθ and moment transmitted to the soil–rotation relationships are shown in **Figure 4.58**.

4.4.3 Fundamental Period

The fundamental period–deck displacement relationship of UR is shown in **Figure 4.59**. As expected, this is a more flexible system leading to greater periods and a fundamental period for small displacements T_0 = 0.81 s.

Figures of Chapter 4

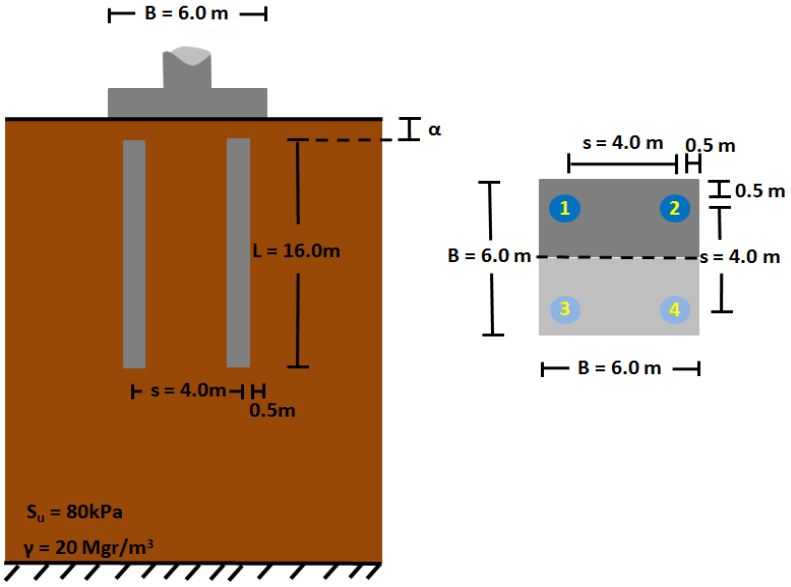

Fig. 4.1: Section and plan view of the first unconnected pile foundation tested.

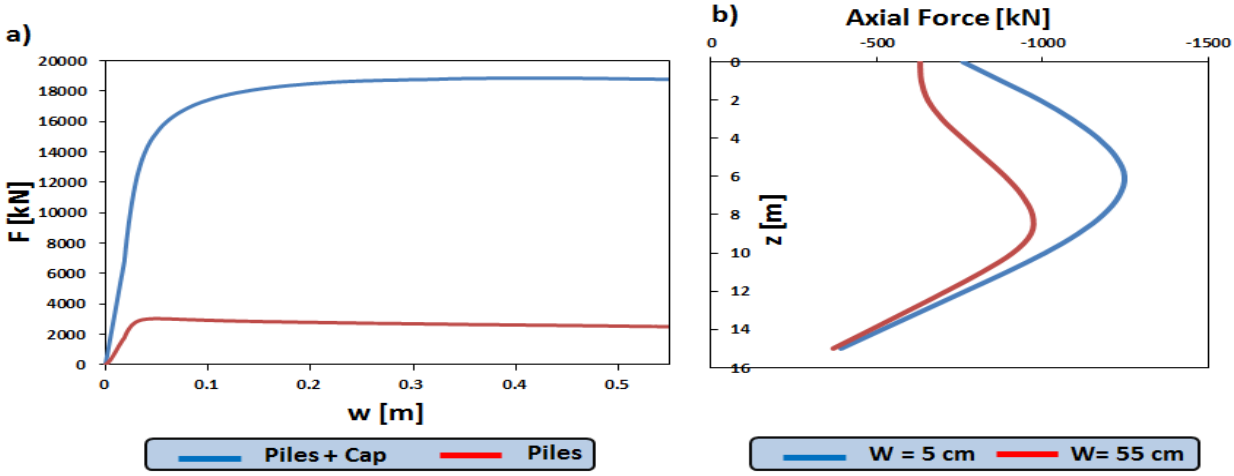

Fig. 4.2: Response of System 1 for α = 1.0 m. (a) Applied force on top of the pier and sum of forces on pile heads, versus settlement; (b) distribution of axial force on Pile 1 for settlements equal to 5 cm and 55 cm.

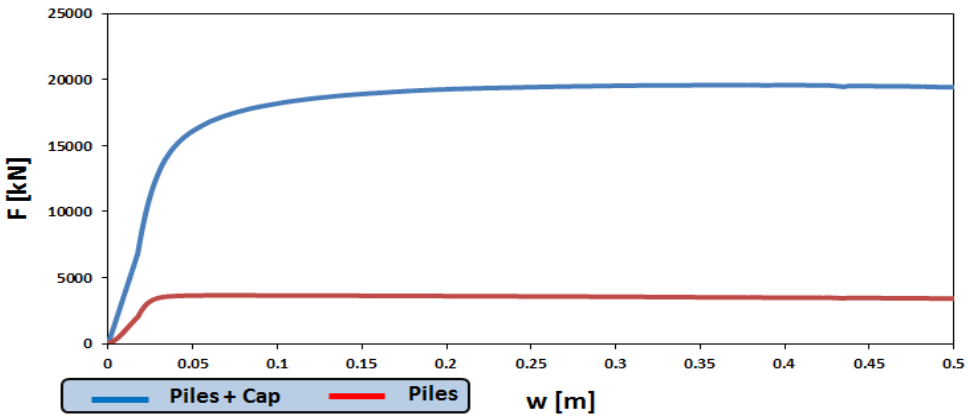

Fig. 4.3: Force–settlement relationship of System 1 for α = 0.5 m during vertical loading.

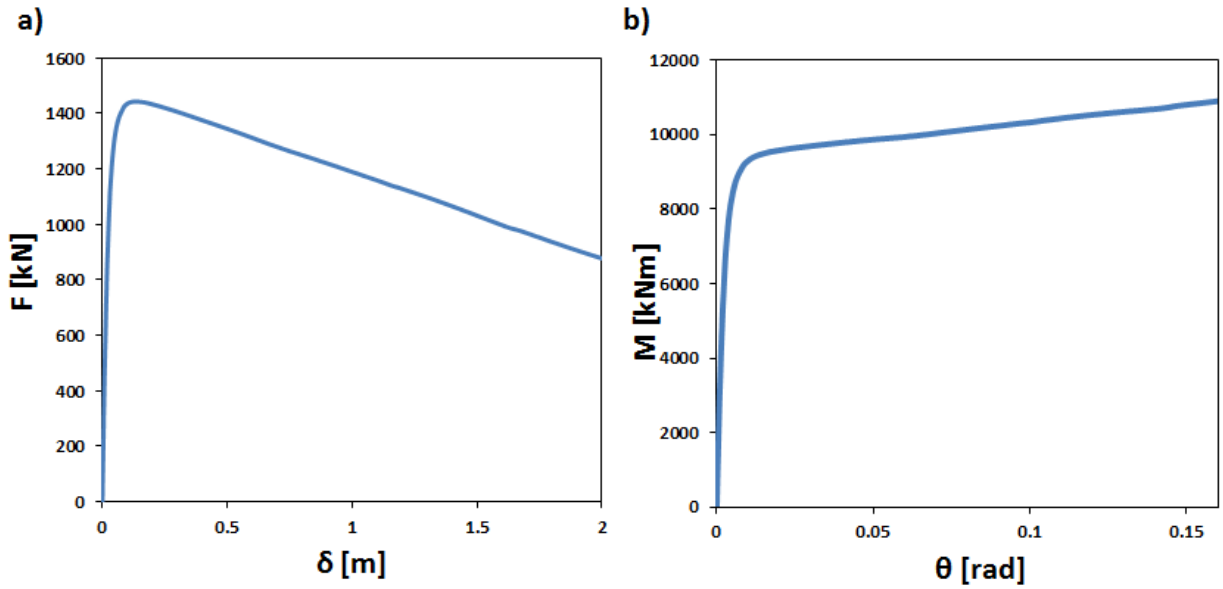

Fig. 4.4: (a) Force–displacement and (b) Moment at the base of the pier–rotation relationships of System 1 for α = 1.0 m.

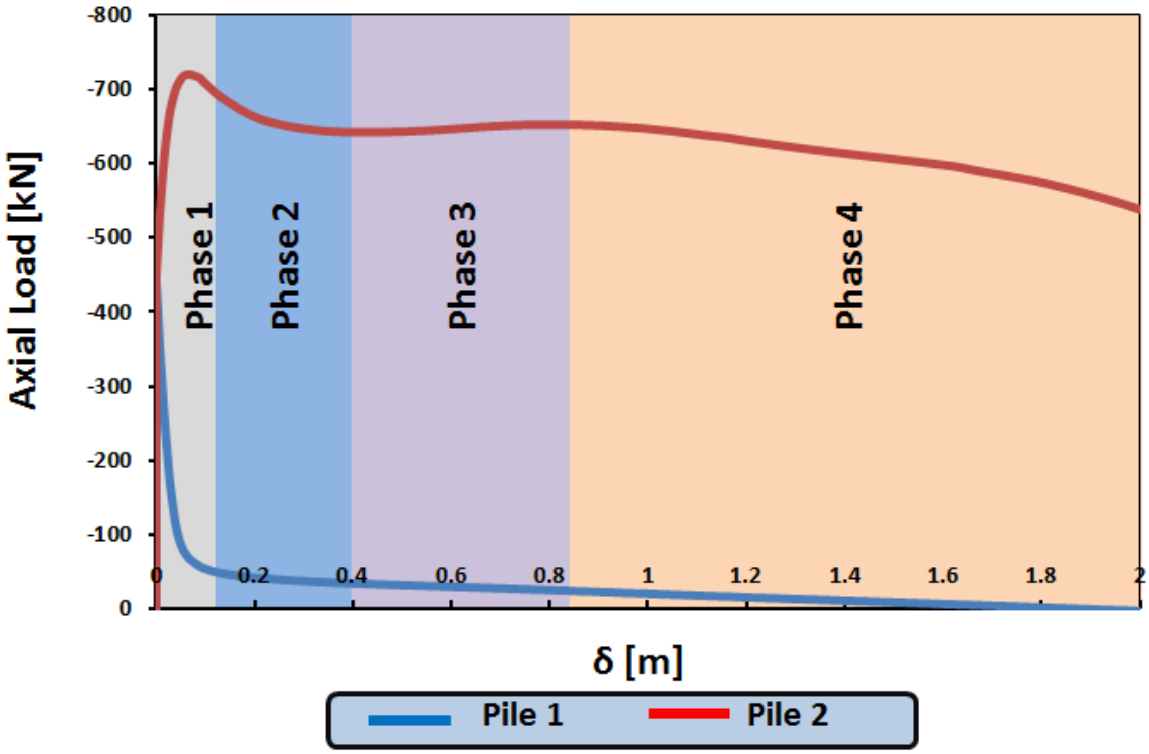

Fig. 4.5: Variation of axial load on the heads of the piles with displacement, divided in the four loading phases of Pile 2.

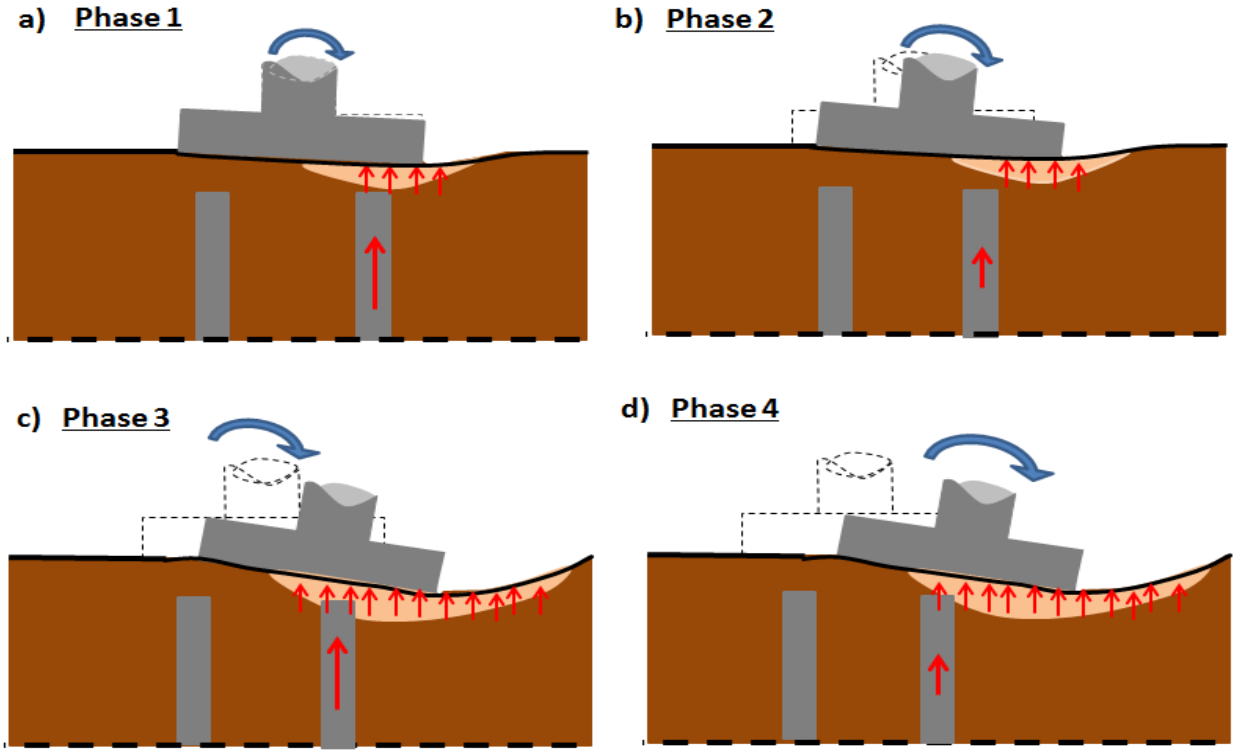

Fig. 4.6: Schematic illustration of system's response leading to loading and unloading of Pile 1.

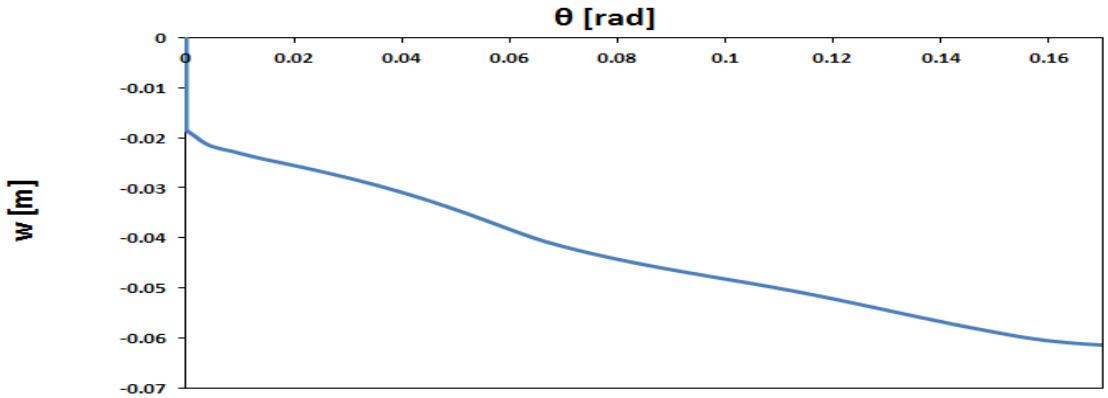

Fig. 4.7: Settlement–rotation response of System 1 for α = 1.0 m.

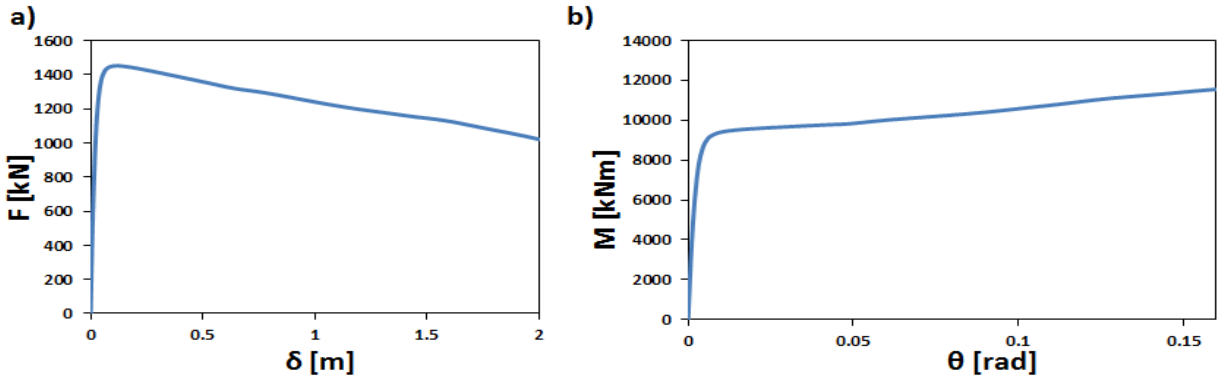

Fig 4.8: (a) Force–deck displacement **(**b) Moment–rotation relationships for System 1 and α = 0.5m.

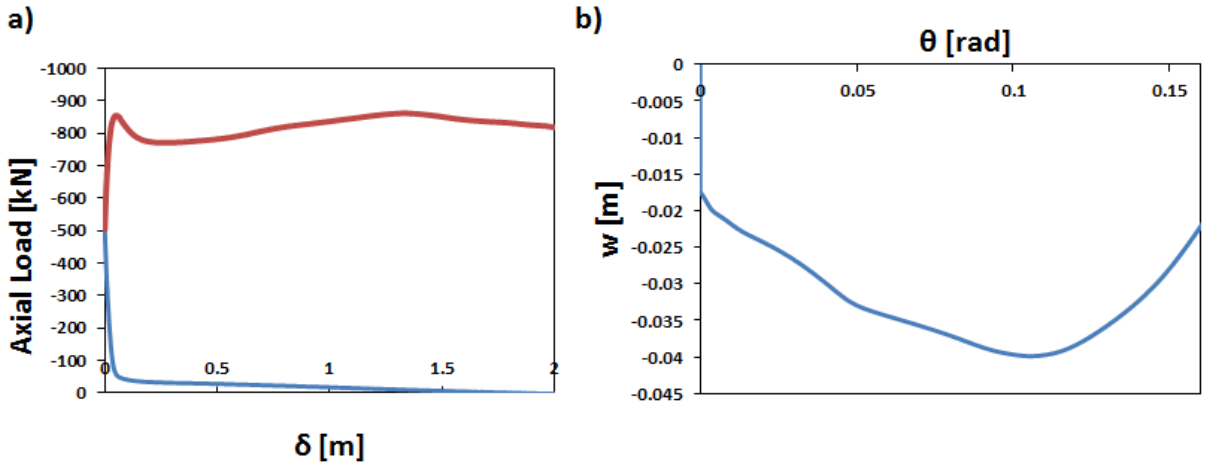

Fig. 4.9: (a) Variation of axial load on pile heads with displacement **(**b) settlement–rotation behavior of System 1 for α = 0.5 m.

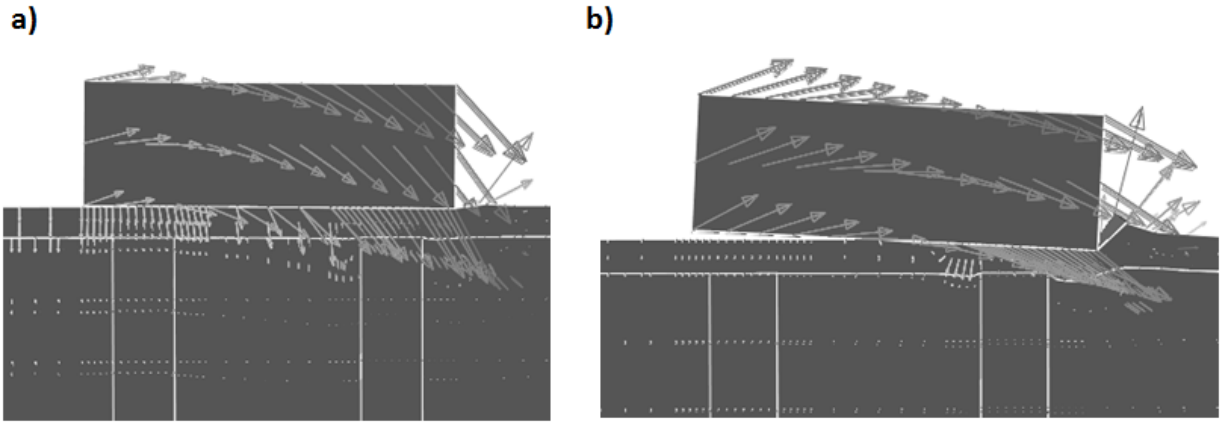

Fig. 4.10: Displacement vectors showing **(**a) sinking **(**b) uplifting response of the system for different displacements.

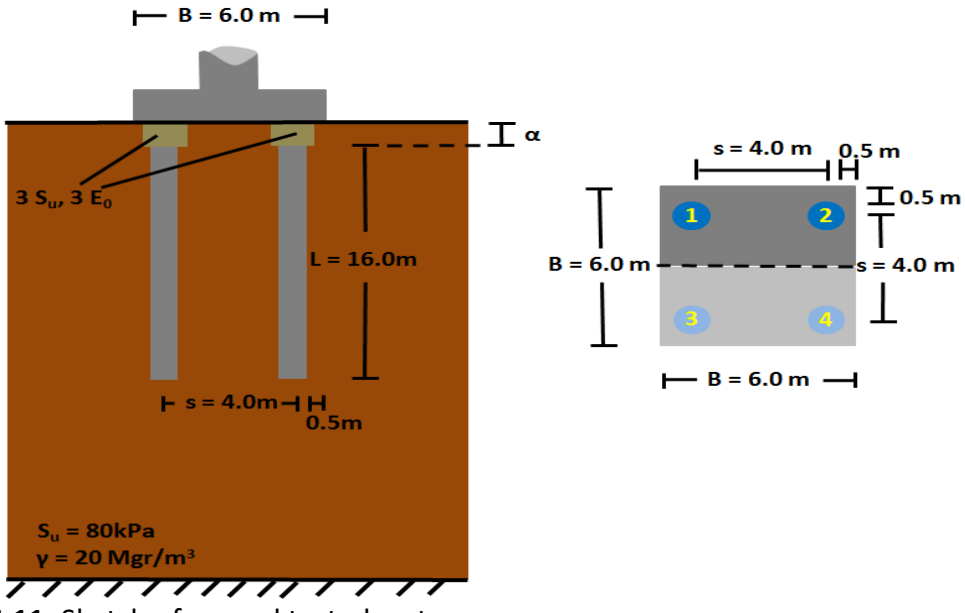

Fig. 4.11: Sketch of second tested system.

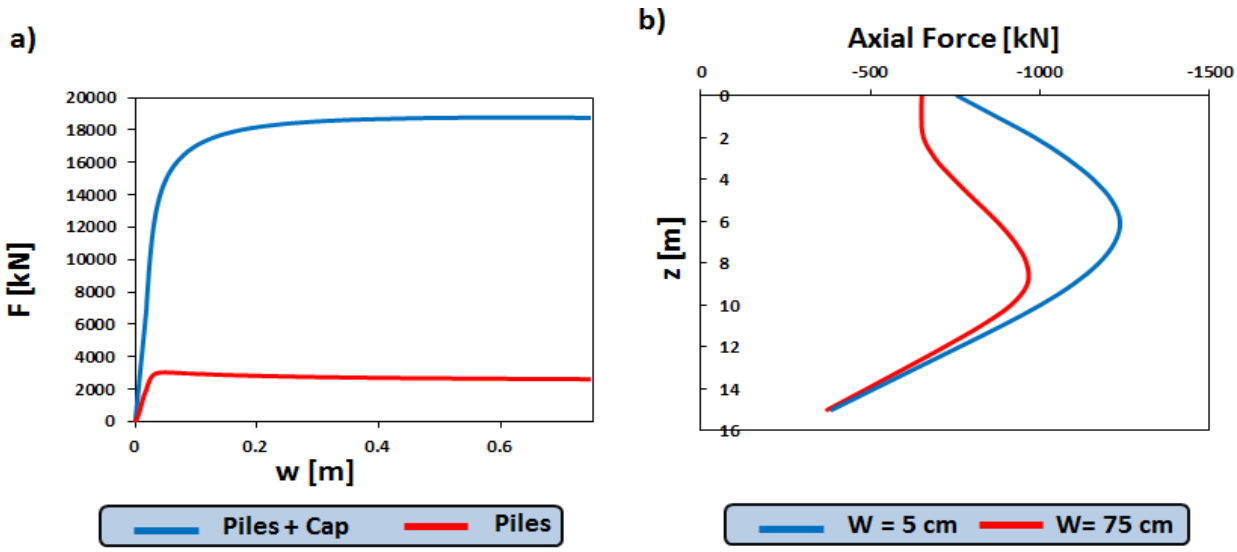

Fig. 4.12: Response in the vertical push-over of System 2 for α = 1.0 m. **(**a) Applied force and sum of forces on piles heads versus settlement **(**b) distribution of axial force on Pile 1 for settlements equal to 5 cm and 75 cm.

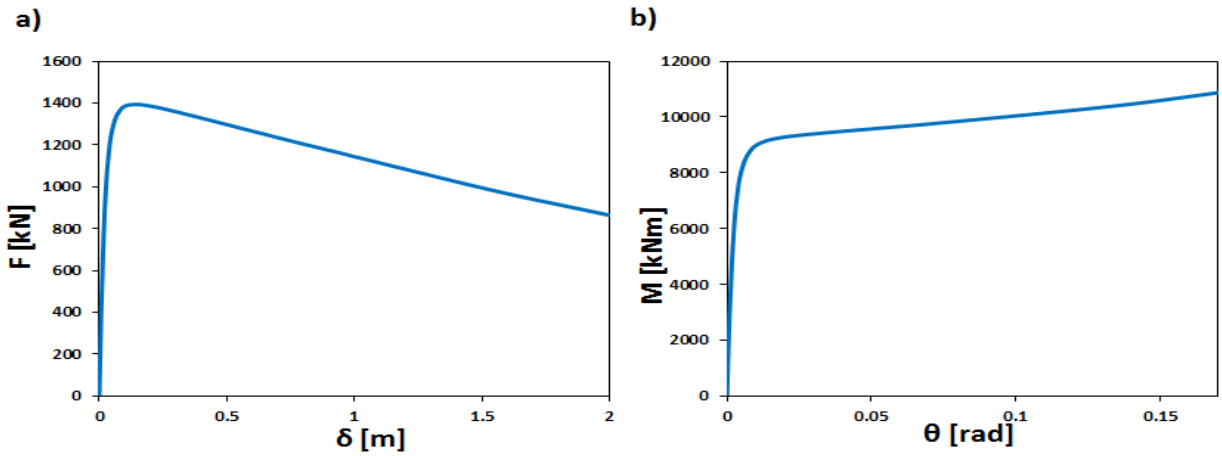

Fig. 4.13: (a) Force–deck displacement **(**b) Moment–rotation relationships for System 2 and α = 1.0 m.

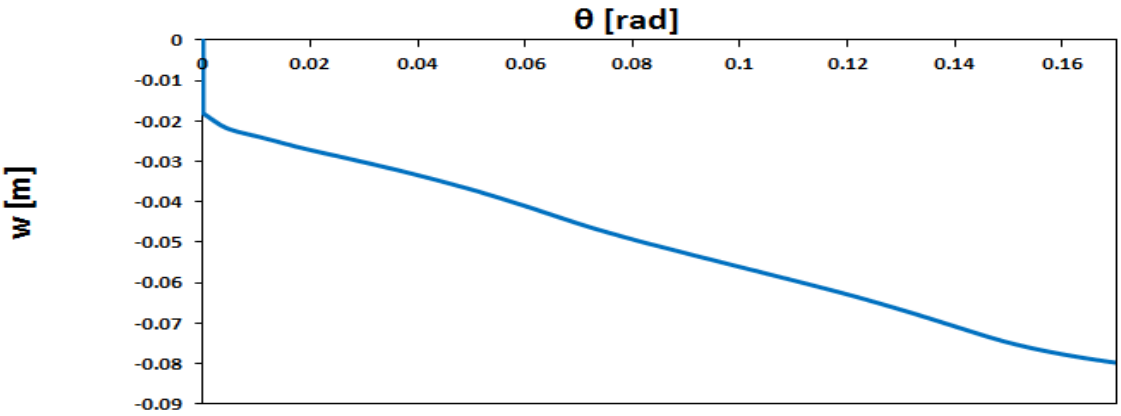

Fig. 4.14: Evolution of settlement in respect of pile cap rotation.

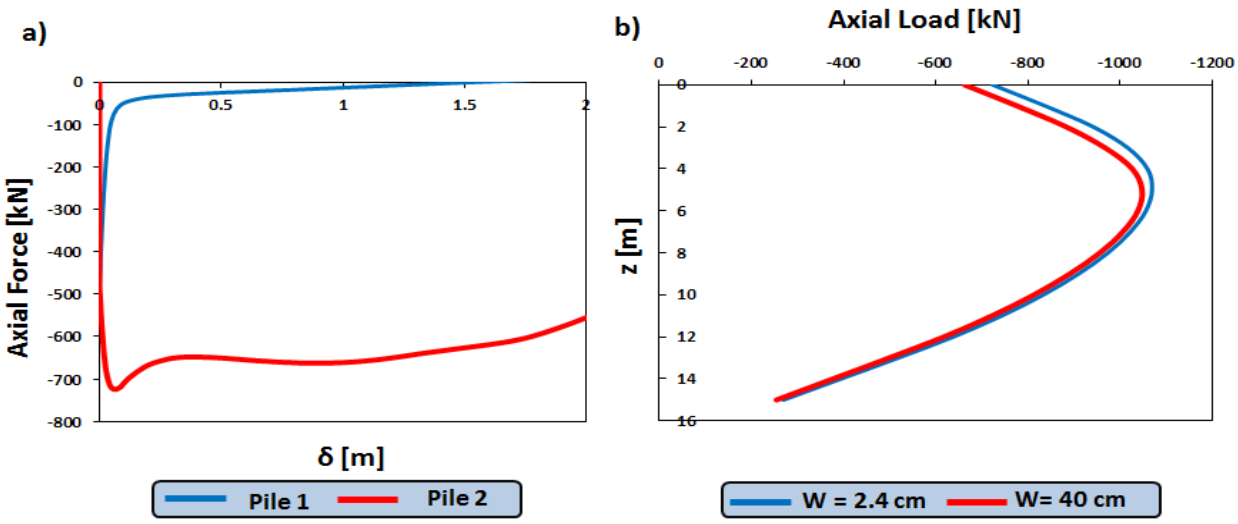

Fig 4.15: (a) Axial force of piles versus displacement **(**b) distribution of axial force along the piles.

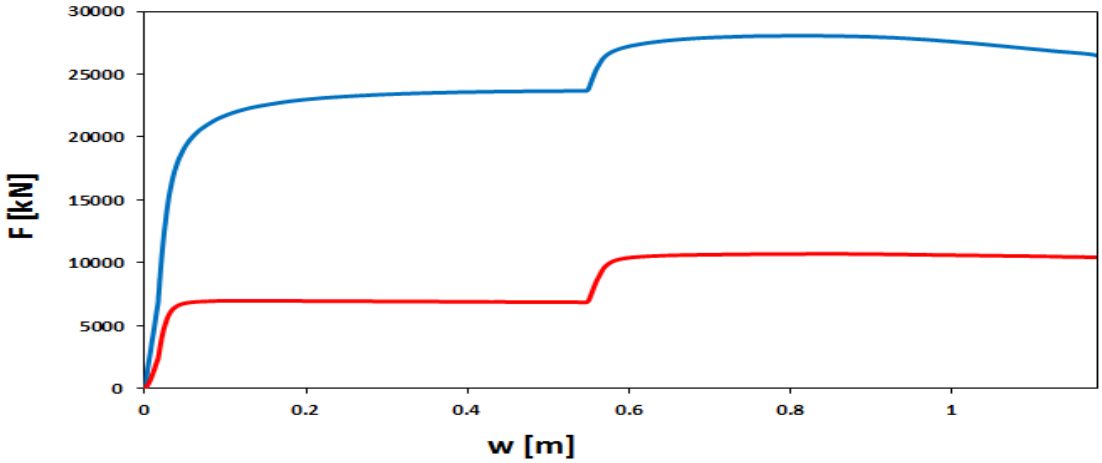

Fig. 4.16: Force–settlement relationship from the vertical push-over analysis.

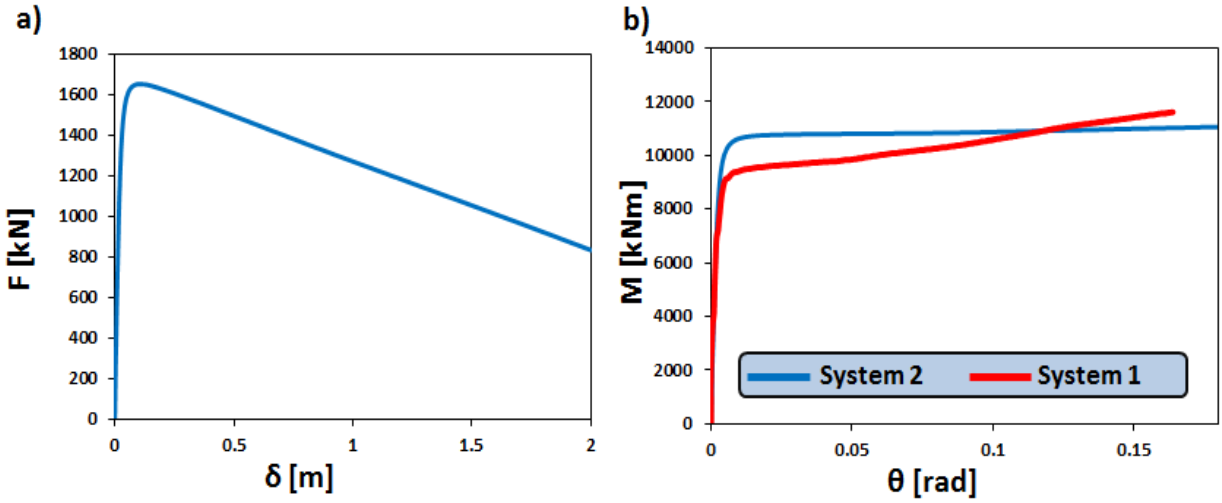

Fig. 4.17: Response on horizontal loading **(**a) force–displacement **(**b) moment–rotation.

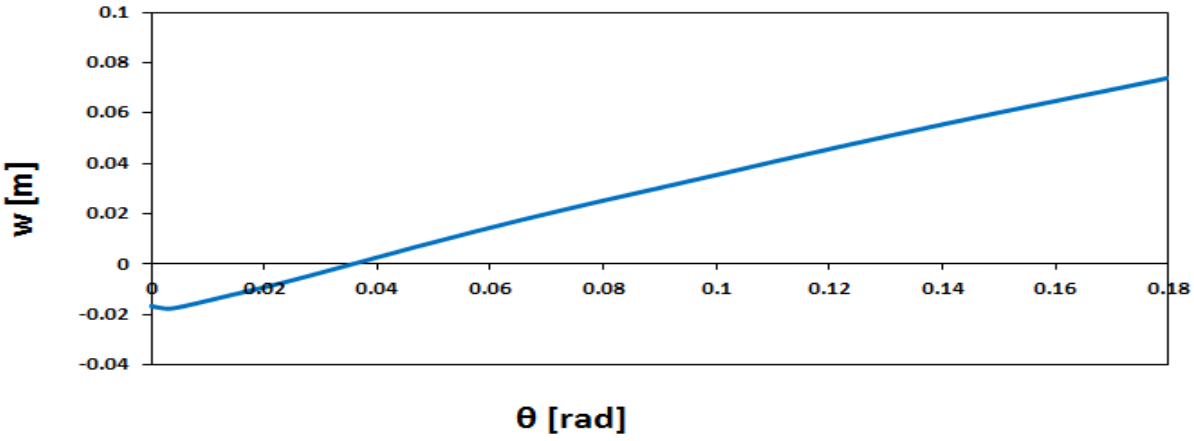

Fig. 4.18: Settlement–rotation response of System 2 for α = 0.5 m showing uplifting of the foundation.

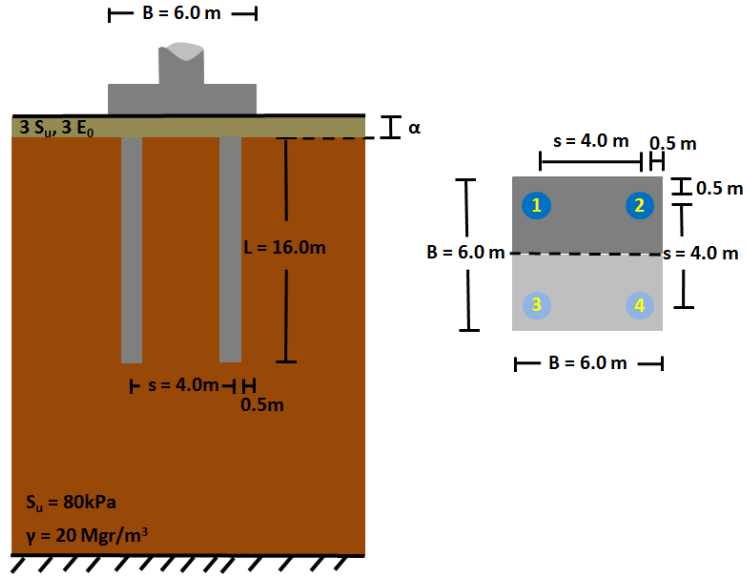

Fig. 4.19: Configuration of the third tested system.

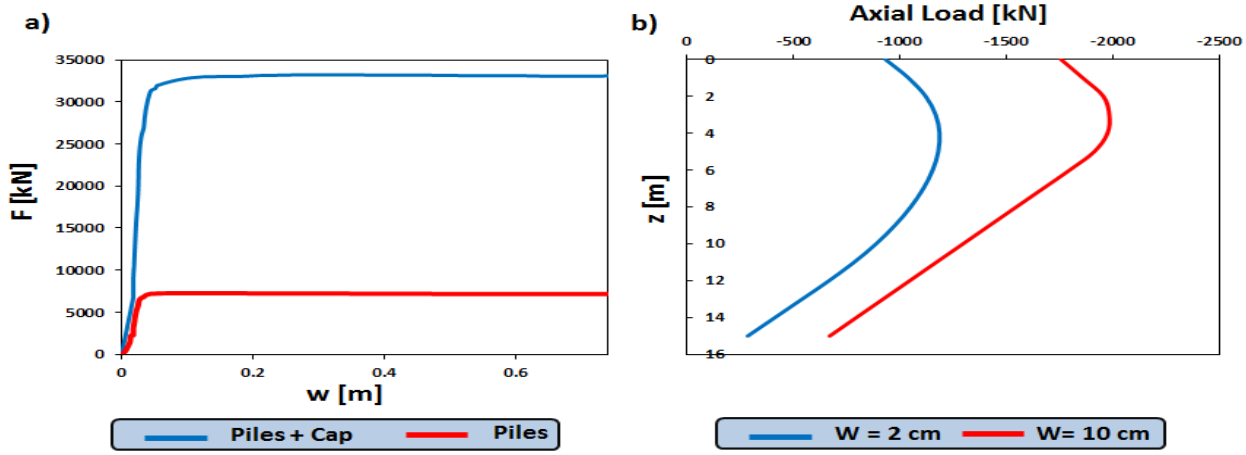

Fig. 4.20: **(**a) Applied force on the pier and sum of piles' axial force in respect with settlement **(**b) distribution of axial force along Pile 1 for settlement equal to 2 and 10 cm.

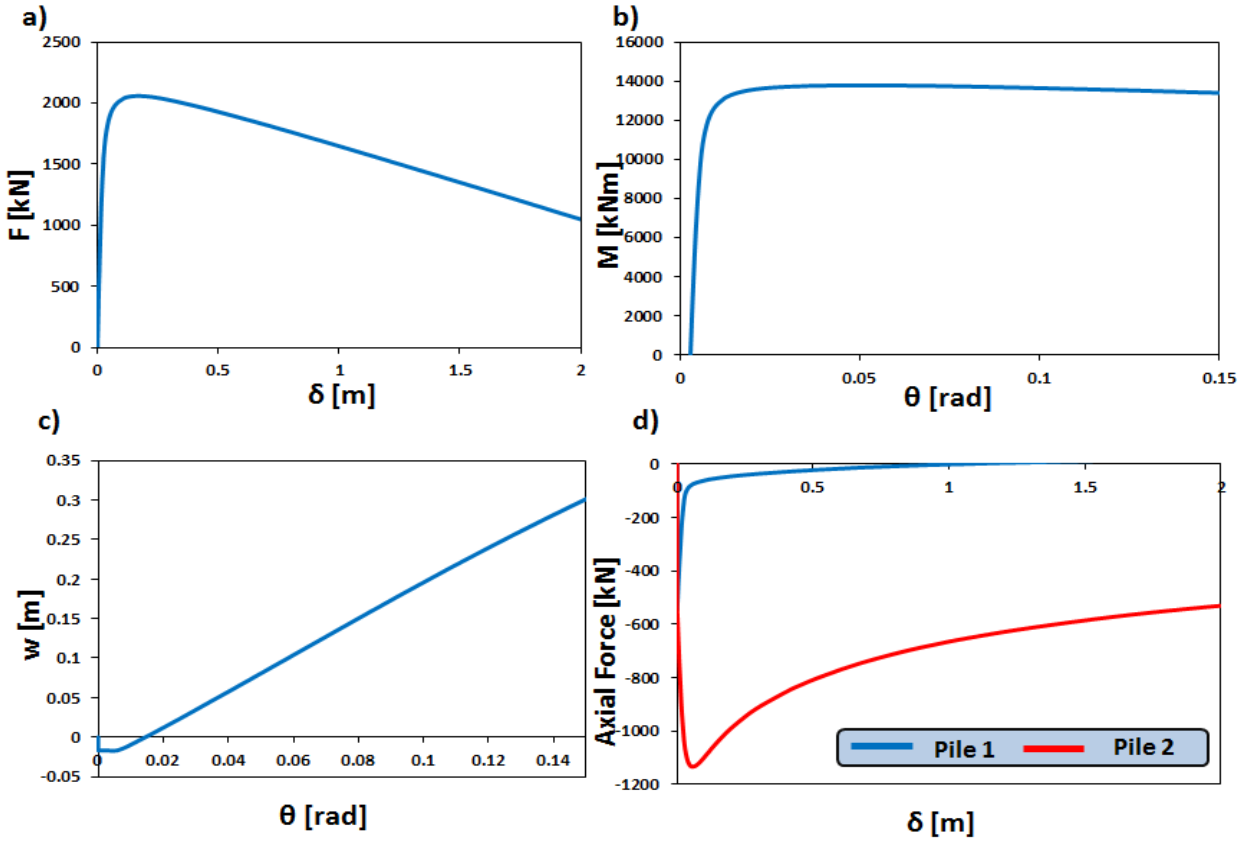

Fig. 4.21: Response of third system in horizontal loading in terms of **(**a) Force–deck displacement **(**b) Moment–rotation c) settlement–rotation d) Axial on pile heads–deck displacement.

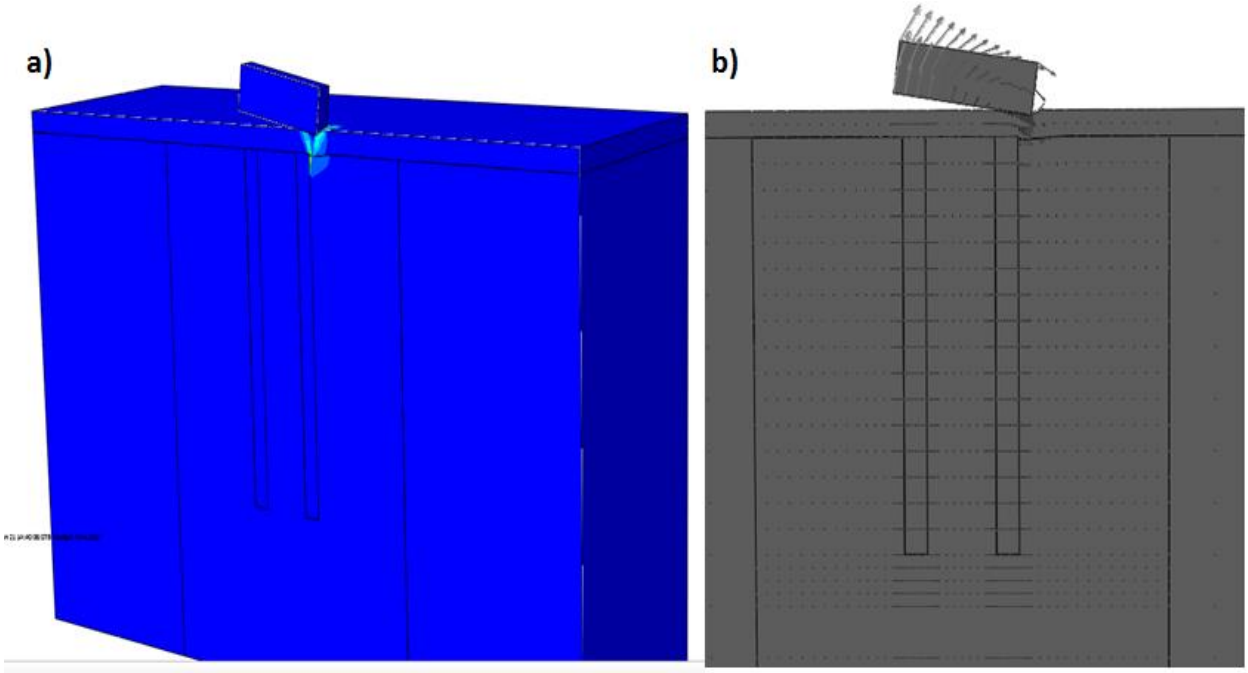

Fig. 4.22: (a) Deformed geometry with contours of plastic deformations b) displacement vectors showing uplifting of the foundation.

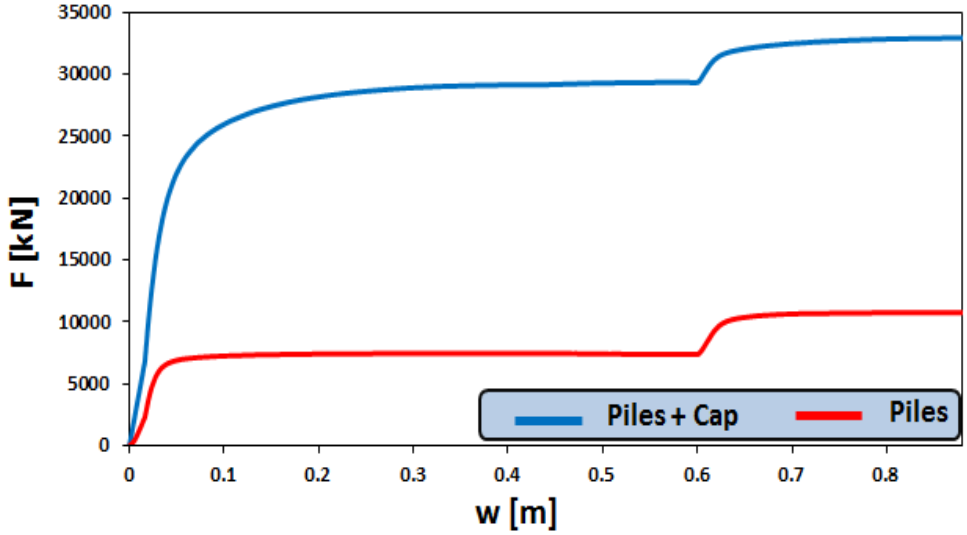

Fig 4.23: Force – settlements relationship for System 3 and α = 0.5 m. The total axial load of the piles is also presented.

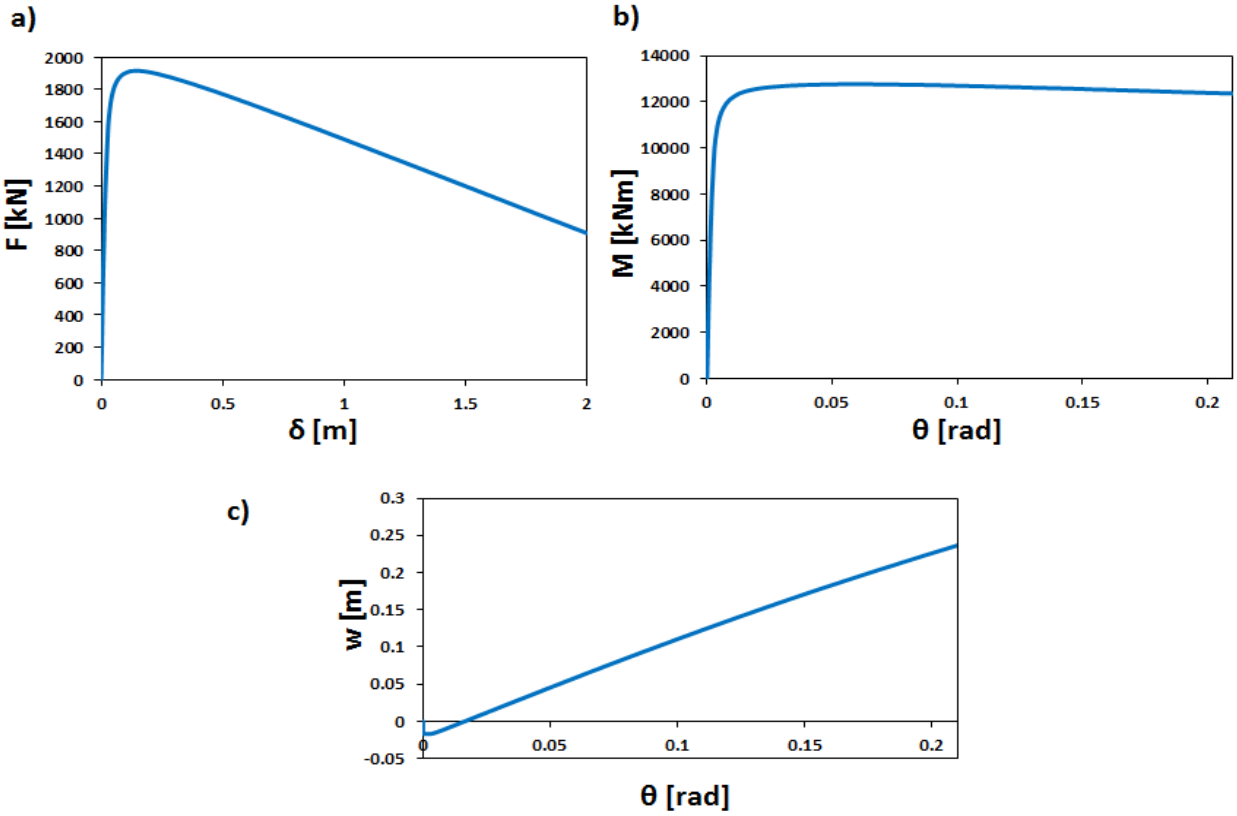

Fig. 4.24: Response of third System, for α = 0.5 m, in horizontal loading in terms of **(**a) Force–deck displacement **(**b) Moment–rotation **(**c) settlement–rotation

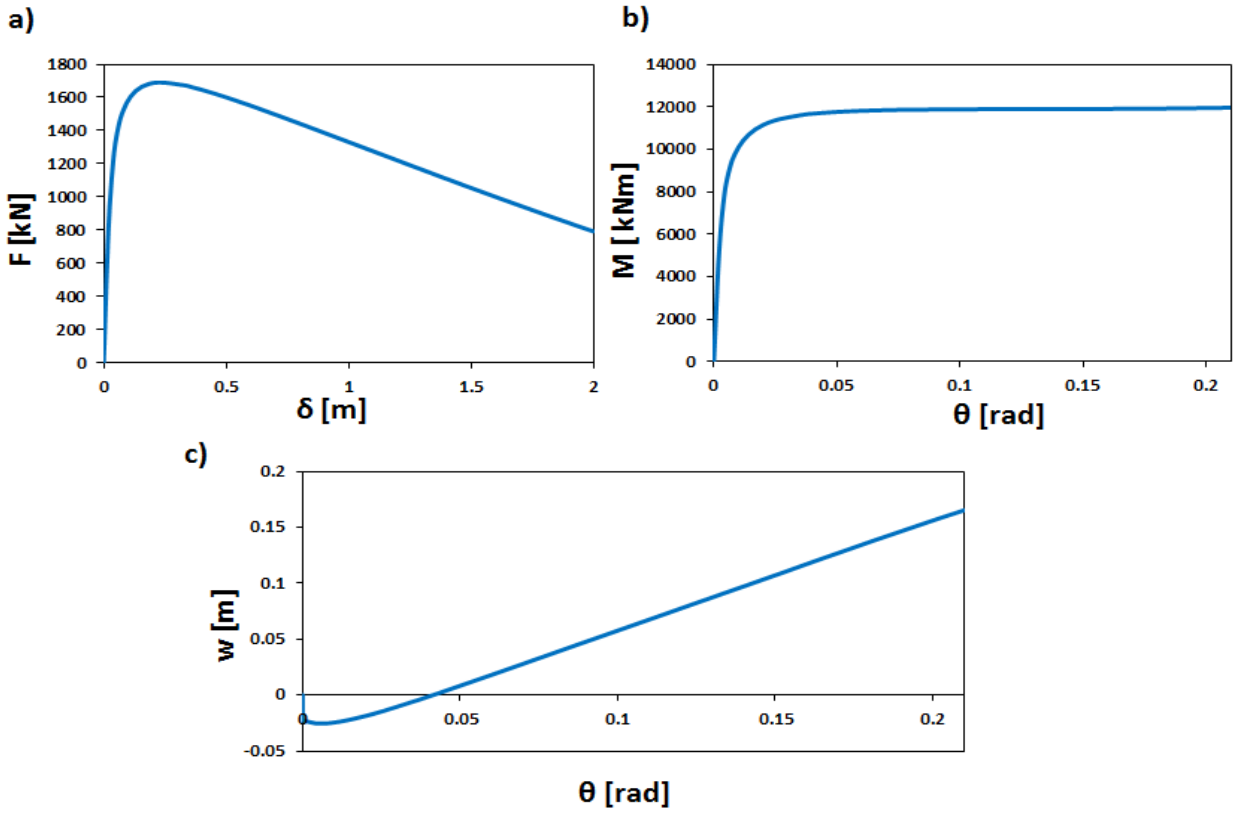

Fig. 4.25: Response of shallow foundation with dimensions of System 3's Pile Cap.

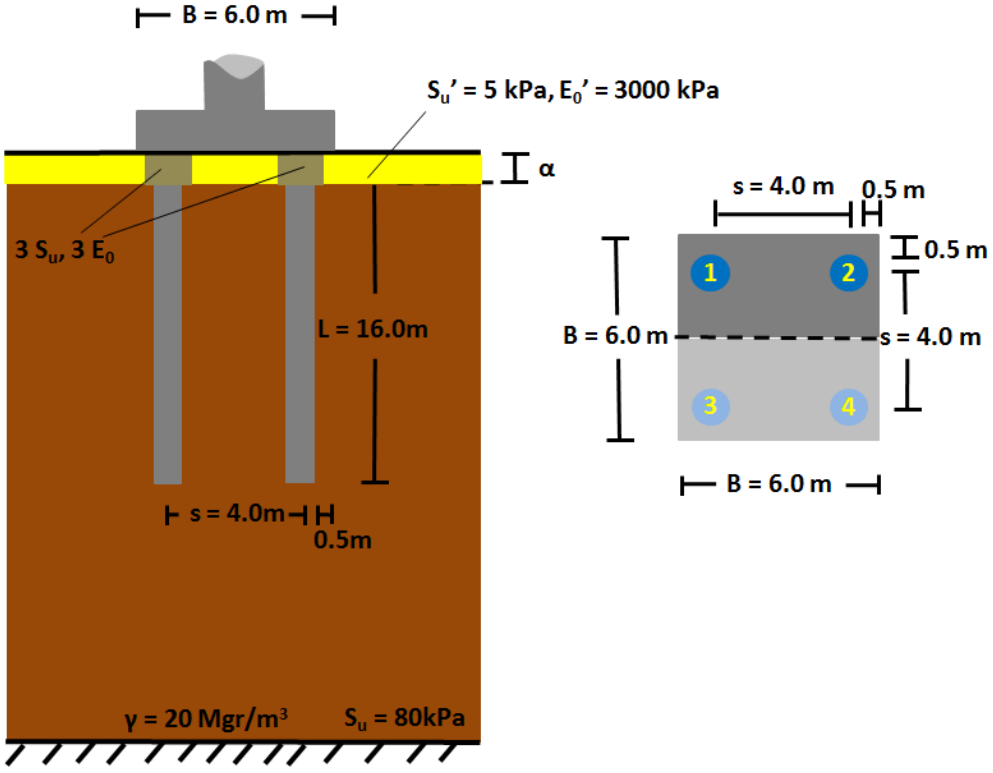

Fig. 4.26: Design of the fourth tested system with unconnected piles.

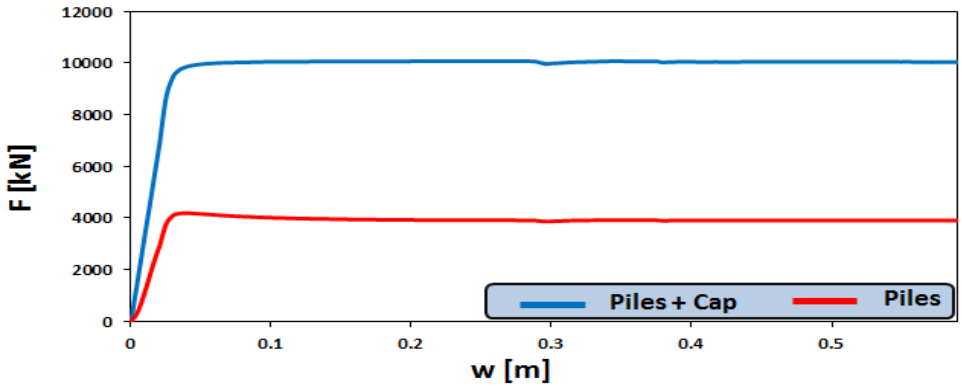

Fig. 4.27: Response of System 4 in vertical loading in terms of total resistance and the resistance of the piles.

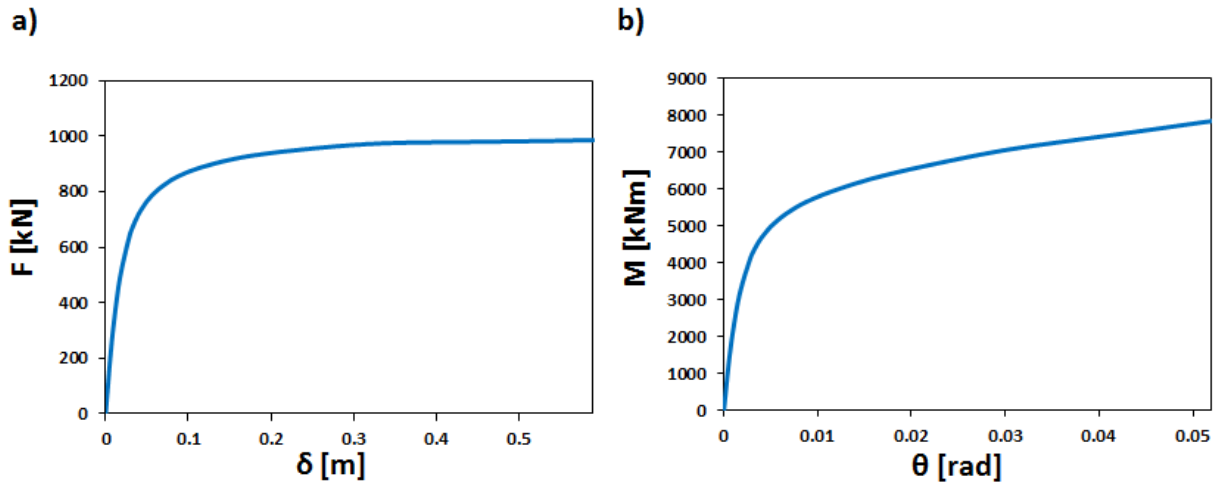

Fig. 4.28: Response of System 4 in horizontal push-over analysis **(**a) Force–deck displacement **(**b) Moment–rotation relationships.

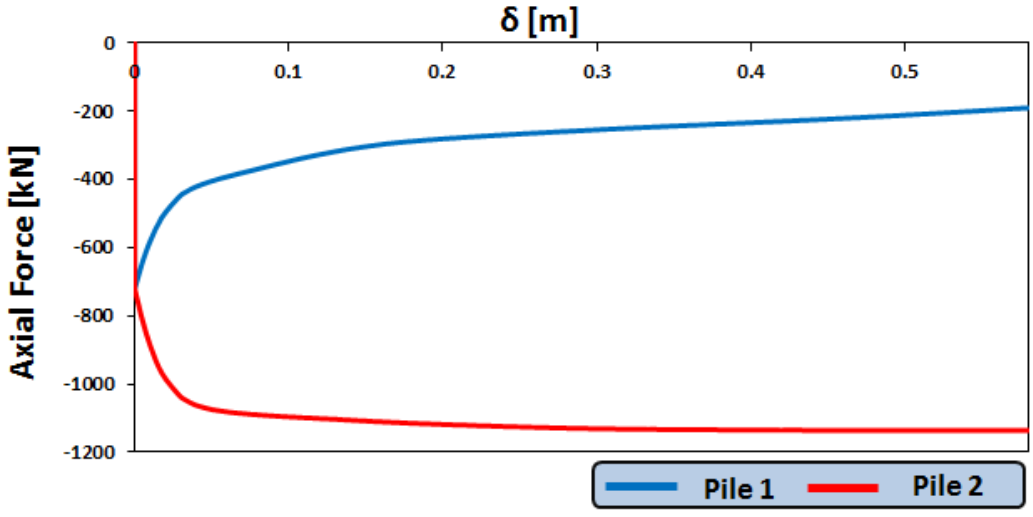

Fig. 4.29: Evolution on axial force on pile heads with deck displacement.

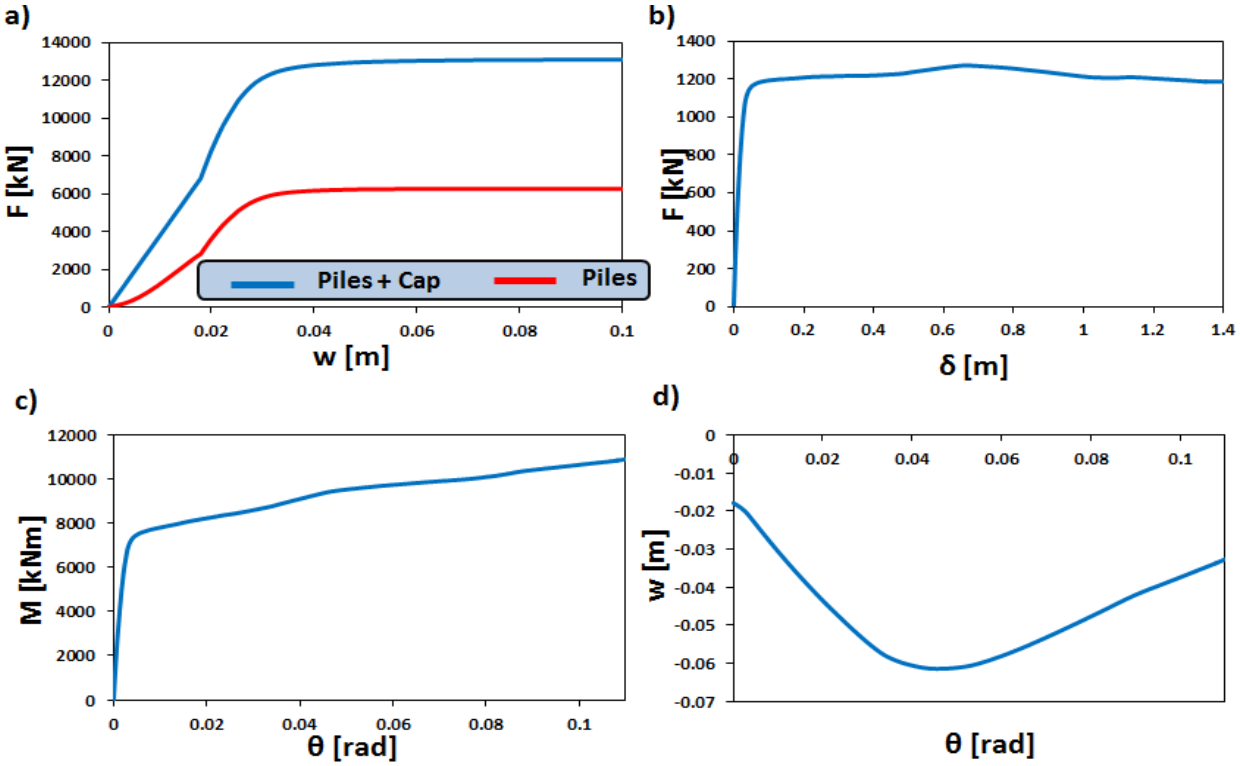

Fig. 4.30: Behavior of System 4 for α = 0.5 m. **(**a) Force–Settlement for vertical loading **(**b) Force–Deck displacement and **(**c) Moment–Rotation **(d**) Settlement–Rotation relationships for horizontal loading.

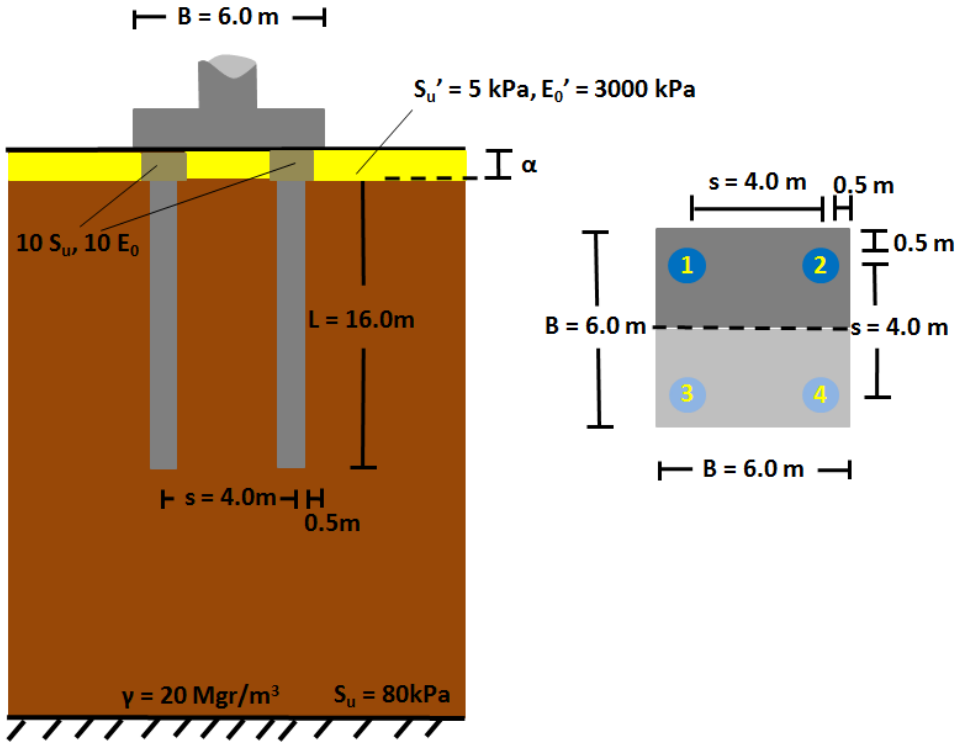

Fig. 4.31: Fifth tested system on unconnected piles. Identical with System 4 but $S_u{}^* = 10S_u$ and $E_0{}^* = 10E_0$ in the improved soil area.

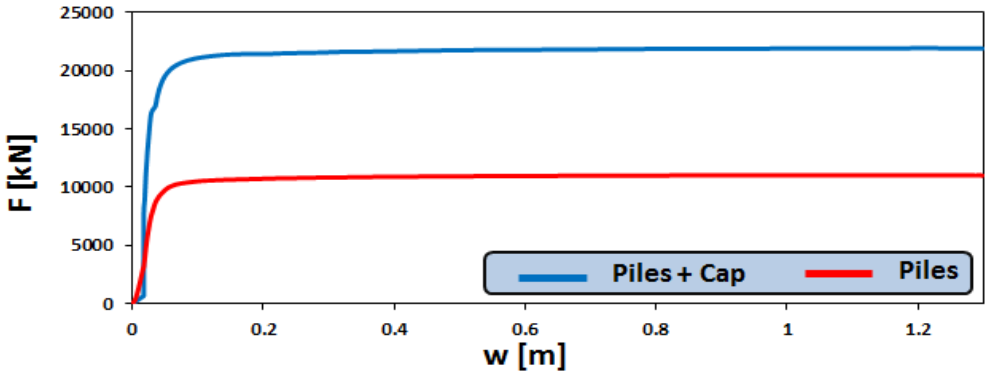

Fig. 4.32: Response of System 5 in vertical loading, for α = 1.0 m.

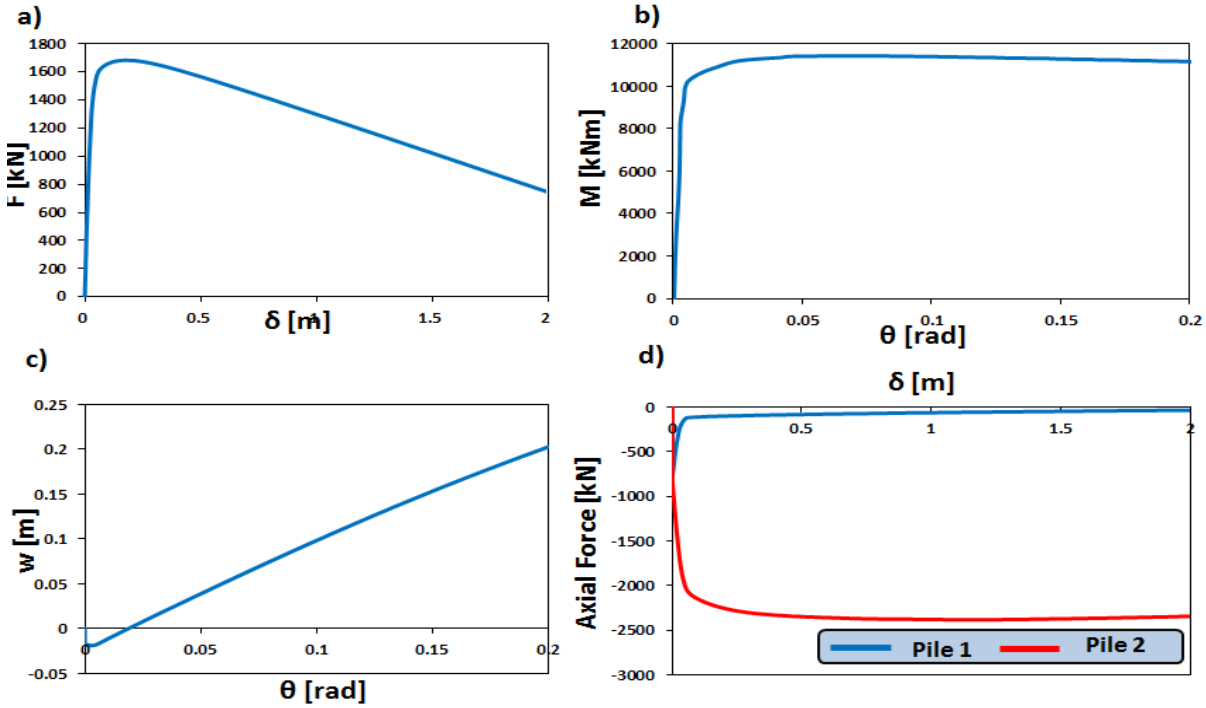

Fig. 4.33: Response of System 5 in horizontal loading, for α = 0.5 m. **(**a) Force–deck displacement **(**b) Moment–Rotation **(**c) Settlement–Rotation and **(**d) Axial load on pile heads -deck displacement relationships.

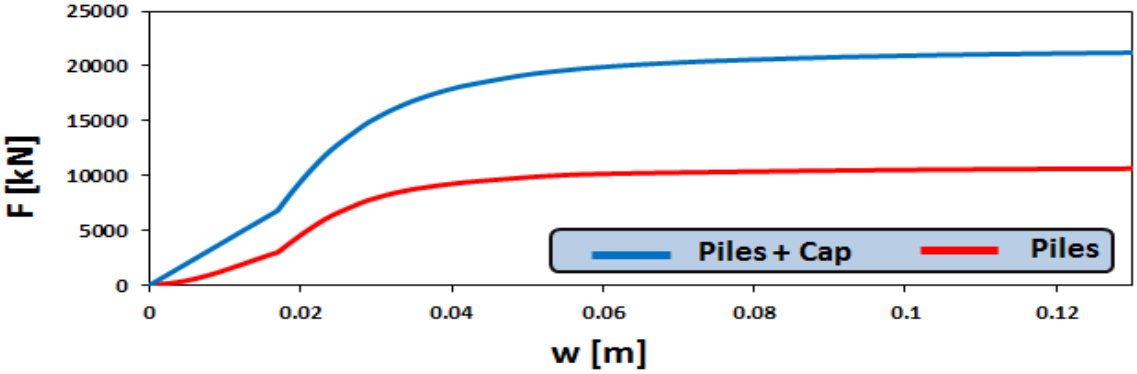

Fig. 4.34: Response of System 5 in vertical loading, for α = 0.5 m.

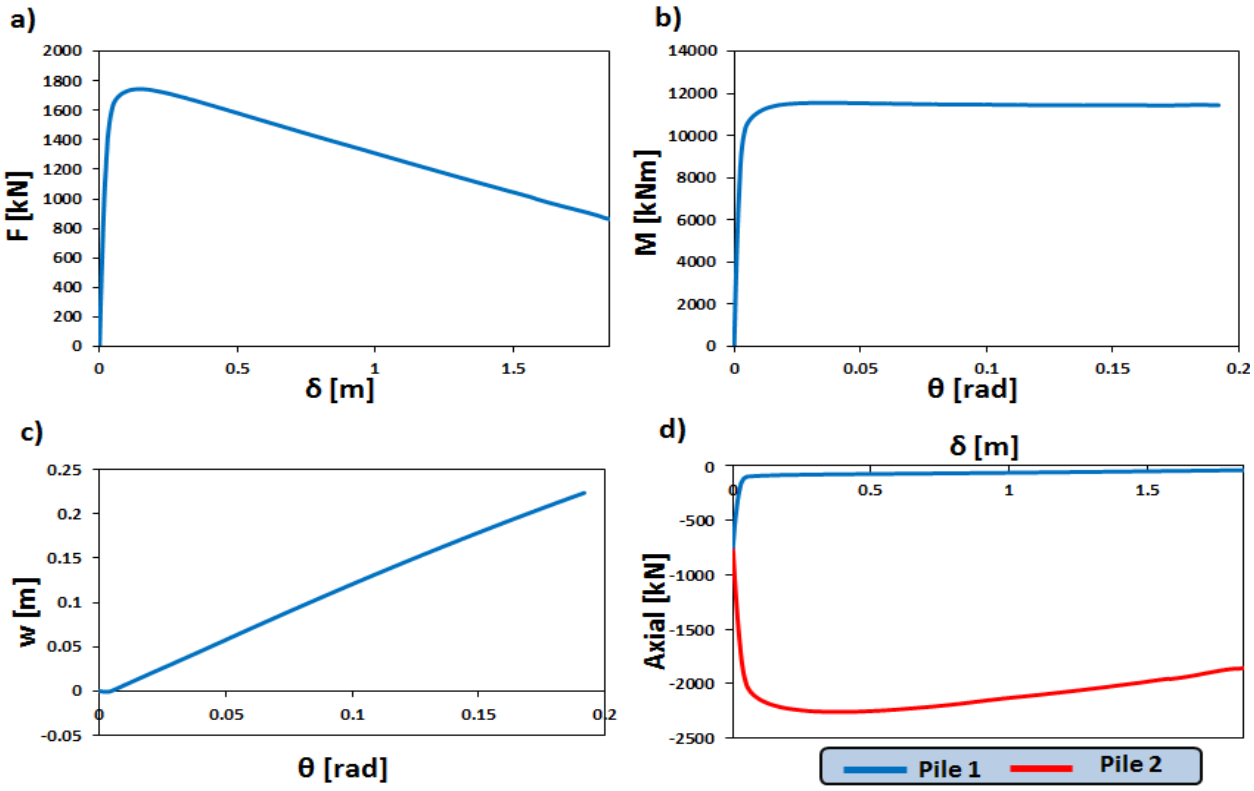

Fig. 4.35: Response of System 5 in horizontal loading, for α = 0.5 m. (a) Force–deck displacement (b) Moment–Rotation (c) Settlement–Rotation and (d) Axial load on pile heads–deck displacement relationships.

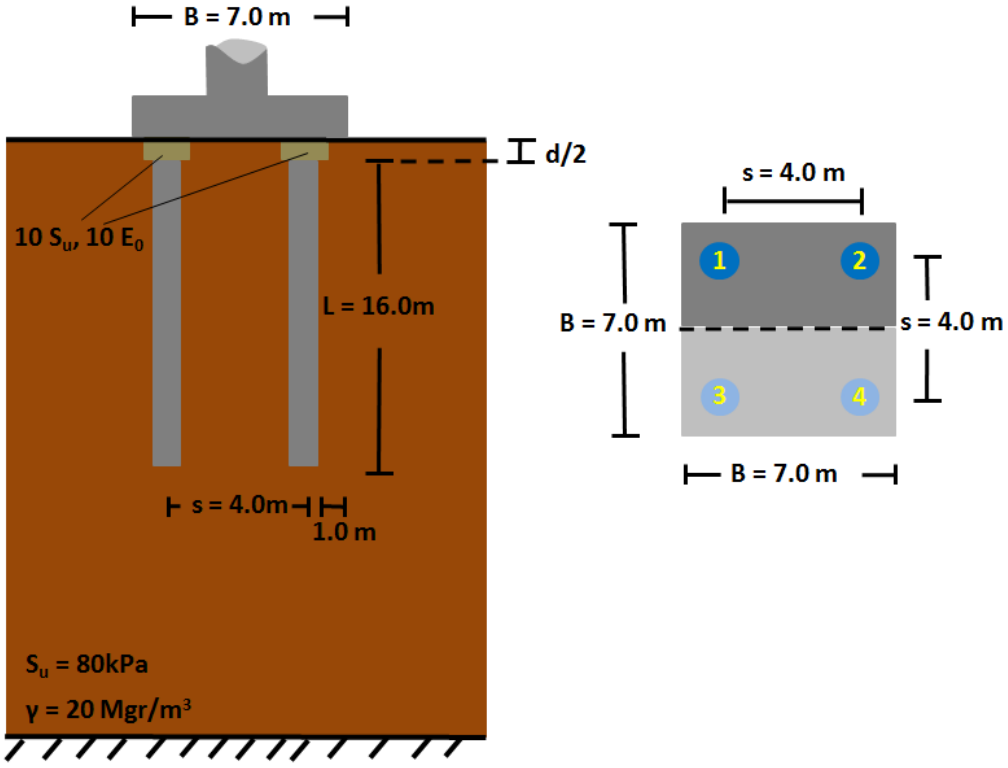

Fig. 4.36: Sixth tested design of unconnected pile foundation.

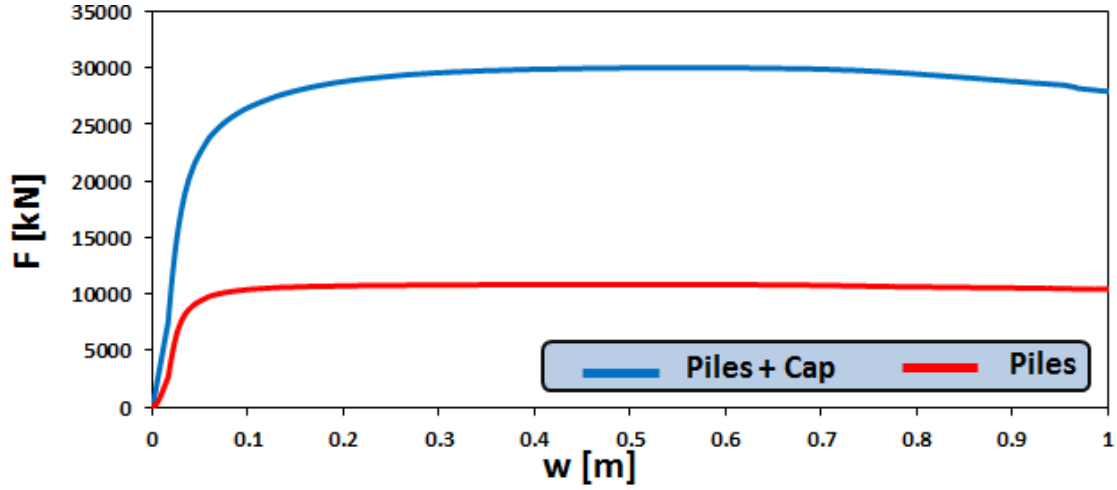

Fig. 4.37: Response of System 6 under vertical loading.

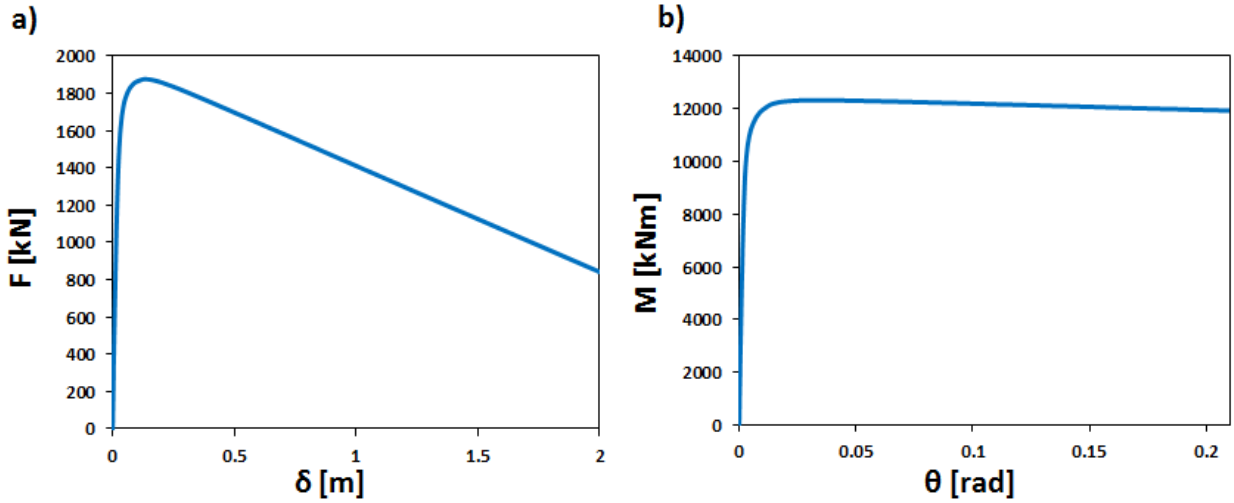

Fig. 4.38: (a) Force–deck displacement (b) Moment–rotation behavior of System 6 under horizontal loading.

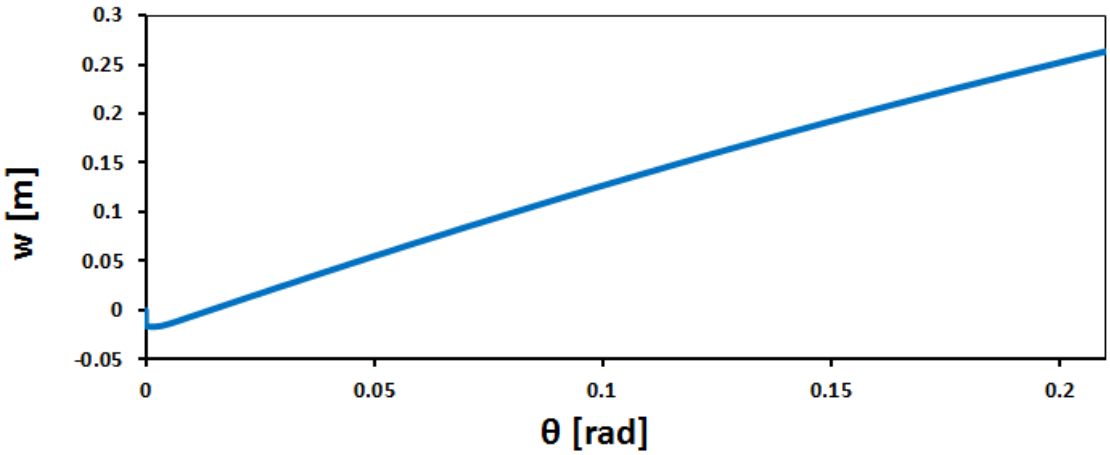

Fig. 4.39: Settlement–rotation curve showing the uplifting dominated response of System 6.

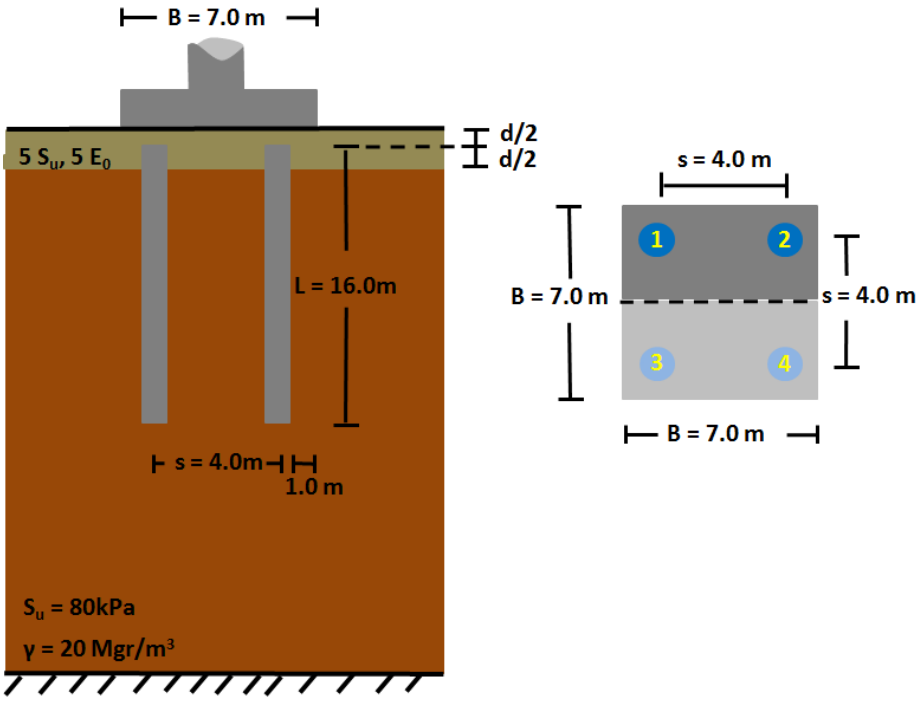

Fig. 4.40: Section and plan view of System 7.

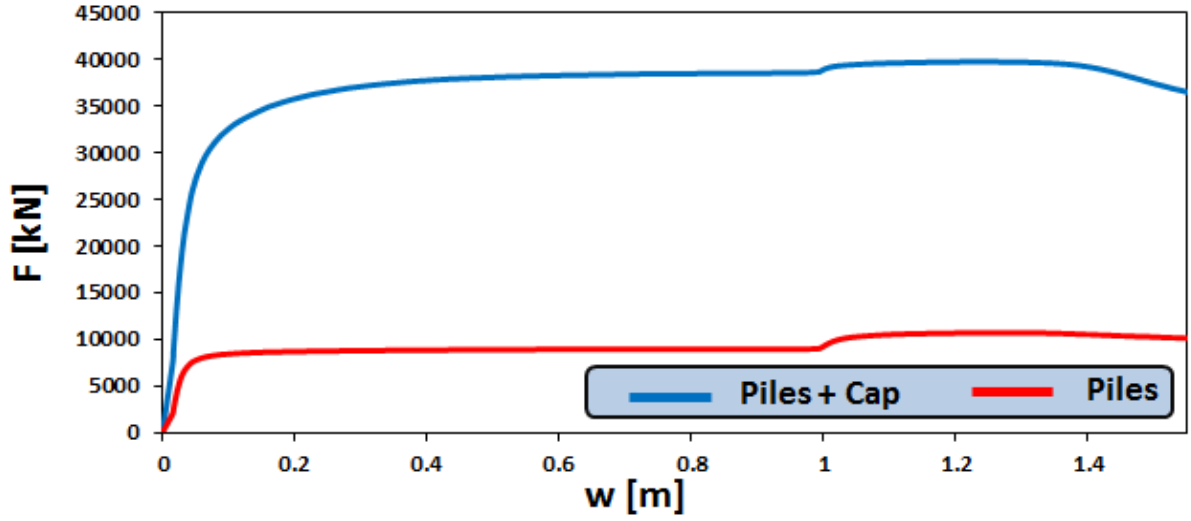

Fig. 4.41: Response of System 7 under vertical loading.

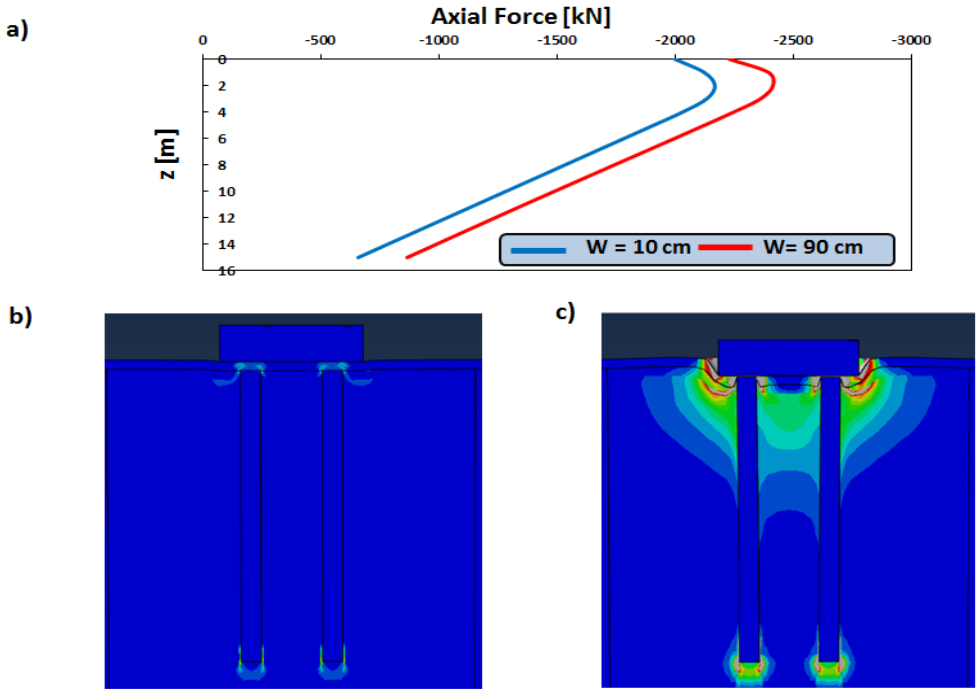

Fig. 4.42: (a) Distribution of axial forces along Pile 1. Deformed geometry and contours of plastic strains for settlement equal to (b) 10 cm and (c) 90 cm.

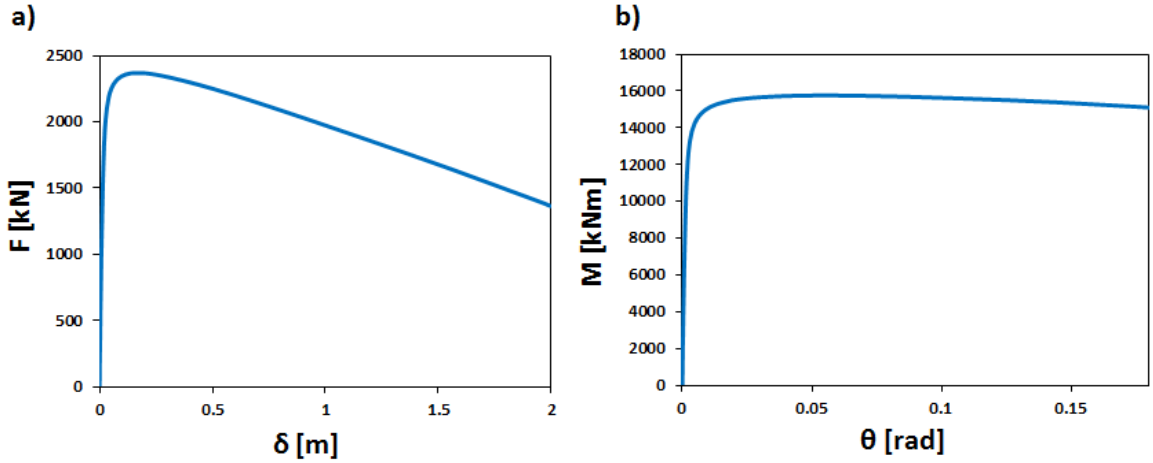

Fig. 4.43: System 7 response on horizontal loading (a) Force–deck displacement (b) Moment–rotation.

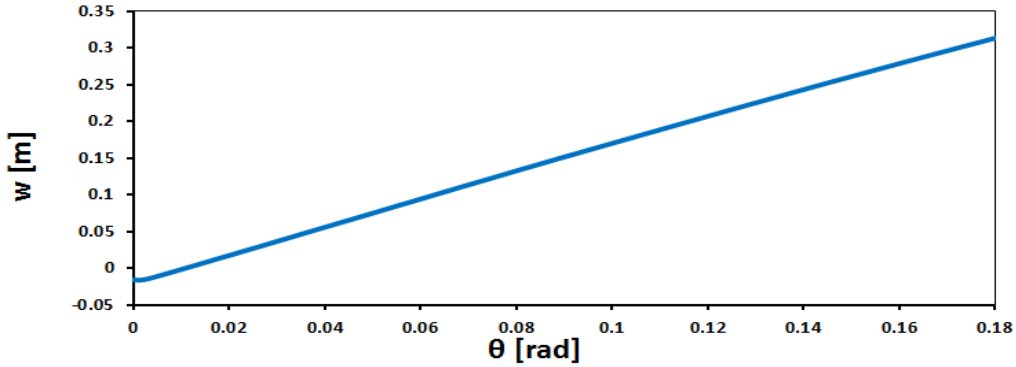

Fig. 4.44: Settlement–rotation behavior of System 7.

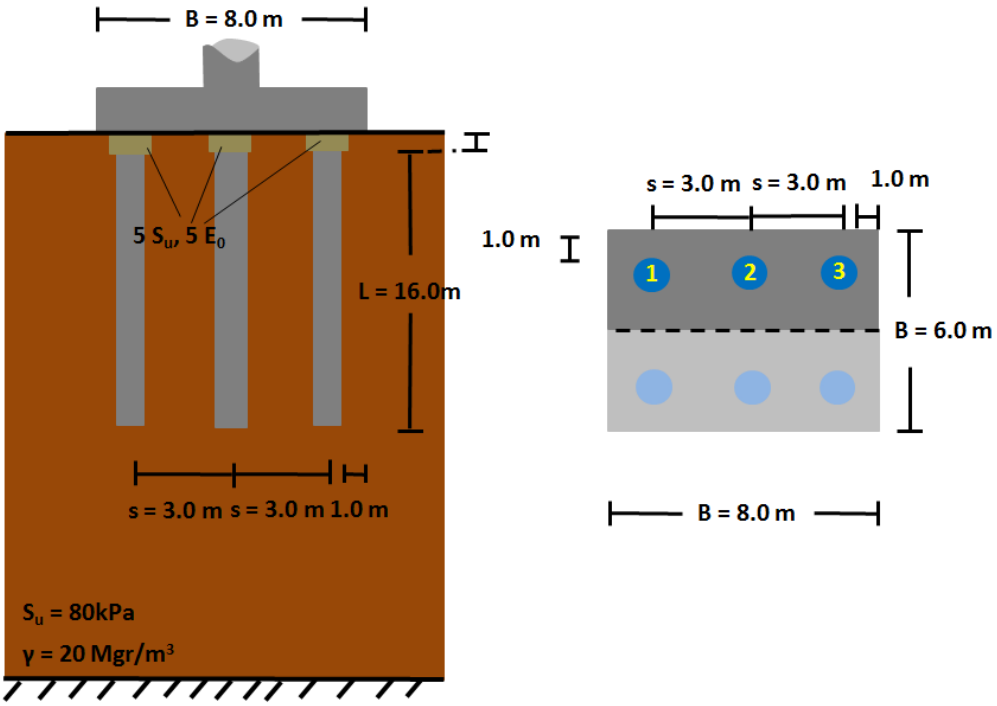

Fig. 4.45: System8 configuration consisted of a 2χ3 pile group.

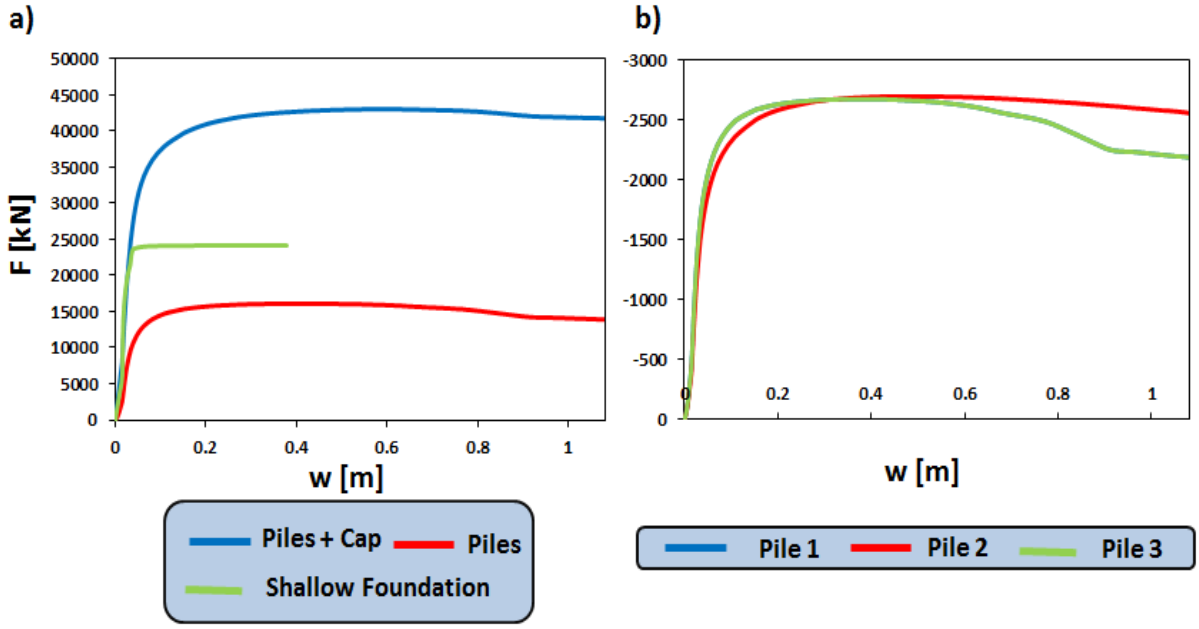

Fig. 4.46: (a) Force–settlement relationship of System 8 compared with the load received by the piles and a shallow foundation of same dimensions without unconnected piles (b) Axial load–settlement relationships of the three piles.

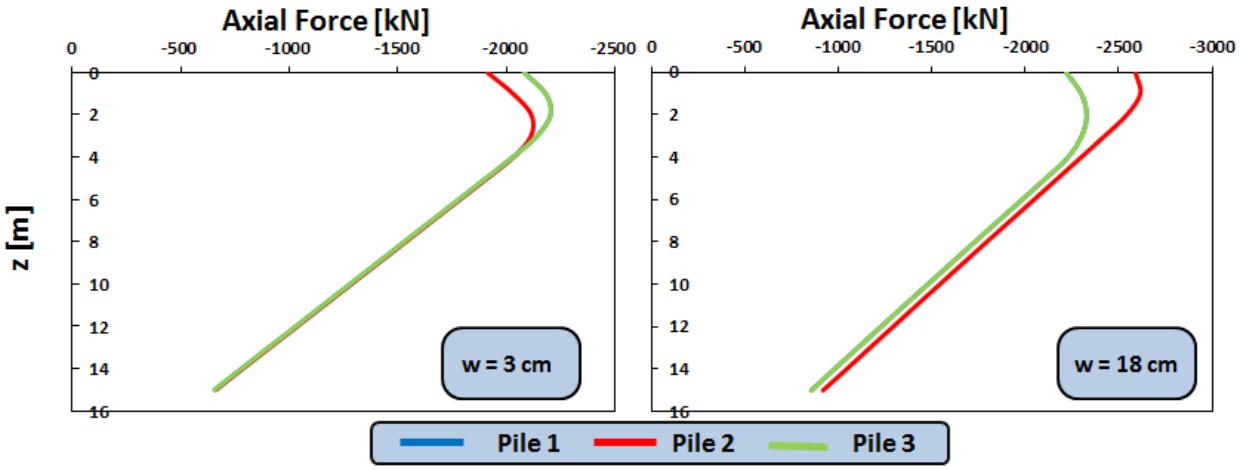

Fig. 4.47: Distribution of axial forces along the piles of System 8, in the case of vertical loading, for settlements equal to 3 and 18 cm.

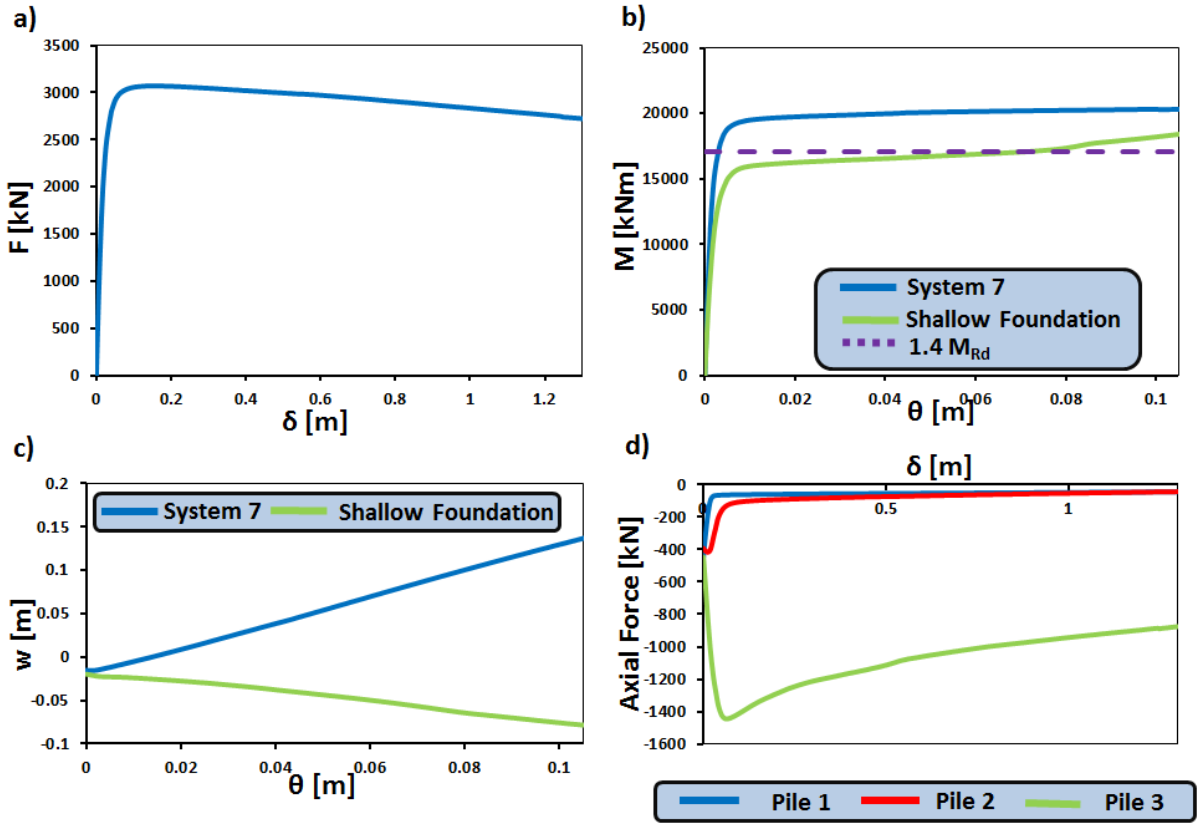

Fig. 4.48: Response of System 8 under horizontal loading and comparison with shallow foundation. (a) force–displacement (b) moment–rotation (c) settlement–rotation and d) axial force on piles–displacement relationships for the system.

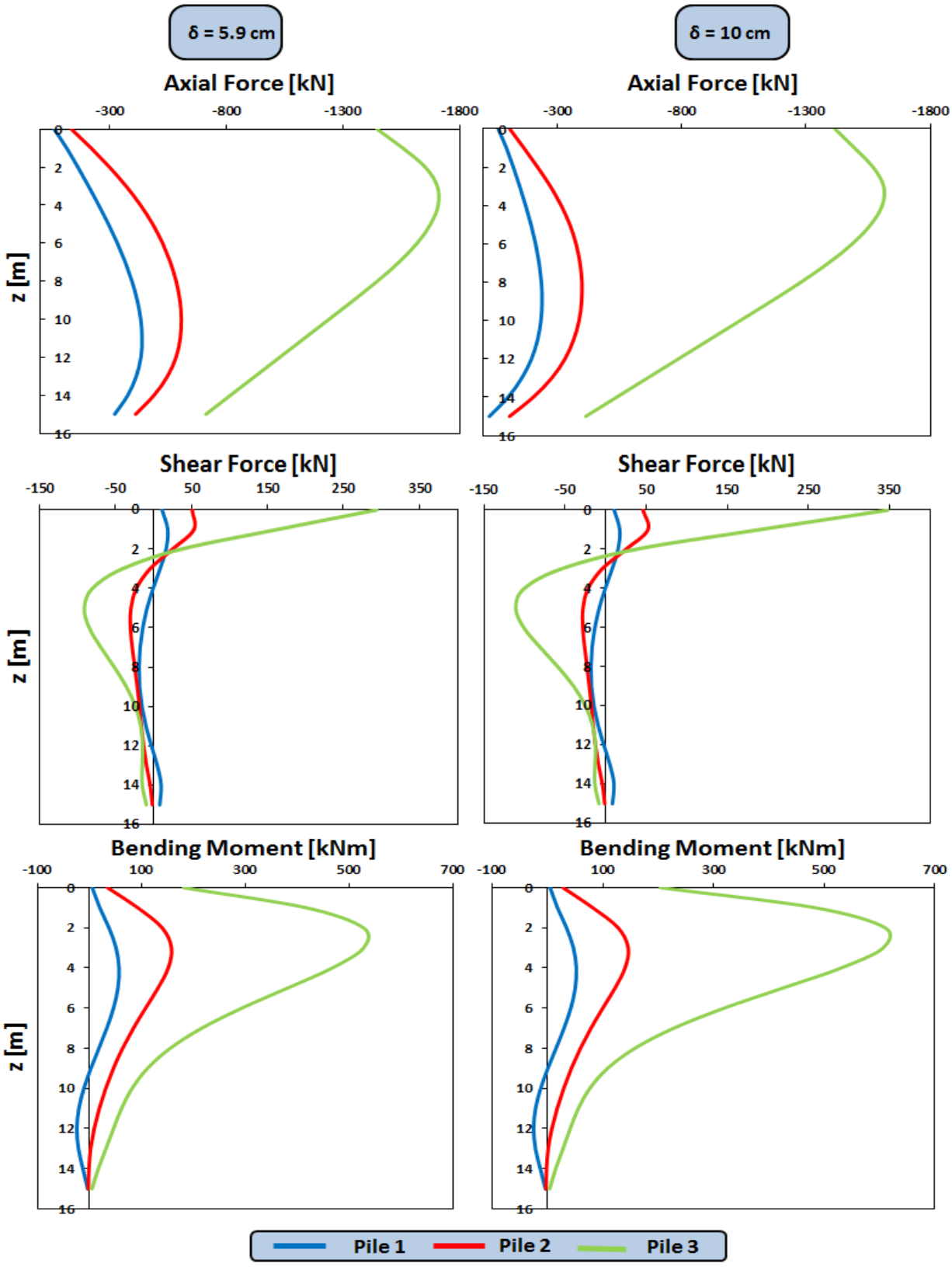

Fig. 4.49: Distribution of axial forces, shear forces and bending moments along the piles for deck displacements 5.9 cm and 10 cm.

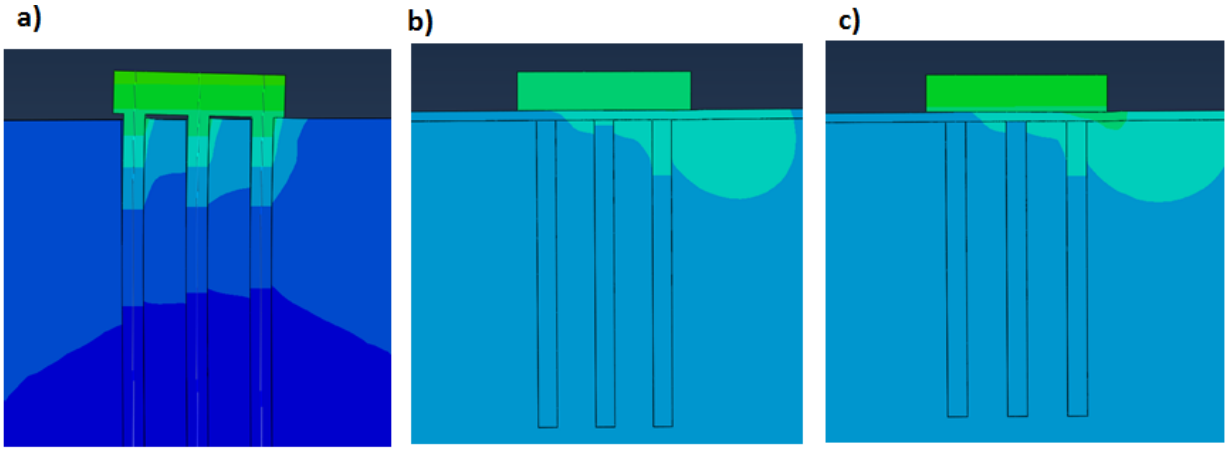

Fig. 4.50: Contours of horizontal displacements in the cases of (a) connected piles and deck displacement 10 cm (b) unconnected piles and deck displacement 5.9 cm (c) unconnected piles and deck displacement 10 cm.

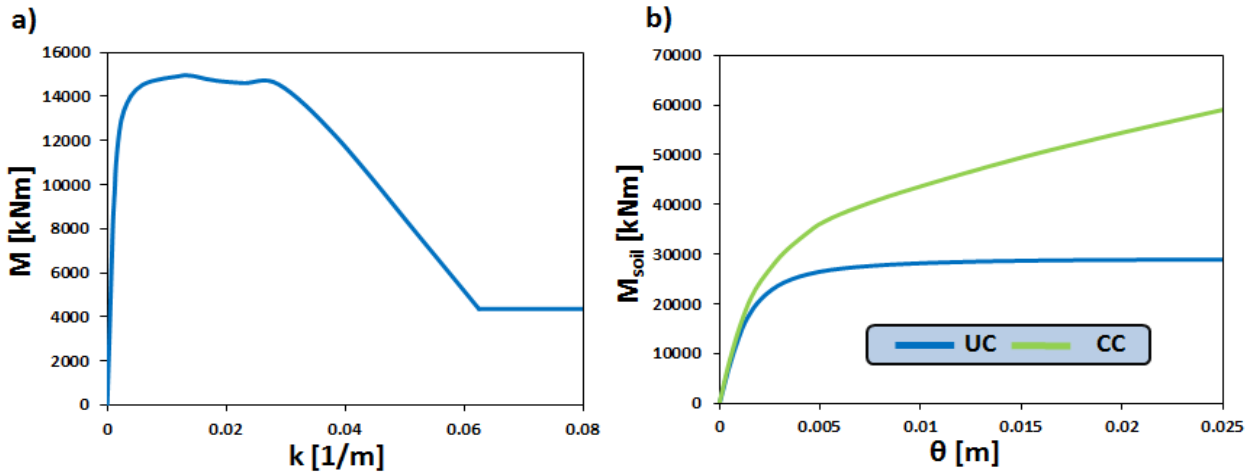

Fig. 4.51: (a) Moment–curvature relationship at the base of the pier by the horizontal push–over analysis (b) moment transmitted to the soil–rotation relationships of the two systems.

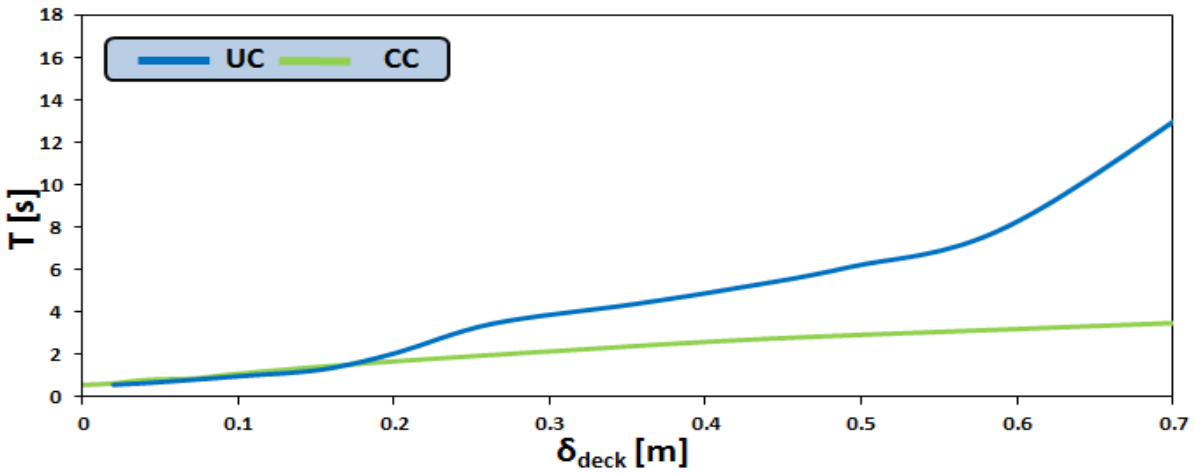

Fig. 4.52: Evolution of Fundamental period of CC and UC systems.

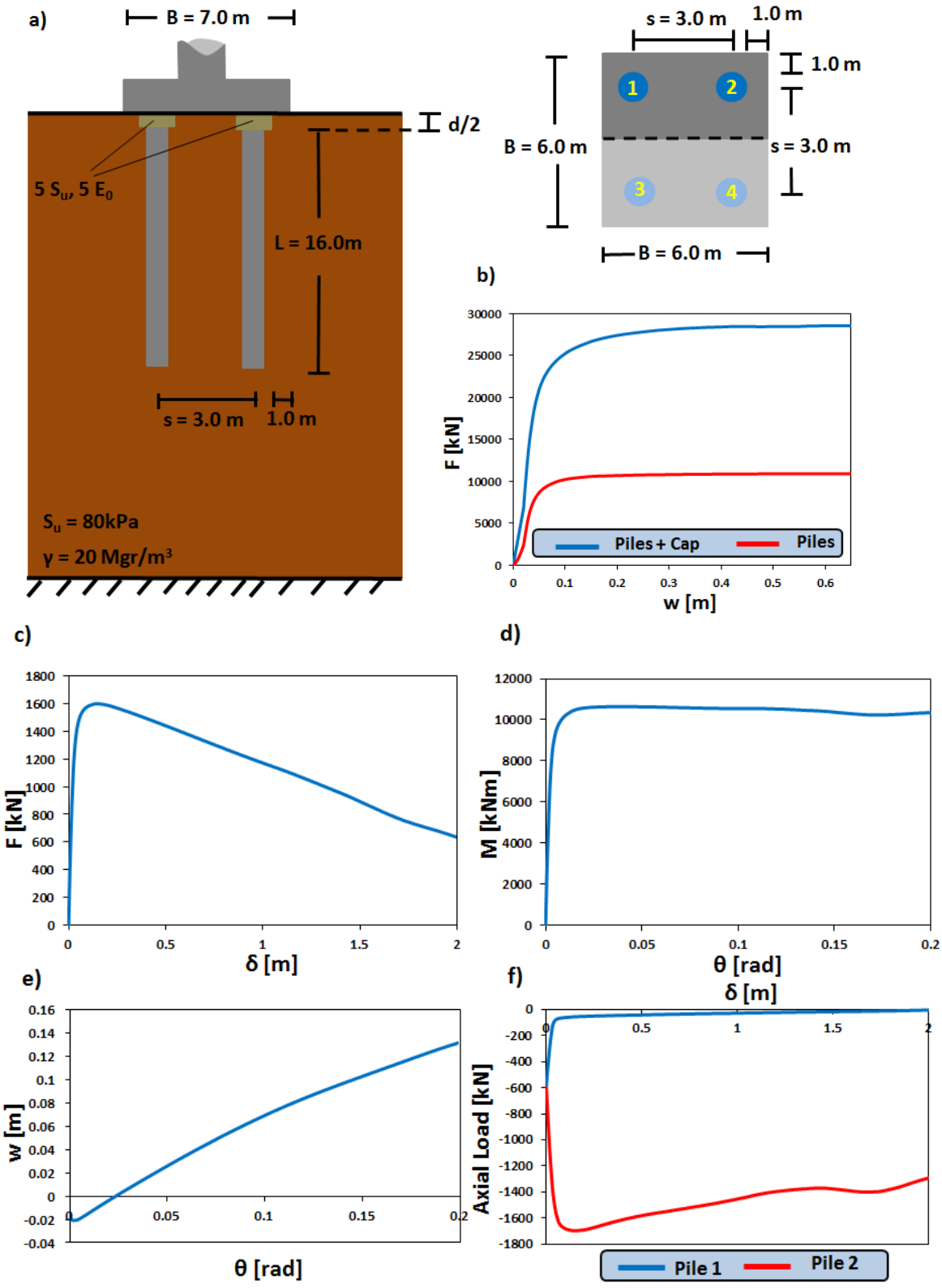

Fig. 4.53: (a) Design of first rocking foundation tested (b) its response on vertical loading and (c) force–deck displacement (d) moment–rotation (e) settlement–rotation (f) axial load on pile heads–deck displacement relationships for horizontal loading.

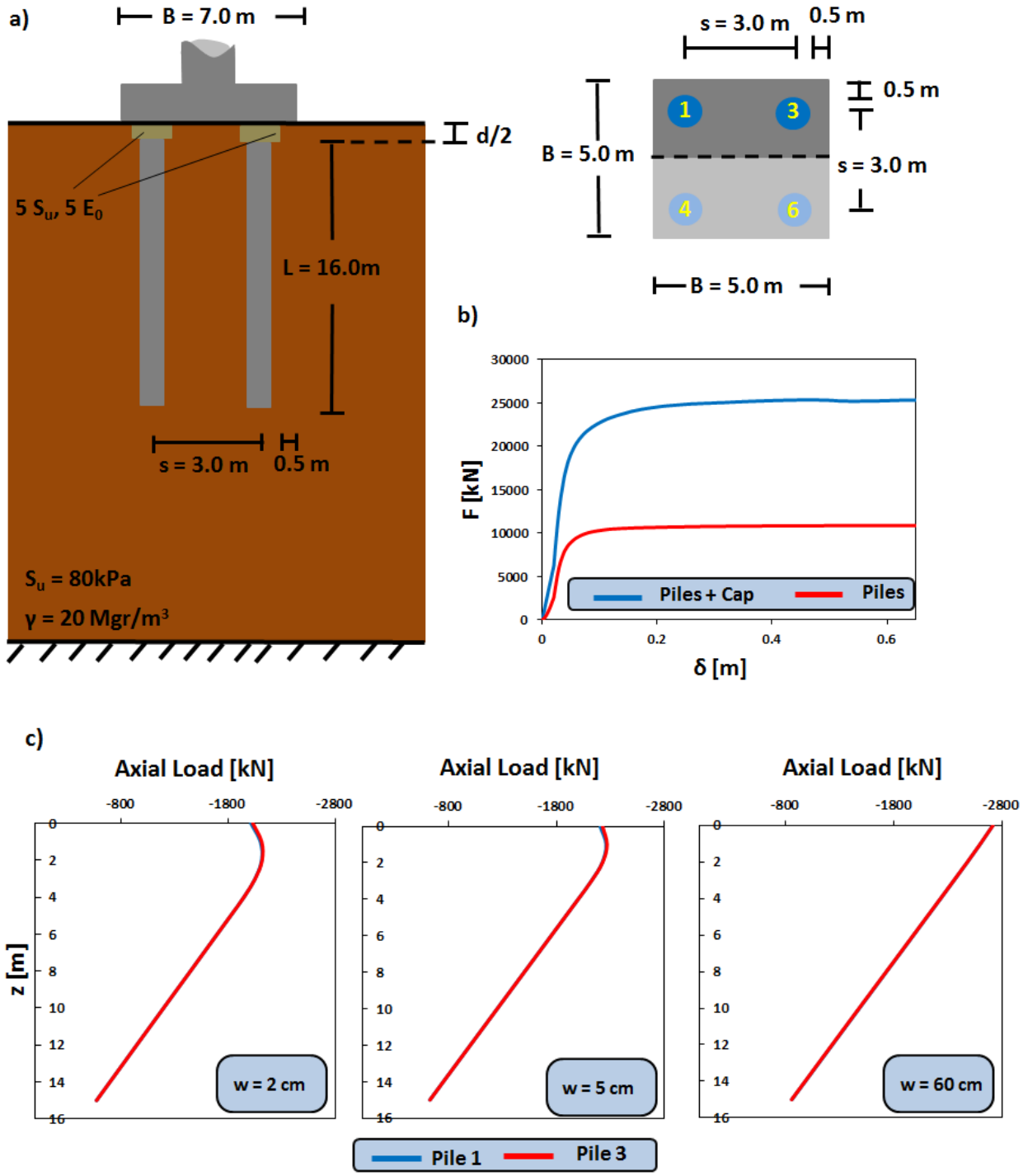

Fig. 4.54: (a) Second rocking foundation tested (b) force–settlement curve comparing the total load of the foundation with the total load of the pile heads (c) distribution of axial forces along the piles for settlements equal to 2, 5 and 60 cm.

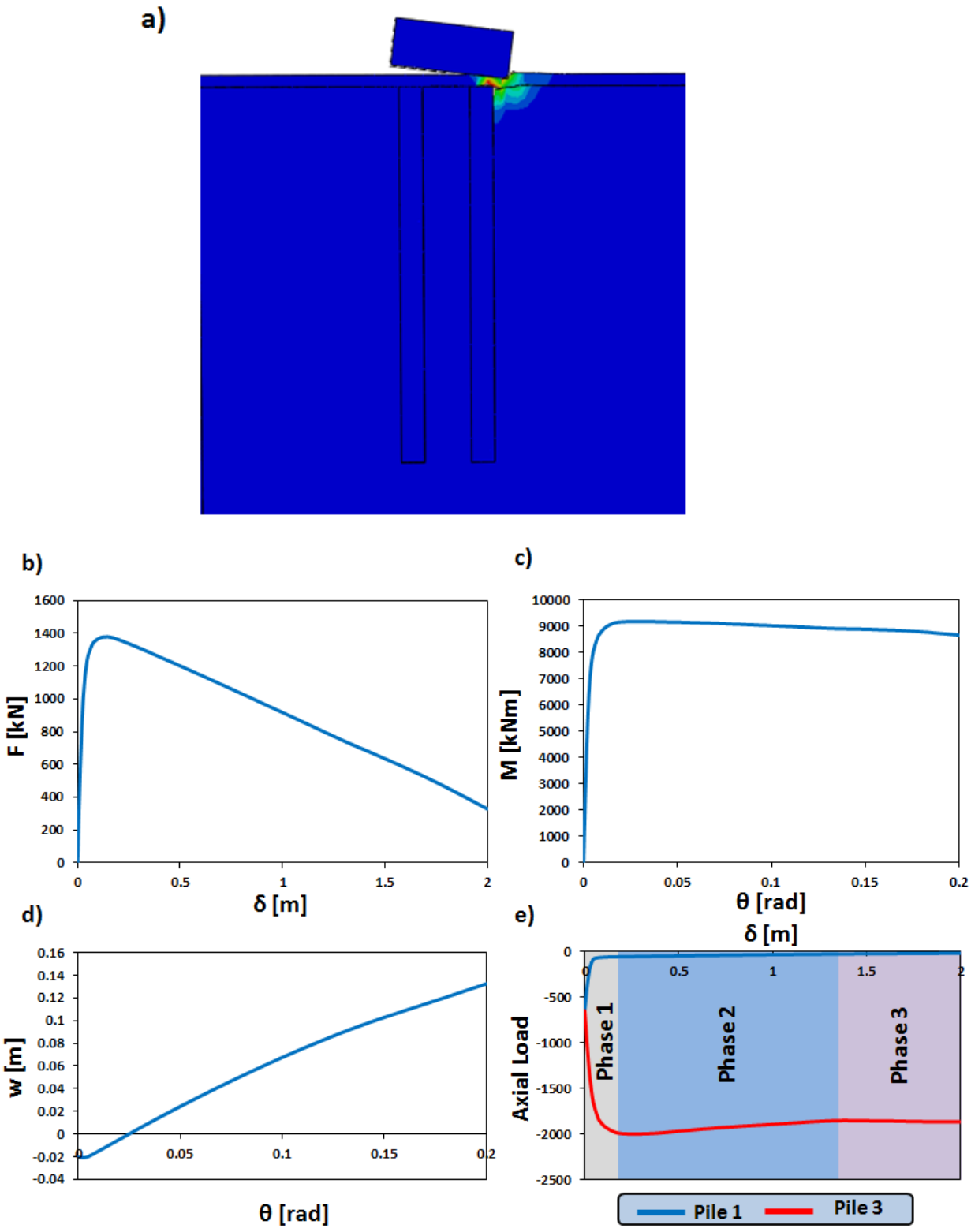

Fig. 4.55: Response of Rocking System 2 in horizontal loading. (a) Deformed geometry showing the magnitude of plastic strains (b) force–displacement (c) moment–rotation (d) settlement–rotation and (e) axial load on pile heads–displacement relationships. The latter diagram highlights the different phases of pile loading.

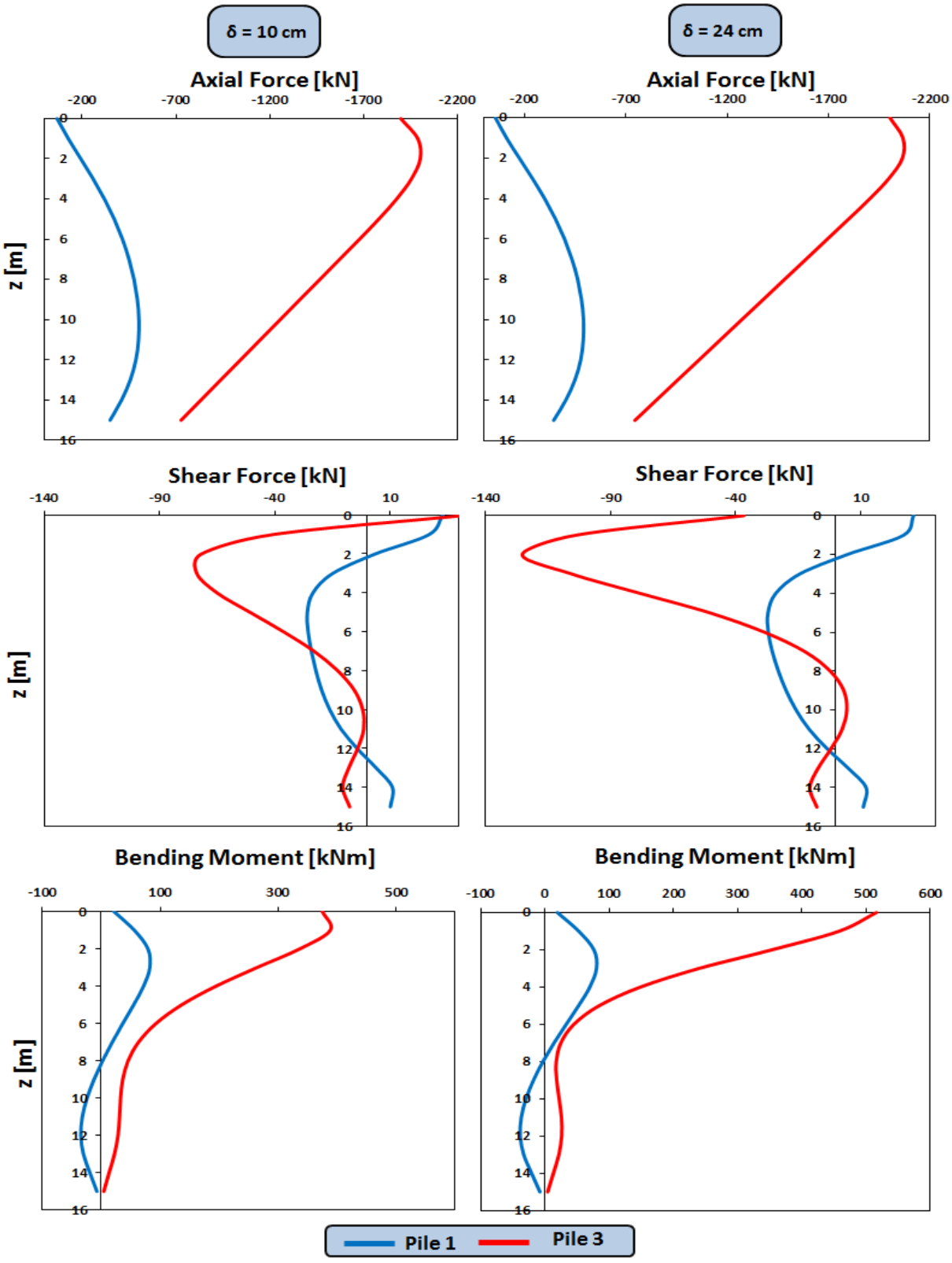

Fig. 4.56: Distribution of axial forces, shear forces and bending moments along the piles for deck displacements 5.9 cm and 10 cm.

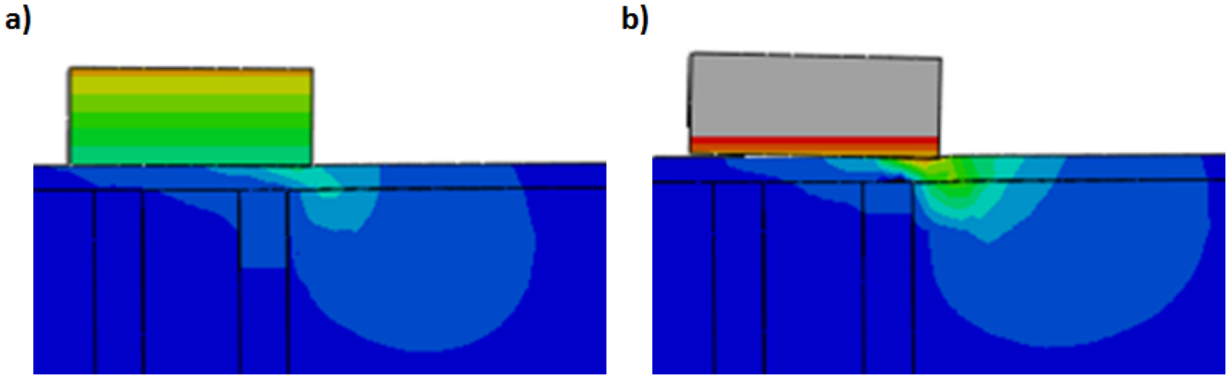

Fig. 4.57: Contours of horizontal displacements for deck displacement equal to (a) 10 cm (b) 24 cm.

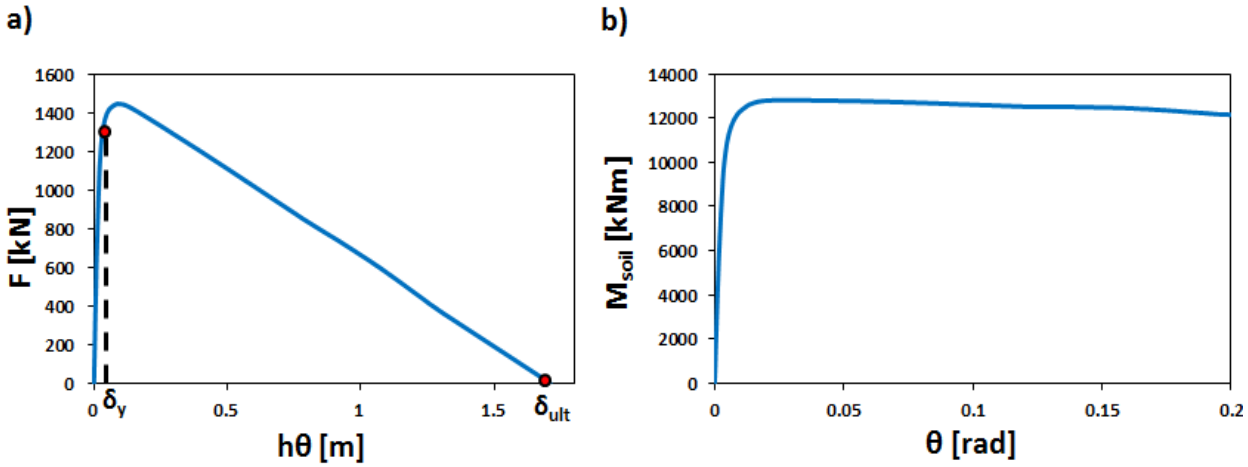

Fig. 4.58: Relationships between (a) applied force on pier top and deck displacement due to foundation rotation (b) moment transmitted to the soil and rotation of the foundation.

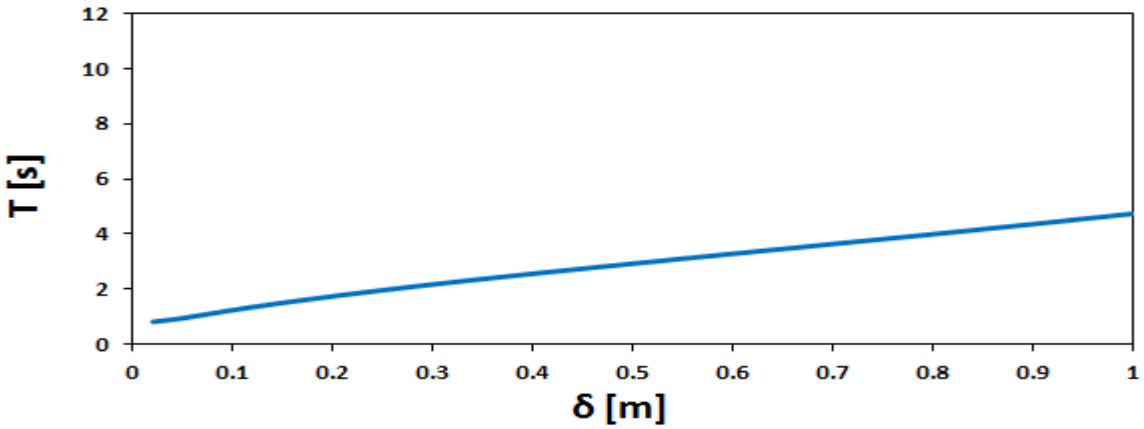

Fig. 4.59: Evolution of Fundamental period of rocking foundation.

Chapter 5

Dynamic Analysis of the Short Pier

5.1 Selected Earthquakes

In this chapter the dynamic response of the short pier supported on the three different foundations will be studied. In addition, the reasons that each system performs better or worse than the others will be discussed. In order to do so, four real earthquake timehistories, with different characteristics, were applied at the base of the model. Two of them, Kalamata (1986) and Aegion (1995), were characterized as design–level earthquakes and were fitted to the elastic design spectrum. The other two, Lixouri (2014) and Shinkobe (from the 1995 Kobe earthquake), were characterized as very strong earthquakes and were used to test the systems in earthquakes exceeding the design requirements. The four accelerograms and their elastic spectra, both in the base of the model and at the foundation level, are shown in **Figure 5.1** and **5.2** respectively. From them, amplifications at the spectral accelerations corresponding approximately to periods 1.40 s and 0.50 s can be observed. This can be explained from the natural periods of the soil:

$$T_i = \frac{4H}{(2i-1)V_s} \tag{5.1}$$

$$V_s = \sqrt{\frac{G}{\rho}} \tag{5.2}$$

where, V_s the shear wave velocity of the soil, G the soil shear modulus, H the height of the soil layer and T_i the i–th natural period of the soil layer. Hence, the first two natural periods of the studied soil layer are 0.95 s and 0.32 s. However, these equations correspond to elastic homogeneous soil; these periods increase due to soil nonlinearilty.

5.2 Dynamic Analysis of Connected and Unconnected Conventional Pile Foundations

First, a comparison between the connected and unconnected pile groups satisfying the capacity design will be presented. In order to compare the behavior of the two systems it is important to note the three different components of the total deck displacement. As shown in **Figure 5.3**, the total deck displacement, δ, consists of the displacement of the base, δ_b, the rigid body displacement from the rotation of the pile cap, $\delta_r = h\theta$, and the structural deformation of the pier, δ_s.

Dynamic analysis of the two systems was performed on Abaqus and the results of Shinkobe excitation are presented in here while the rest are presented in **Appendix A**. **Figures 5.4 – 5.10** present and compare the results of the earthquake excitations of the two systems. It can be observed that the acceleration of the pile cap is reduced in UC system compared to CC. As it was discussed in the introduction, disconnecting the piles from the pile cap can reduce the transmitted acceleration to it. In addition from the base shear–displacement diagram it can be seen that at about 2000 kN there is a gradual stiffness deterioration. This is due to the sliding of

the pile cap, which also limits the accelerations. In both cases the base acceleration is able to excite the structure enough for it to develop its maximum moment capacity. Thus, the deck accelerations of the two systems are essentially the same, with a cut–off value equal to $a_{max} = \frac{M_{pier,ult}}{hm} \approx 0.45\ g$. Equal moments develop at both pier bases, however the moment–curvature curves show a slight reduction of curvature demand in the system with unconnected piles resulting from rotational compliance of the foundation. This is explained by the reduction of rotational stiffness when piles are disconnected form the pile cap, as it was discussed in **Chapter 4**.

The displacement timehistory of the pile cap shows reduction of residual displacement of the pile cap with unconnected piles. In the UC case this displacement is due to sliding, while in the CC the plasticization of the soil around the piles leads to a permanent horizontal displacement. As expected, from what was previously discussed, the rotations of UC are greater leading to greater hθ. However, the moments transmitted to the soil are significantly smaller than the capacity of the foundation and so these rotations are mostly elastic ones not leading to permanent rotations. From the moment–curvature relationship it was expected that the structural deformations of the pier supported on unconnected piles will be reduced, something that is proven from its timehistory (**Figure 5.6 (c)**). In total, the deck displacement of the unconnected system is reduced compared to the conventional one. More importantly, there is a 30% reduction of the residual deck displacement. The beneficial role of foundation's flexibility is also reflected on the timehistory of ductility demand over ductility capacity of the pier, where this ratio is always small for UC.

Another very positive outcome is that settlements have not increased in UC. From the settlement–rotation curve some uplifting of the foundation is observed. In contrast the conventional foundation with connected piles to the pile cap has a pure sinking response. This difference is what makes both systems to perform equally well in terms of settlements. It is believed that if UC had a sinking response instead of an uplifting one its settlements would have been larger that CC's due to large plastification of the soil under the pile cap. It is interesting to note in **Table 5.1,** that summarizes the response of the two systems in eight important parameters, that only in the two larger earthquakes UC's settlements are smaller or equal. In the design–level earthquakes its settlements are slightly larger than CC's because the foundation's rotations are smaller and uplifting does not appear. **Figure 5.10** shows the settlements of the soil and the pile cap in the case of unconnected piles at the end of the excitation and at the time where the moment transmitted to the soil takes its maximum value. It is interesting to note that above the pile heads the settlement of the soil is reduced compared to the surrounding soil. It will be proven in the next paragraph that this behavior is very important in the rocking foundations on top of unconnected piles.

Figure 5.9 shows the distribution of axial forces, shear forces and bending moments along Piles 1, 2 and 3 and their maximum value, at the moment when the maximum moment is transmitted to the soil. In the unconnected piles the maximum axial force

is reduced 45% compared to the connected piles. As in the case of monotonic loading this maximum value is not developed on the head of the pile due to negative skin friction from the relative settlements between the soil and the piles. The interaction between the piles can be observed by the increasing with depth axial force on Pile 1. The shear forces and bending moments on the unconnected piles are significantly smaller, with their maximum values reduced by 84% and 61% respectively. Bending moment is developed on the compressed pile's head due to the eccentric loading of the overlaying soil, as explained in **Chapter 4**.

Table 5.1: Results of dynamic analysis in each earthquake of the two systems. Compared in eight parameters: residual deck displacement, residual pier deformation, maximum ratio of ductility demand over ductility capacity in terms of displacement and curvature, total settlement, maximum developed axial force, shear force and bending moment on the piles.

	KALAMATA		AEGION		LIXOURI		SHINKOBE	
	CC	UC	CC	UC	CC	UC	CC	UC
Residual U_{top} (m)	0.035	0.015	0.050	0.045	0.090	0.070	0.100	0.075
Pier Deformation (m)	0.025	0.010	0.045	0.040	0.080	0.066	0.090	0.070
$(\mu_{demand}/\mu_{capacity})_{\Delta}$	0.32	0.23	0.44	0.37	0.68	0.67	0.72	0.59
$(\mu_{demand}/\mu_{capacity})_{r}$	0.17	0.12	0.39	0.37	0.54	0.65	0.73	0.70
w (cm)	3.0	3.0	2.5	2.5	7.5	6.5	5.5	5.5
max Pile Axial (kN)	2433	1521	2361	1401	2413	1355	2544	1407
max Pile shear (kN)	490	269	568	175	638	250	656	104
max Pile Moment (kNM)	624	456	757	292	1021	527	1117	433

In **Table 5.1** the performance of both systems in the four earthquakes is summarized. The key goal of unconnected pile foundation was to reduce the stresses on the piles in order to avoid failure under strong earthquakes. From the above analyses it is concluded that this is achieved. This reduction is not as great in the other earthquakes as it was in Shinkobe excitation, which was meticulously analyzed, but it is still satisfying. Furthermore, there is slight improvement in all the other factors, including settlements. In addition, in Lixouri earthquake the maximum ratio of ductility demand to ductility capacity is increased compared to the conventional system with connected piles, but, as it was only observed in one earthquake, this is characterized as a random result due to the specific acceleration timehistory.

5.3 Dynamic Analysis of Unconnected Conventional and Rocking Pile Foundations

The foundation with unconnected piles designed with the factors of safety of current codes proved to both satisfy its goal to reduce stresses on the piles and perform slightly better than the conventional pile group under seismic loading. Hence, in this chapter its behavior will be compared with the rocking foundation on top of unconnected piles.

Figures 5.11 – 5.18 show the response of the two systems under Lixouri earthquake while the responses in the rest earthquakes are presented in **Appendix A**. Due to the large rotations of the rocking system, 2 extra seconds of free oscillation were allowed in order to predict the residual values of each parameter more accurately.

In the rocking foundation the accelerations on the structure are bounded by the moment capacity of the foundation. This can be observed by their timehistories. The deck acceleration has a cut-off value $a_{max} = \frac{M_{f,ult}}{hm} \approx 0.28\, g$. The maximum moments on the base of the pier are also limited leading to a completely elastic response of the pier. On the other hand, highly inelastic response is observed at the foundation level. From the foundation moment–rotation response it is observed the foundation reached its capacity. This also led to a plateau of the base shear.

The displacement timehistories show that the horizontal displacement at the top of the pile cap has larger both maximum and residual values for the rocking foundation. It should be noted that the pile cap displacements are not only due to sliding but also due to rotation of the pile cap. From the highly inelastic behavior of the foundation larger rotations are developed leading to significant deck displacements hθ, with a maximum value of 28 cm and residual 3.5 cm. These are notable larger than those of the conventional system. On the other hand, as the pier remains elastic, the deck displacement due to structural deformations is minimal, remaining smaller than 1 cm. The total deck displacement took a maximum value of 12 cm in the conventionally designed foundation, while the same value was 38 cm for the rocking foundation. The residual deck displacement however, has less than 1 cm deviation between the two systems.

The conventional system demands 65% of its capacity while the rocking system only 15%, proving that the margins of safety against collapse are greatly increased.

The price to pay, when using such a system, is the larger settlement. Despite the significant uplifting of the rocking foundation, its settlement is 12 cm at the end of the excitation, twice that of the conventional system. **Figure 5.18** tries to explain the main reasons of this. Firstly, in the rocking foundation the soil under the pile cap develops large plastic deformations. This leads to permanent settlements. It is interesting to note that soil plastification mainly takes place above the piles, where soil is improved, and towards the corners of the pile cap. In addition as it was also observed in the conventional system with unconnected piles in an area above the

piles the settlement of the soil was reduced compared to the surroundings. This is also the case in UR but now the differential settlement between the head of the pile and the pile cap is quite large. Hence, two possible ways to reduce the settlement are either to use improved soil in a layer below the pile cap, and not just in areas above the piles, or have a smaller distance between the piles and the pile caps. Of course, these should be tested in order to confirm whether they improve the behavior.

From the same figure the main difference of the two systems can be observed. In UC plastic deformations develop on the superstructure but are minimal in the soil, while in UR, the pier remains elastic but excessive soil plastification develops under the footing.

Table 5.2: Results of dynamic analysis in each earthquake of the two systems. Compared in seven parameters: residual deck displacement, residual pier deformation, maximum ratio of ductility demand over ductility capacity in terms of displacement, total settlement, maximum developed axial force, shear force and bending moment on the piles.

	KALAMATA		**AEGION**		**LIXOURI**		**SHINKOBE**	
	UC	**UR**	**UC**	**UR**	**UC**	**UR**	**UC**	**UR**
Residual U_{top} (m)	0.015	0.080	0.045	0.005	0.070	0.075	0.075	0.065
Pier Deformation (m)	0.01	0.005	0.040	0.002	0.065	0.005	0.070	0.005
$(\mu_{demand}/\mu_{capacity})_{\Delta}$	0.23	0.14	0.37	0.09	0.67	0.16	0.59	0.14
w (cm)	3.0	7.0	2.5	5.5	6.5	11.0	5.5	11.5
max Pile Axial (kN)	1521	2169	1401	2078	1355	1897	1407	2261
max Pile shear (kN)	269	94.5	175	138	250	99.0	84	146
max Pile Moment (kNM)	456	578	292	402	527	817	244	621

Fig 5.17 shows the distribution of forces and moments along the piles when the maximum moment is transmitted to the soil. Since the participation of the piles in the moment resistance of the foundation is increased, their axial forces are also increased. In addition larger bending moments are developed on the piles of the rocking foundation despite the smaller shear forces on them. As it was previously discussed, the eccentric loading of the compressed pile leads to bending moments and rotations on its head. Both shear forces and bending moments are still smaller than on the connected piles.

Table 5.2 the responses of both systems in the four earthquakes are summarized. Since, the pier on rocking foundation remains elastic ductility in terms of curvature does not have any meaning and is not included in this table. Both negative and

positive characteristics of rocking foundation on top of unconnected piles are observed. First of all, the margins of safety against collapse are significantly increased for the rocking system, with its ductility demand over ductility capacity remaining smaller than 16% in all earthquakes. In most cases, except Kalamata, the residual deck displacement does not vary importantly between the two systems while the pier deformation of the rocking system is greatly decreased. However, under all excitation the maximum deck displacement of UR highly exceeds that of UC. Another price to pay in order to achieve rocking isolation is the increase of settlements and stresses on the piles.

Figures of Chapter 5

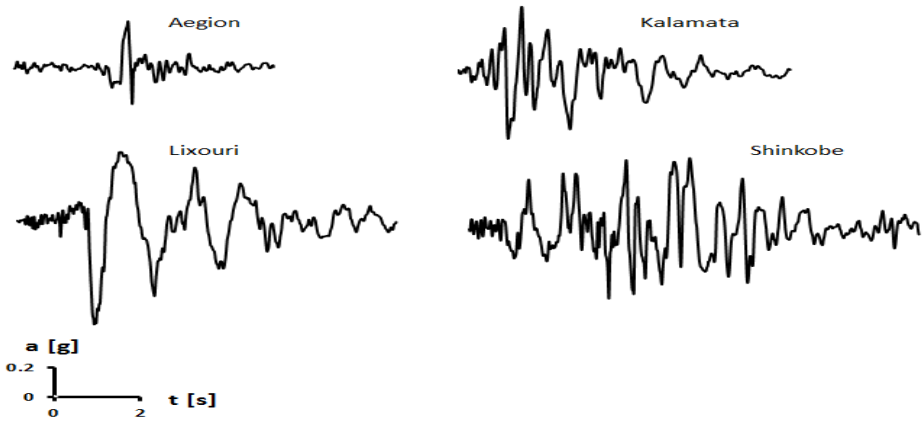

Fig. 5.1: Real earthquakes used for the dynamic analysis of the three systems. Aegion and Kalamata fitted to design spectrum.

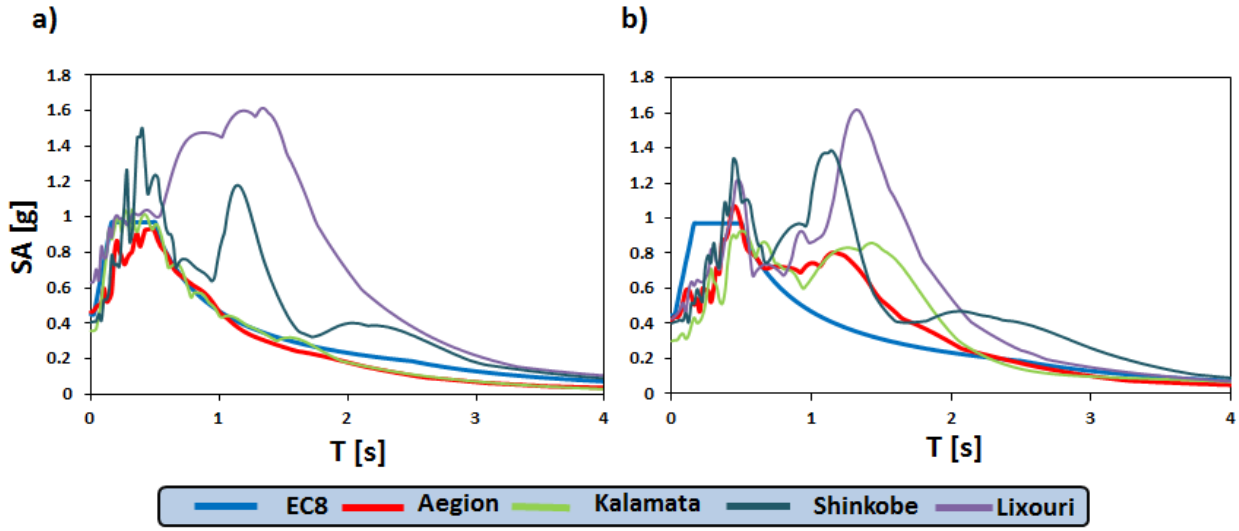

Fig 5.2: Response spectra of the used accelerograms compared to design response spectrum at (a) base of the model (b) free field.

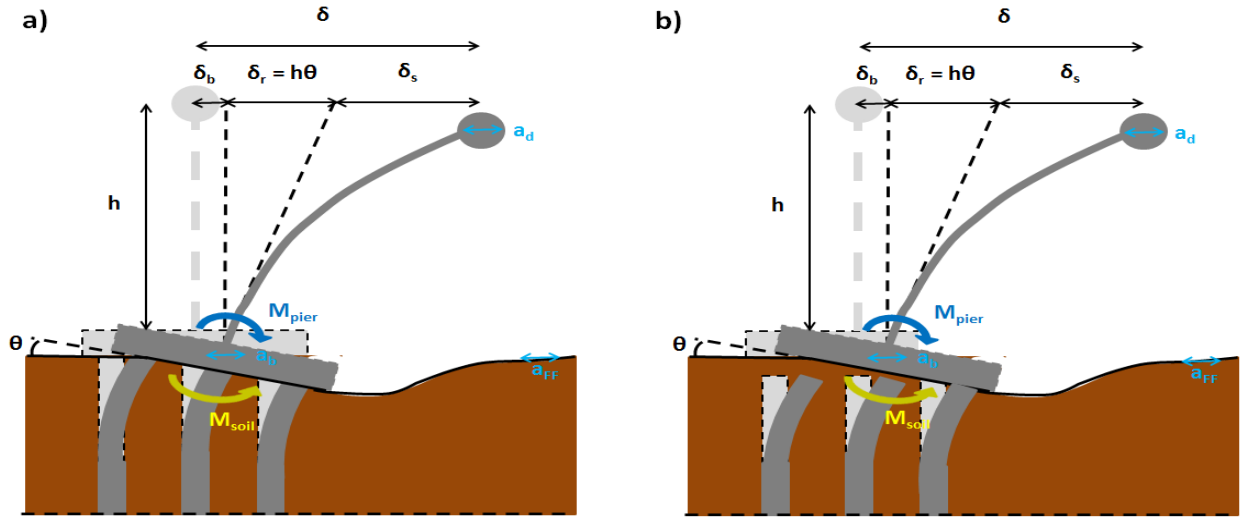

Fig. 5.3: Positions of recorded accelerations and components of the total deck displacement in the case of (a) connected piles (b) unconnected piles.

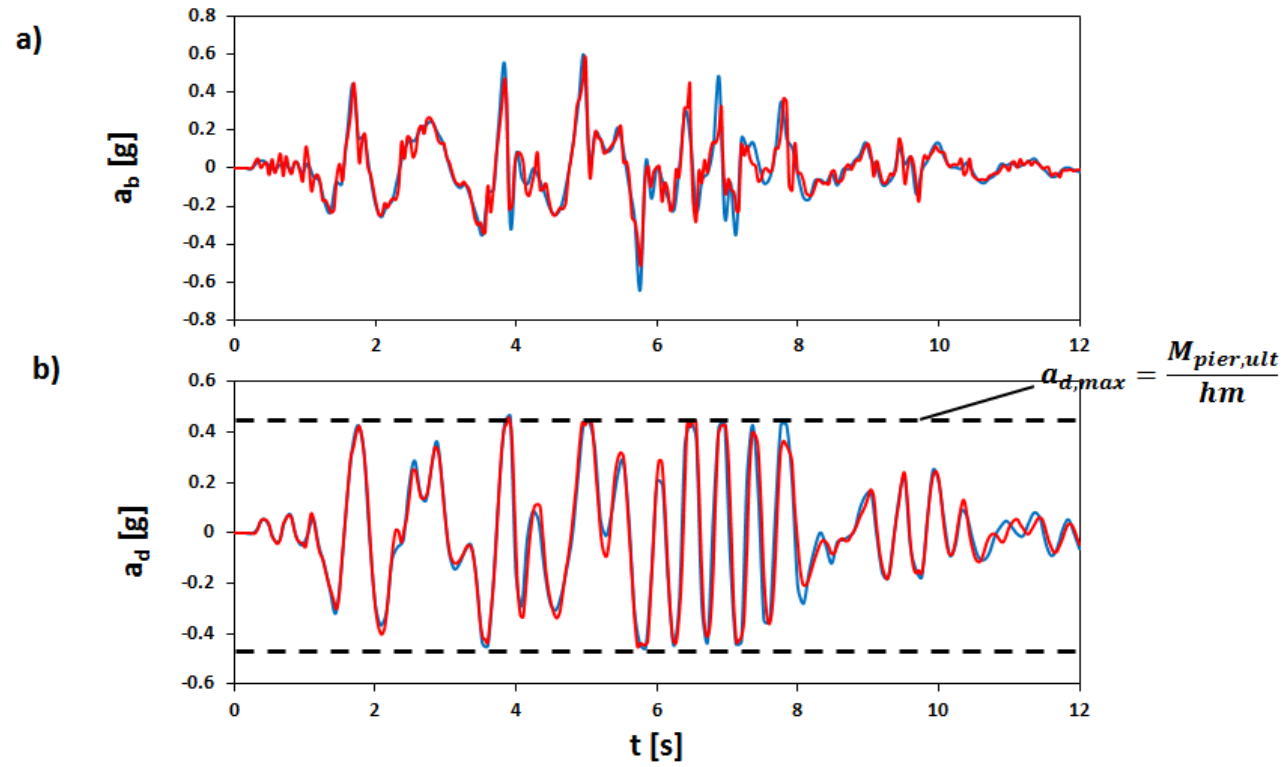

Fig. 5.4: Acceleration timehistory during Shinkobe excitation at (a) the base of the pier (b) the deck for the case connected (blue) and unconnected (red) piles.

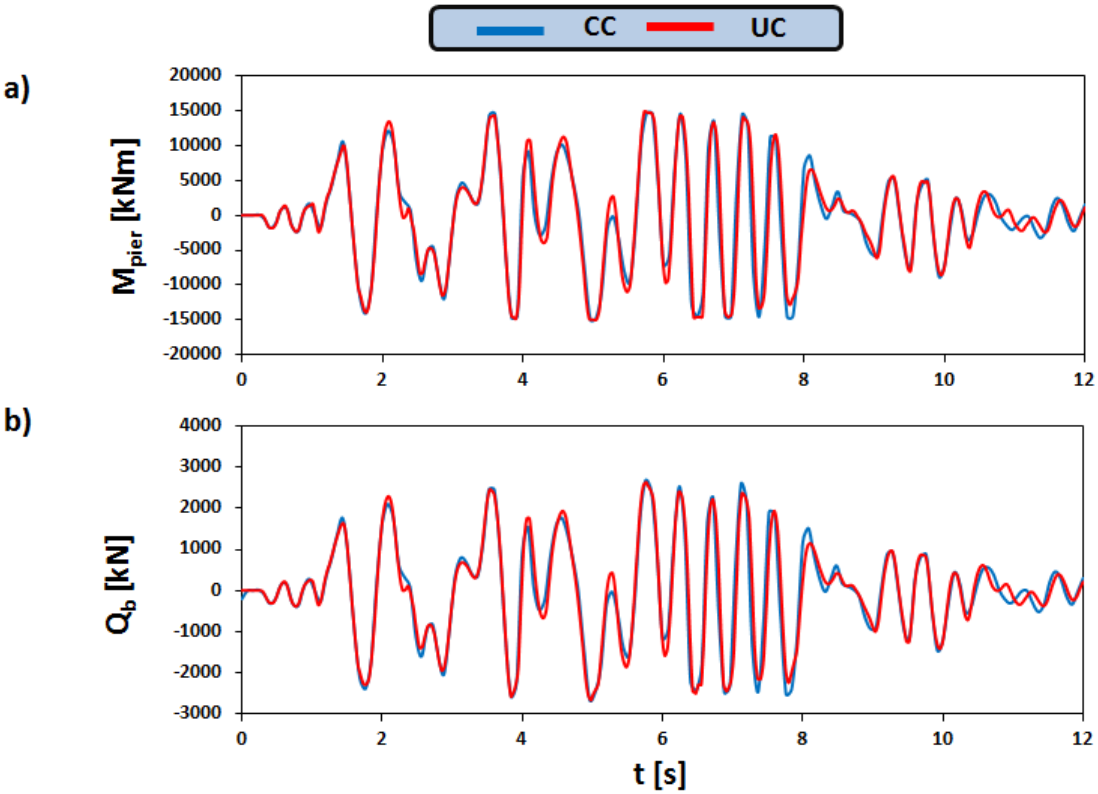

Fig. 5.5: Timehistories of (a) bending moment b) shear force at the base of the pier during Shinkobe excitation for the case of connected (blue) and unconnected (red) piles.

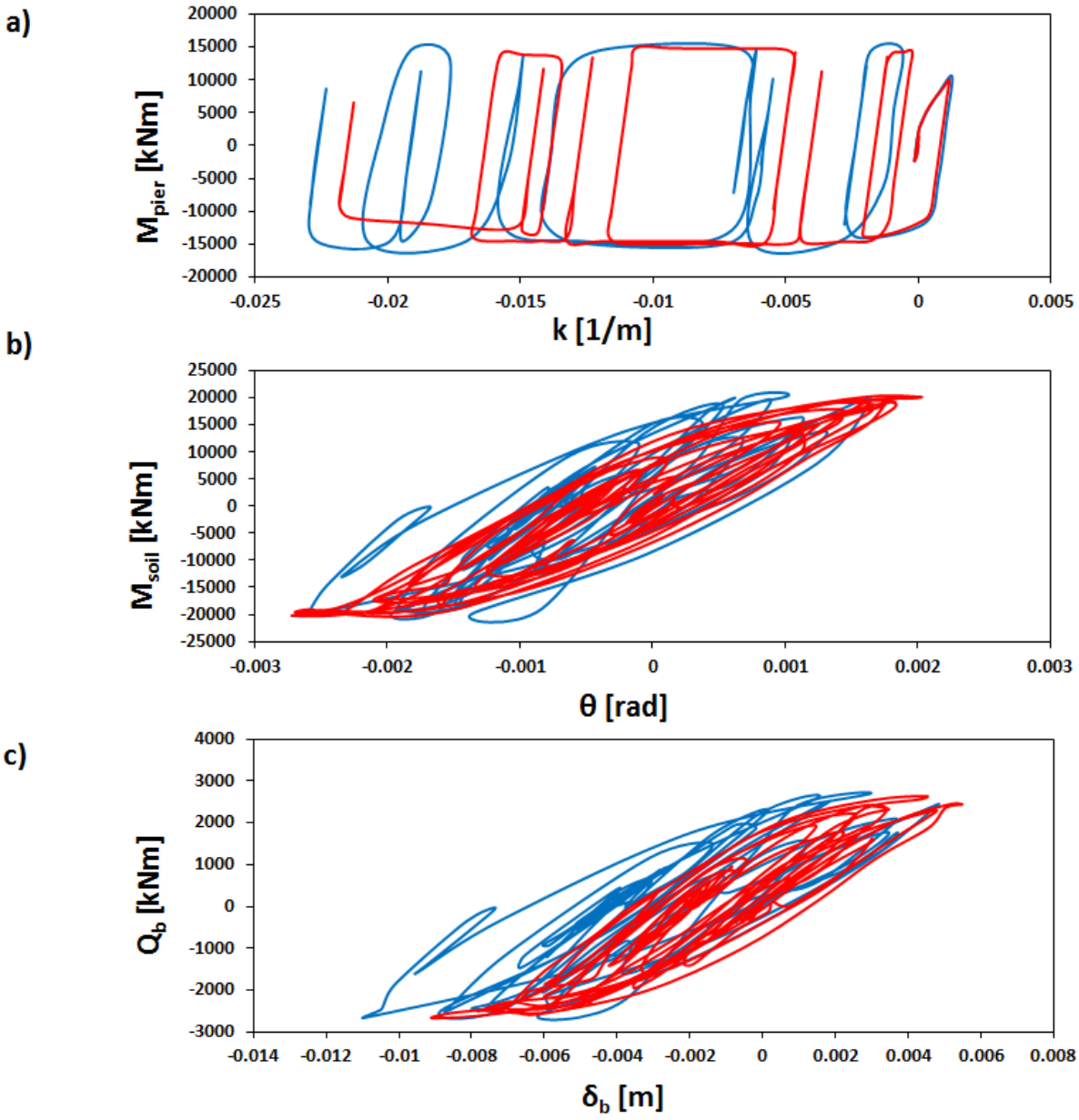

Fig. 5.6: Comparison of the response of the two conventionally designed systems with connected (blue) and unconnected (red) piles in terms of (a) bending moment – curvature at the base of the pier (b) moment–rotation of the foundation level (c) base shear–displacement of the foundation.

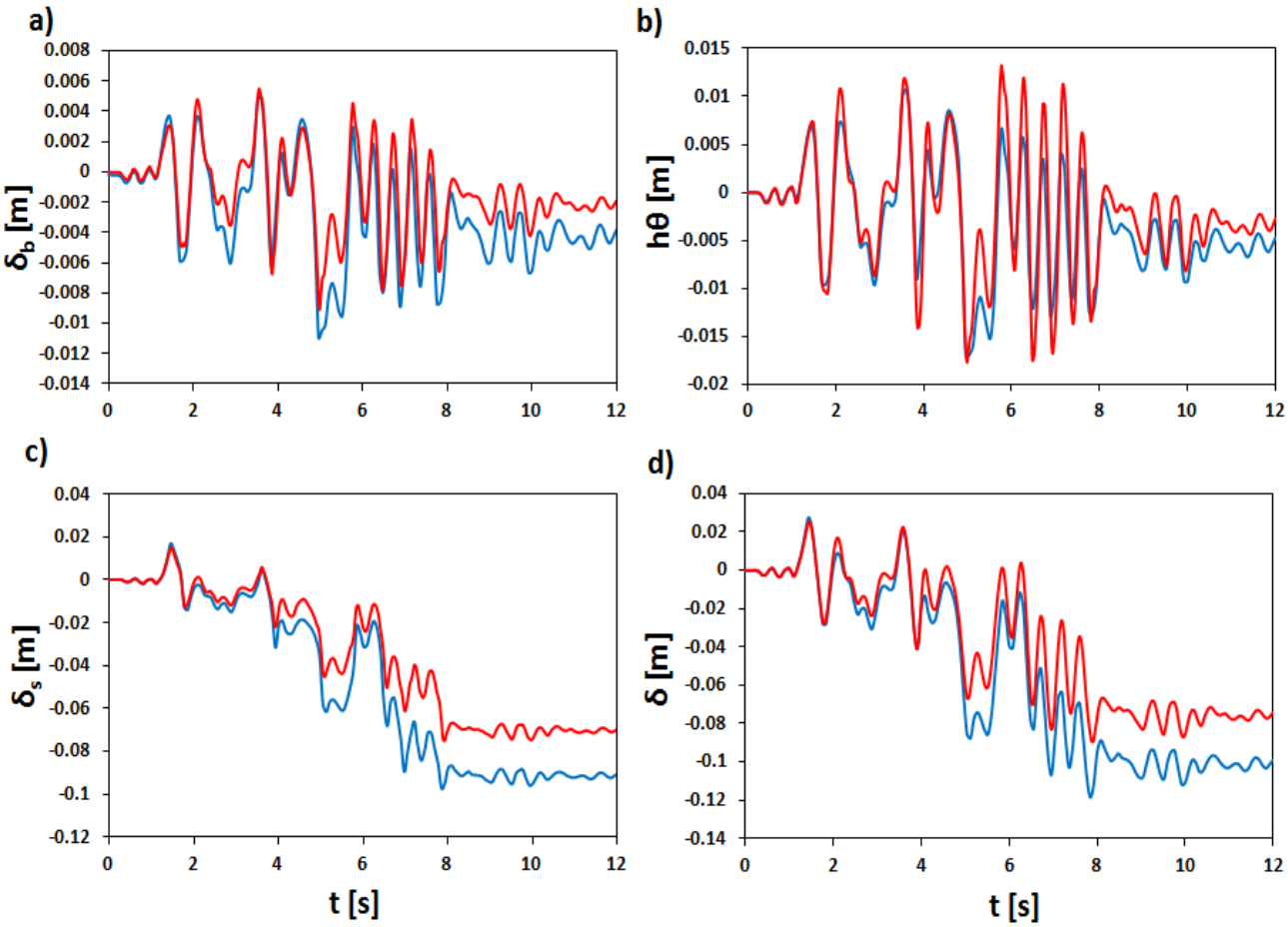

Fig. 5.6: Comparison of the response of the two conventionally designed systems with connected (blue) and unconnected (red) piles in terms of (a) foundation displacement (b) displacement due to the rotation of the foundation (c) structural deformation of the pier (d) total deck displacement.

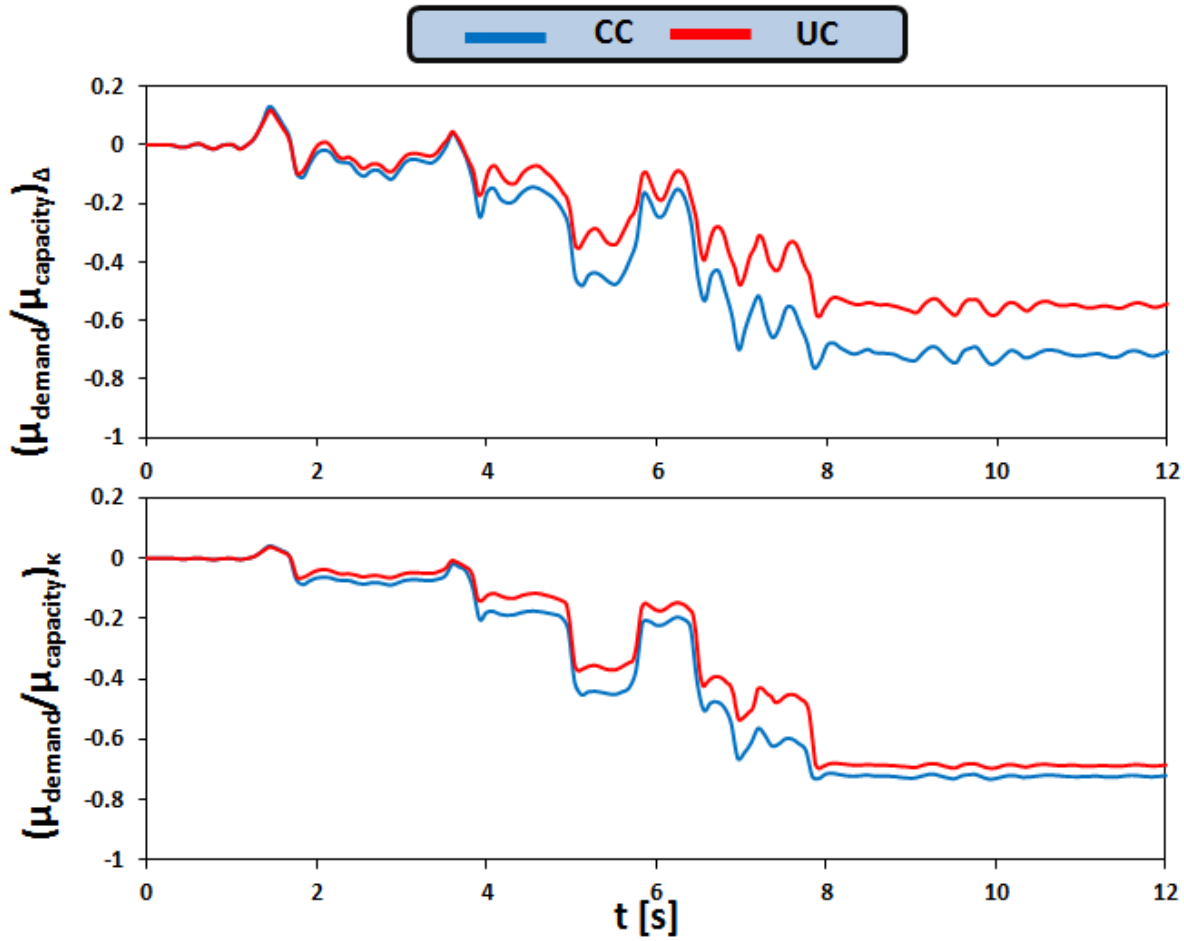

Fig 5.7: Comparison of ductility demand over ductility capacity of the two conventionally designed systems in terms of (a) displacement (b) curvature for Shinkobe earthquake.

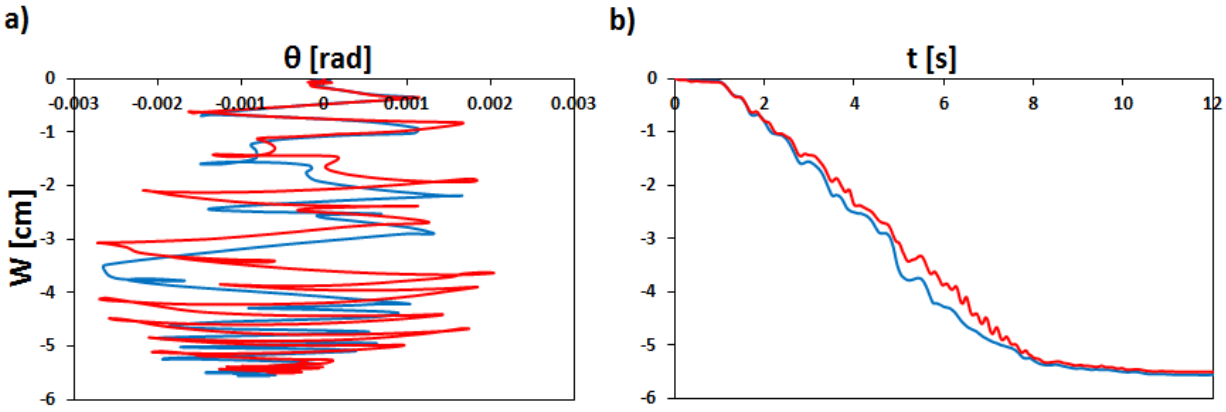

Fig. 5.8: Comparison of the settlements of the two alternative conventional designs subjected to Shinkobe earthquake in terms of (a) settlement – rotation and (b) settlement timehistory.

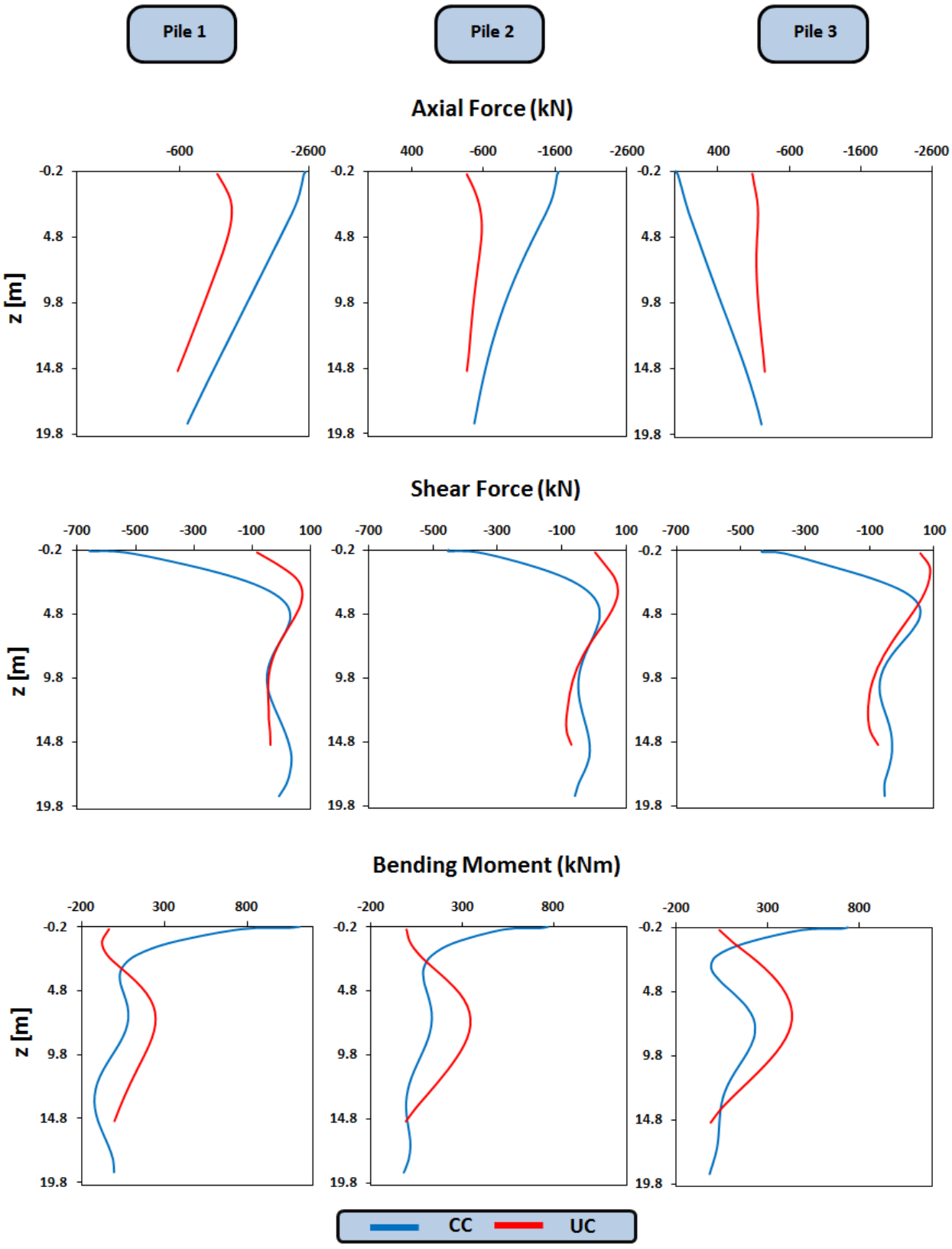

Fig. 5.9: Distribution of axial forces, shear forces and bending moments along the piles when maximum moment is transmitted to the soil (Shinkobe).

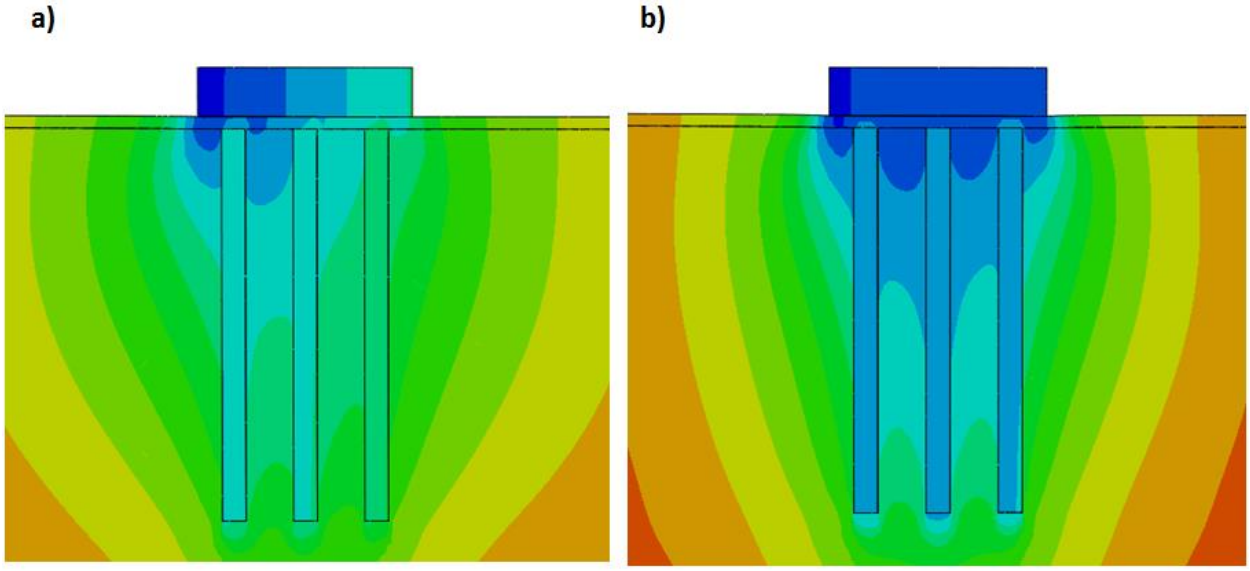

Fig. 5.10: Contours of vertical displacements of the soil, piles and pile cap in the case of unconnected piles (a) when maximum moment is transmitted to the soil (b) at the end of the Shinkobe earthquake.

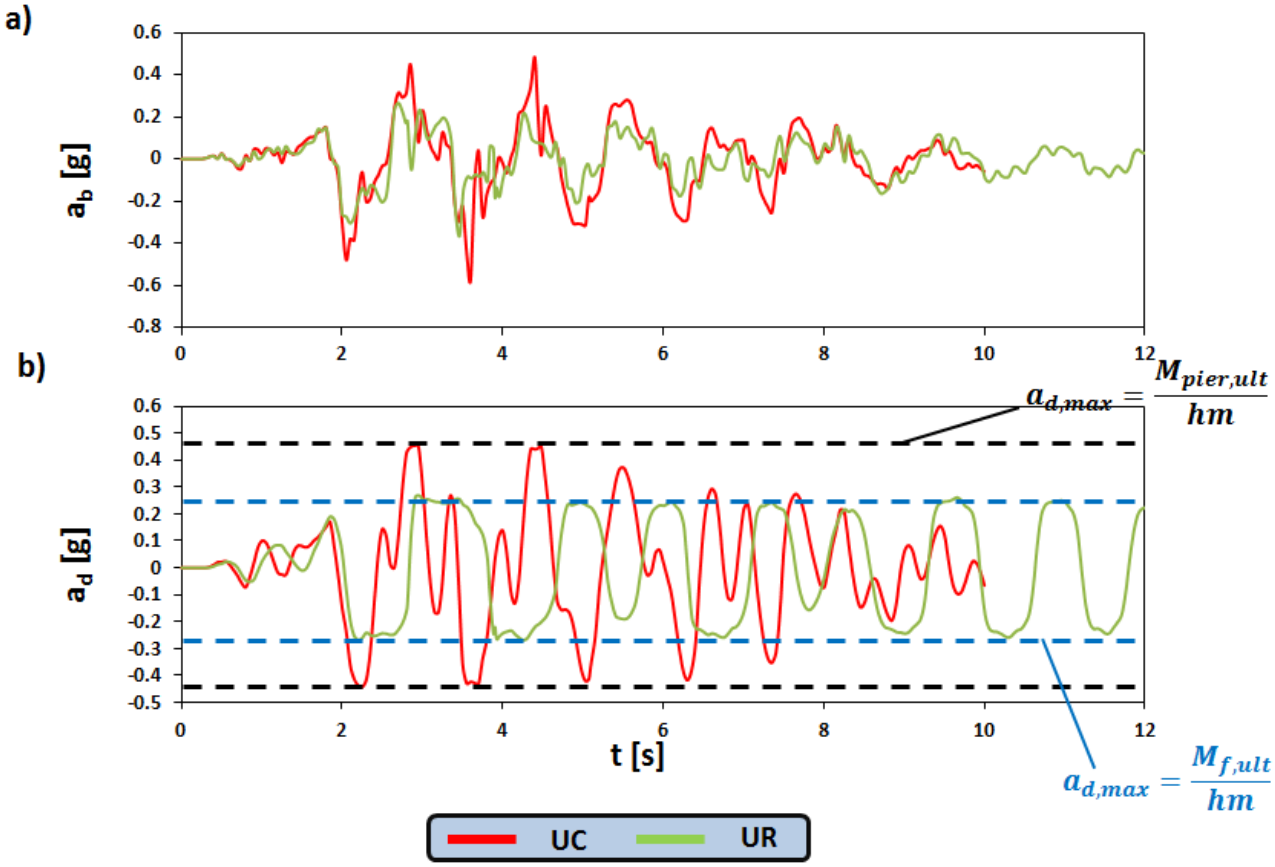

Fig. 5.11: Comparison of the response of conventional (UC) and rocking (UR) foundations on unconnected piles in terms of (a) pier base and (b) deck accelerations for Lixouri earthquake.

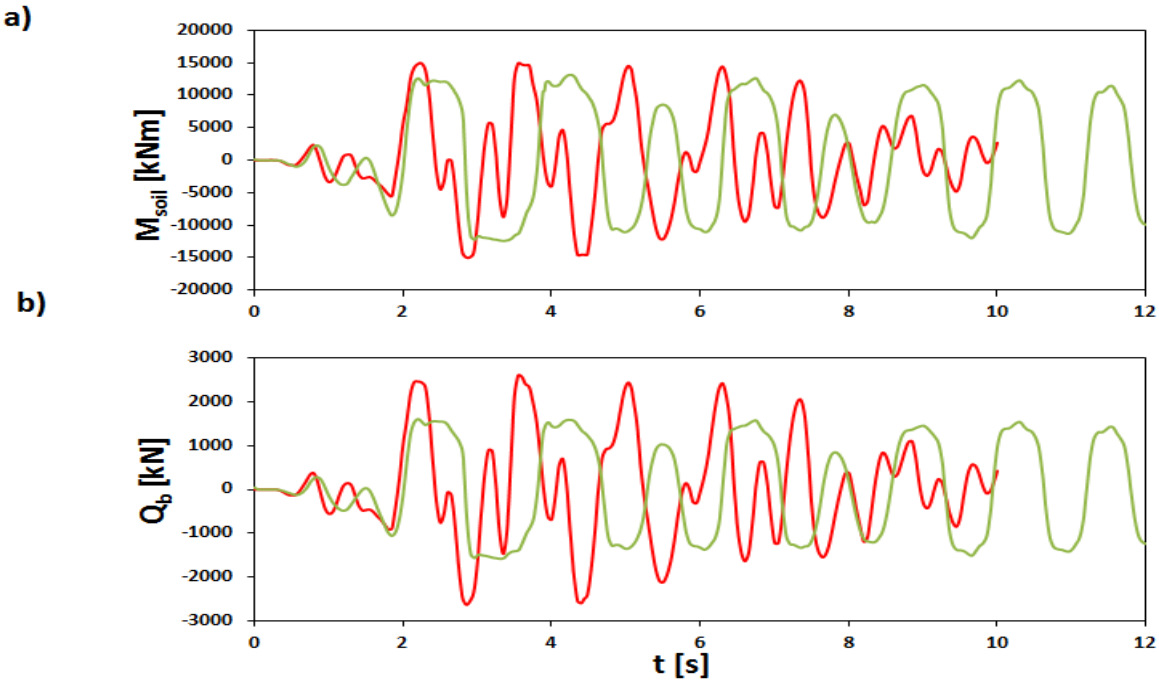

Fig. 5.12: Timehistories of (a) foundation moment (b) base shear of conventional (UC) and rocking (UR) foundations on unconnected piles for Lixouri earthquake.

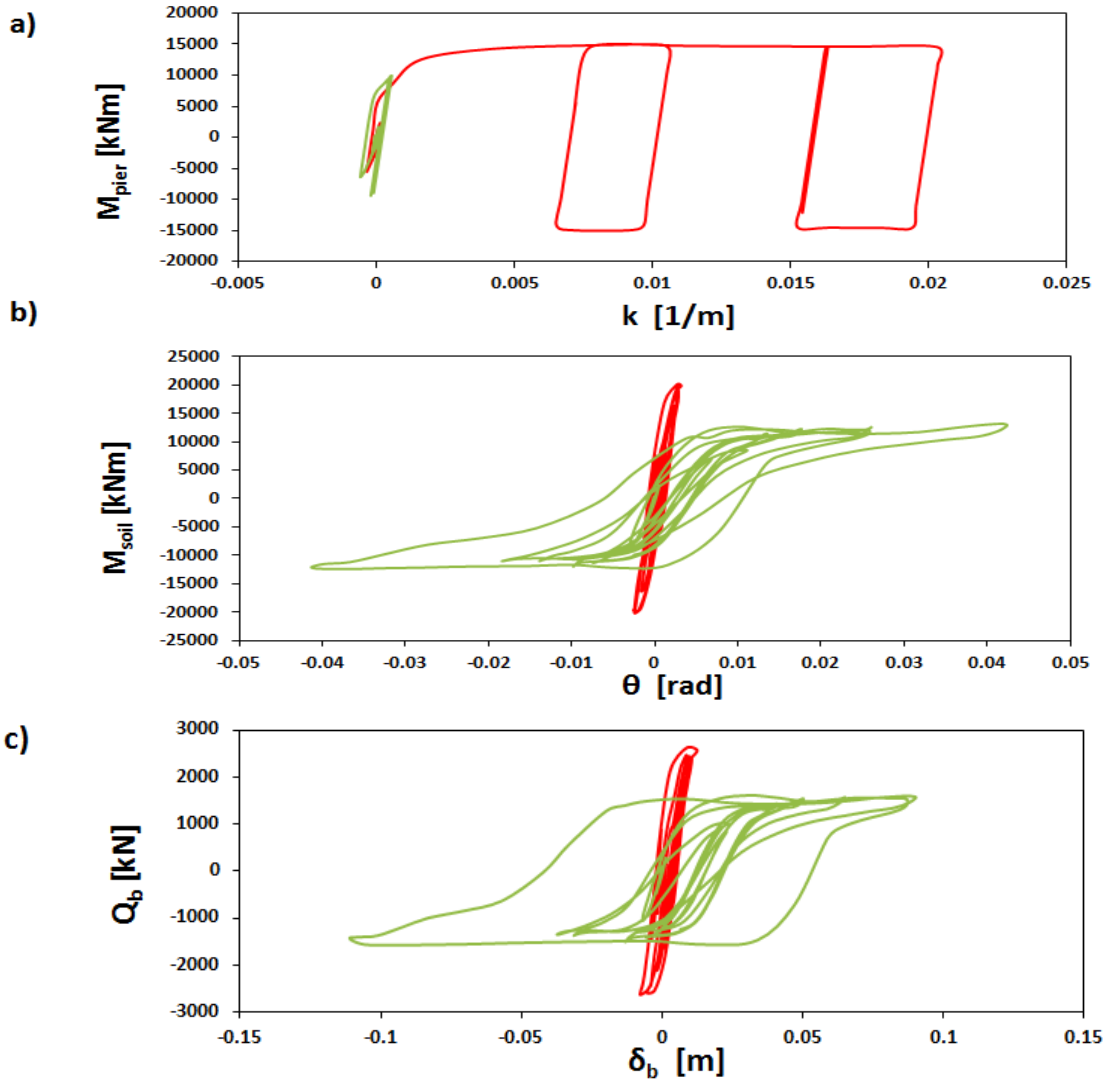

Fig. 5.13: Comparison of UC and UR subjected to Lixouri earthquake in terms of developed (a) moment–curvature at the base of the pier (b) moment–rotation at the foundation level and (c) base shear–dispalcement at the base of the pier.

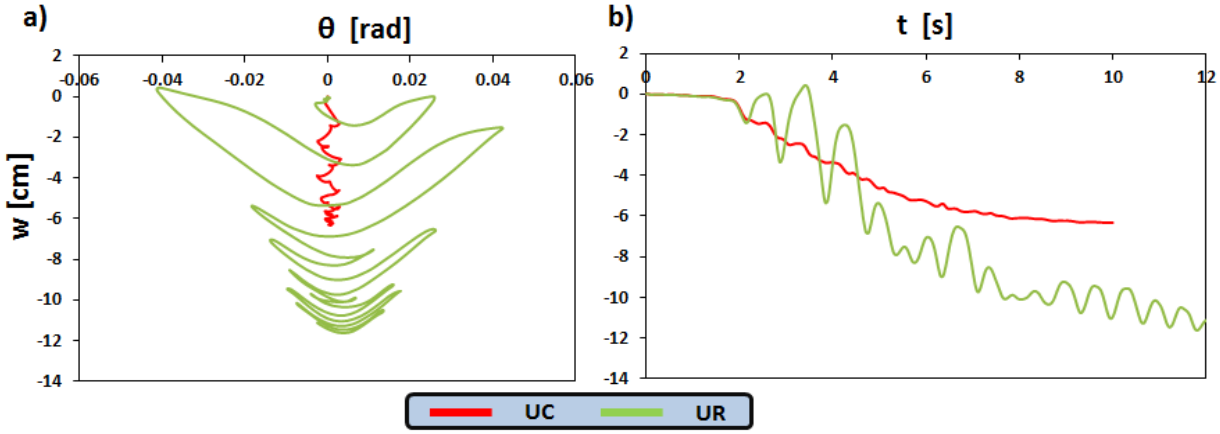

Fig. 5.14: Comparison of the response of the two laternatives subjected to Lixouri earthquake in terms of (a) settlement–rotation and (b) settlement timehistory.

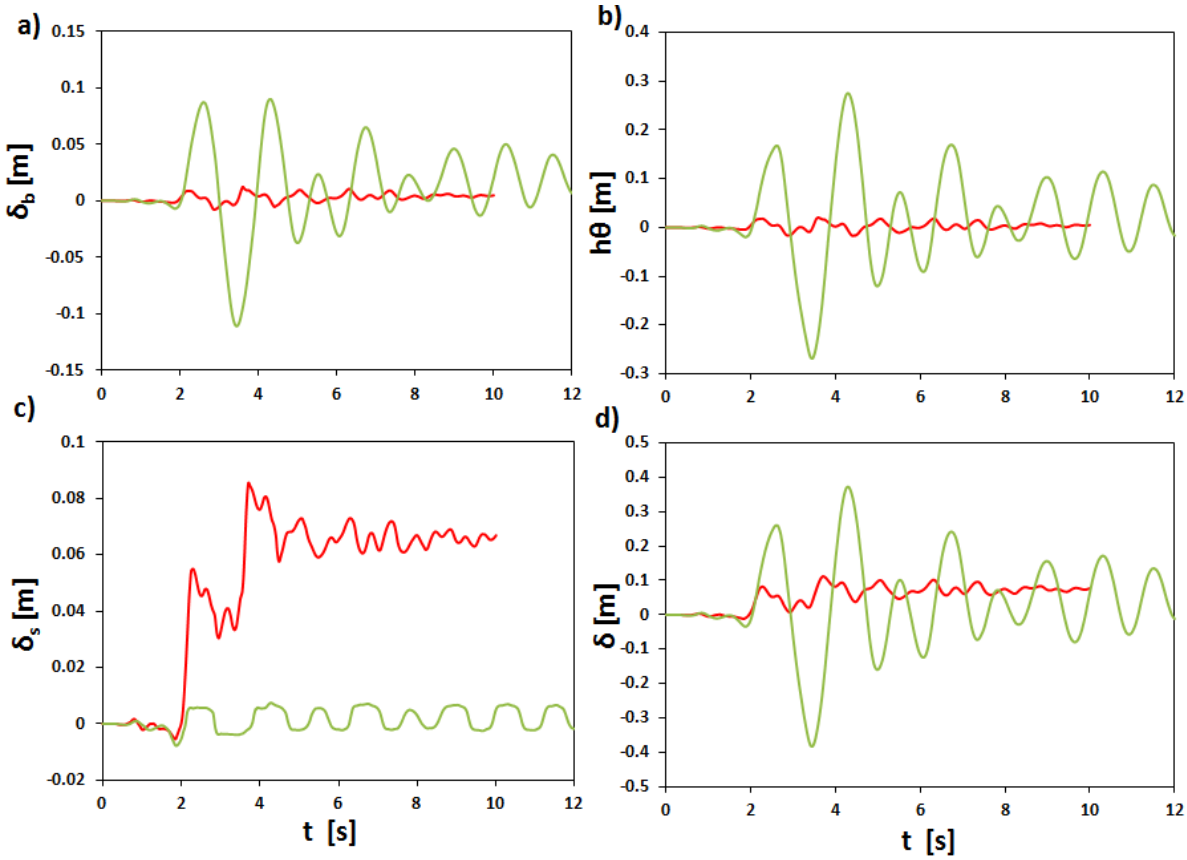

Fig. 5.15: Comparison of the response of conventional (UC) and rocking (UR) foundations with unconnected piles in terms of (a) foundation displacement (b) displacement due to the rotation of the foundation (c) structural deformation of the pier (d) total deck displacement (Lixouri).

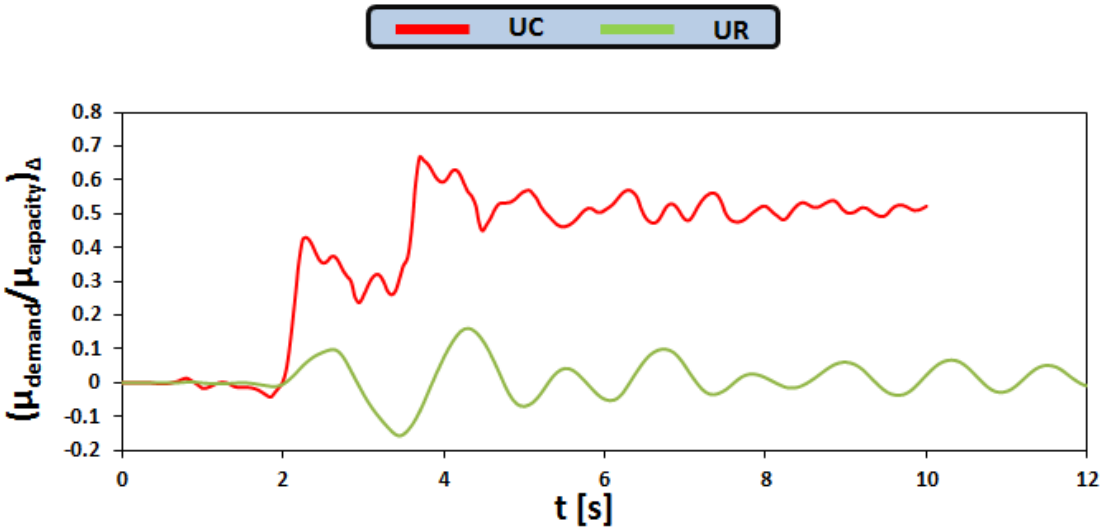

Fig. 5.16: Comparison of ductility demand over ductility capacity in terms of displacement of conventional and rocking foundations.

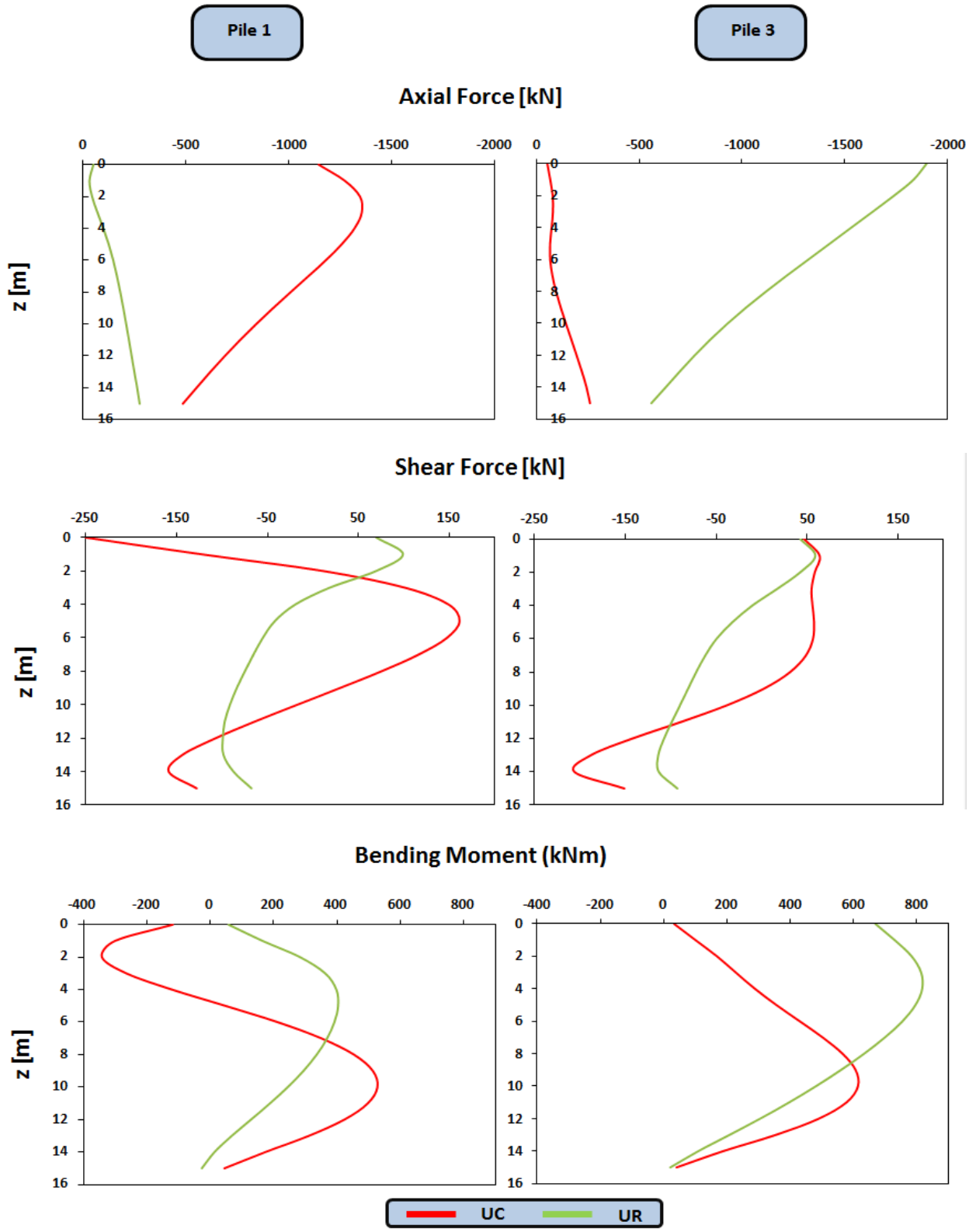

Fig. 5.17: Distribution of axial forces, shear forces and bending moments on the outermost piles of the two alternative designes with unconnected piles, when maximum moment is transmitted to the soil, Lixouri earthquake.

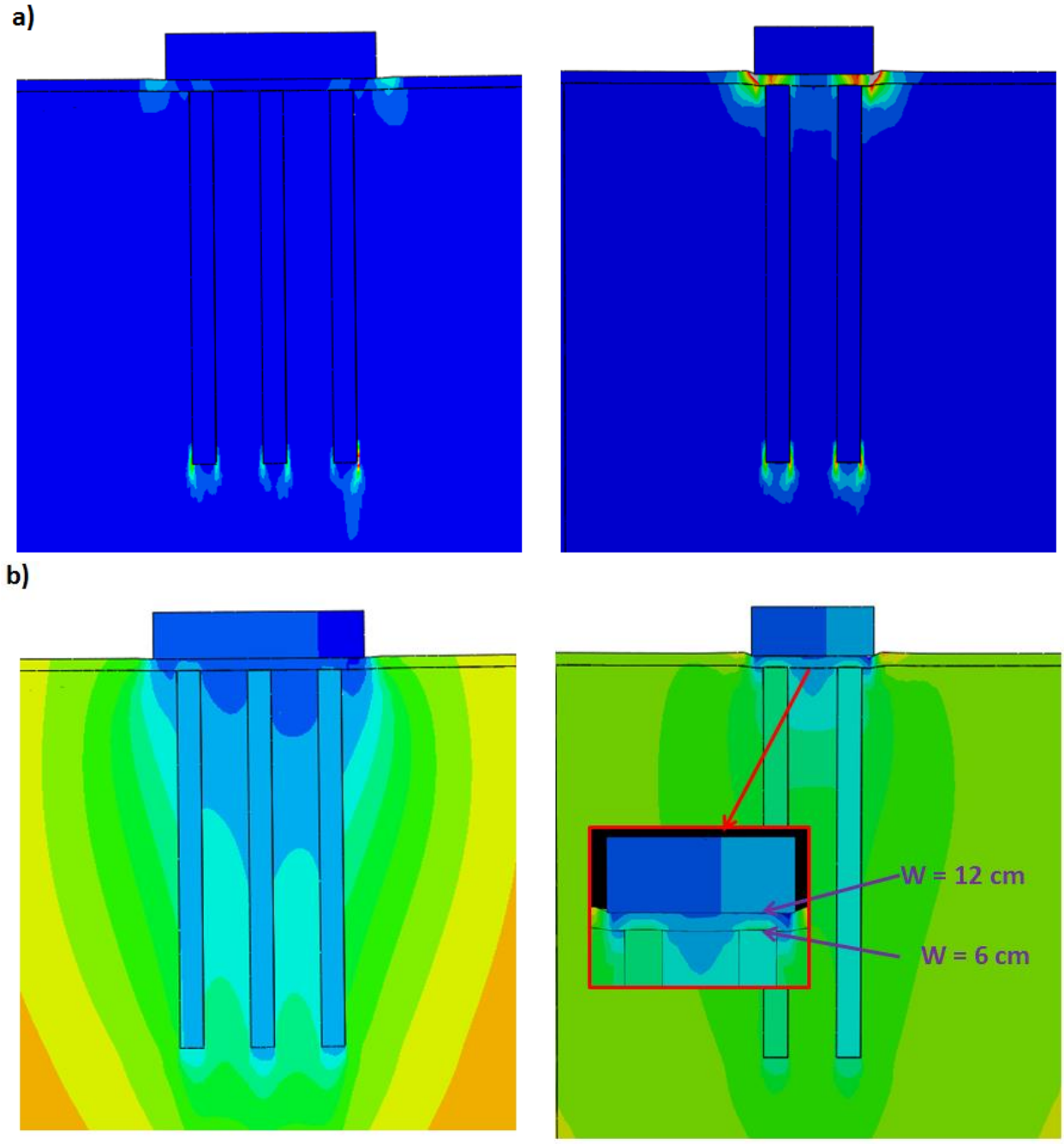

Fig 5.18: (a) Contours of soil plastic deformations, showing the excessive plastification under the pile cap in the case of rocking foundation (b) contours of settlements showing the 6 cm differential settlement between the soil just below the pile cap and above the pile in the case of rocking foundation.

Chapter 6

Design of the Tall Pier

6.1 Conventional Design

6.1.1 Design

The same procedure was followed for the design of the tall pier. Its fundamental period, taking into account the soil–structure interaction, was calculated T_{SSI} = 1.53 s and the design acceleration 0.10 g. The loads acting on the base of the pier according to EC8 and those resulting from capacity design are shown in **Figure 6.1**. For the final design it was selected:

- 40Φ32 longitudinal reinforcement
- Φ12/10 transverse reinforcement

The moment–curvature relationship of the pier base is shown in **Figure 6.2**, from which the ductility capacity of the system was found equal to μ_k = 11.1 and μ_Δ = 3.30 in terms of curvature and displacements respectively.

Capacity design was also used to design the foundation. The acting forces and the design forces on the foundation are shown in **Figure 6.3**. The foundation used for the short pier was also found satisfying for the tall pier, with the vertical load being again critical for the design, due to the reduced design spectral acceleration. **Figure 6.4** shows the final design of the conventional foundation with connected piles.

6.1.2 Comparison with the Short Pier

The response of the foundation under vertical loading is not affected by the height of the pier so only horizontal push over analysis was performed on the tall pier and its response was compared with the response of the short pier. The force–deck displacement and the shear force–displacement at the head of the piles relationships are presented in **Figure 6.5**. It can be observed that for a given displacement the shear forces both on the base of the pier and on the piles are reduced compared to the short pier. Shadow effects can also be observed in this case. **Figure 6.6** shows the sinking response of this foundation.

The axial force on the piles of the tall pier are larger than in the short pier for a given applied horizontal force, as shown in **Figure 6.7**. However, they reach the same maximum value. In addition from the same graph the interaction between the piles can be seen, since the piles of the inner row (4, 6) develop larger forces than the piles of the outer row (1, 3) at the beginning of the horizontal loading.

Figure 6.8 shows the distribution of axial forces, shear forces and bending moments along the piles for deck displacements 10 cm and 21 cm, corresponding to pile head displacements 2 cm and 3.7 cm respectively. Compared to the short pier the axial forces on the piles of the tall pier are slightly larger for the same pile displacements. On the other hand the bending moments are slightly decreased, while the decease of the shear forces is significant. From the last two figures it is concluded that the increase of slenderness leads to increase of foundation's rotation and piles' axial

forces for a given deck displacement but decrease of shear forces and bending moments on the piles.

6.2 Unconnected Conventional Pile Foundation

The requirements of this foundation are the same as in the short pier case. The same configuration (**Figure 6.9)** was tested with a horizontal push–over analysis and its response is presented in **Figure 6.10**. The ultimate moment capacity of the foundation is 25315 kNm, showing that as the shear to moment ratio has been decreased the moment capacity of the foundation increased. The settlement–rotation relationship shows an uplifting dominated response.

Figure 6.11 shows the distribution of axial force, shear forces and bending moments along the piles for deck displacements equal to 10 cm and 15 cm, which corresponds to the maximum axial moment of Pile 3. As it was also observed in the connected pile foundation, for a given deck displacement the axial loads on the piles are increased while the shear forces and bending moments are significantly decreased compared to the unconnected piles of the short pier. Since, the moment to shear ration at the base of the foundation is increased the soil reacts more with vertical stresses than shear stresses leading to higher axial forces and smaller shear forces and bending moments on the piles. Additionally, the maximum axial force on Pile 3 is developed for smaller deck displacement than in the shorter pier.

6.3 Unconnected Rocking Pile Foundation

The same configuration, as in the tall pier case, was tested for the rocking foundation and is shown in **Figure 6.12**. From the results of the unconnected conventional pile foundation it was expected the moment capacity of the rocking foundation would also increase due to increase of structure's slenderness. A horizontal push–over analysis was employed and its results are presented in **Figure 6.13**. The foundation has the desired uplifting response but, as expected, its capacity has increased and $\frac{M_f}{M_{Rd}} = 0.95$. It was selected as the final design of rocking foundation, because any further reduction of the distance between the piles and the edge of the pile cap or between the piles would not be acceptable. The selection is also justified from the fact the actual pier capacity is 1.27 time greater than the design one, and hence $\frac{M_f}{M_{pier,max}} = 0.75$ — which is sufficiently small.

Figure 6.14 shows the distribution of axial force, shear forces and bending moments along the piles for deck displacements equal to 10 cm and 66 cm, which corresponds to the maximum axial moment of Pile 3. It is interesting to note that while in the conventionally designed unconnected pile foundation Pile 3 reached its maximum axial force in smaller displacement in the case of the tall pier compared to the case of the short, here the opposite happens. In addition for deck displacement 10 cm axial forces, shear forces and bending moments are all slightly reduced in the case of the tall pier. The reason for that is the extremely small rotation and horizontal

displacement of the pile cap at that moment. Hence, there are two competing effects of slenderness. As it increases, for a given horizontal force larger moments are transmitted to the soil and so the soil has greater normal stresses, while at the same time for a given displacement the displacement and rotation of the pile cap is smaller leading to smaller stresses on the unconnected piles. However, the axial force reaches higher maximum value.

Figures of Chapter 6

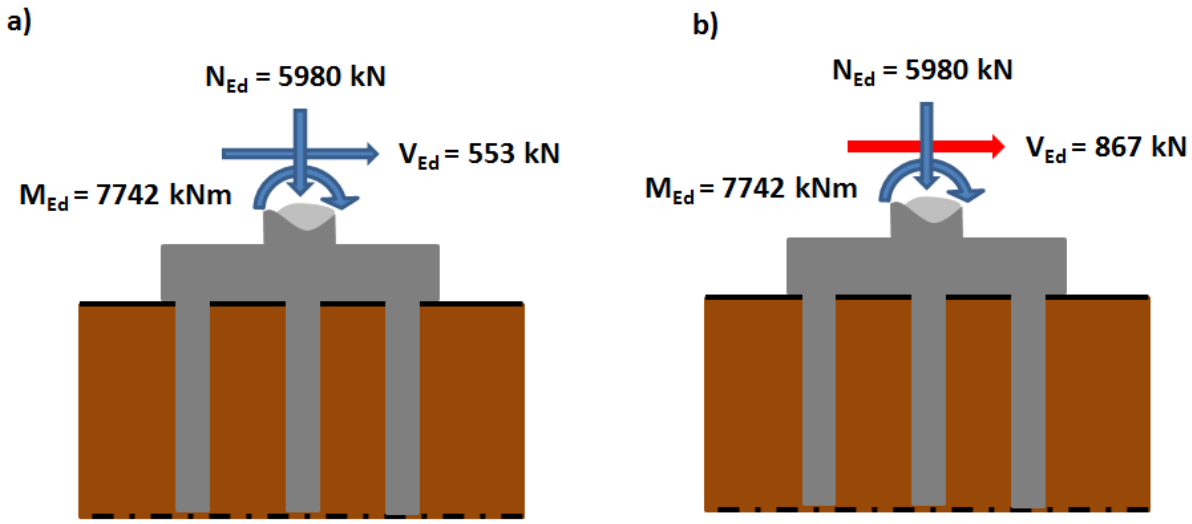

Fig. 6.1: (a) acting and (b) design forces after capacity design at the base of the tall pier.

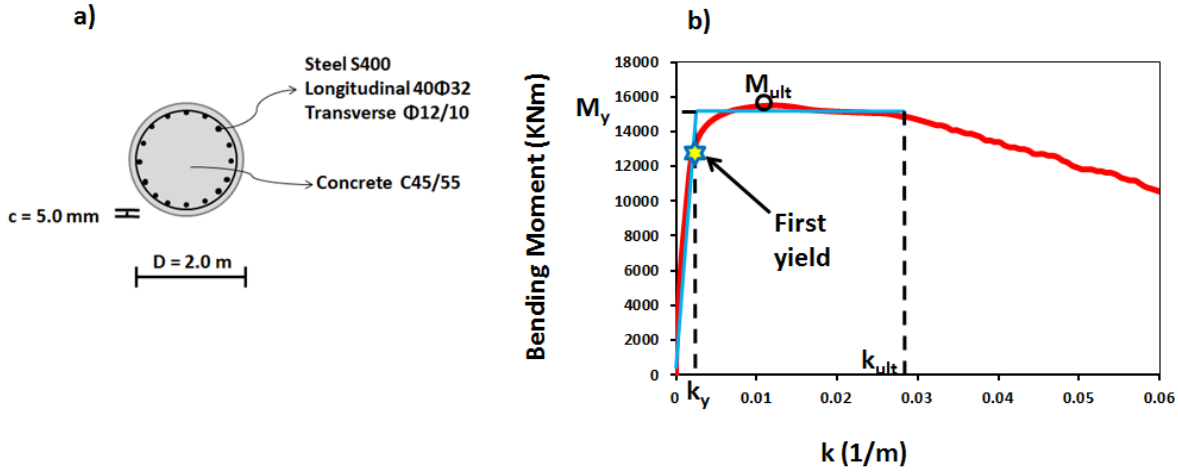

Fig. 6.2: (a) Geometry and reinforcement of the reinforced concrete sections (b) moment – curvature relationship at the pier base.

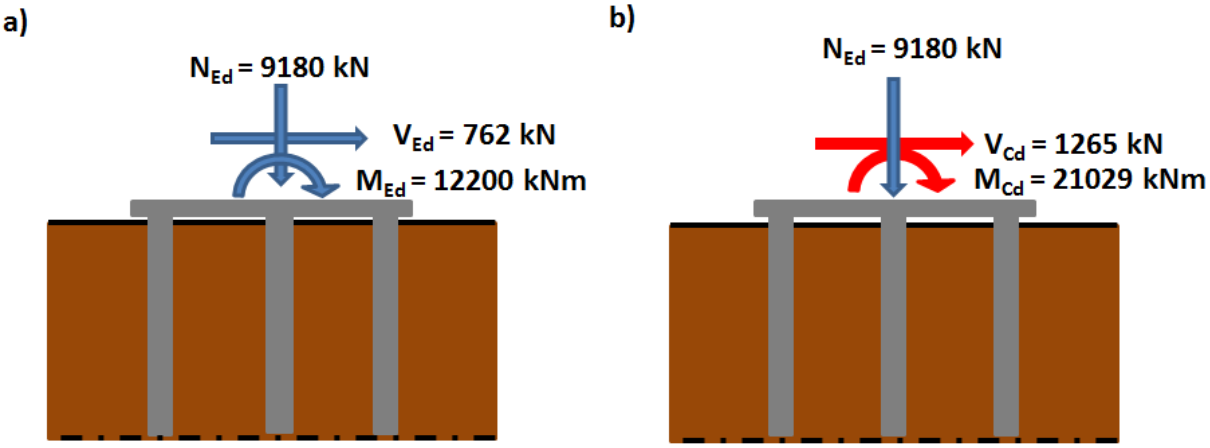

Fig. 6.3: (a) Static and seismic loads acting on the foundation (b) Static and seismic design loads accounting for the overstrength factors.

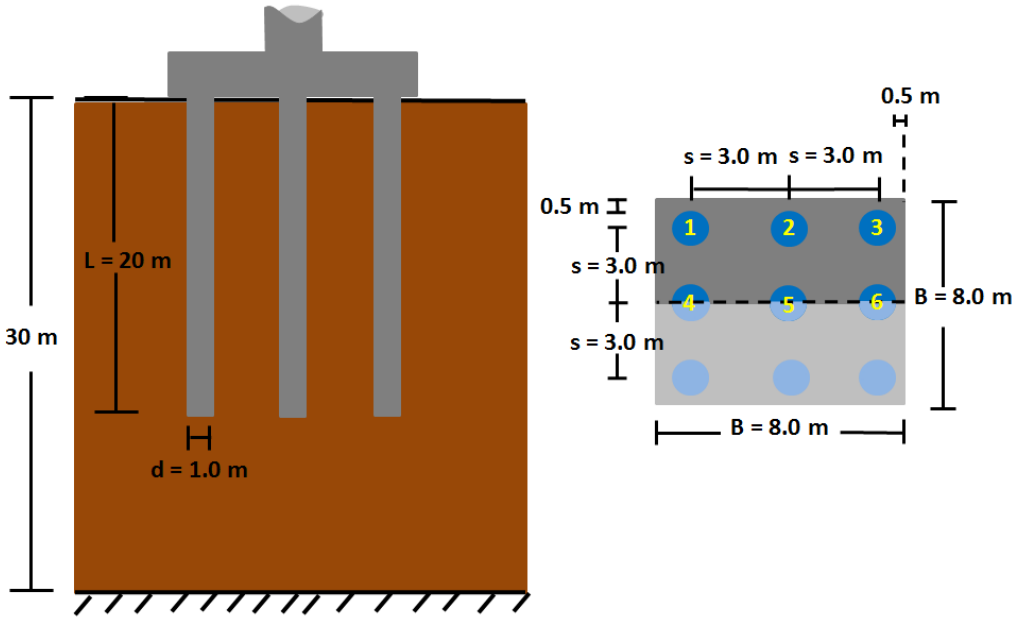

Fig. 6.4: Final configuration of the conventional pile foundation. Section and plan view.

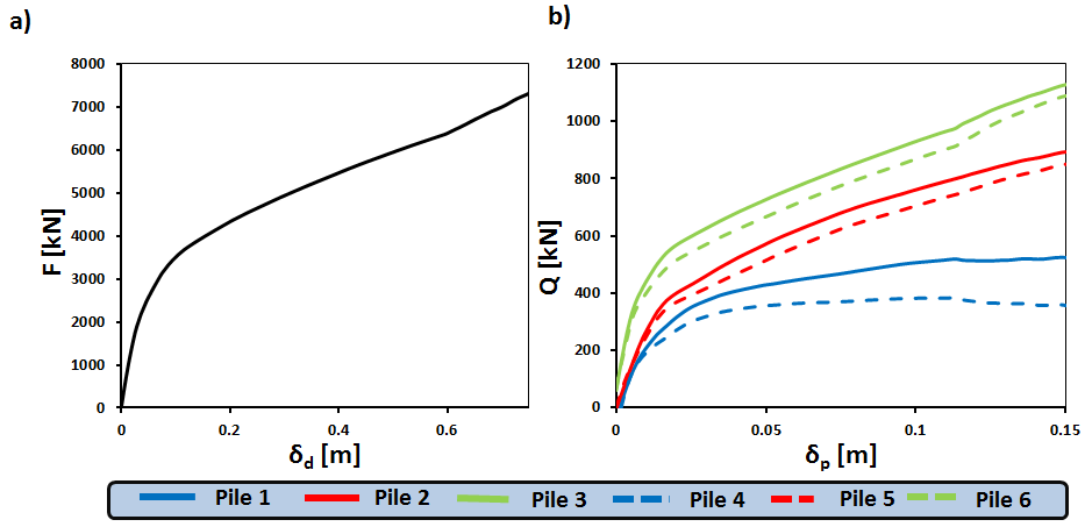

Fig. 6.5: (a) Force-displacement relationship at the top of the pier (b) shear force–displacement at the heads of the piles.

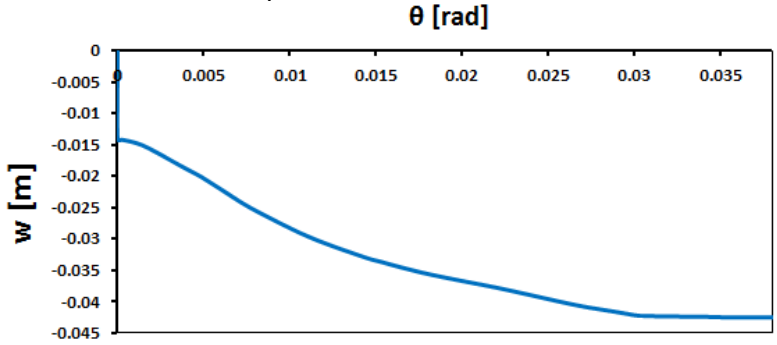

Fig. 6.6: Settlement-rotation relationship of the foundation showing sinking response.

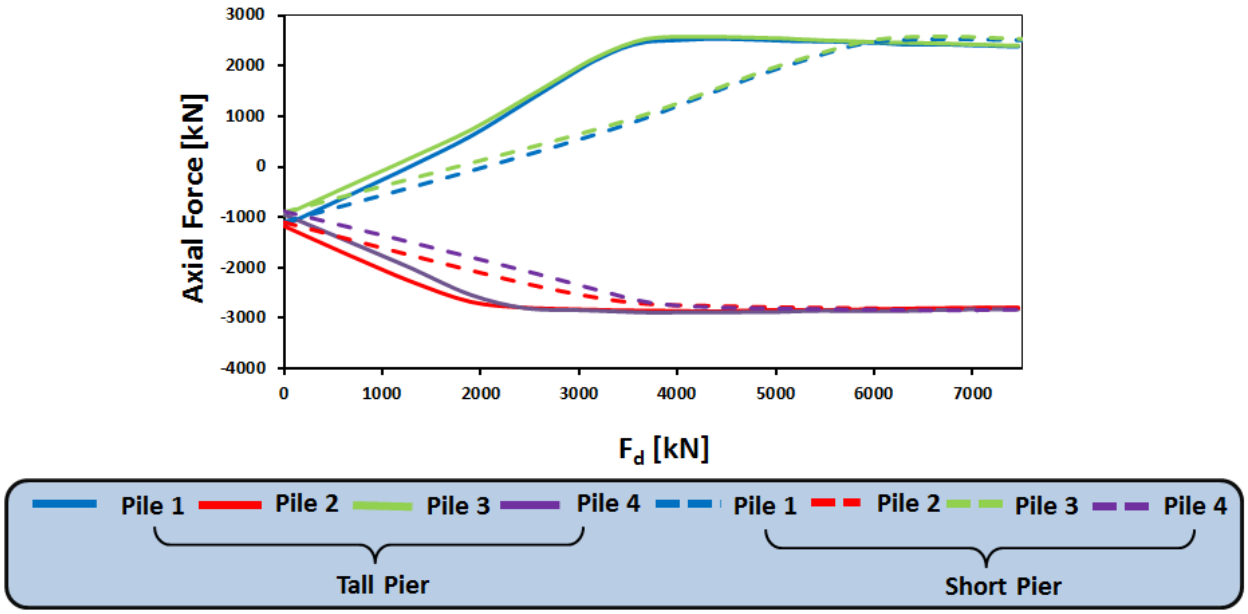

Fig. 6.7: Comparison of axial loads on pile heads for a given applied force on the deck for tall and short pier cases.

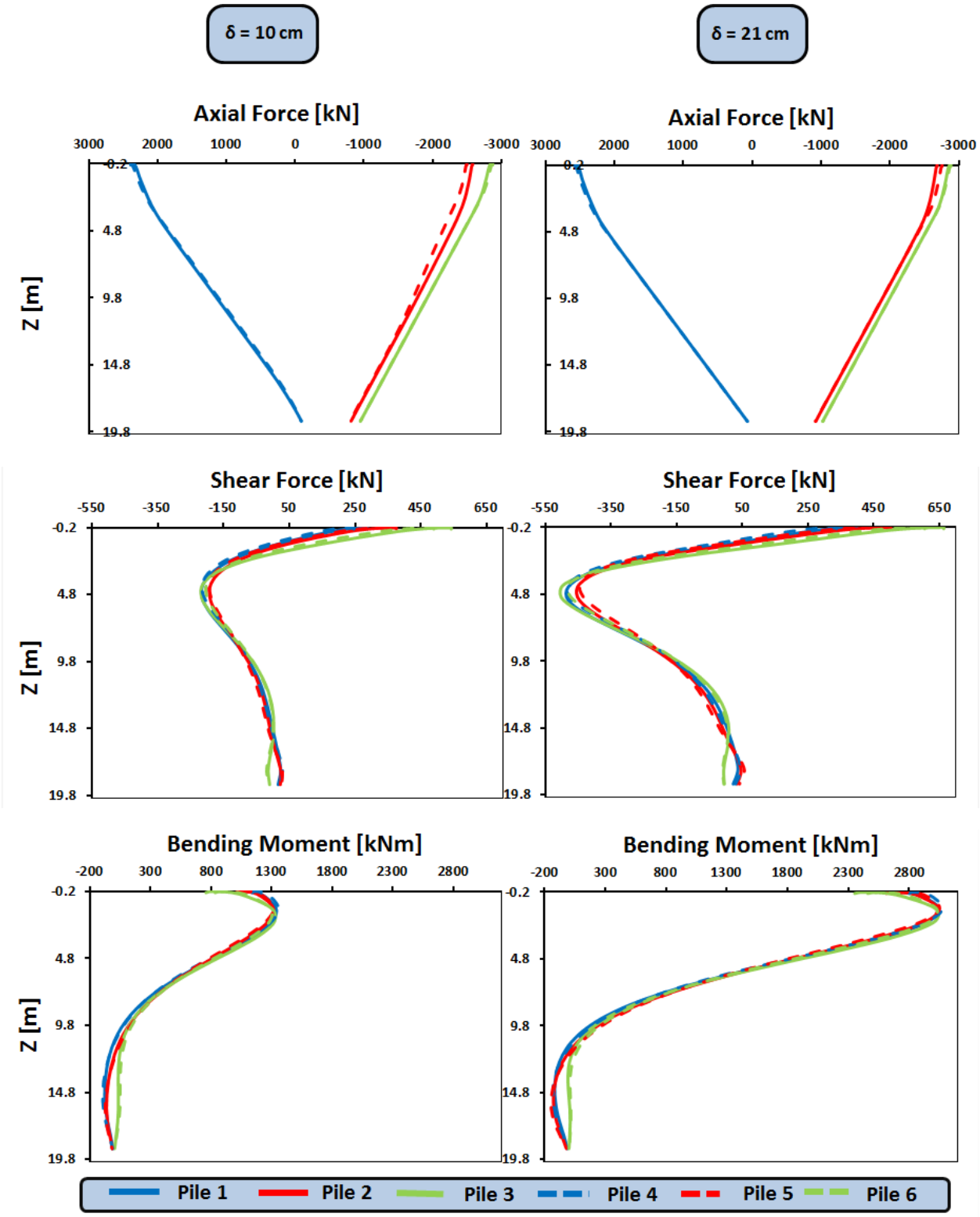

Fig. 6.8: Distribution of axial forces, shear forces and bending moments along the piles for horizontal deck displacements 10 cm and 21 cm.

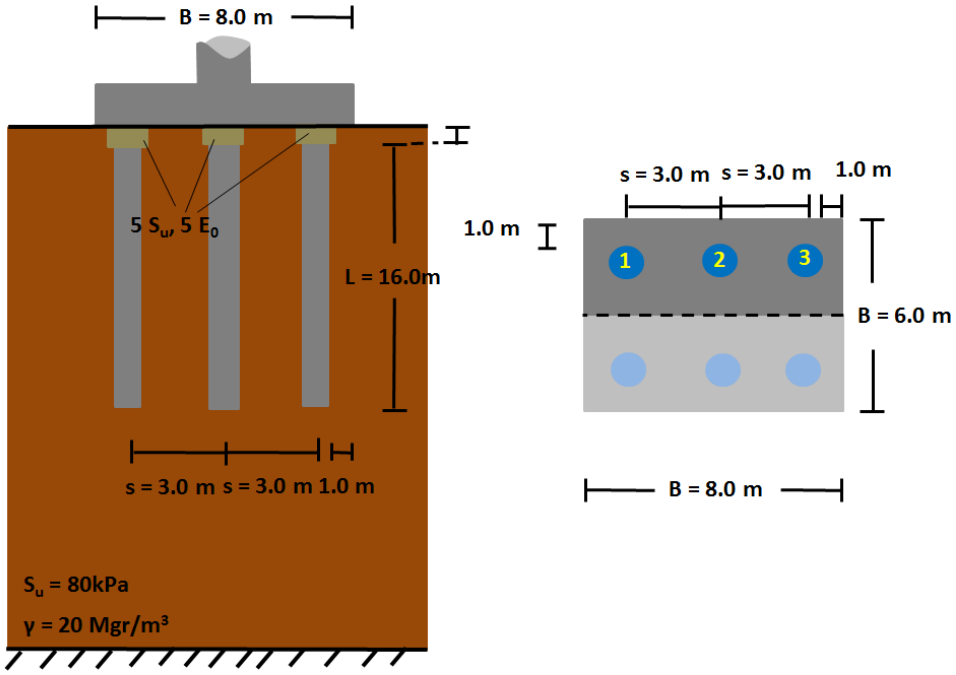

Fig 6.9: Design of the conventional unconnected pile foundation (UC). Section and plan view.

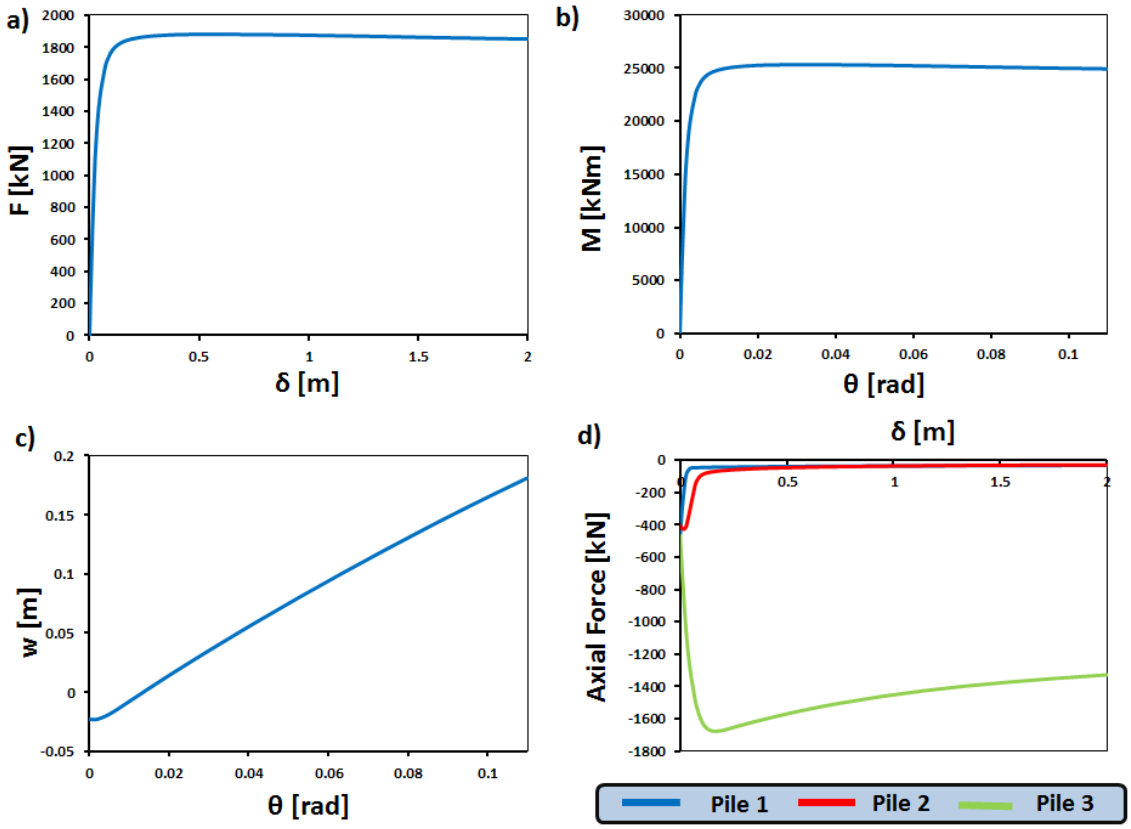

Fig. 6.10: Response of the foundation under horizontal loading in terms of (a) force-displacement on the deck (b) moment-rotation (c) settlement-rotation, showing uplifting response (d) axial loads on the pile heads versus deck displacement.

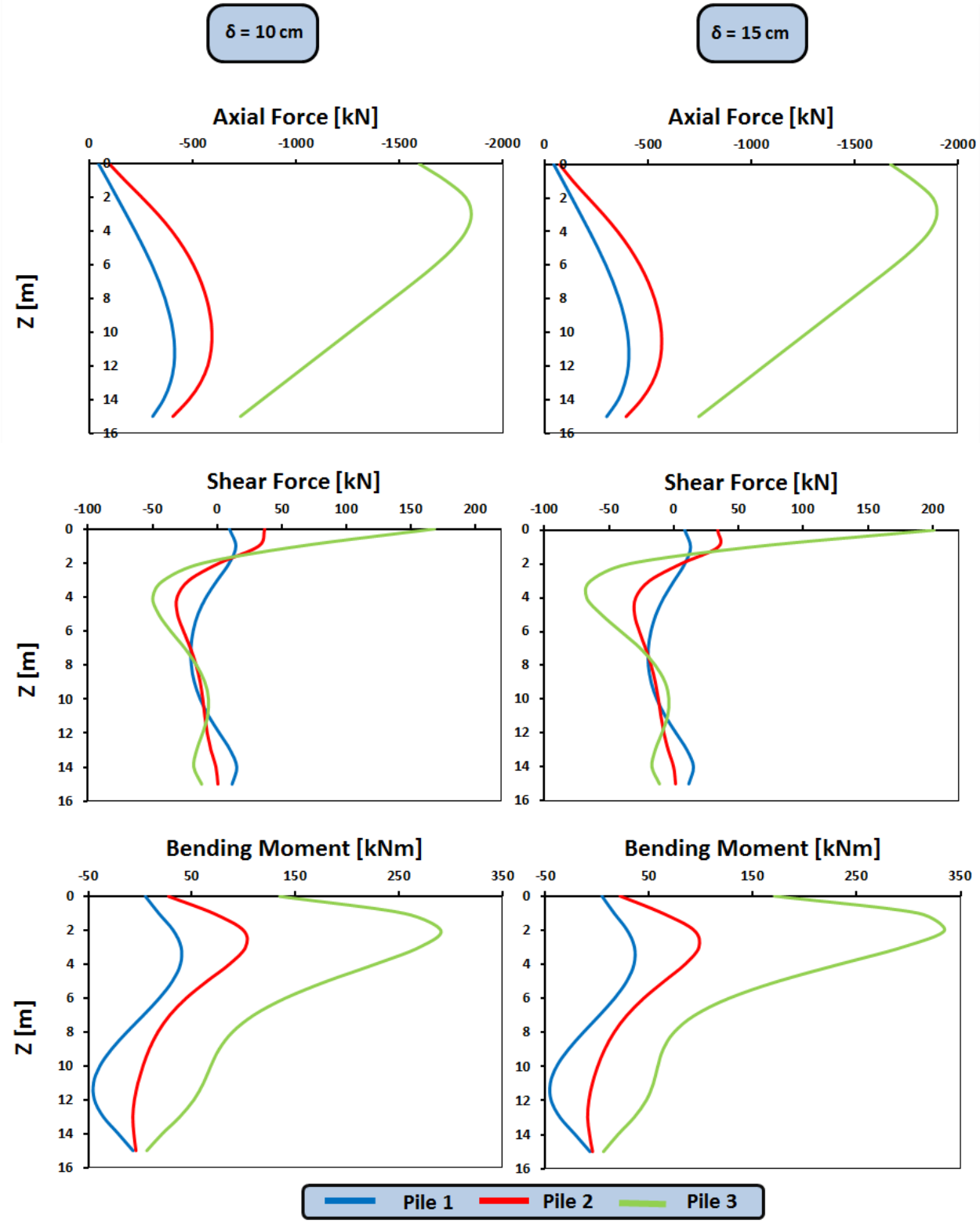

Fig. 6.11: Distribution of axial forces, shear forces and bending moments along the piles for horizontal deck displacements 10 cm and 15 cm, which corresponds to the maximum axial load on pile 3.

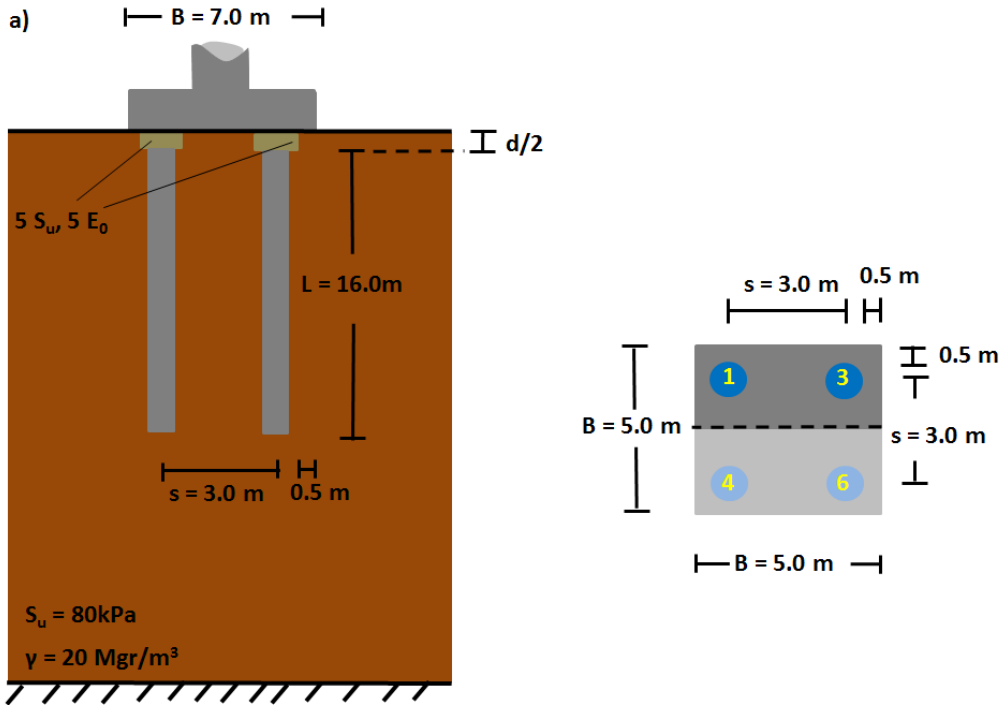

Fig. 6.12: Final design of the rocking foundation (UR). Section and plan view.

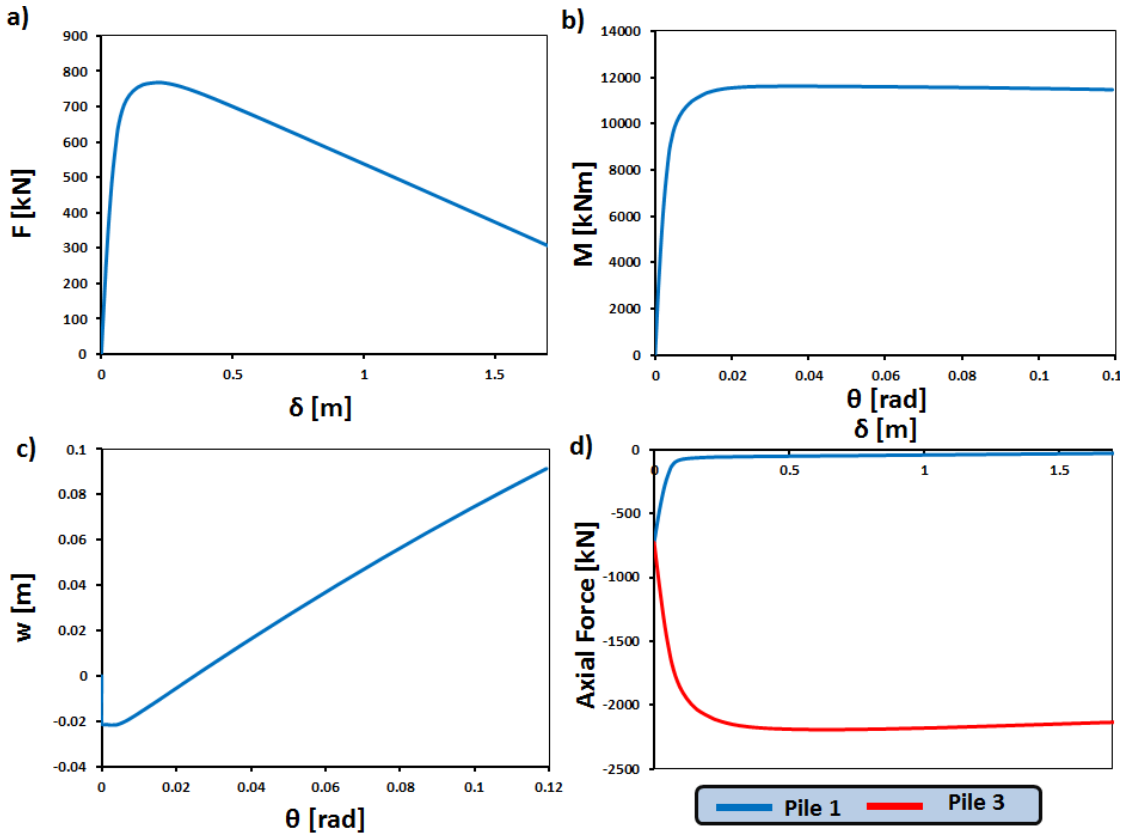

Fig. 6.13: Response of the rocking foundation under horizontal loading in terms of (a) force-displacement on the deck (b) moment-rotation (c) settlement-rotation, showing uplifting response (d) axial loads on the pile heads versus deck displacement.

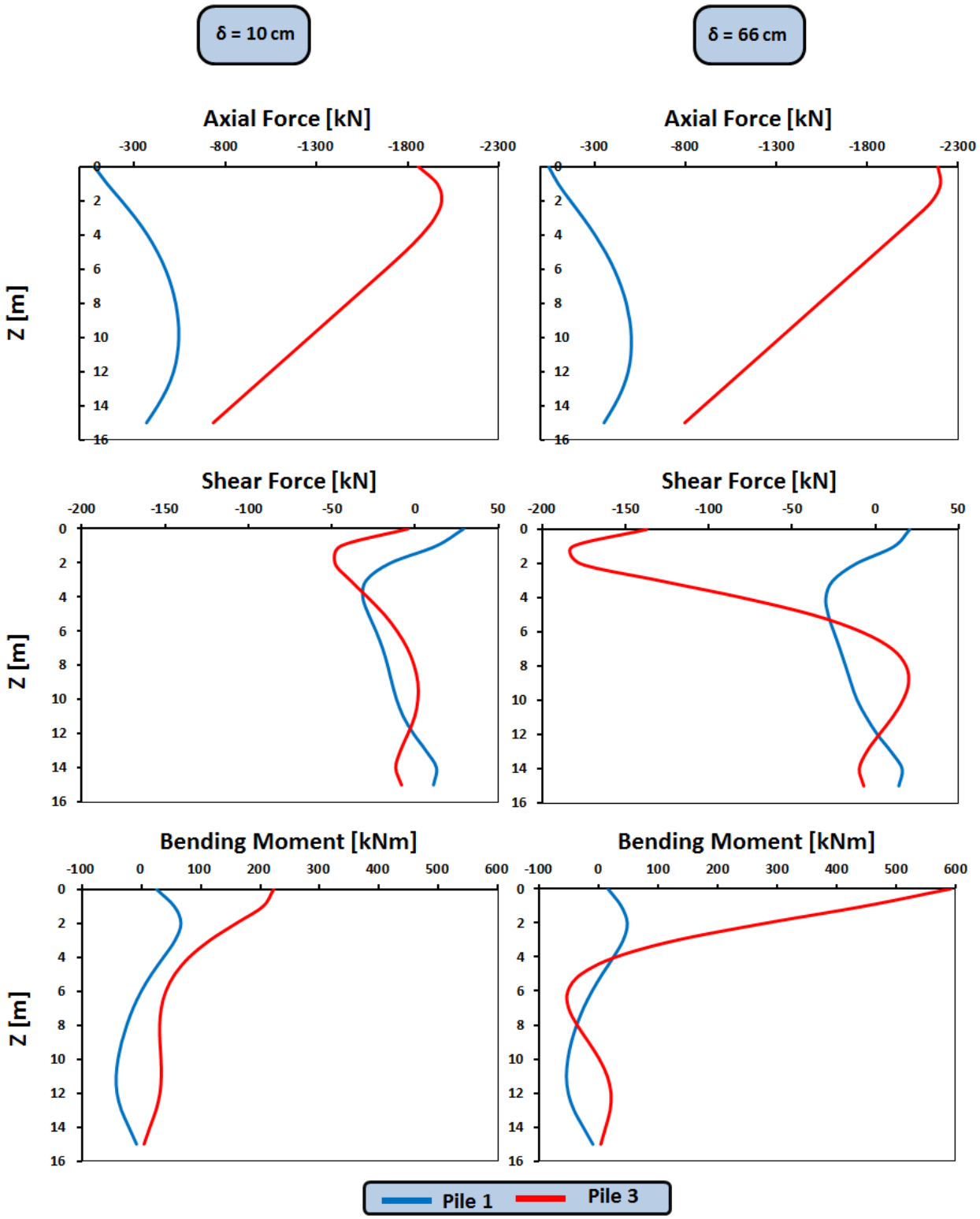

Fig. 6.14: : Distribution of axial forces, shear forces and bending moments along the piles for horizontal deck displacements 10 cm and 66 cm, which corresponds to the maximum axial load on pile 3.

CHAPTER 7

Dynamic Analysis of the Tall Pier

7.1 Selected Earthquakes

In order to test the response of tall piers on all of the designed foundations, three earthquake motions were used. First, as design–level earthquake Aegion (1995) was used. However, due to soil amplification the spectral acceleration of the original Aegion earthquake was significantly amplified at the fundamental period of the pier. Hence, a modified excitation was used, where the acceleration values were divided by two. Kalamata (1986) fitted to the elastic spectrum of Eurocode and Lixouri (2014), both exceeding design–level earthquakes. From Lixouri response spectrum on the free field, which was presented in **Chapter 5**, it can be seen that its maximum value corresponds to the natural period of the structure. Hence, the rocking foundation would lead to greater natural period and smaller accelerations, definitely having an advantageous response. For this reason its time step was multiplied by 1.2. The resulting earthquake is extremely devastating, having 0.59 g peak acceleration and very long–period pulses. The timehistories and the response spectra of the earthquakes at the base and the top of the model are presented in **Figure 7.1** and **7.2** respectively.

7.2 Dynamic Analysis of Connected and Unconnected Conventional Pile Foundations

Figures 7.3 – 7.9 show the response of the two piers on conventionally designed foundations in Kalamata earthquake. The base accelerations of the two systems are almost identical while the deck accelerations of the system with unconnected piles are slightly reduced. Despite that, UC system seems to have a small increase of the ductility demand in terms of curvature. From base shear–displacement graph the stiffness degradation can be observed but is not as prominent as in the short pier. Due to increased moment to shear ratio this degradation takes places at smaller shear forces.

From the displacement timehistories it can be seen that the maximum and the residual values of base displacement, displacement due to rotation and structural deformation are smaller in the case of unconnected piles. Of course, this leads to smaller deck displacements and ductility demand in terms of displacement. On the other hand, as mentioned in the previous paragraph, the ductility demand in terms of curvature is somewhat increased in UC system. This is probably due to concentrated deformation of the pier at each base. In the short pier it was concluded that disconnecting the piles from the pile cap leads to reduction of rotational stiffness resulting in greater rotations but less deformation of the pier. This does not seem to be the case in this studied earthquake. In addition it should be mentioned that both systems are close to collapse, which can be seen from the ductility demand over capacity timehistories. This is expected since the earthquake exceeds the design–level earthquake.

The distribution of axial forces, shear forces and bending moments along the piles at the time when maximum moment is transmitted to the soil are shown in **Figure 7.9**.

The main goal to reduce the stresses on the piles have been achieved with reductions of 45%, 75% and 45% in maximum axial forces, shear forces and bending moments respectively. There is a negligible, less than 0.5 cm, increase in the settlement of the foundation on unconnected piles, which cannot be considered a disadvantage of this design.

In **Table 7.1** the performance of the two systems in the two earthquakes is summarized and compared based on eight important parameters. Both systems collapsed during the severe Lixouri excitation and their results are not presented in the table. As it can be seen in **Appendix B**, their response was similar until their collapse and it cannot be stated that the one or the other performed better. From these three dynamic analyses it is concluded that systems in connected or unconnected pile groups, designed according to current codes safety factors response similarly. Disconnecting the piles from the cap successfully reduce stresses on them. Slenderness did not seem to play an important role on the behavior of such systems however the settlements were reduced compared to the short piers.

Table 7.1: Results of dynamic analysis in each earthquake of the two systems. Compared in eight parameters: residual deck displacement, residual pier deformation, maximum ratio of ductility demand over ductility capacity in terms of displacement and curvature, total settlement, maximum developed axial force, shear force and bending moment on the piles.

	AEGION		**KALAMATA**	
	CC	**UC**	**CC**	**UC**
Residual U_{top} (m)	0.060	0.030	0.475	0.435
Pier Deformation (m)	0.050	0.029	0.450	0.425
$(\mu_{demand}/\mu_{capacity})_{\Delta}$	0.25	0.21	1.06	0.99
$(\mu_{demand}/\mu_{capacity})_{r}$	0.12	0.12	0.82	1.01
w (cm)	1.0	1.5	3.0	3.5
max Pile Axial (kN)	2389	1420	2464	1343
max Pile shear (kN)	366	46	457	115
max Pile Moment (kNM)	380	146	905	495

7.3 Dynamic Analysis of Unconnected Conventional and Rocking Pile Foundations

In the previous paragraph conventional foundation with unconnected piles was studied under earthquake loading and its response was found similar to the conventionally designed foundation with connected piles, while the piles stresses significantly reduced. As its response was satisfying, here it is compared to the response of a rocking foundation on top of unconnected piles. The same two

earthquakes were applied and their responses in Kalamata are presented in **Figures 7.10 – 7.18** while in Lixouri and Aegion in **Appendix B**.

The aim of Rocking Isolation was the maximum deck acceleration to be bounded by $a_{max} = \frac{M_{f,ult}}{hm} \approx 0.18\ g$ and the pier to remain elastic. From the timehistories it can be seen that this is achieved. On the other hand excessive soil plastification takes place, which can be seen from the foundation's moment–rotation and shear–displacement curves. As expected, this leads to large rotations and "rocking displacements", hθ, as well as displacements of the pile cap but minimal structural deformations. As a result, the total deck displacement of the rocking system is reduced compared to the conventional one having smaller both maximum and residual values.

The system designed according to conventional factors of safety consumes almost all its ductility capacity while the rocking system only 13%. Hence, the most salient improvement of this new design philosophy is the avoidance of collapse. It is noted that in Lixouri excitation, that both conventional systems collapsed, the rocking had a ductility demand over capacity ratio only 19%.

Of course, there are drawbacks in this system as well. The settlement has increased as well as the axial forces, shear forces and bending moments on the piles as they participate more in the vertical and lateral loading of the system. However, the piles still have smaller forces and moments then the connected piles of the conventional system.

Table 7.2: Results of dynamic analysis in each earthquake of the two systems. Compared in seven parameters: residual deck displacement, residual pier deformation, maximum ratio of ductility demand over ductility capacity in terms of displacement, total settlement, maximum developed axial force, shear force and bending moment on the piles.

	AEGION		**KALAMATA**		**LIXOURI**	
	UC	**UR**	**UC**	**UR**	**UC**	**UR**
Residual U_{top} (m)	0.030	0.010	0.435	0.100	–	0.160
Pier Deformation (m)	0.029	0.020	0.425	0.045	–	0.020
$(\mu_{demand}/\mu_{capacity})_{\Delta}$	0.21	0.05	0.99	0.13	–	0.19
w (cm)	1.5	2.5	3.5	5.5	–	11.0
max Pile Axial (kN)	1420	2163	1343	2221	–	2105
max Pile shear (kN)	46	63	115	154	–	183
max Pile Moment (kNM)	146	288	495	732	–	690

Table 7.2 summarizes the response of the two systems in the three earthquakes according to seven important parameters. From the dynamic analyses of the short and the tall pier it appears that while the conventionally designed foundation with

unconnected piles is not affected by structure's slenderness, the rocking system is. The total deck displacements at the tall rocking pier were reduced compared to the conventional ones, but this is not always the case for the short pier. It is also important to note that in the tall pier even the maximum deck displacements are not larger in UR than in UC. Moreover, in the Lixouri excitation applied in the short pier the ductility demand of the rocking system is 16% while in the extremely devastating modified Lixouri used for the tall piers the rocking system increases its ductility demand only to 19%. Although the settlements of the rocking system are increased, they are considered acceptable for Aegion and Kalamata earthquakes and a small price to pay compared to the collapse of the conventional systems during Lixouri excitation. The response of the rocking system in Lixouri is illustrated in **Appendix B**.

Figures of Chapter 7

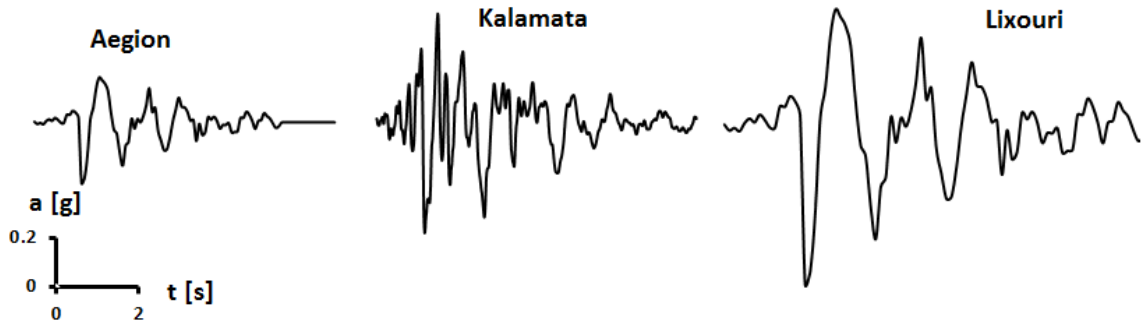

Fig. 7.1: Earthquakes timehistories used for the dynamic analysis of the three systems. Aegion accelerations have been divided by 2, Kalamata has been fitted to design spectrum and Lixouri timestep has been multiplied by 1.2.

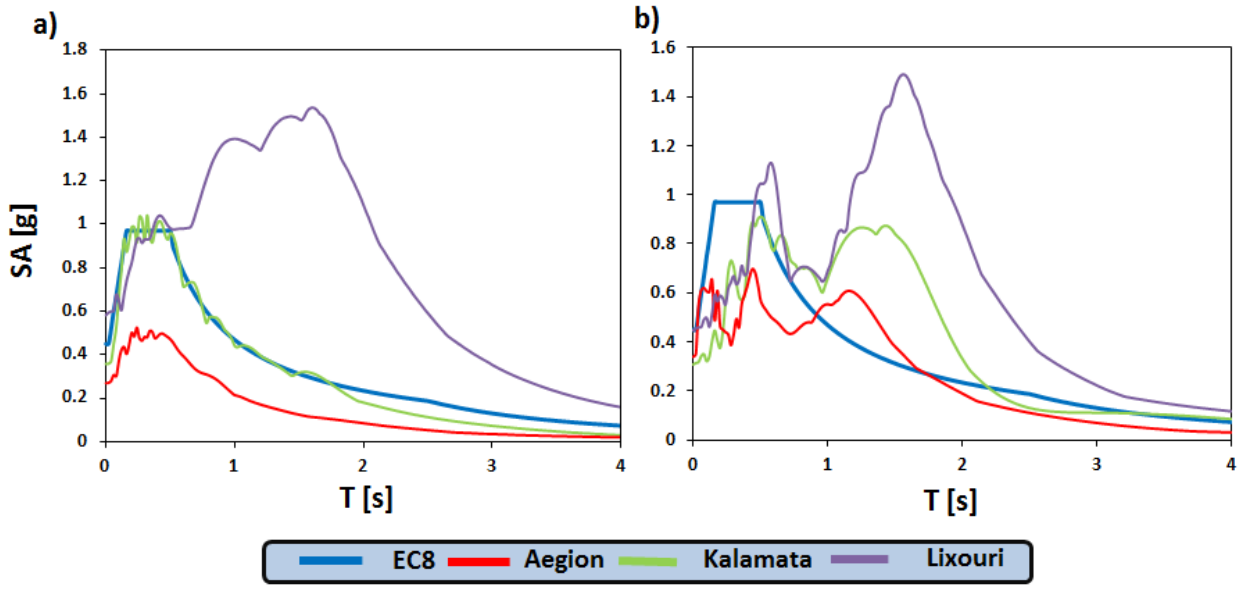

Fig 7.2: Response spectra of the used accelerograms compared to design response spectrum at (a) base of the model (b) free field.

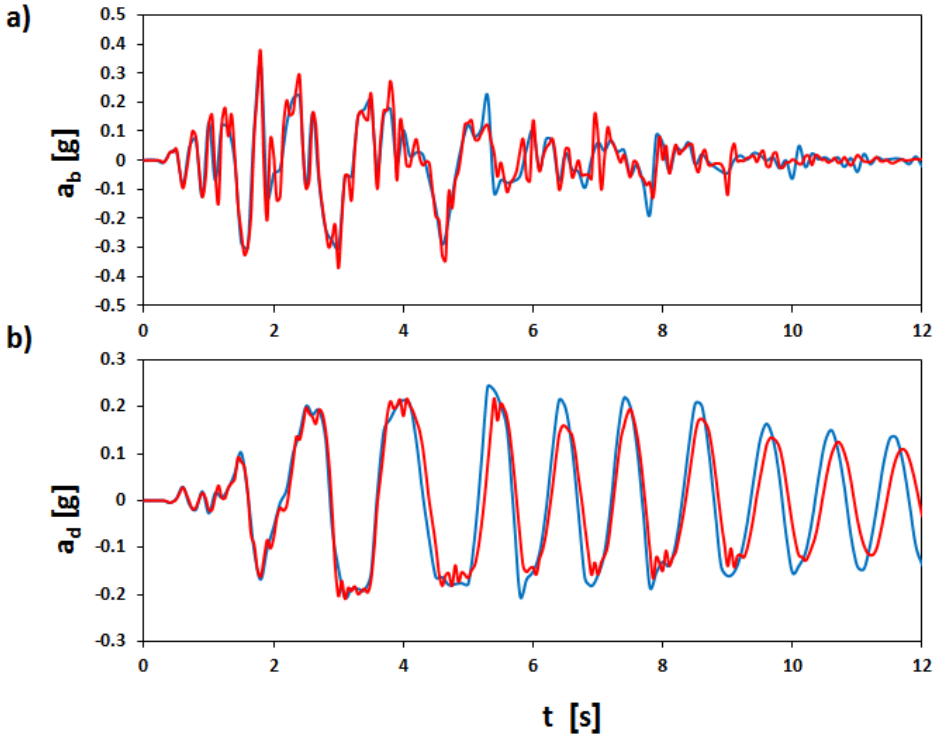

Fig. 7.3: Acceleration timehistory during Kalamata excitation at (a) the base of the pier (b) the deck for the case connected (blue) and unconnected (red) piles.

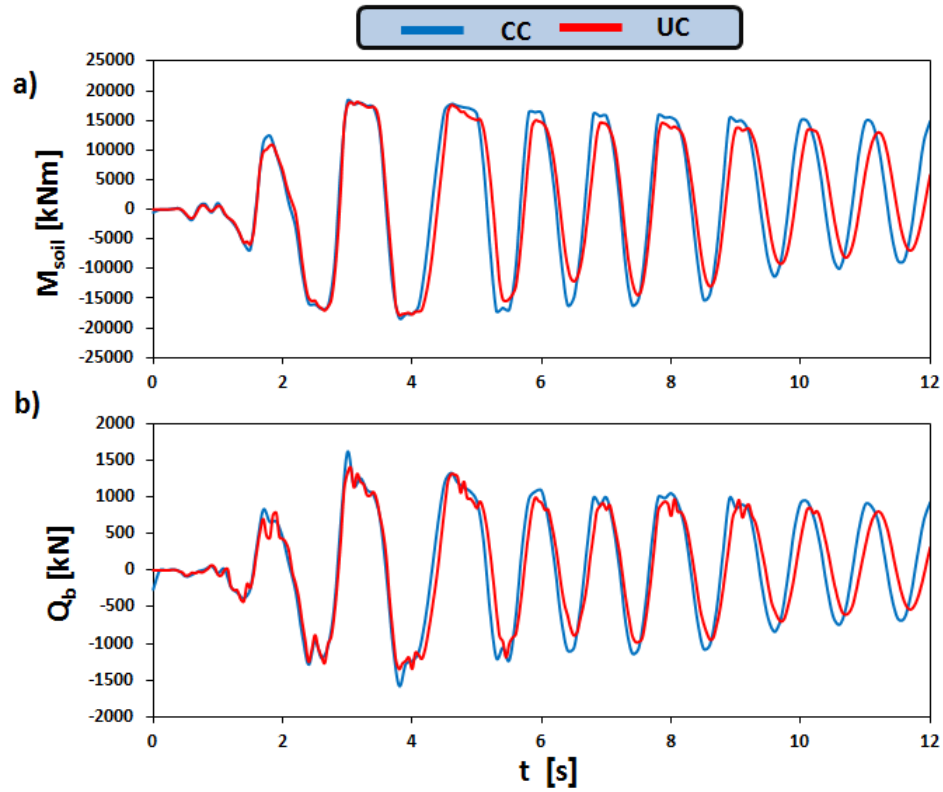

Fig. 7.4: Timehistories of (a) bending moment (b) shear force at the base of the pier during Kalamata excitation for the case of connected (blue) and unconnected (red) piles.

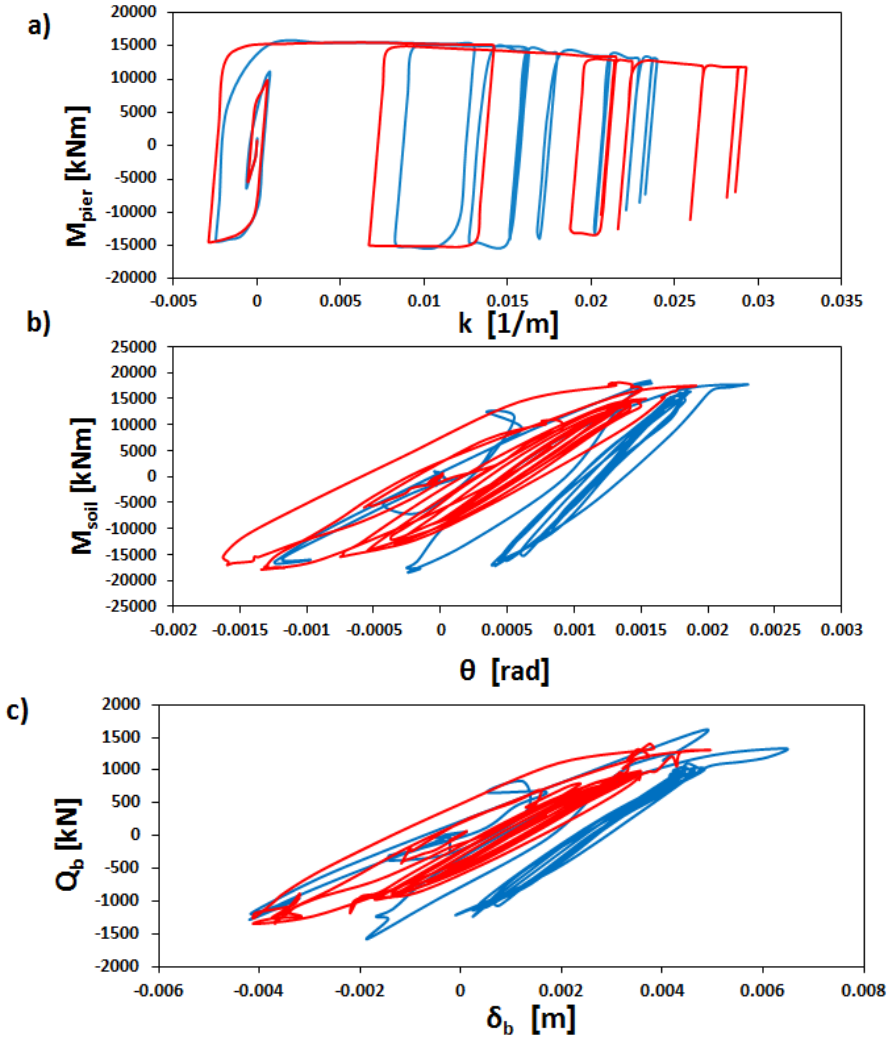

Fig. 7.5: Comparison of the response of the two conventionally designed systems with connected (blue) and unconnected (red) piles in terms of (a) bending moment–curvature at the base of the pier (b) moment–rotation of the foundation level (c) base shear–displacement of the foundation.

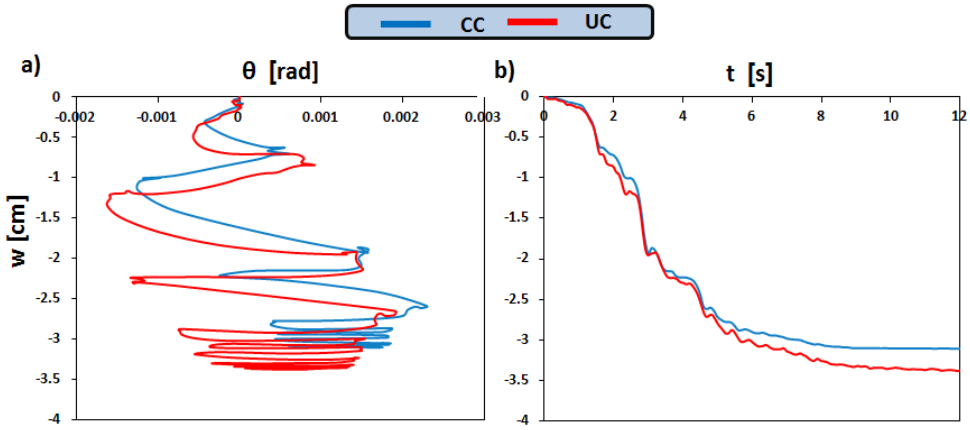

Fig. 7.6: Comparison of the settlements of the two alternative conventional designs subjected to Kalamata earthquake in terms of (a) settlement–rotation and (b) settlement timehistory.

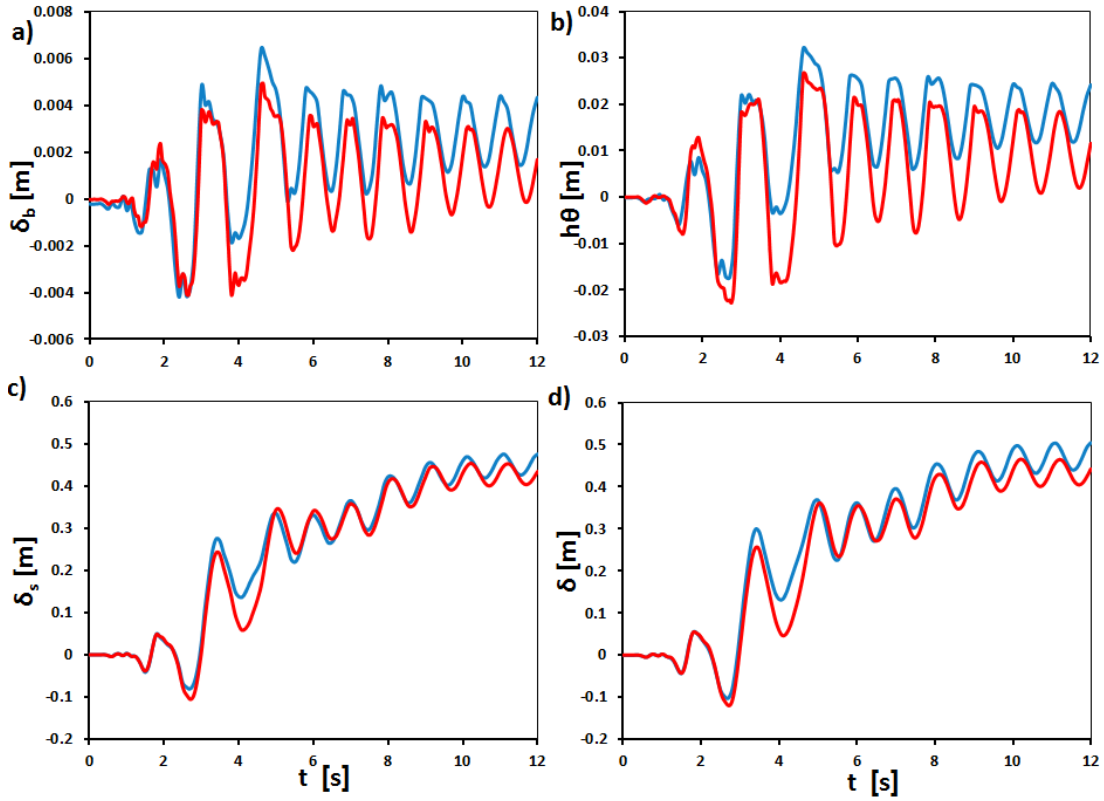

Fig. 7.7: Comparison of the response of the two conventionally designed systems with connected (blue) and unconnected (red) piles in terms of (a) foundation displacement (b) displacement due to the rotation of the foundation (c) structural deformation of the pier (d) total deck displacement.

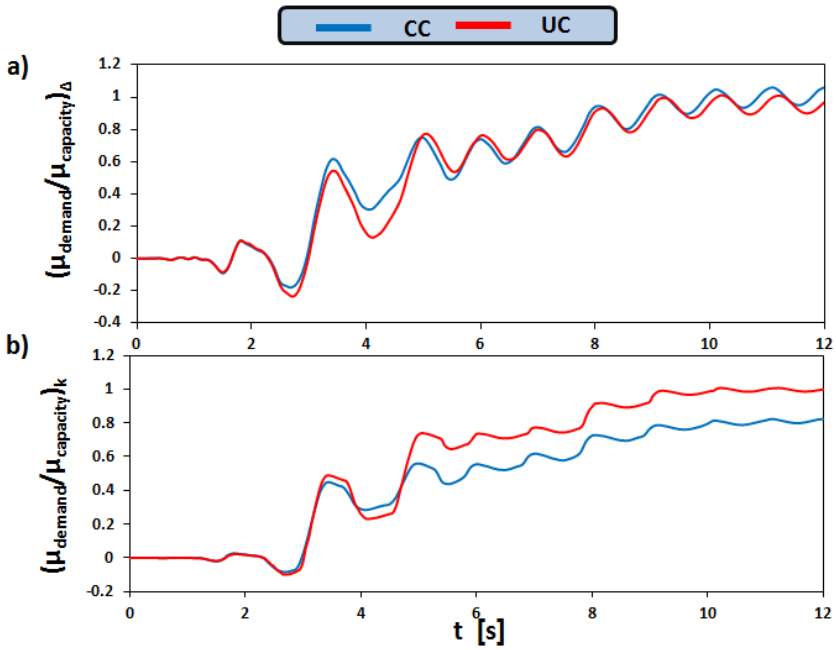

Fig 7.8: Comparison of ductility demand over ductility capacity of the two conventionally designed systems in terms of (a) displacement (b) curvature for Kalamata earthquake.

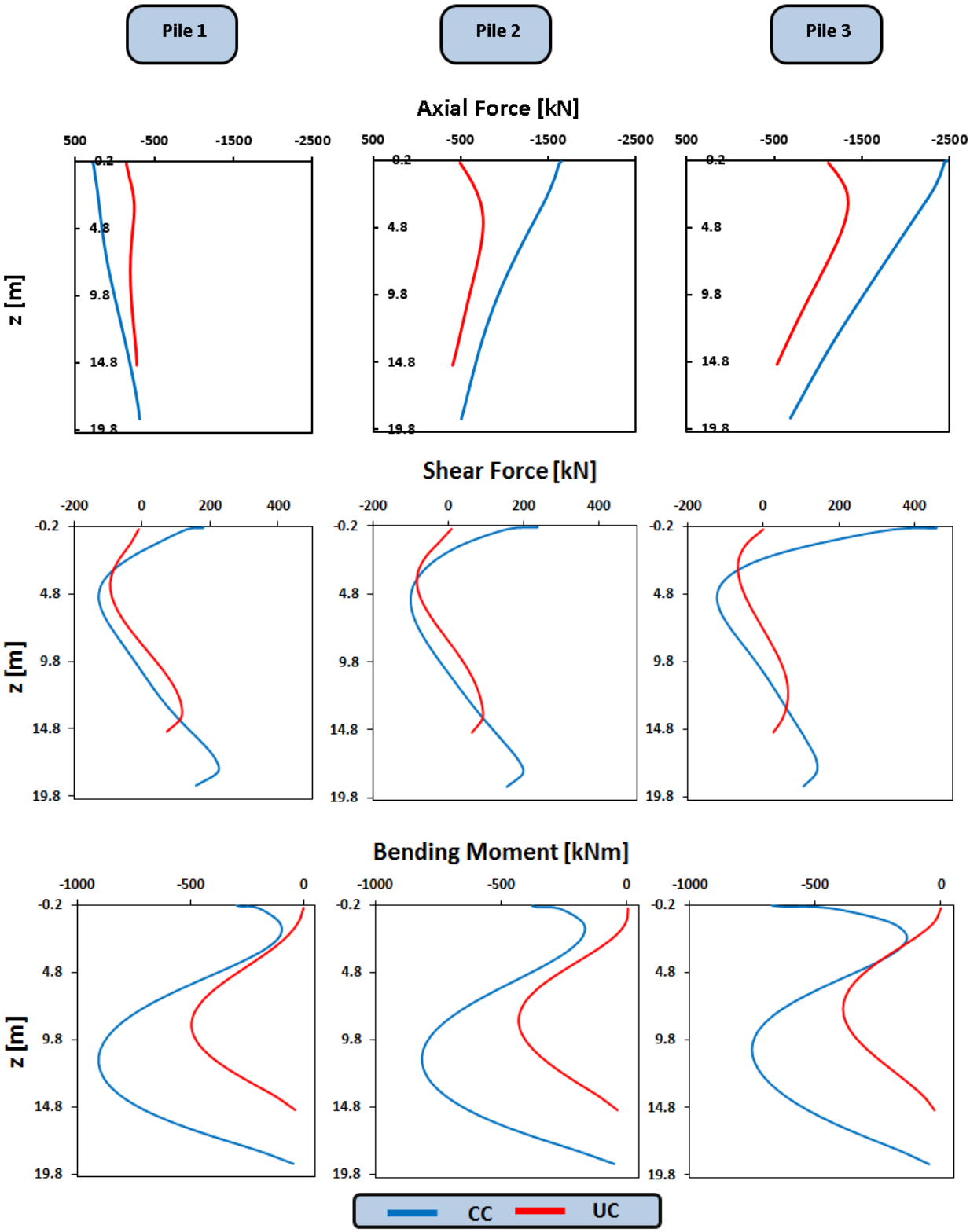

Fig. 7.9: Distribution of axial forces, shear forces and bending moments along the piles when maximum moment is transmitted to the soil (Kalamata).

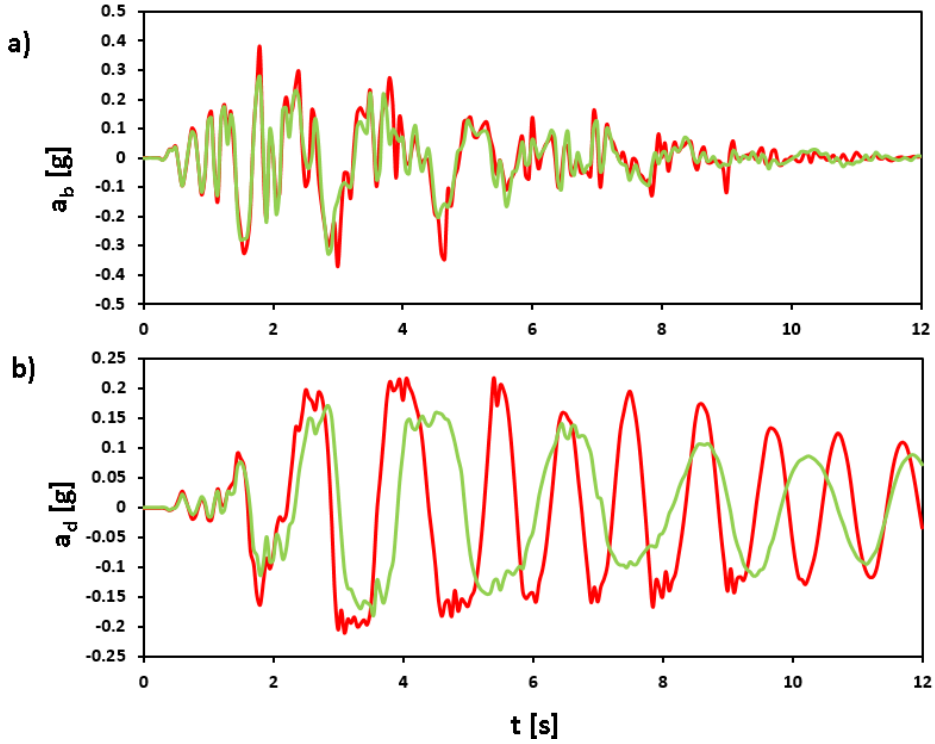

Fig. 7.10: Comparison of the response of conventional (UC) and rocking (UR) foundations on unconnected piles in terms of (a) pier base and (b) deck accelerations for Kalamata earthquake.

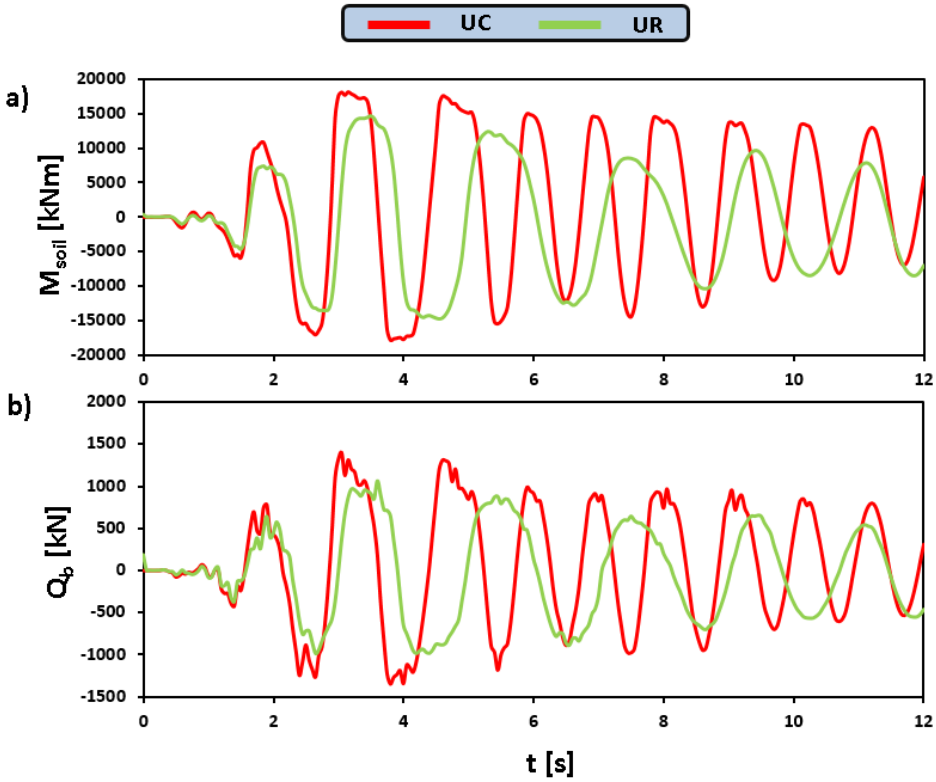

Fig. 7.11: Comparison of the response of conventional (UC) and rocking (UR) foundations on unconnected piles in terms of (a) pier base and (b) deck accelerations for Kalamata earthquake.

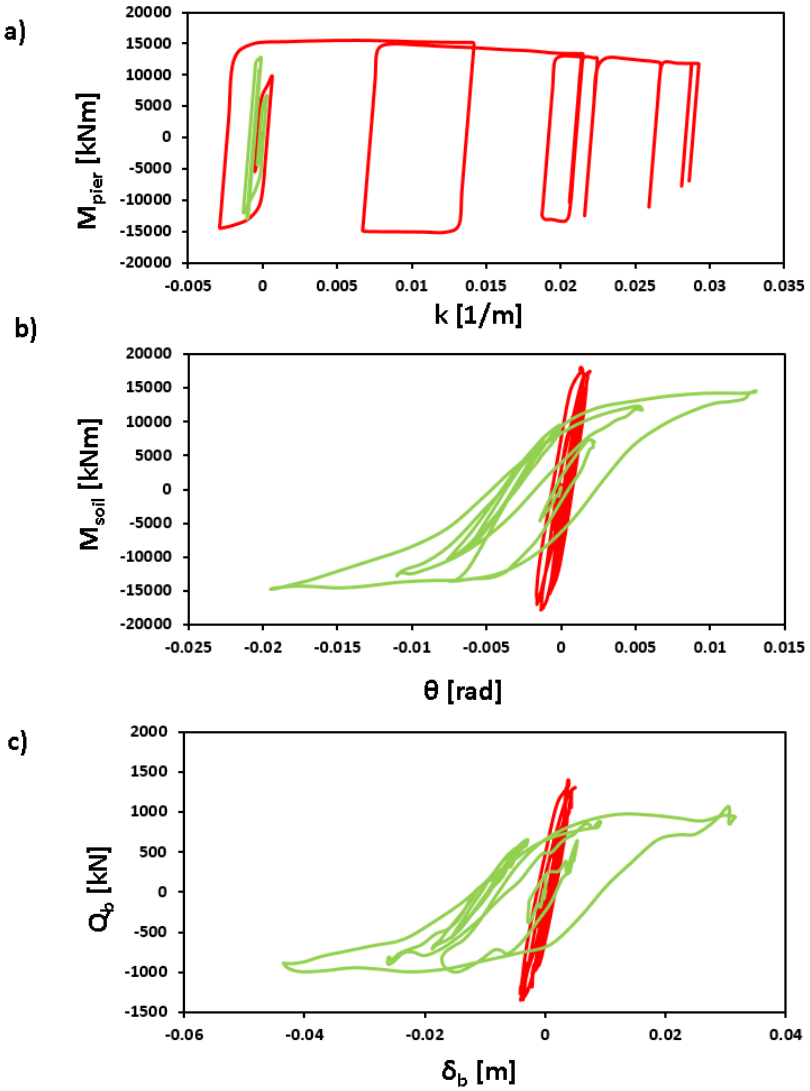

Fig. 7.12: Comparison of the two alternatives unconnected pile foundations, conventional (UC) and rocking (UR), in terms of (a) moment–curvature at the base of the pier (b) Moment–rotation at the foundation level (c) shear-displacement at the pier base for Kalamata earthquake.

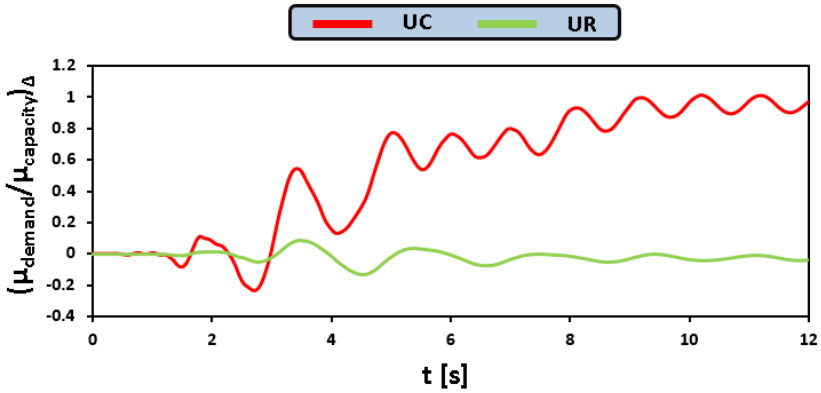

Fig. 7.13: Comparison of ductility demand over ductility capacity, in terms of displacements, of the two alternatives unconnected pile foundations for Kalamata earthquake.

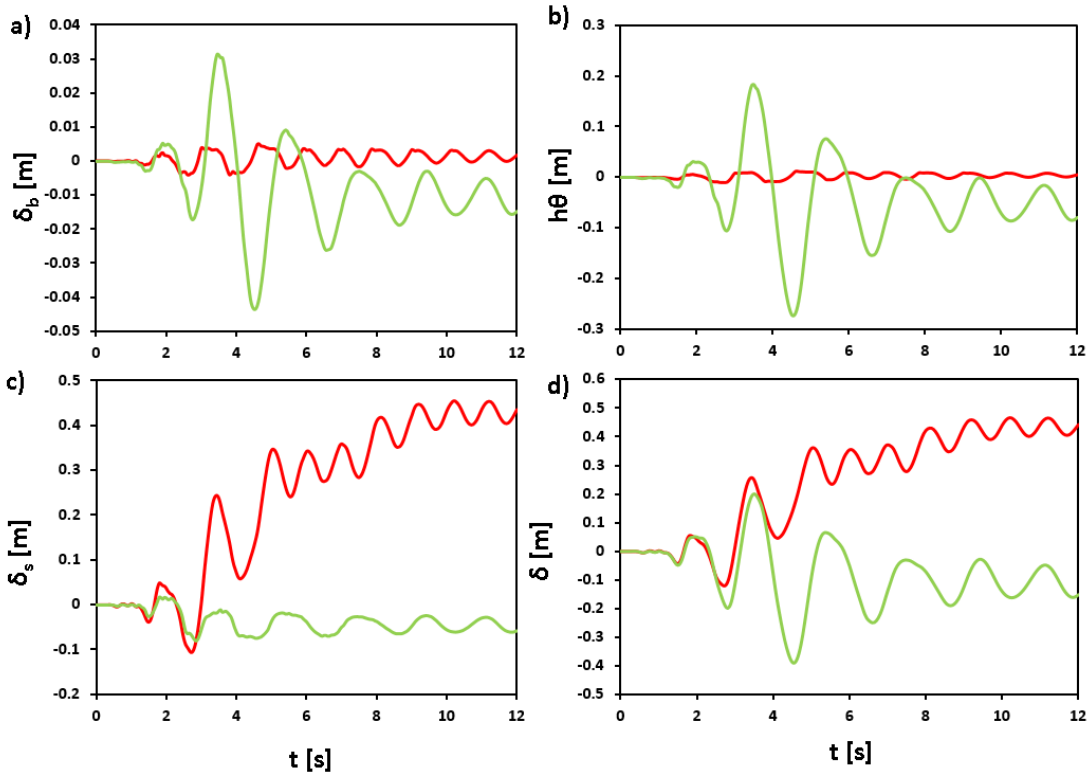

Fig. 7.14: Comparison of the two alternatives unconnected pile foundations, conventional (UC) and rocking (UR), in terms of (a) foundation displacement (b) displacement due to the rotation of the foundation (c) structural deformation of the pier (d) total deck displacement. (Aegion earthquake)

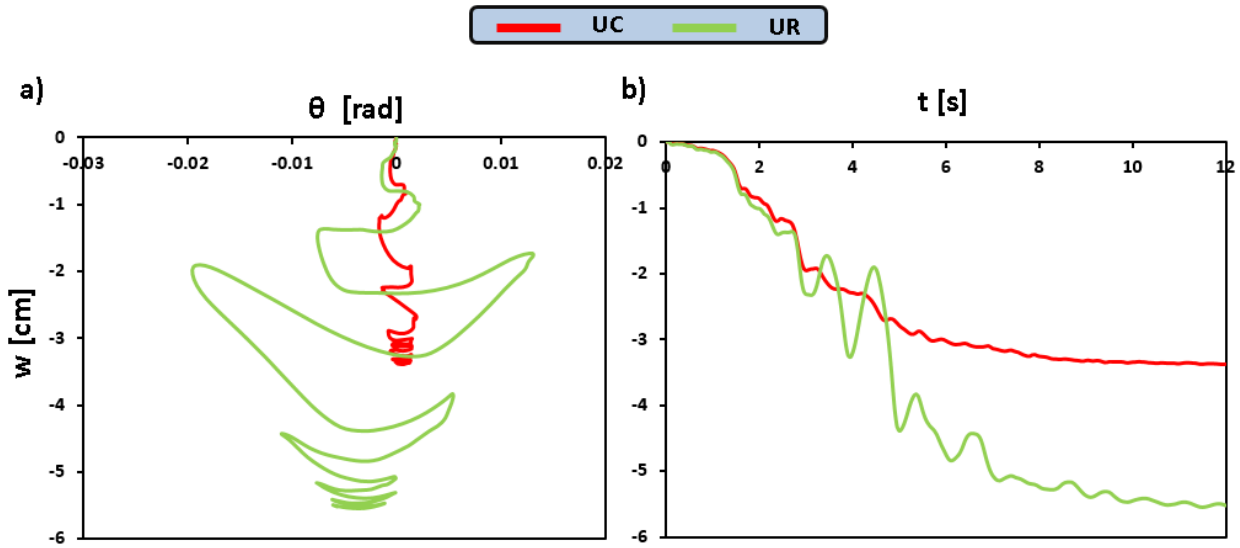

Fig. 7.15: Comparison of the settlements of the two alternative conventional designs subjected to Aegion earthquake in terms of (a) settlement–rotation and (b) settlement timehistory.

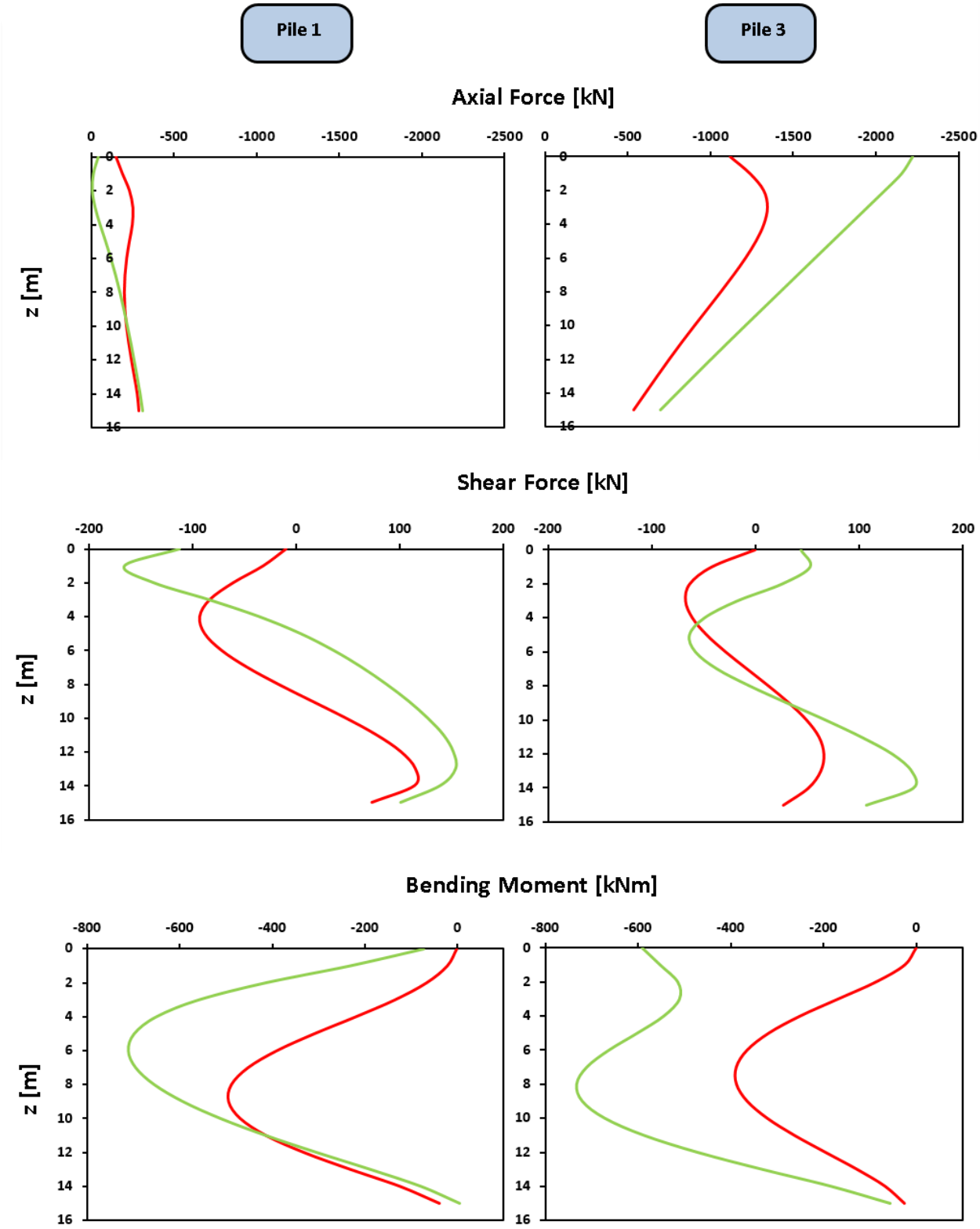

Fig. A.28: Distribution of axial forces, shear forces and bending moments along the piles when maximum moment is transmitted to the soil (Kalamata earthquake).

CHAPTER 8

Conclusions

In this study the dynamic response of bridge piers supported on foundations with connected and unconnected piles was studied. In order to examine the effects of slenderness a short and a tall pier were subjected to earthquake excitations on Abaqus. Two foundations with unconnected piles were studied. The first one was designed conventionally, with the ultimate moment capacity of the foundation being greater than that of the pier. In the second the foundation was designed with smaller moment capacity than the pier in order to achieve rocking isolation. Since no analytical solution exist to design such systems, vertical and horizontal push–over analyses were employed in order to estimate their vertical and horizontal capacity. The main conclusions of the study are:

- The dynamic response in terms of ductility demand, total deck displacements and settlements of the conventionally designed foundation with unconnected piles was slightly improved compared to that with connected piles.
- The axial forces, bending moments and shear forces on the unconnected piles were significantly reduced compared to the connected ones.
- Slenderness does not play an important role in the response of bridge piers on conventionally designed foundations with unconnected piles.
- In both cases of the short and the tall pier the rocking foundation led to elastic response of the pier and significant decrease of the ductility demand over ductility capacity.
- The pier supported on rocking foundation survived all earthquakes, even a severe modified Lixouri excitation where both conventionally designed systems collapsed.
- The unconnected piles of the rocking foundation had slightly increased stressed compared to those of the conventional foundation. However, this was still smaller than the stresses of the connected piles.
- In the tall pier both the residual and the maximum deck displacements were reduced in the case of rocking foundation. On the other hand, in the short pier the residual deck displacements were similar to those of the conventional system but the maximum displacements due to “rocking displacements”, hθ, were significantly larger. Hence, it was concluded that slenderness affects the response of rocking piers.
- The main price to pay when foundations are designed according to the Rocking Isolation Philosophy is the increased settlements.

This studied showed the beneficial aspects of the use of unconnected piles. However there is need for more studies in order to investigate the response of foundations with unconnected piles in different soil conditions, as well as the use end bearing unconnected piles. In addition it should be examined whether the settlement of the pier on rocking foundation with unconnected piles can be reduced if the pile cap–pile distance is reduced. Of course, in order to validate the numerical simulations and allow the use of such systems there is a need for experiments.

APPENDIX A

Earthquake Response of Short Piers

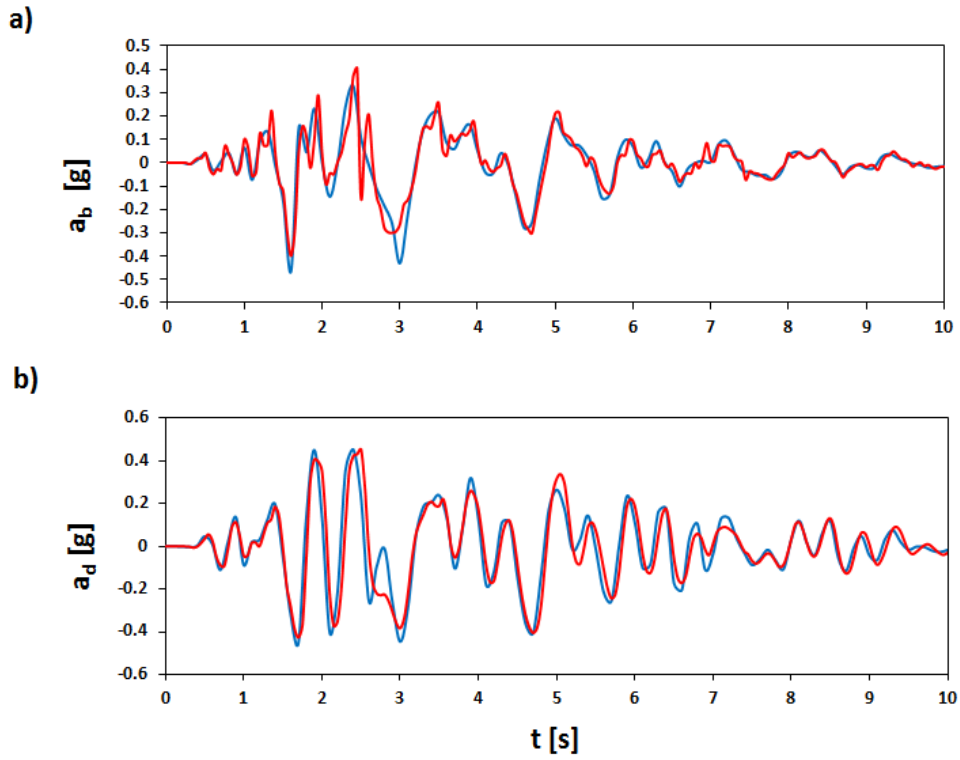

Fig. A.1: Acceleration timehistory during Kalamata excitation at (a) the base of the pier (b) the deck for the case connected (blue) and unconnected (red) piles.

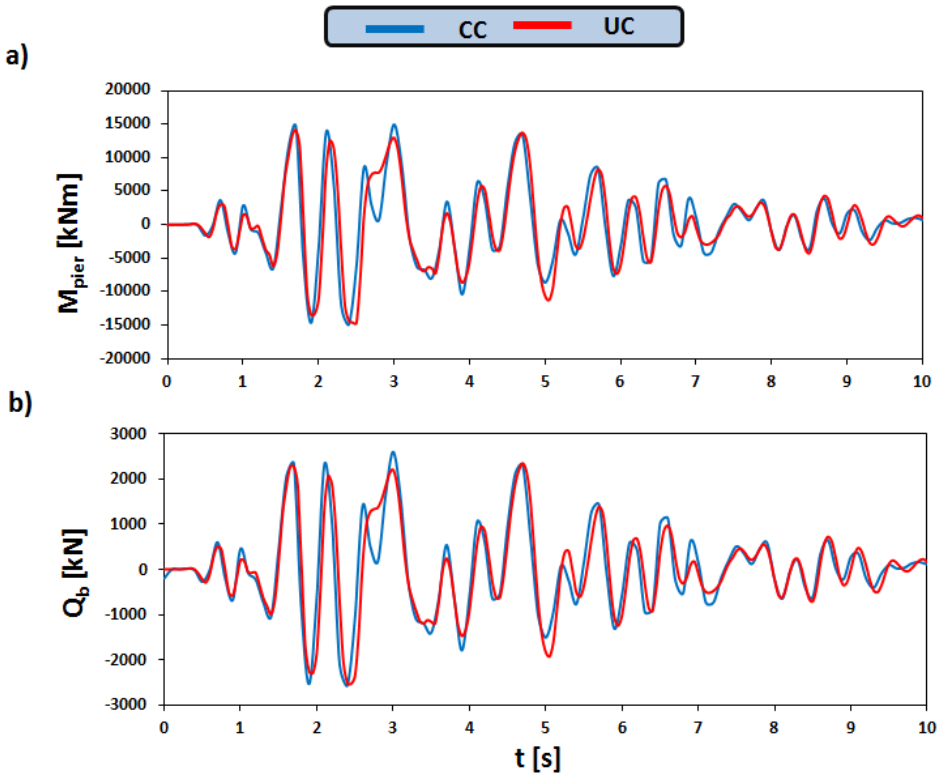

Fig. A.2: Timehistories of (a) bending moment (b) shear force at the base of the pier during Shinkobe excitation for the case of connected (blue) and unconnected (red) piles (Kalamata).

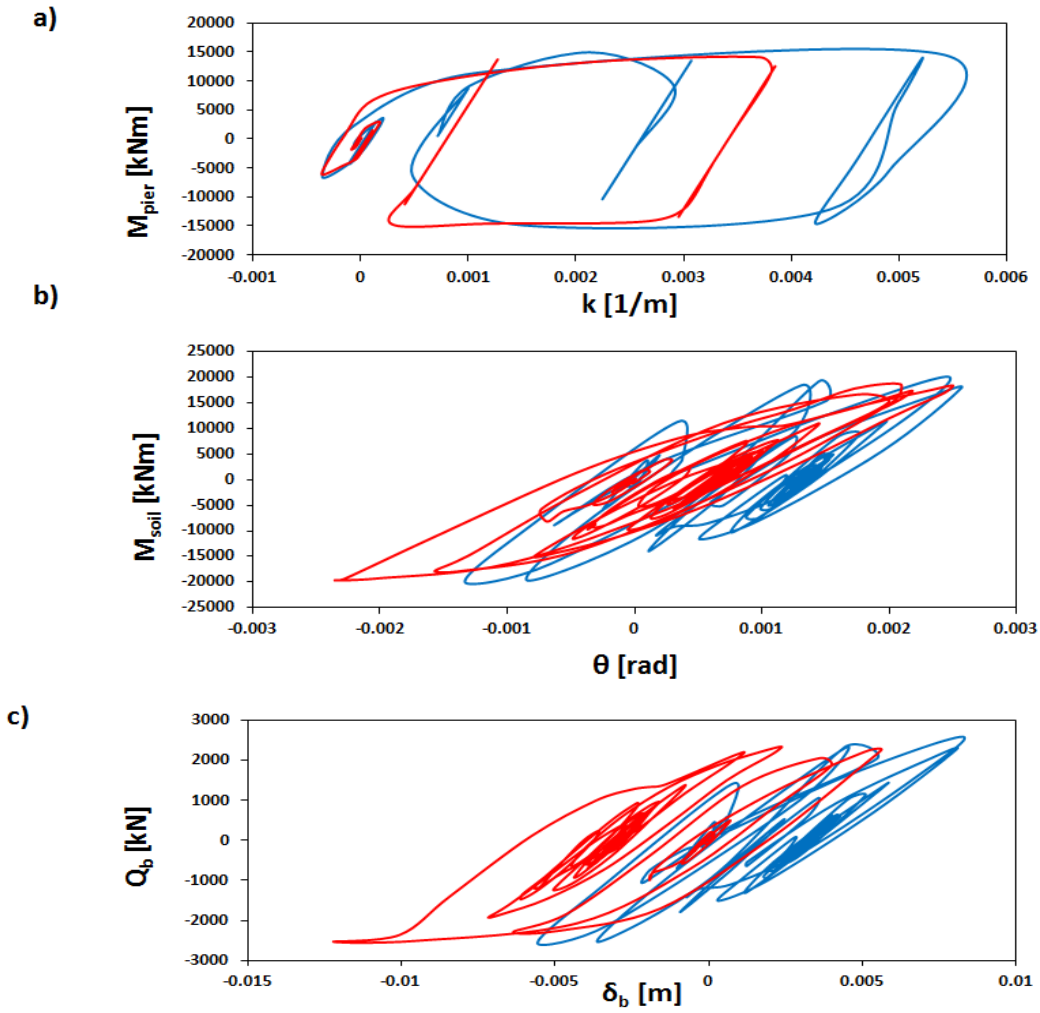

Fig. A.3: Comparison of the response of the two conventionally designed systems with connected (blue) and unconnected (red) piles in terms of (a) bending moment–curvature at the base of the pier (b) moment–rotation of the foundation level (c) base shear–displacement of the foundation. (Kalamata)

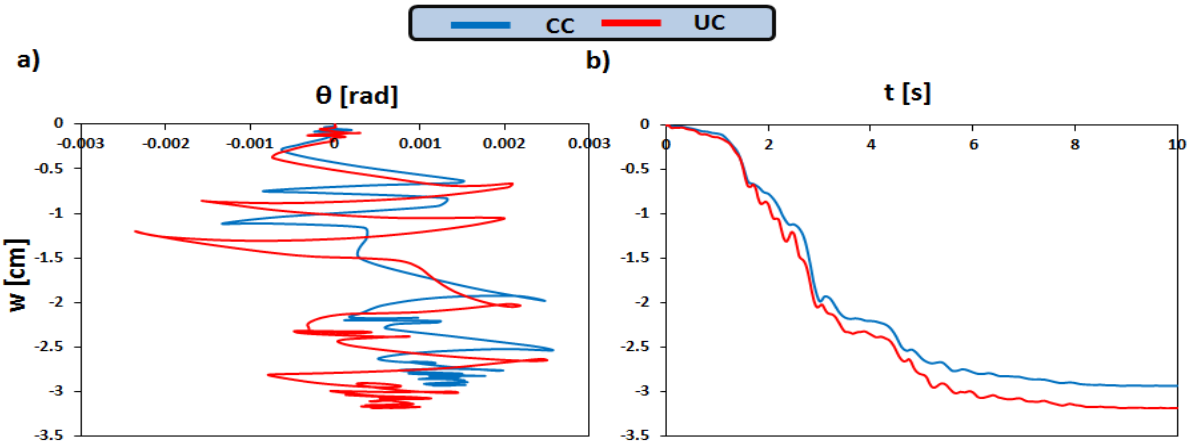

Fig. A.4: Comparison of the settlements of the two alternative conventional designs subjected to Kalamata earthquake in terms of (a) settlement–rotation and (b) settlement timehistory.

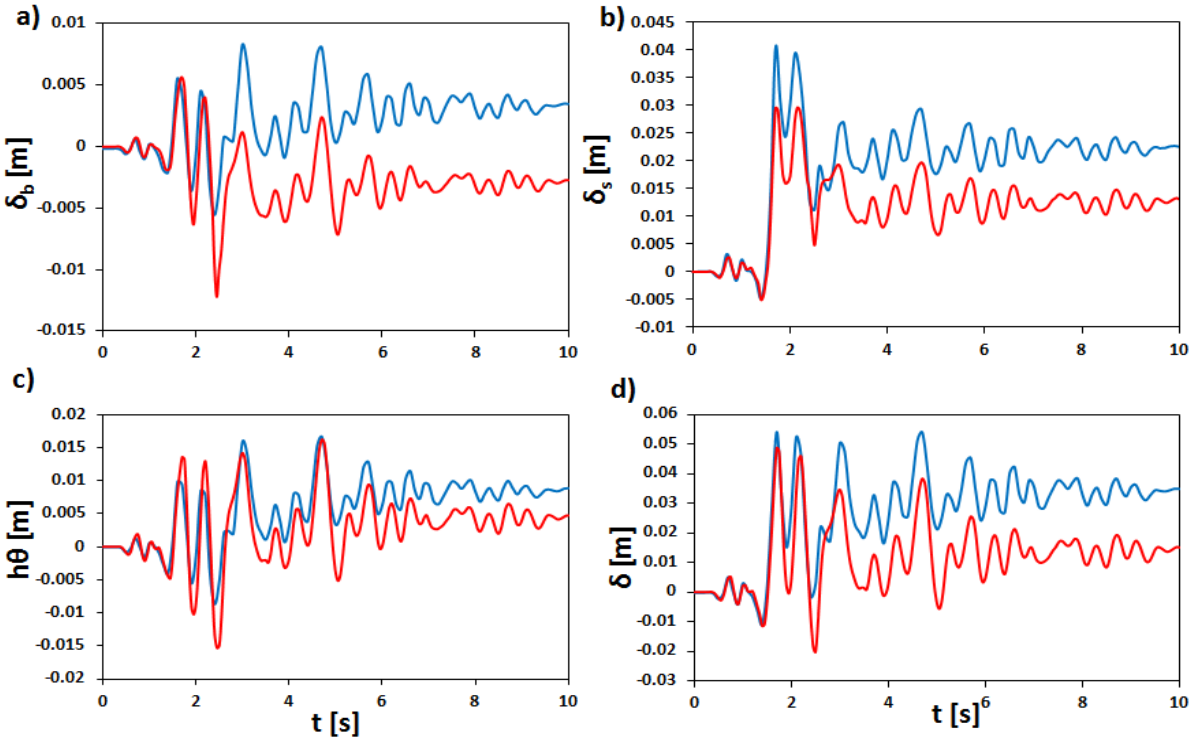

Fig. A.5: Comparison of the response of the two conventionally designed systems with connected (blue) and unconnected (red) piles in terms of (a) foundation displacement (b) displacement due to the rotation of the foundation (c) structural deformation of the pier (d) total deck displacement. (Kalamata)

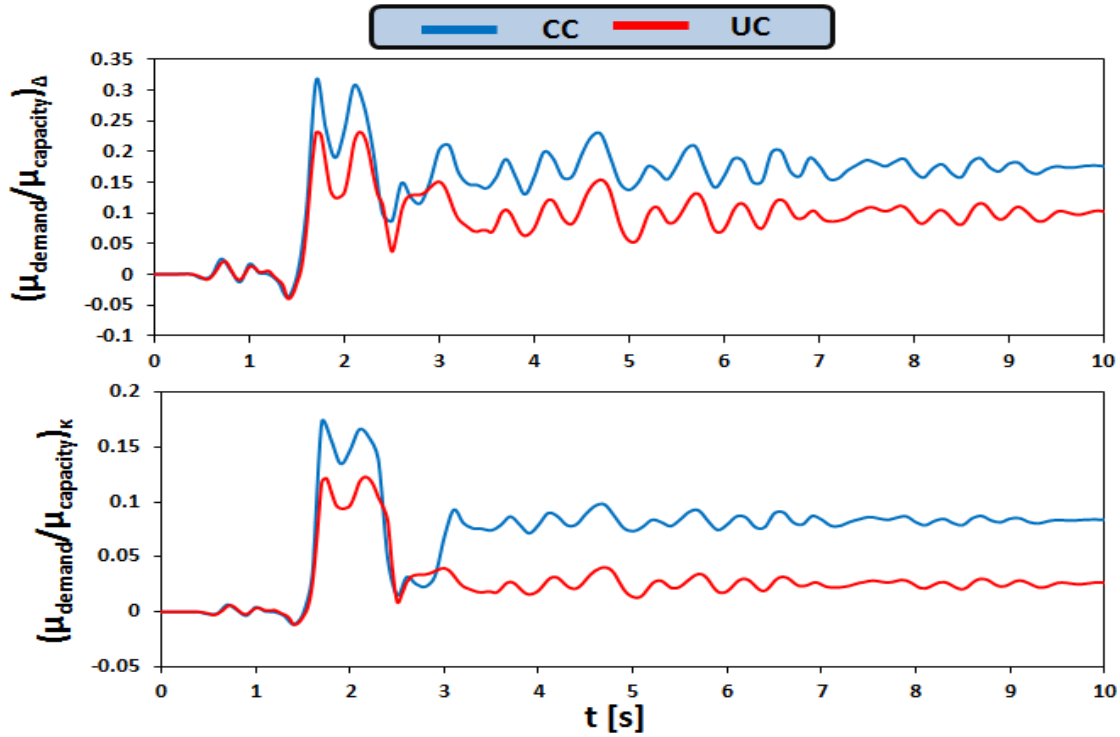

Fig. A.6: Comparison of ductility demand over ductility capacity of the two conventionally designed systems in terms of (a) displacement (b) curvature for Kalamata earthquake.

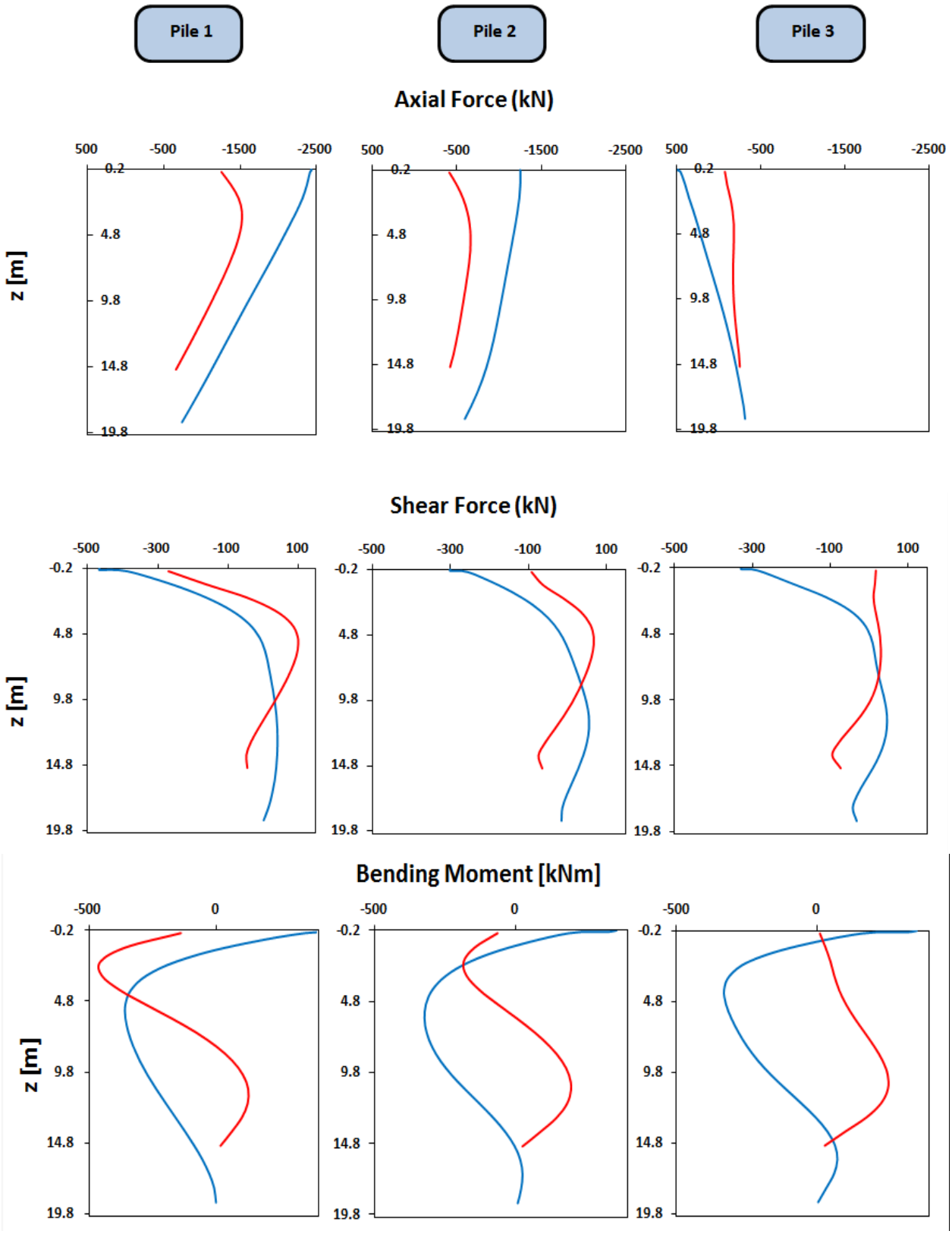

Fig. A.7: Distribution of axial forces, shear forces and bending moments along the piles when maximum moment is transmitted to the soil (Kalamata).

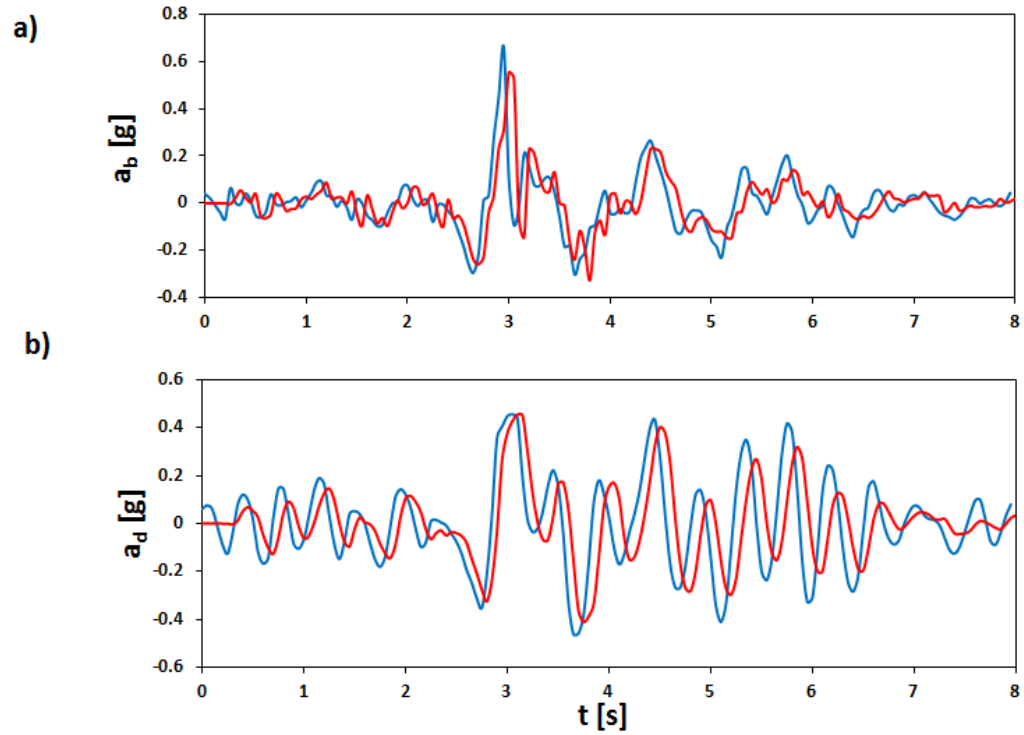

Fig. A.8: Acceleration timehistory during Aegion excitation at (a) the base of the pier (b) the deck for the case connected (blue) and unconnected (red) piles.

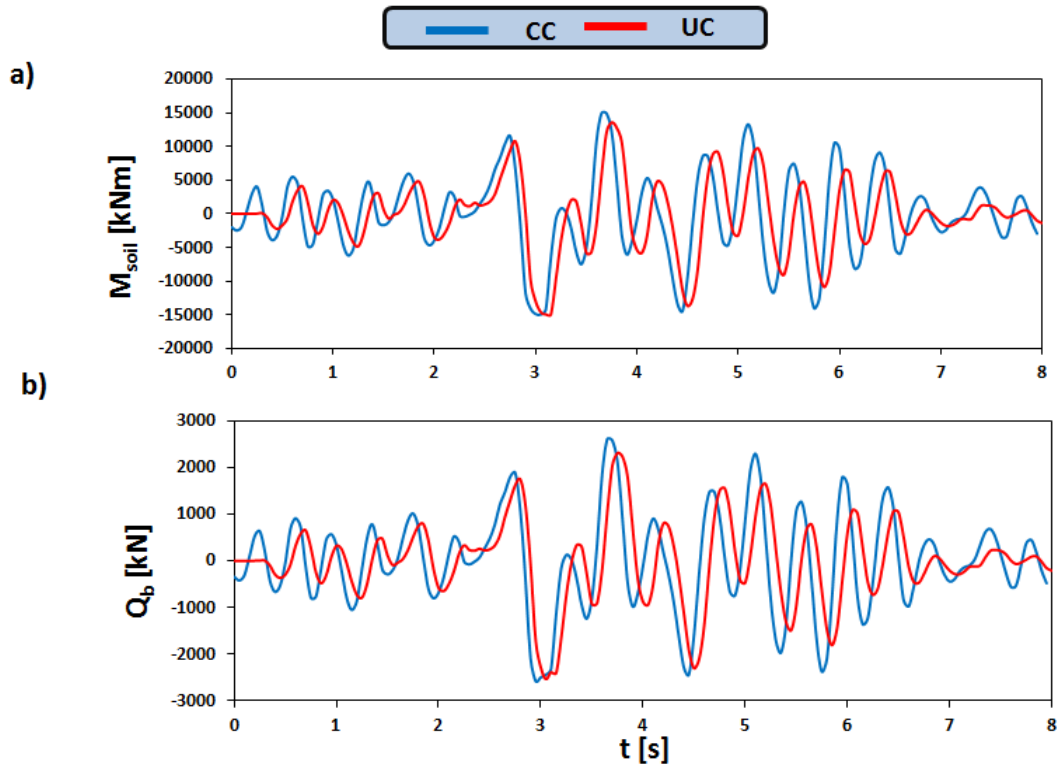

Fig. A.9: Timehistories of (a) bending moment (b) shear force at the base of the pier during Aegion excitation for the case of connected (blue) and unconnected (red) piles.

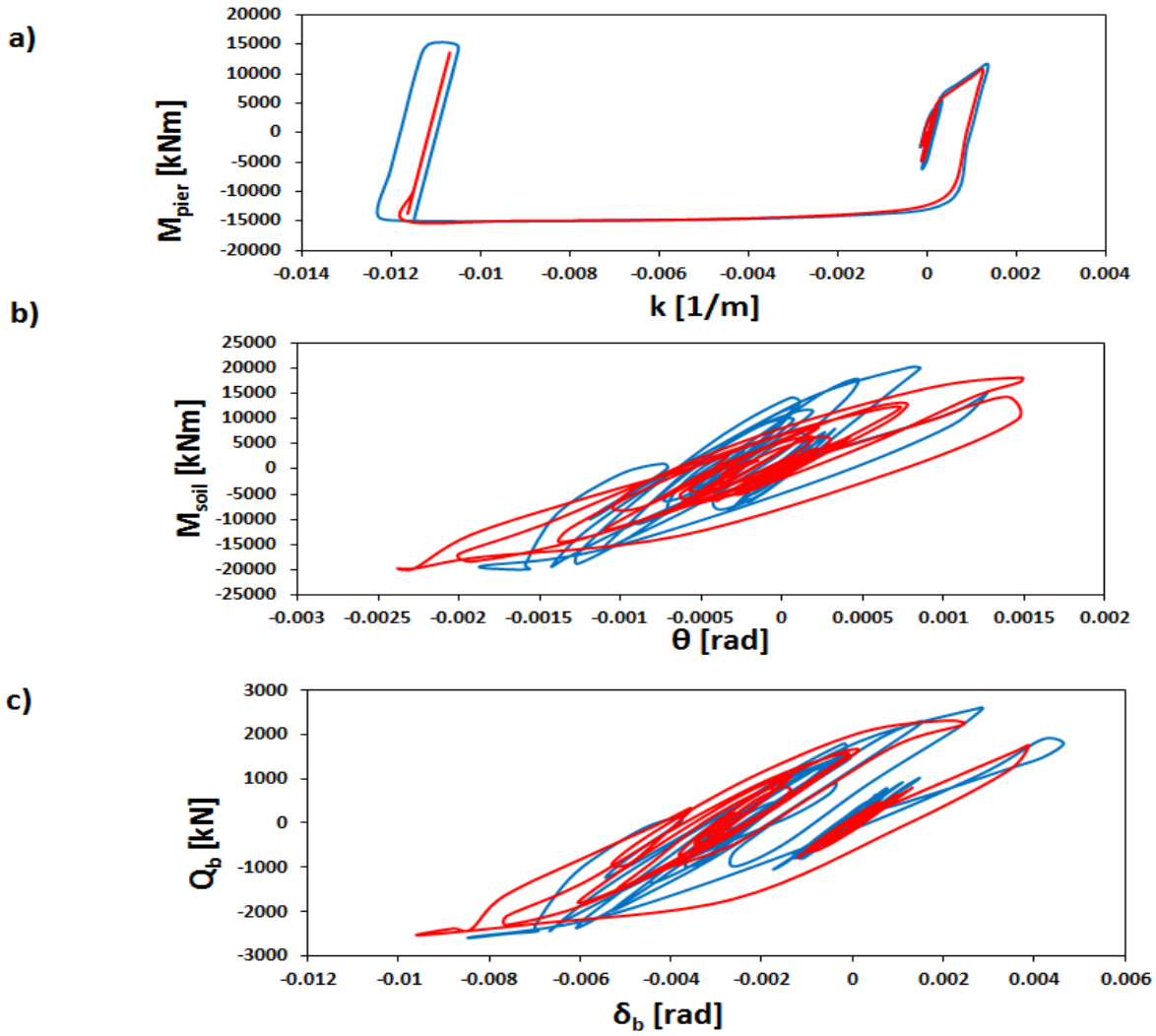

Fig. A.10: Comparison of the response of the two conventionally designed systems with connected (blue) and unconnected (red) piles in terms of (a) bending moment–curvature at the base of the pier (b) moment–rotation of the foundation level (c) base shear–displacement of the foundation. (Aegion excitation)

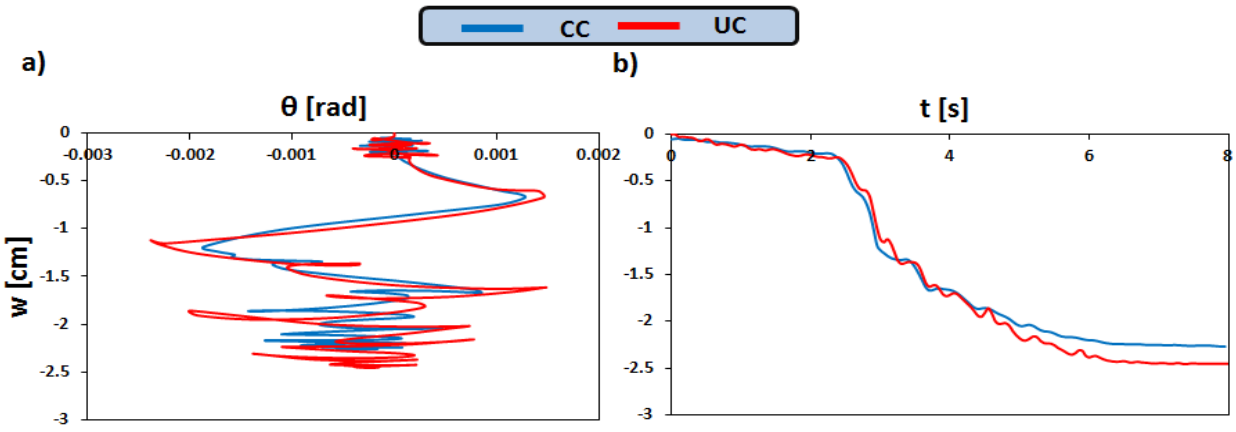

Fig. A.11: Comparison of the settlements of the two conventional aternative designs subjected to Aegion earthquake in terms of (a) settlement–rotation and (b) settlement timehistory.

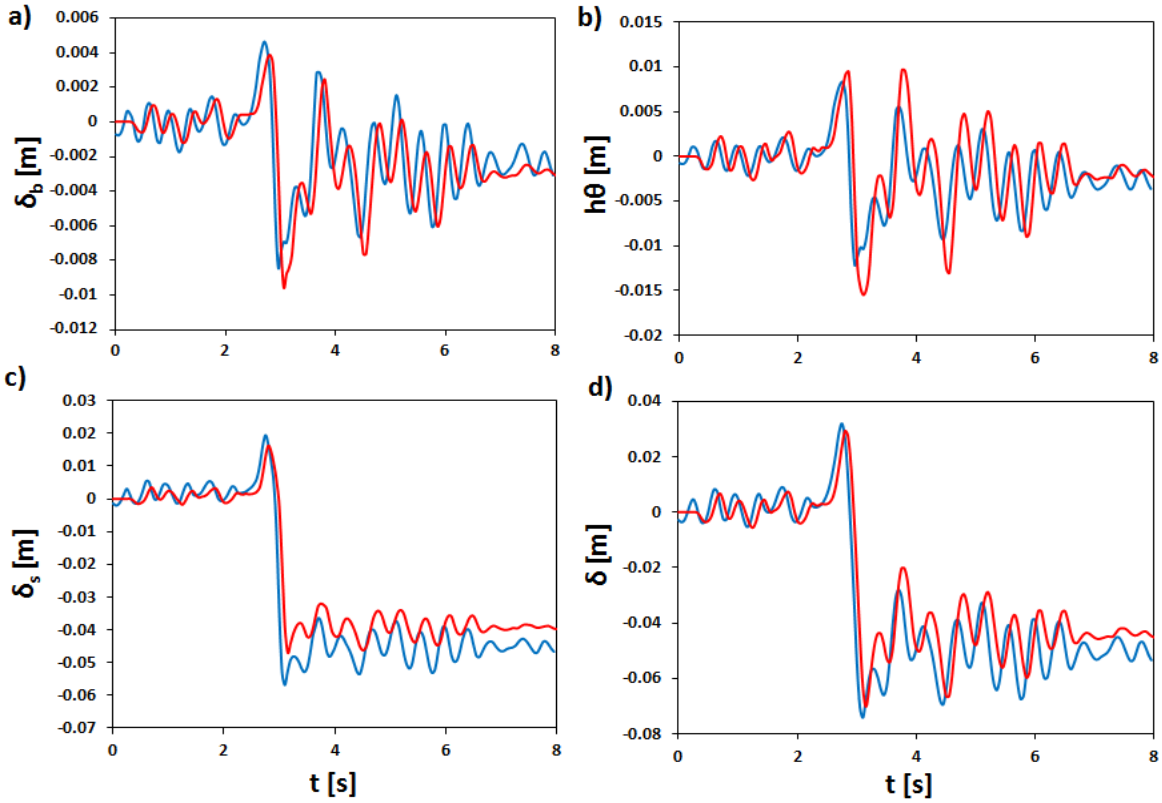

Fig. A.12: Comparison of the response of the two conventionally designed systems with connected (blue) and unconnected (red) piles in terms of (a) foundation displacement (b) displacement due to the rotation of the foundation (c) structural deformation of the pier (d) total deck displacement. (Aegion)

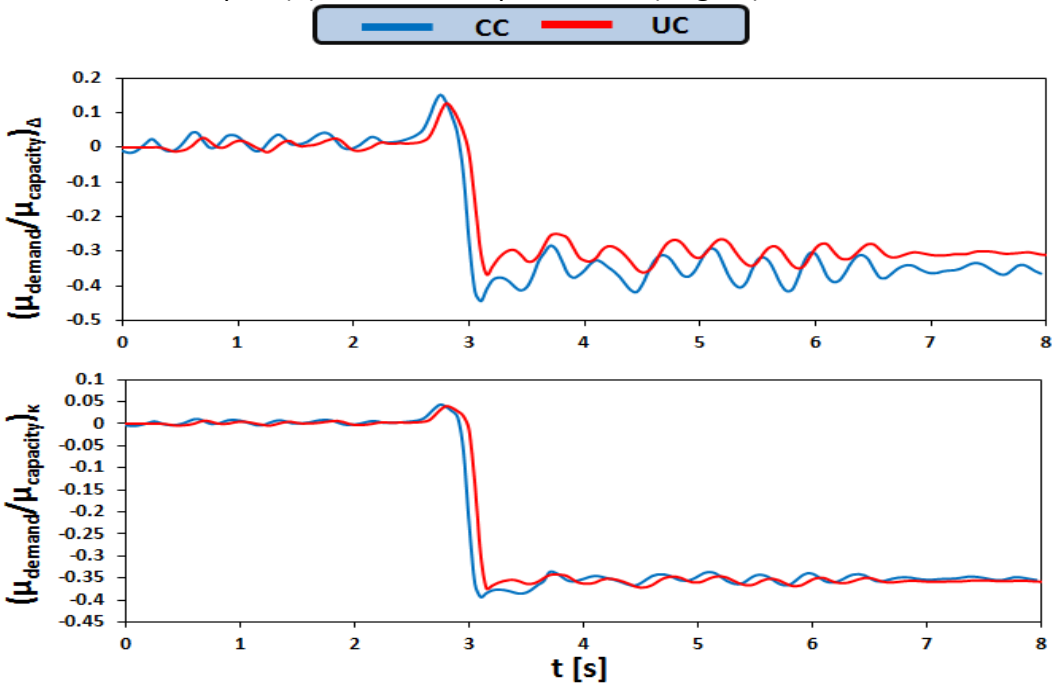

Fig. A.13: Comparison of ductility demand over ductility capacity of the two conventionally designed systems in terms of (a) displacement (b) curvature for Aegion earthquake.

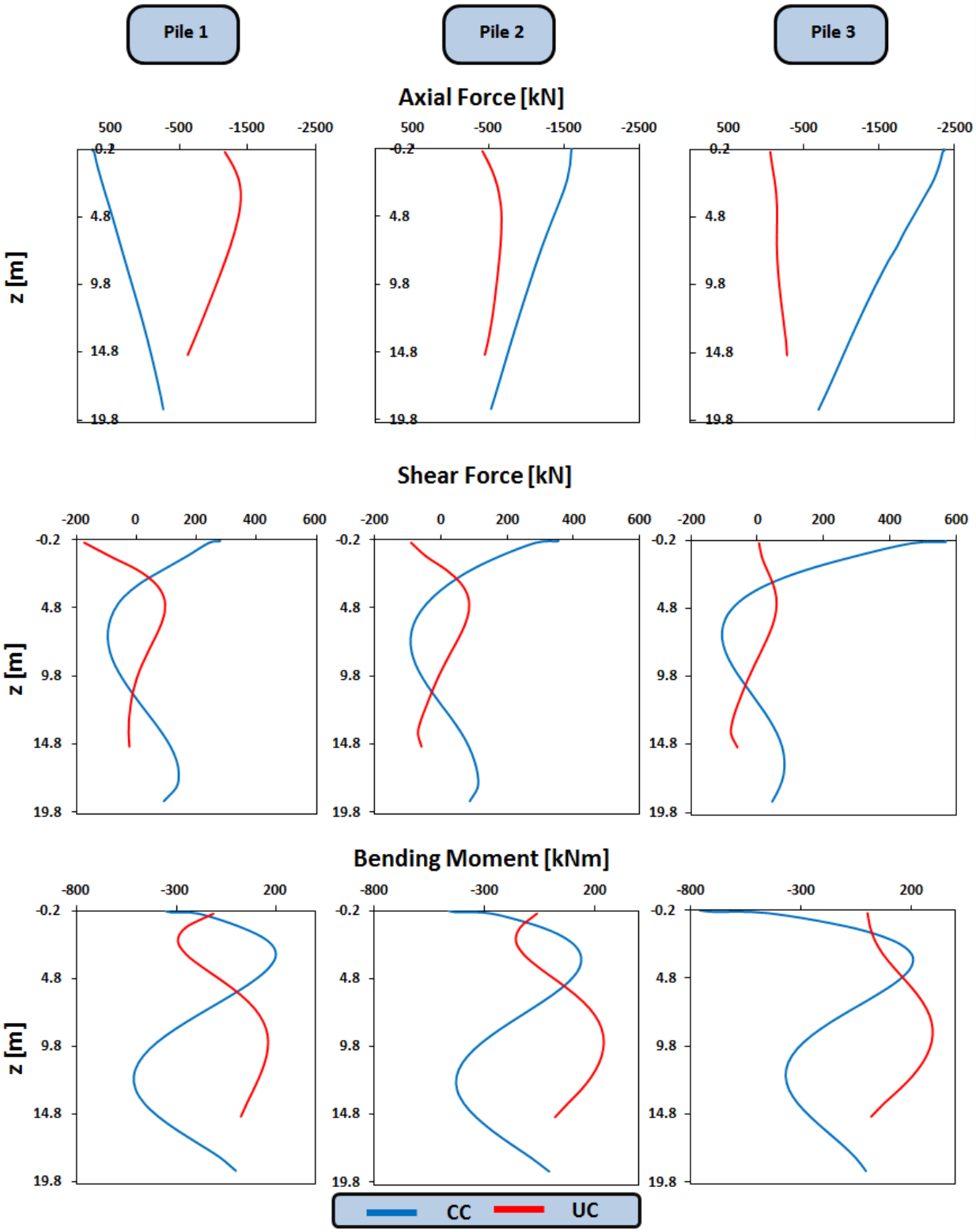

Fig. A.14: Distribution of axial forces, shear forces and bending moments along the piles when maximum moment is transmitted to the soil (Aegion).

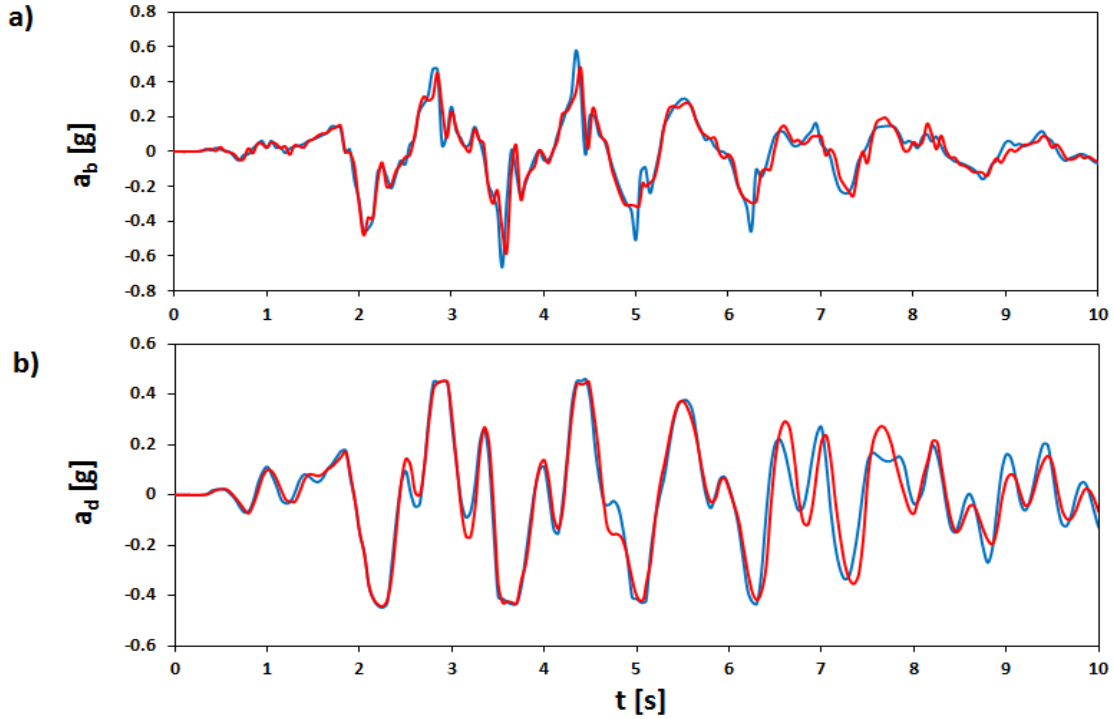

Fig. A.15: Acceleration timehistory during Lixouri excitation at (a) the base of the pier (b) the deck for the case connected (blue) and unconnected (red) piles.

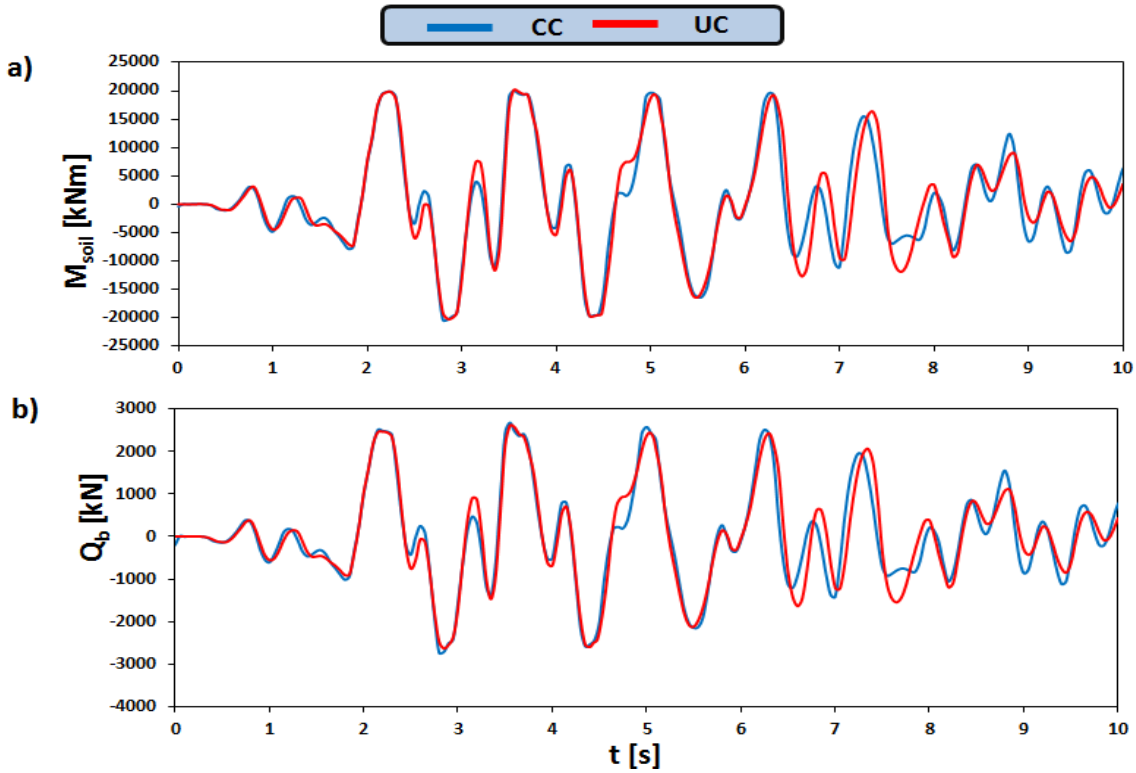

Fig. A.16: Timehistories of (a) bending moment (b) shear force at the base of the pier during Shinkobe excitation for the case of connected (blue) and unconnected (red) piles. (Lixouri earthquake)

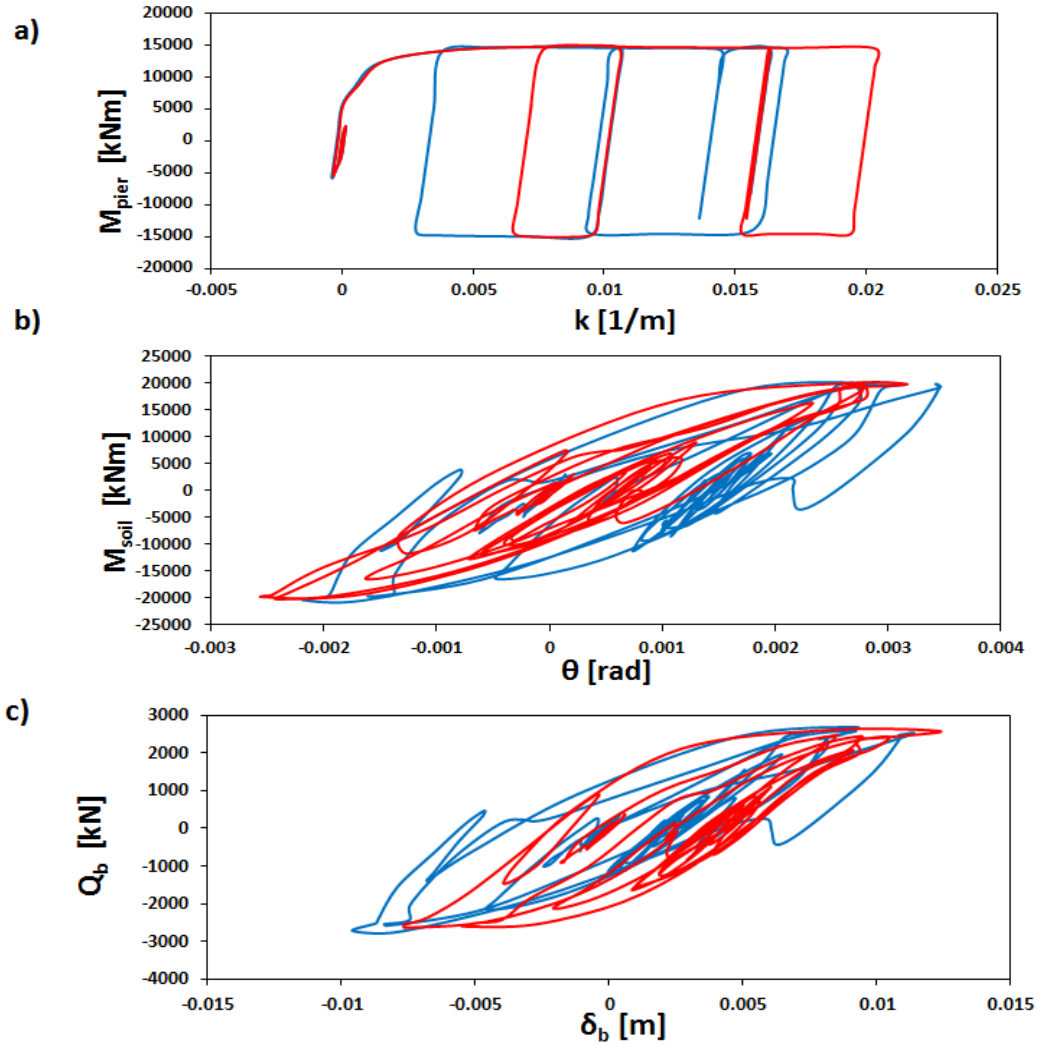

Fig. A.17: Comparison of the response of the two conventionally designed systems with connected (blue) and unconnected (red) piles in terms of (a) bending moment–curvature at the base of the pier (b) moment–rotation of the foundation level (c) base shear–displacement of the foundation. (Lixouri earthquake)

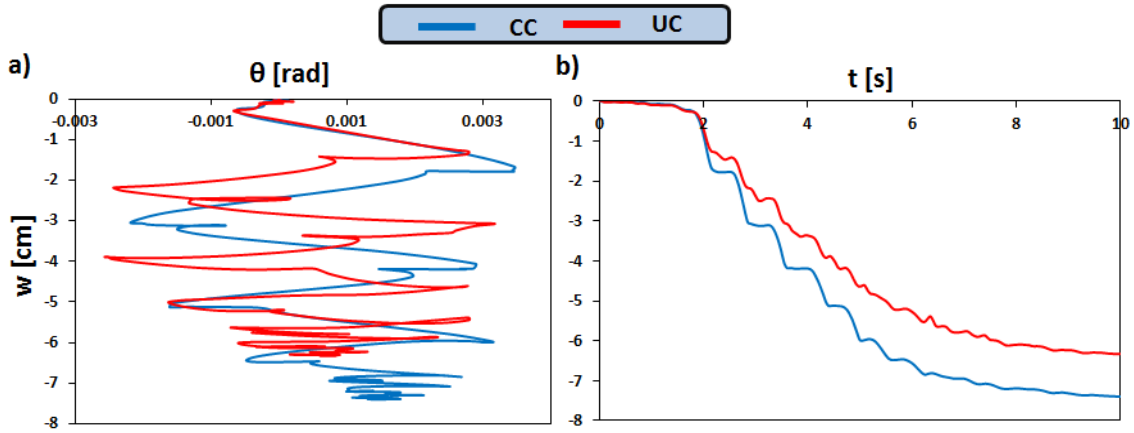

Fig. A.18: Comparison of the settlements of the two alternative conventional designs subjected to Lixouri earthquake in terms of (a) settlement–rotation and (b) settlement timehistory.

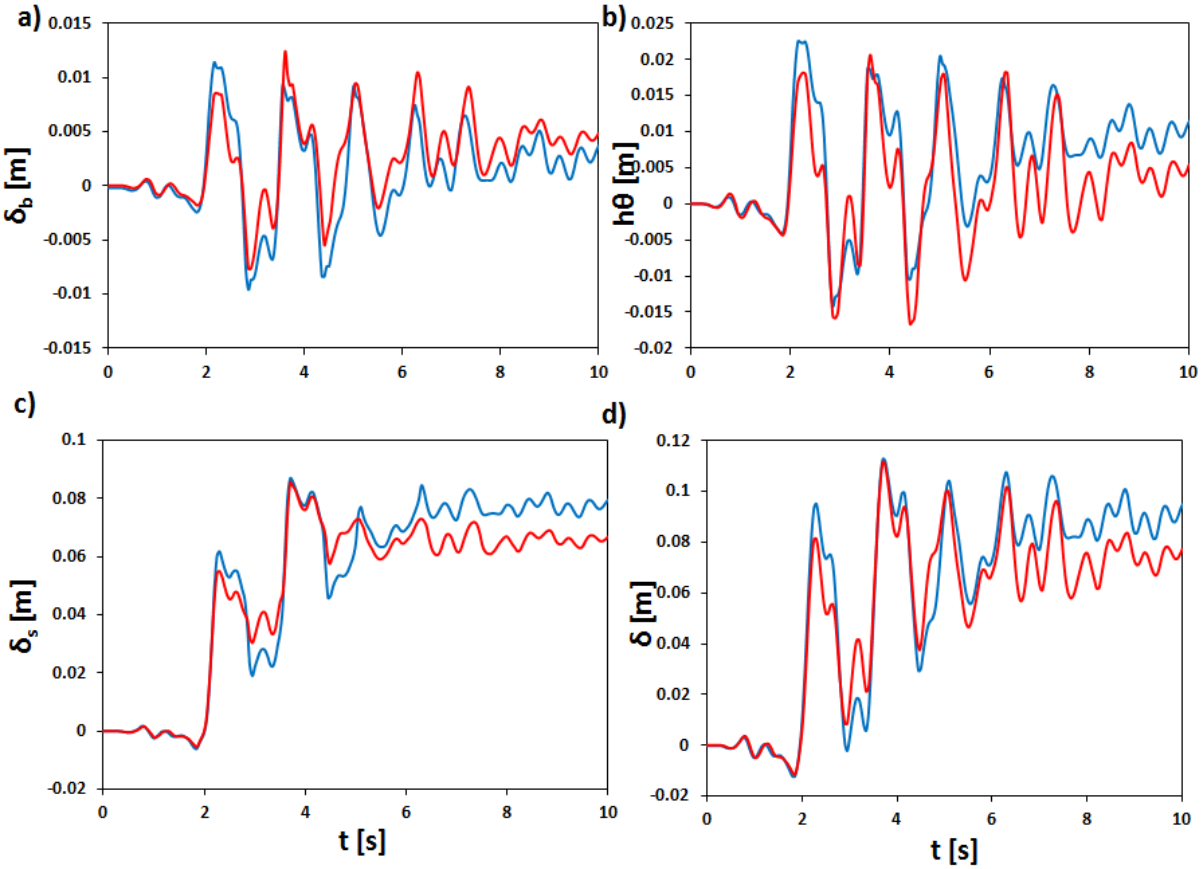

Fig. A.19: Comparison of the response of the two conventionally designed systems with connected (blue) and unconnected (red) piles in terms of (a) foundation displacement (b) displacement due to the rotation of the foundation (c) structural deformation of the pier (d) total deck displacement. (Lixouri earthquake)

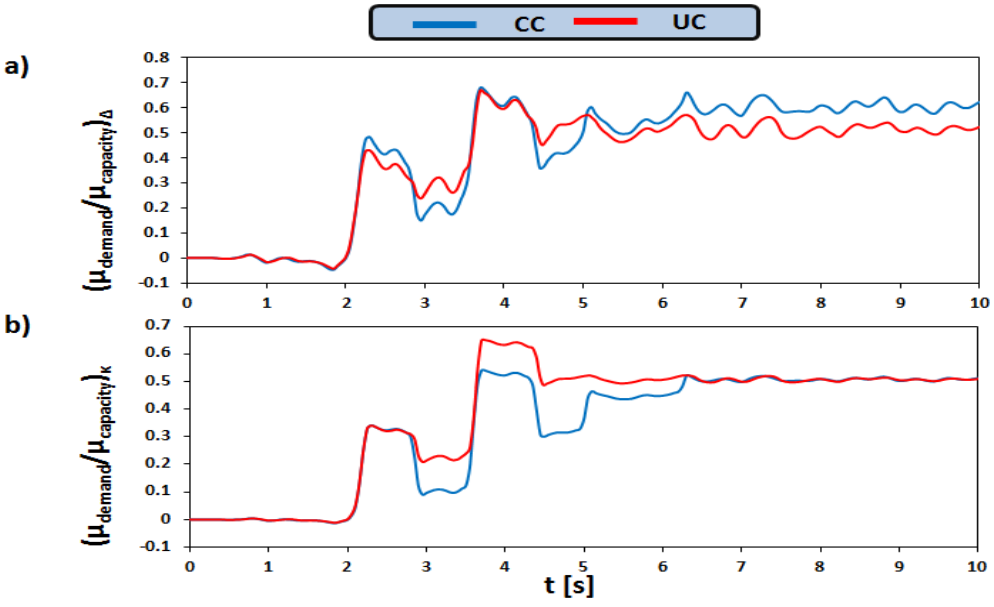

Fig. A.20: Comparison of ductility demand over ductility capacity of the two conventionally designed systems in terms of (a) displacement (b) curvature for Lixouri earthquake.

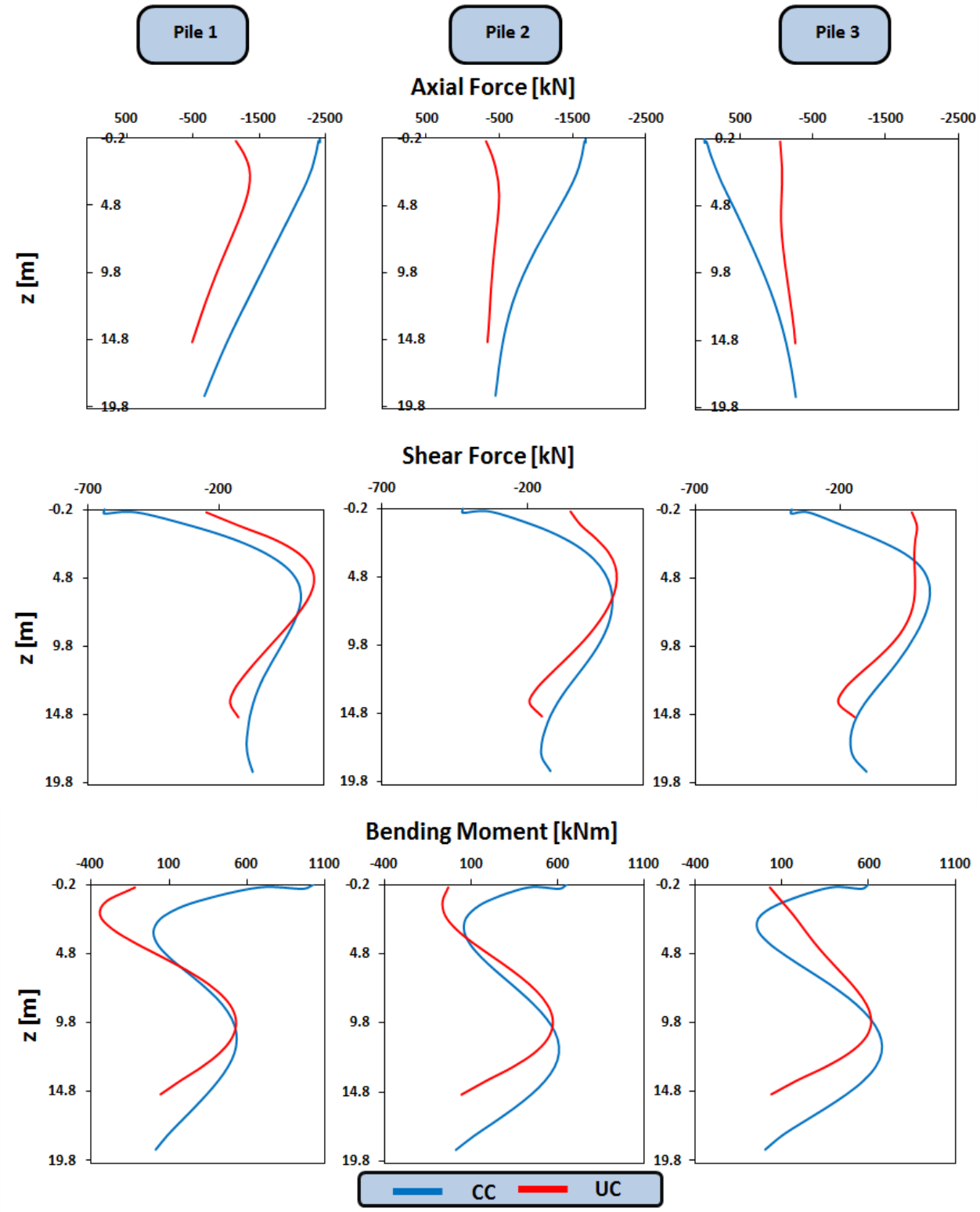

Fig. A.21: Distribution of axial forces, shear forces and bending moments along the piles when maximum moment is transmitted to the soil (Lixouri earthquake).

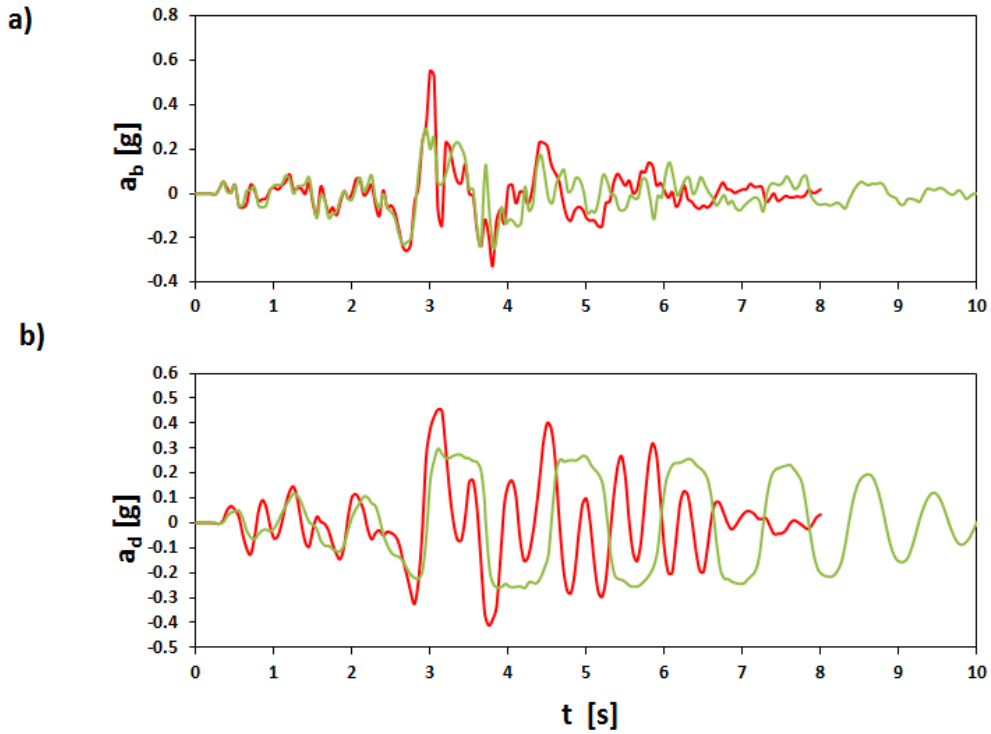

Fig. A.22: Comparison of the accelerations of the two alternative unconnected pile foundations, conventional (UC) and rocking (UR), at the (a) pier base and (b) deck for Aegion earthquake.

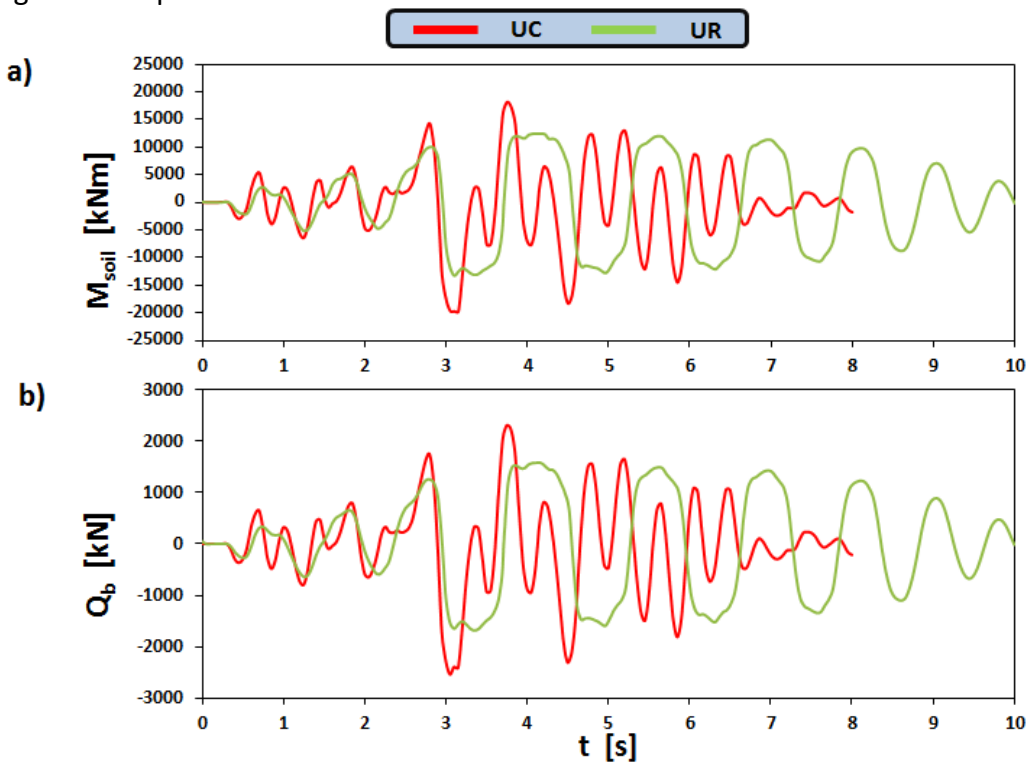

Fig. A.23: Comparison of the two alternative unconnected pile foundations, conventional (UC) and rocking (UR), in terms of (a) moment at the foundation level and (b) shear at the pier base for Aegion earthquake.

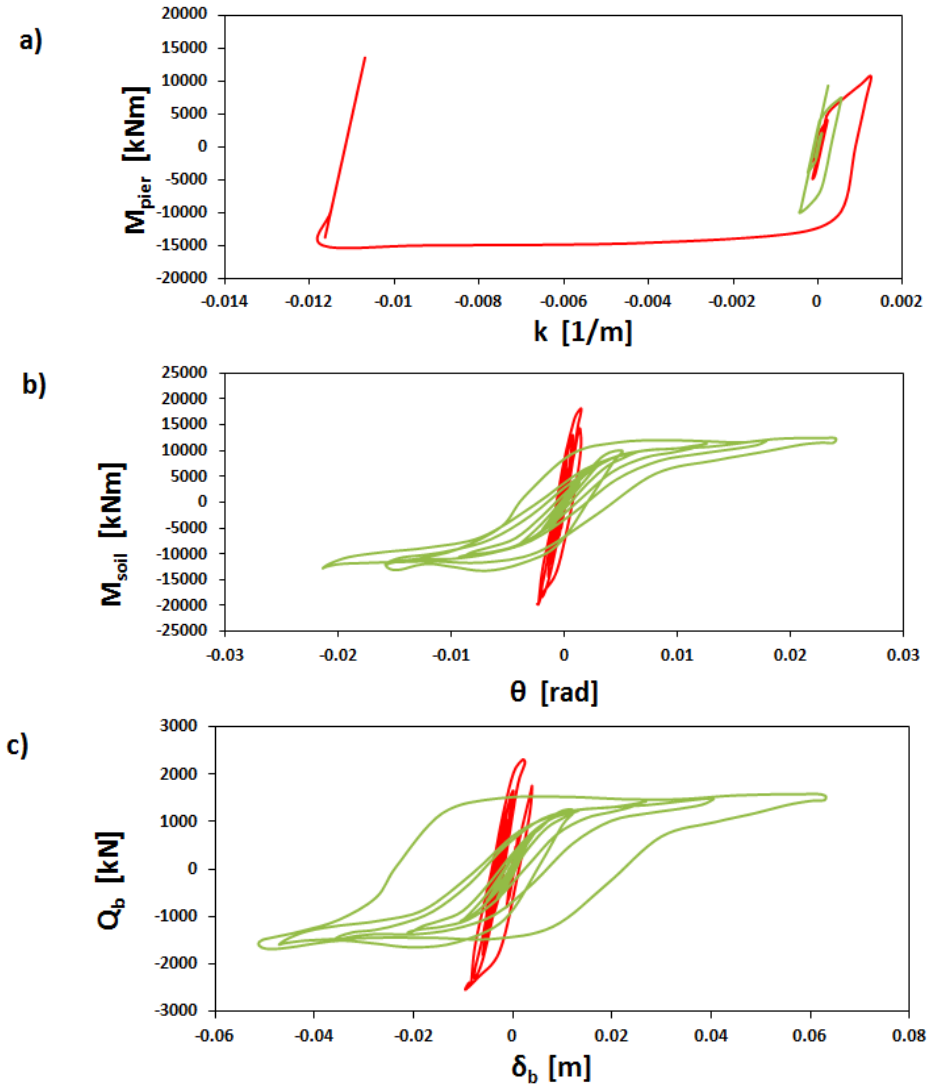

Fig. A.24: Comparison of the two alternative unconnected pile foundations, conventional (UC) and rocking (UR), in terms of (a) moment–curvature at the base of the pier (b) Moment–rotation at the foundation level (c) shear–displacement at the pier base for Aegion earthquake.

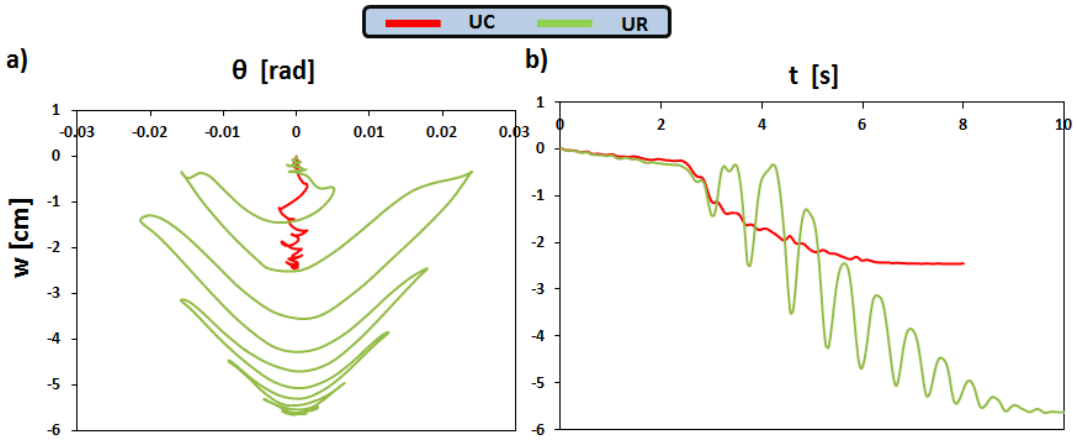

Fig. A.25: Comparison of the settlements of the two alternative designs subjected to Aegion earthquake in terms of (a) settlement–rotation and (b) settlement timehistory.

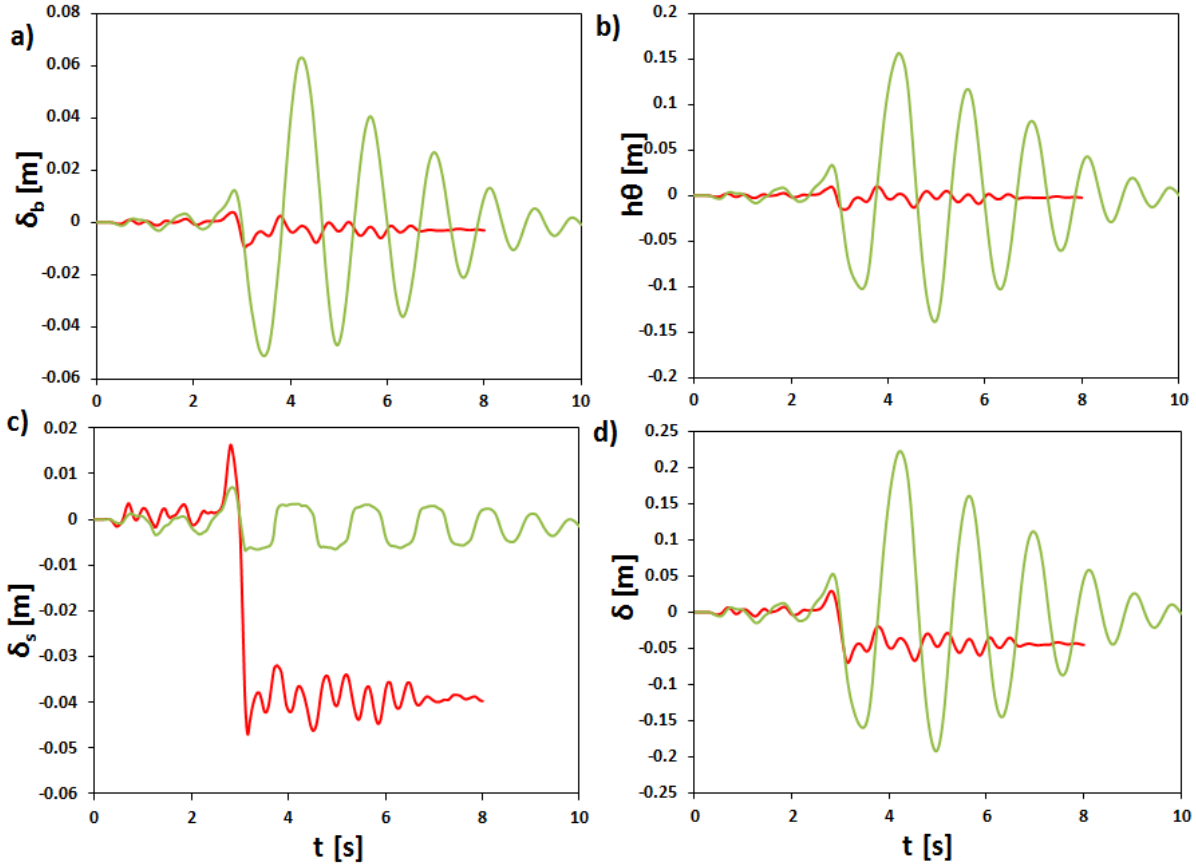

Fig. A.26: Comparison of the two alternative unconnected pile foundations, conventional (UC) and rocking (UR), in terms of (a) foundation displacement (b) displacement due to the rotation of the foundation (c) structural deformation of the pier (d) total deck displacement. (Aegion earthquake)

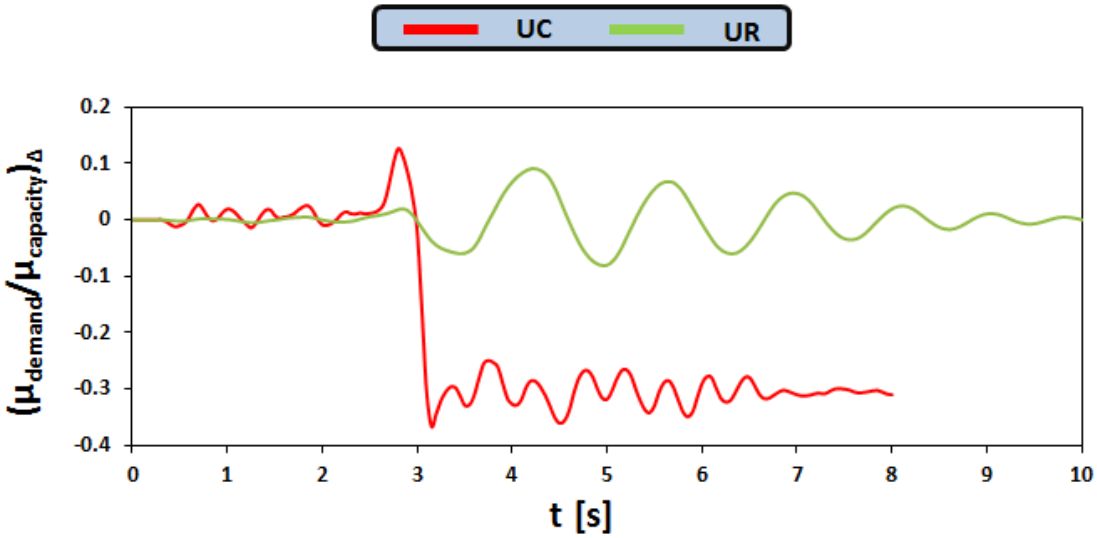

Fig. A.27: Comparison of ductility demand over ductility capacity, in terms of displacements, of the two alternative unconnected pile foundations for Aegion earthquake.

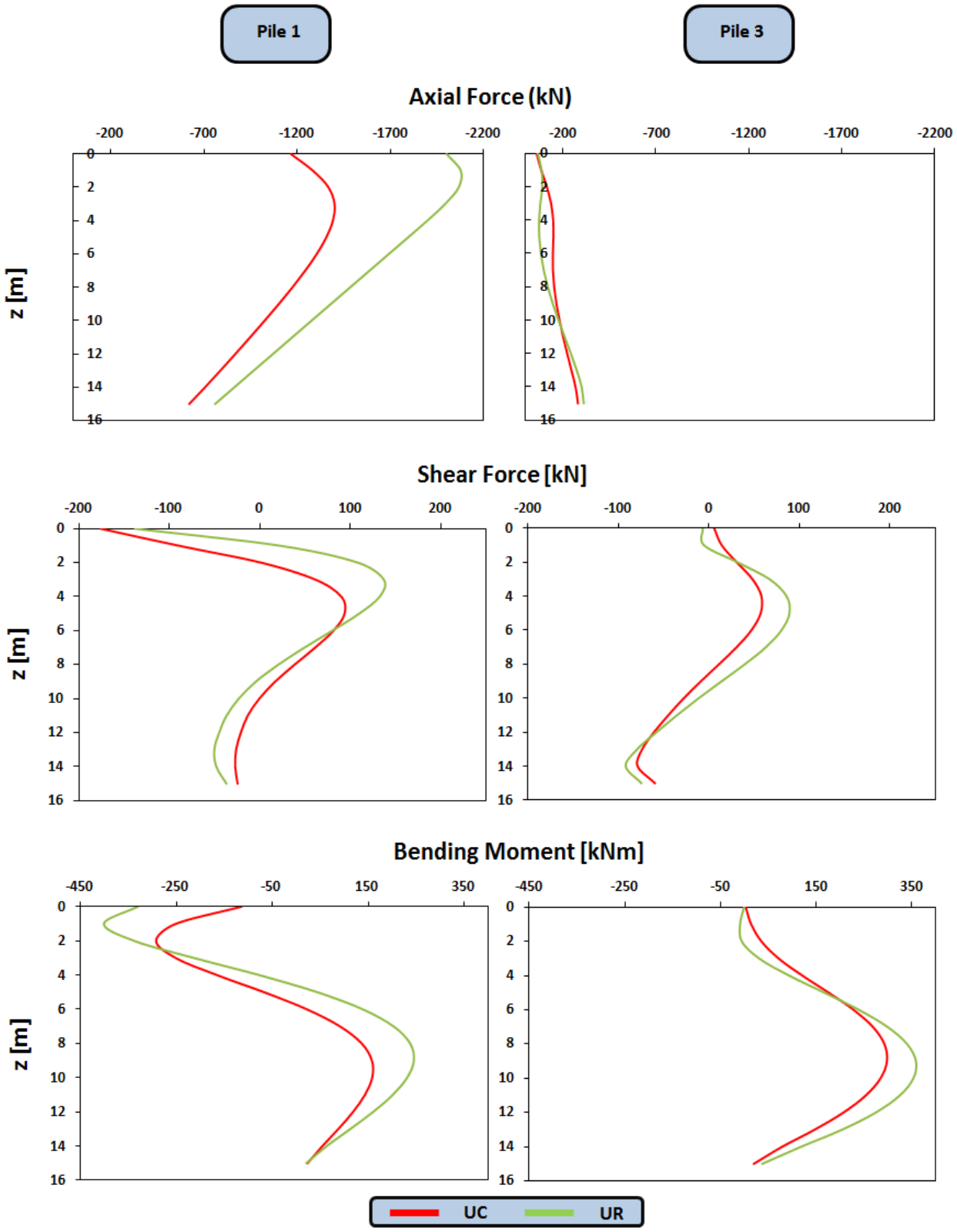

Fig. A.28: Distribution of axial forces, shear forces and bending moments along the piles when maximum moment is transmitted to the soil (Aegion earthquake).

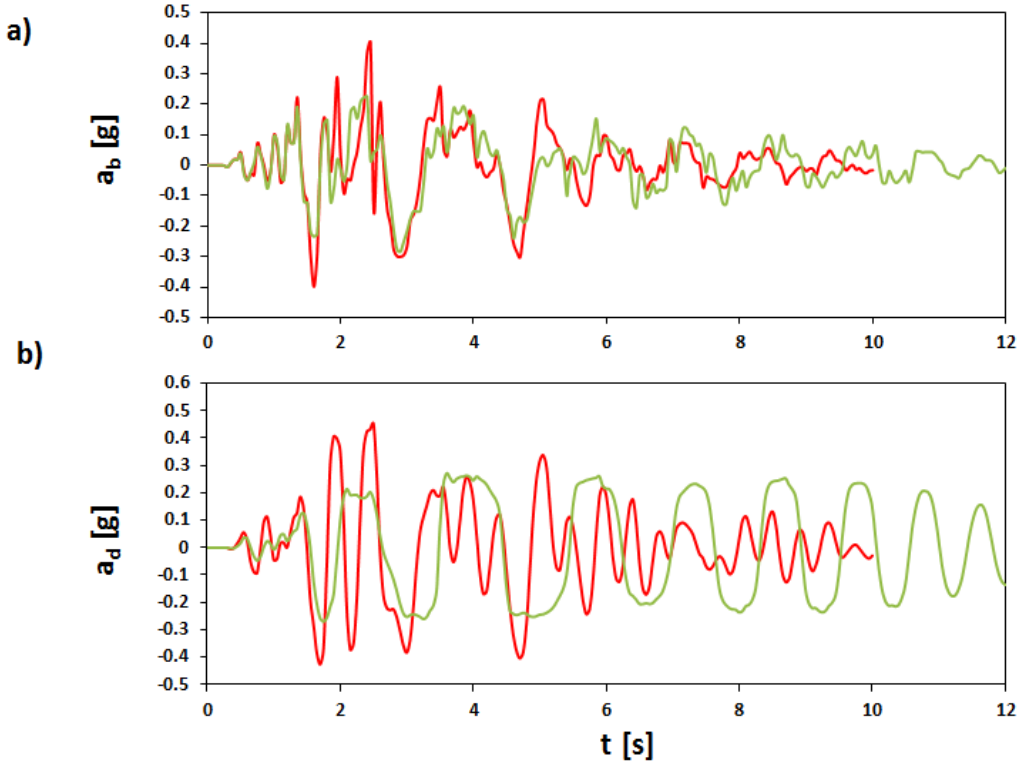

Fig. A.29: Comparison of the accelerations of the two alternative unconnected pile foundations, conventional (UC) and rocking (UR), at the (a) pier base and (b) deck for Kalamata earthquake.

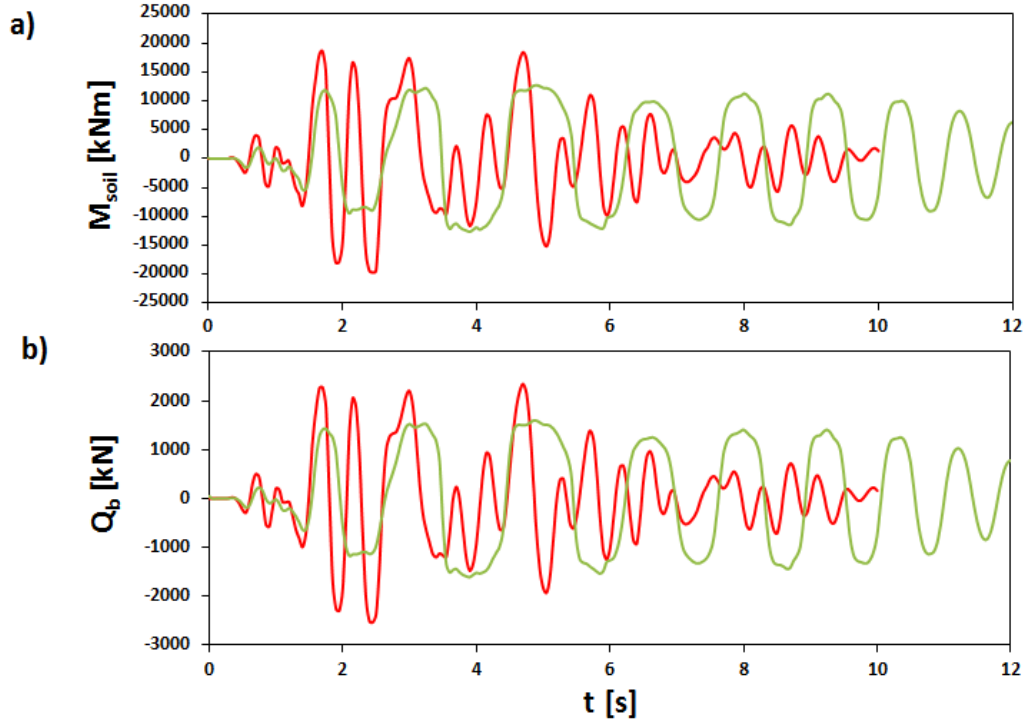

Fig. A.30: Comparison of the two alternative unconnected pile foundations, conventional (UC) and rocking (UR), in terms of (a) moment at the foundation level and (b) shear at the pier base for Kalamata earthquake.

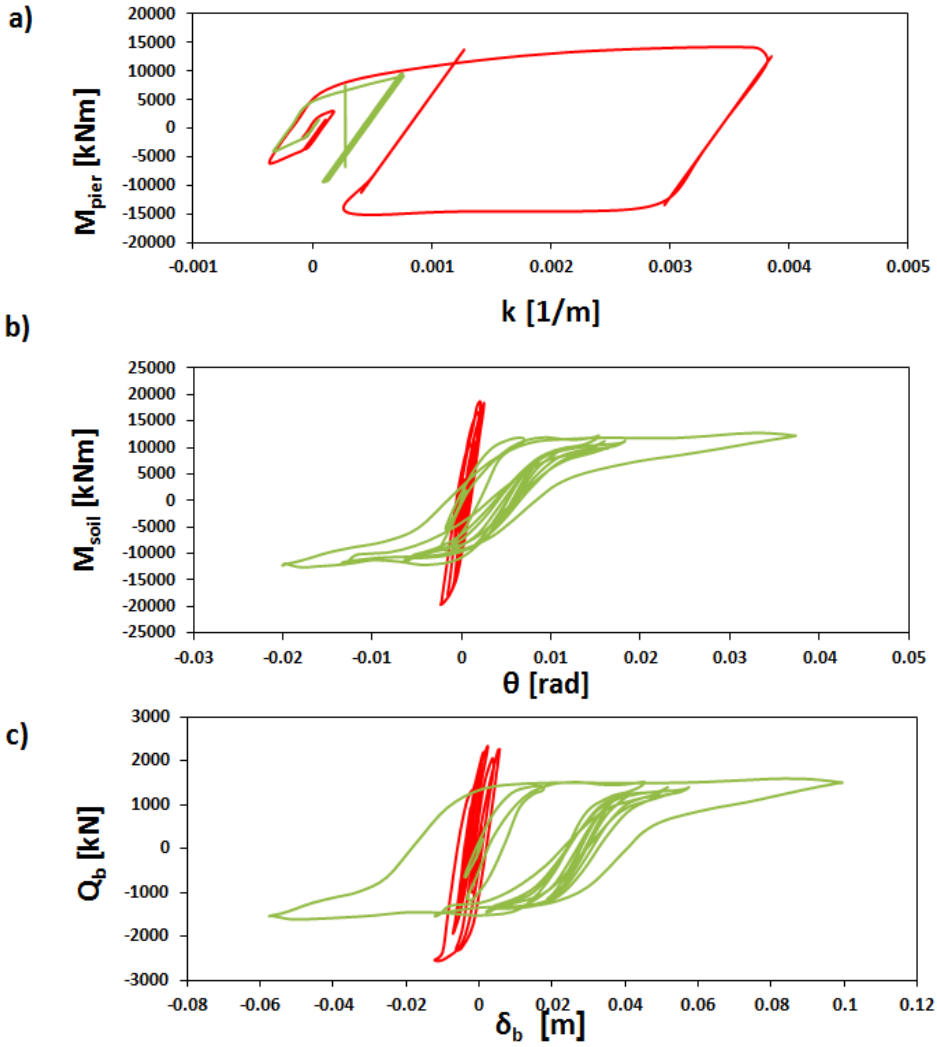

Fig. A.31: Comparison of the two alternative unconnected pile foundations, conventional (UC) and rocking (UR), in terms of (a) moment–curvature at the base of the pier (b) Moment–rotation at the foundation level (c) shear–displacement at the pier base for Aegion earthquake.

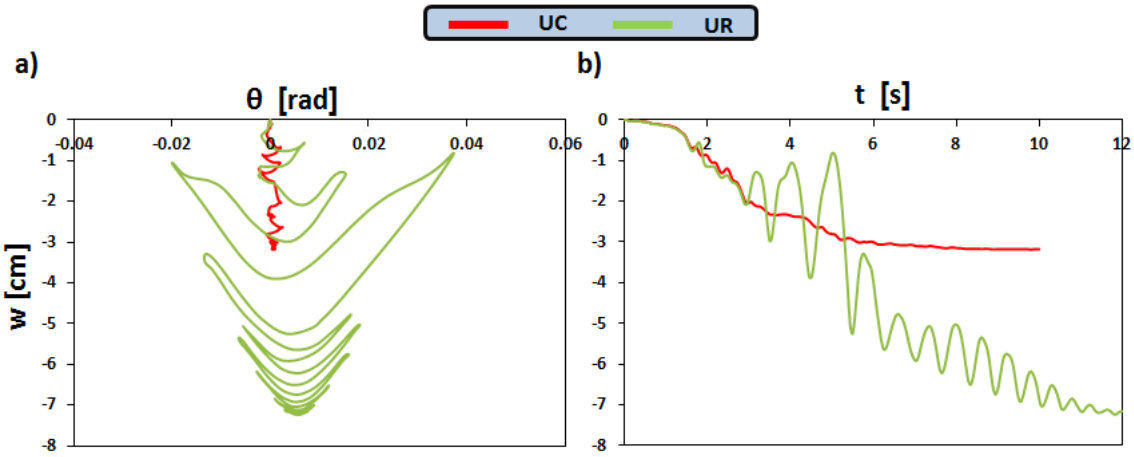

Fig. A.32: Comparison of the settlements of the two alternative designs subjected to Kalamata earthquake in terms of (a) settlement–rotation and (b) settlement timehistory.

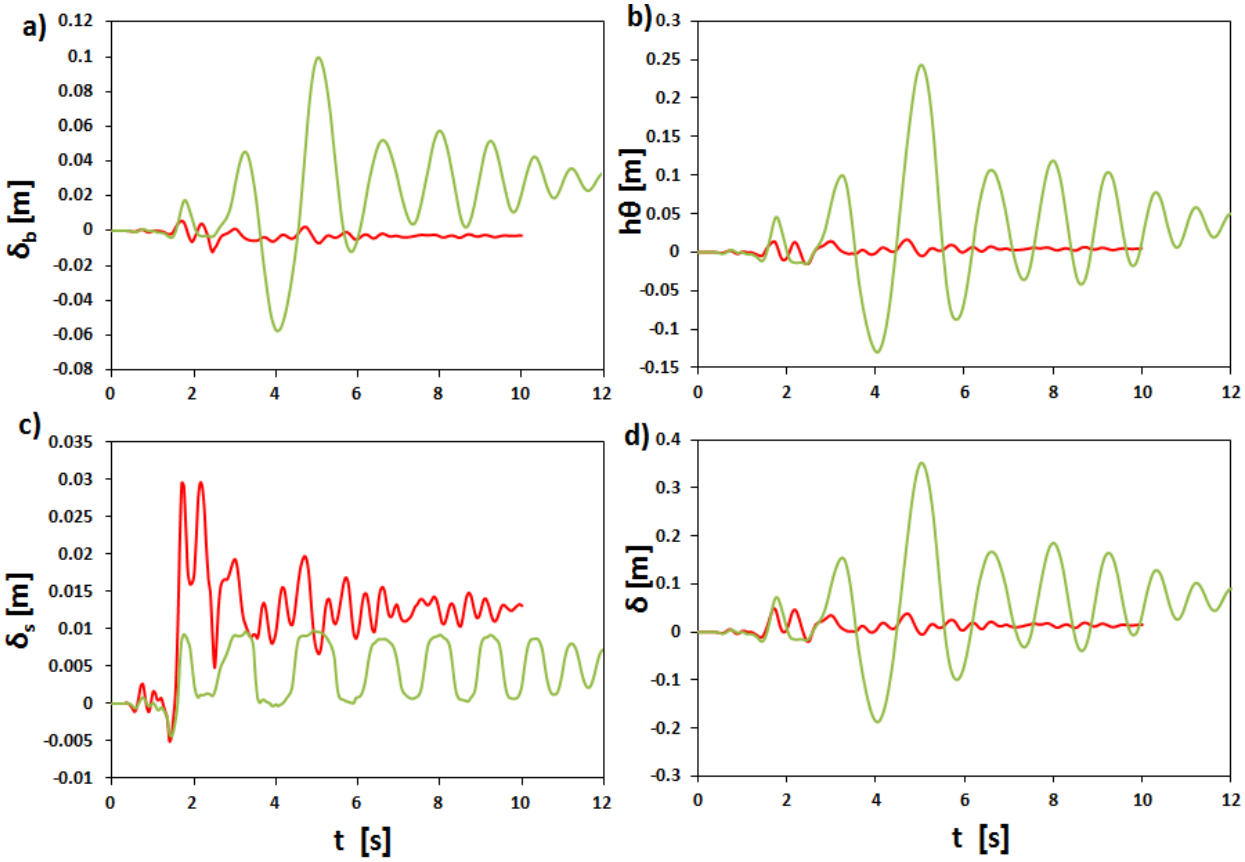

Fig. A.33: Comparison of the two alternative unconnected pile foundations, conventional (UC) and rocking (UR), in terms of (a) foundation displacement (b) displacement due to the rotation of the foundation (c) structural deformation of the pier (d) total deck displacement. (Kalamata earthquake)

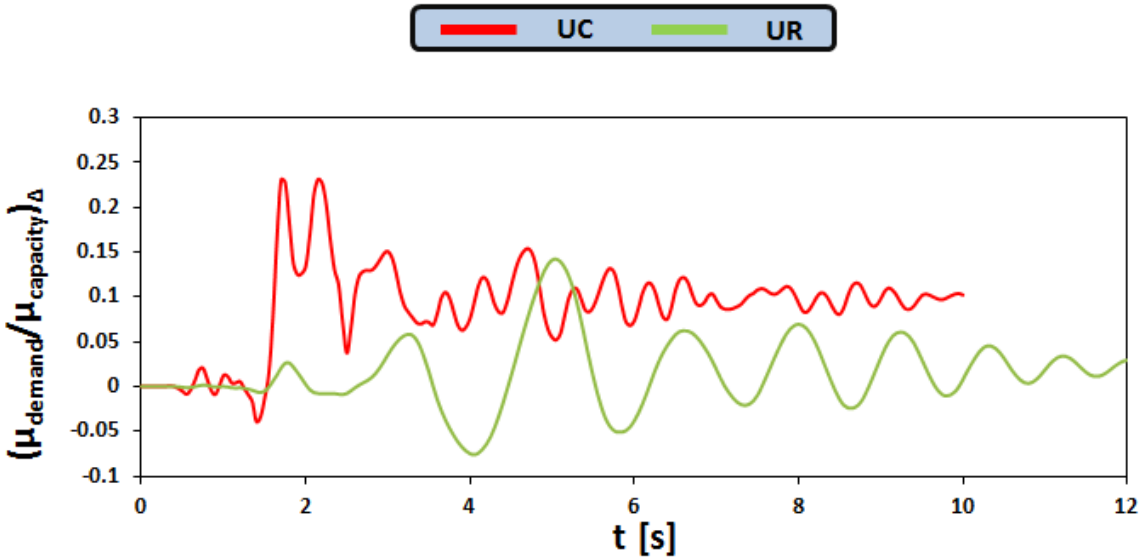

Fig. A.34: Comparison of ductility demand over ductility capacity, in terms of displacements, of the two alternatives unconnected pile foundations for Kalamata earthquake.

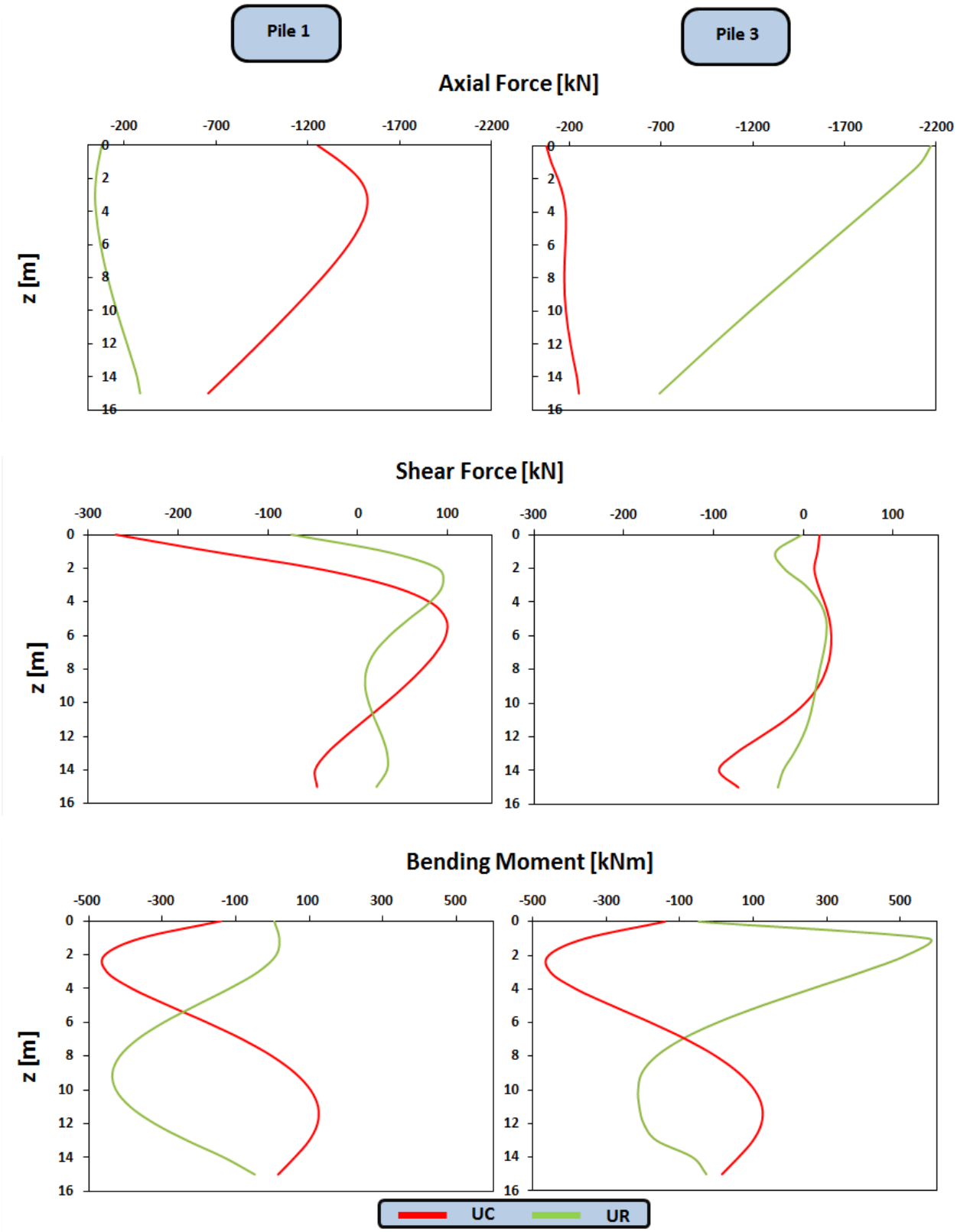

Fig. A.35: Distribution of axial forces, shear forces and bending moments along the piles when maximum moment is transmitted to the soil (Kalamata earthquake).

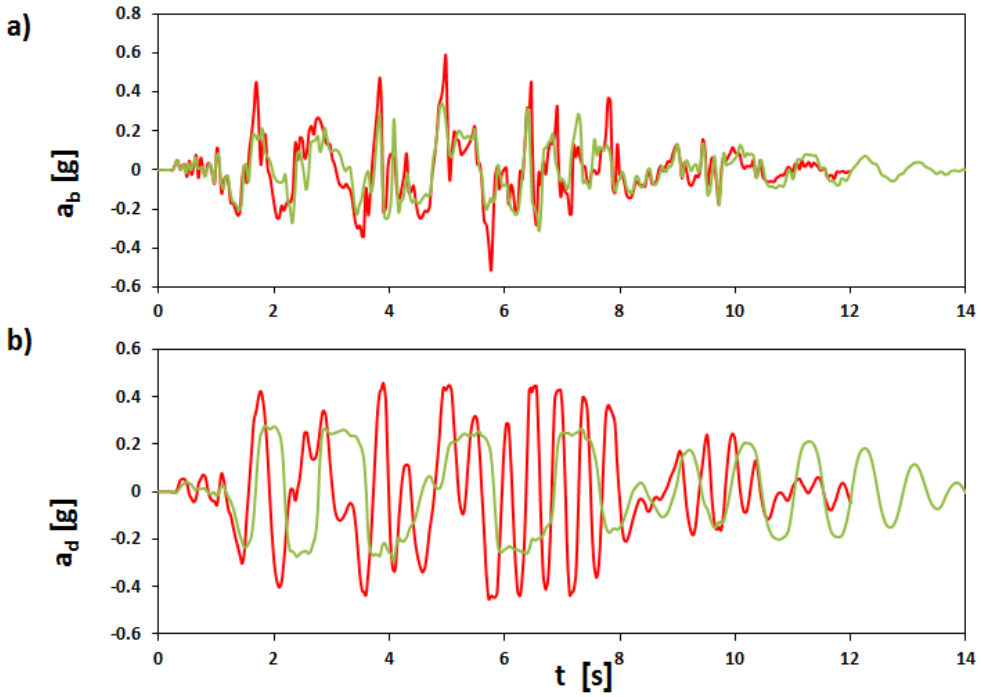

Fig. A.36: Comparison of the acceleration of the two alternatives unconnected pile foundations, conventional (UC) and rocking (UR), at the (a) pier base and (b) deck for Shinkobe earthquake.

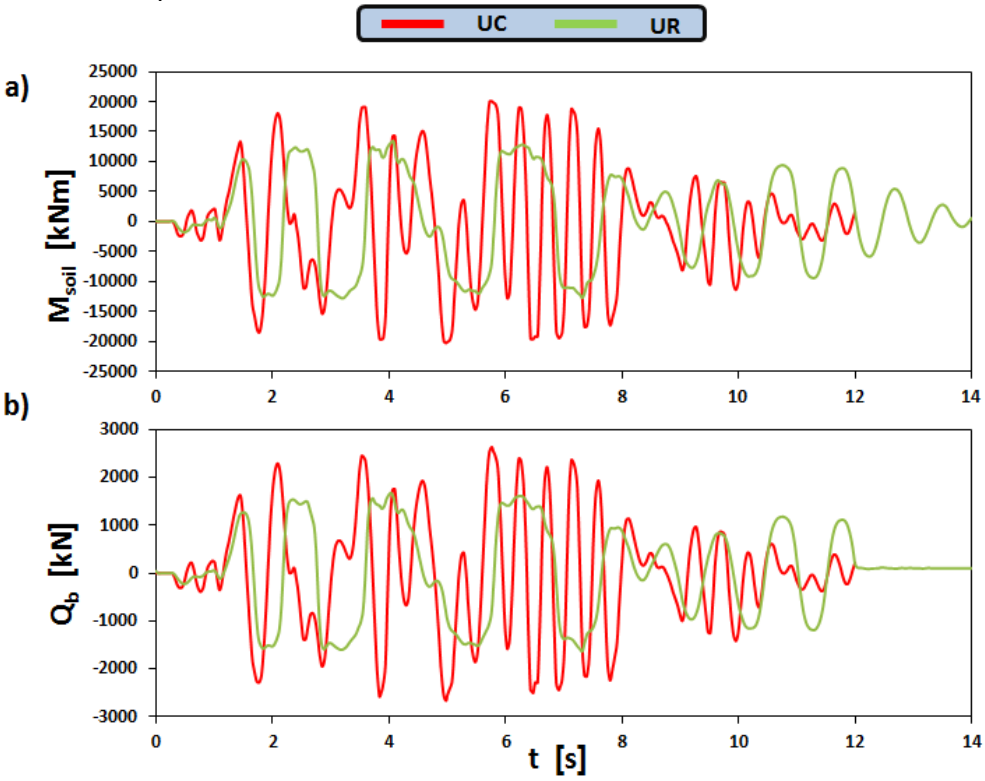

Fig. A.37: Comparison of the two alternative unconnected pile foundations, conventional (UC) and rocking (UR), in terms of (a) moment at the foundation level and (b) shear at the pier base for Shinkobe earthquake.

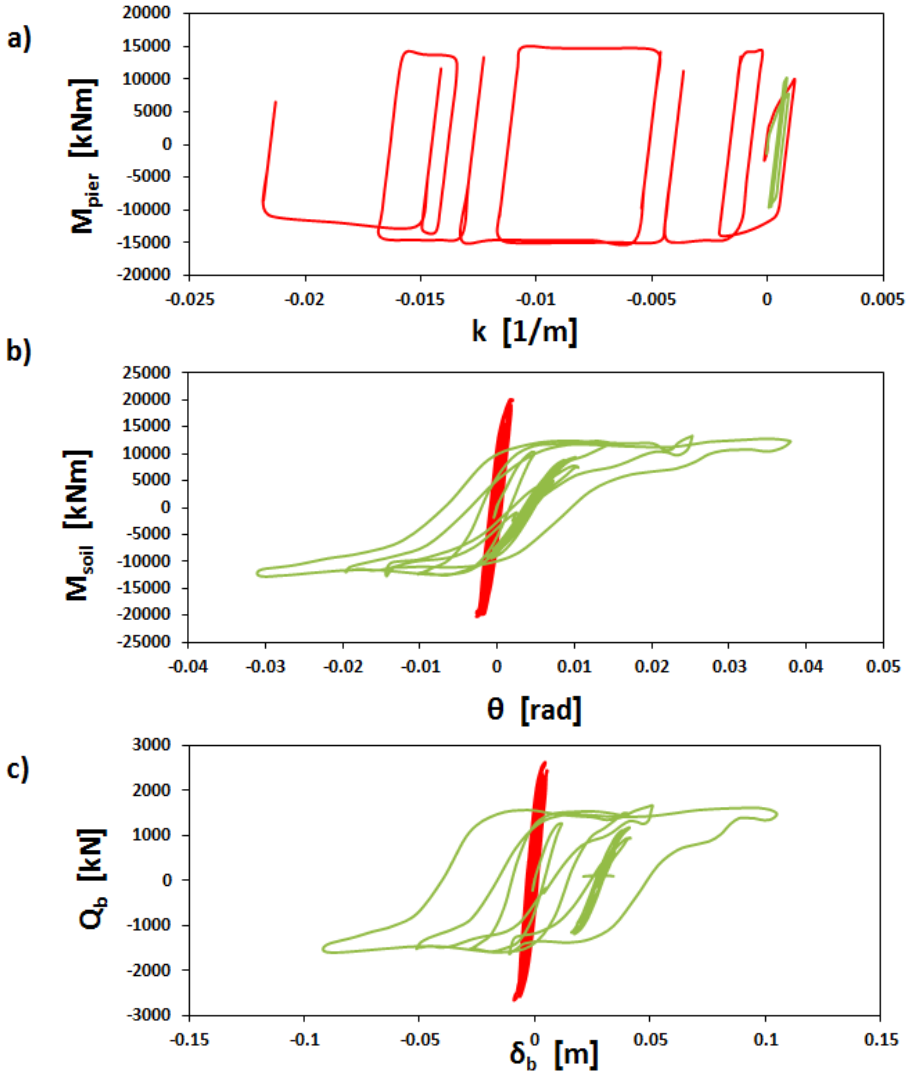

Fig. A.38: Comparison of the two alternative unconnected pile foundations, conventional (UC) and rocking (UR), in terms of (a) moment–curvature at the base of the pier (b) Moment–rotation at the foundation level (c) shear–displacement at the pier base for Shinkobe earthquake.

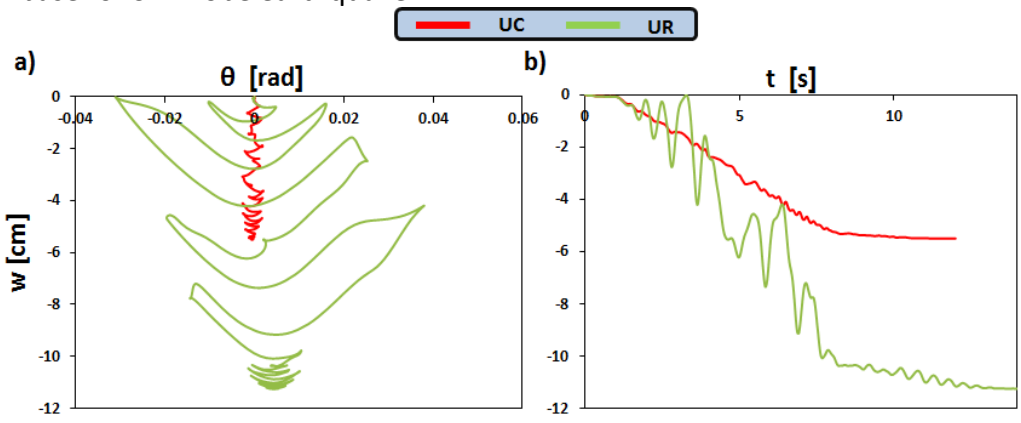

Fig. A.39: Comparison of the settlements of the two alternative designs subjected to Shinkobe earthquake in terms of (a) settlement–rotation and (b) settlement timehistory.

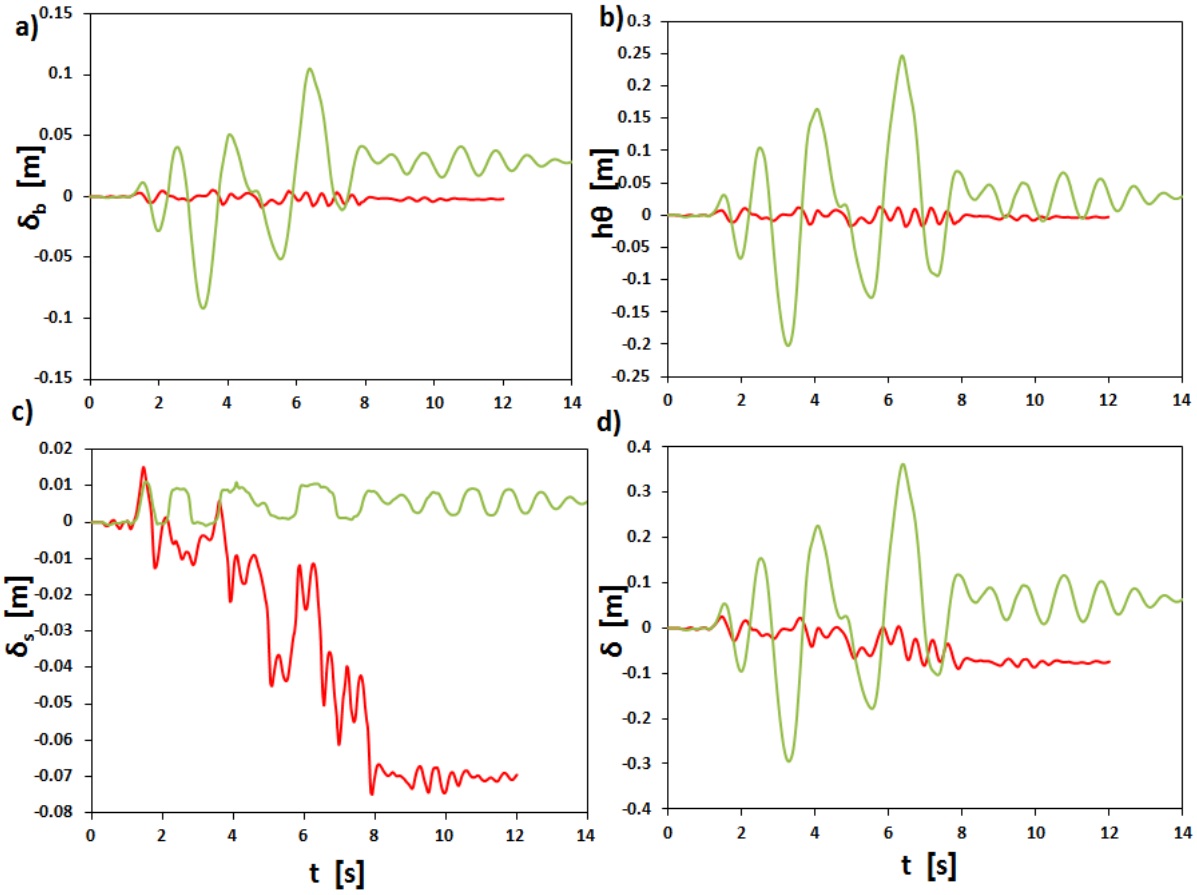

Fig. A.40: Comparison of ductility demand over ductility capacity, in terms of displacements, of the two alternative unconnected pile foundations for Shinkobe earthquake.

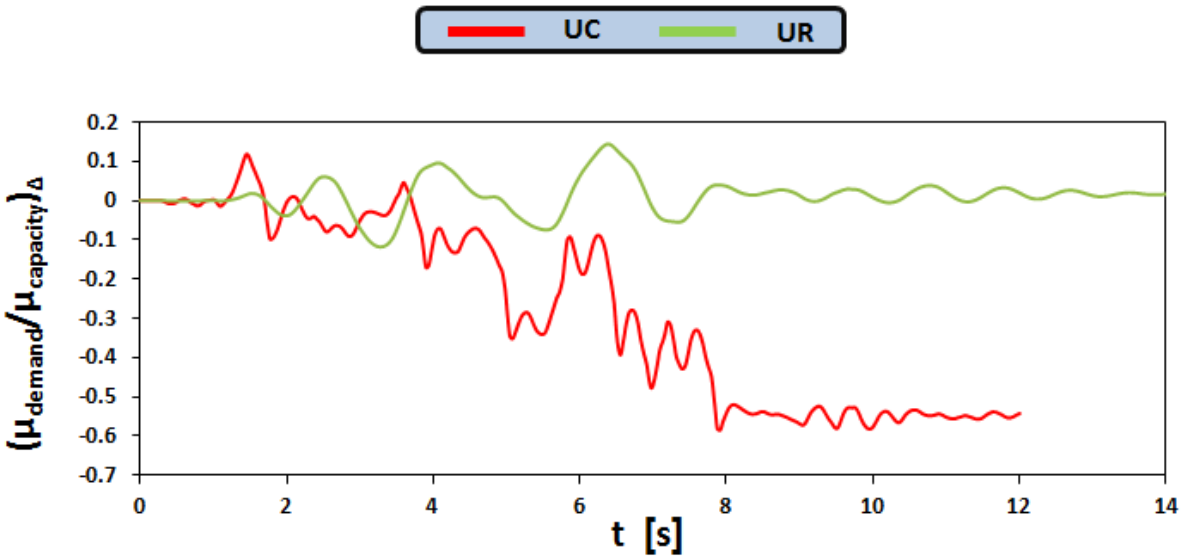

Fig. A.41: Comparison of ductility demand over ductility capacity, in terms of displacements, of the two alternative unconnected pile foundations for Shinkobe earthquake.

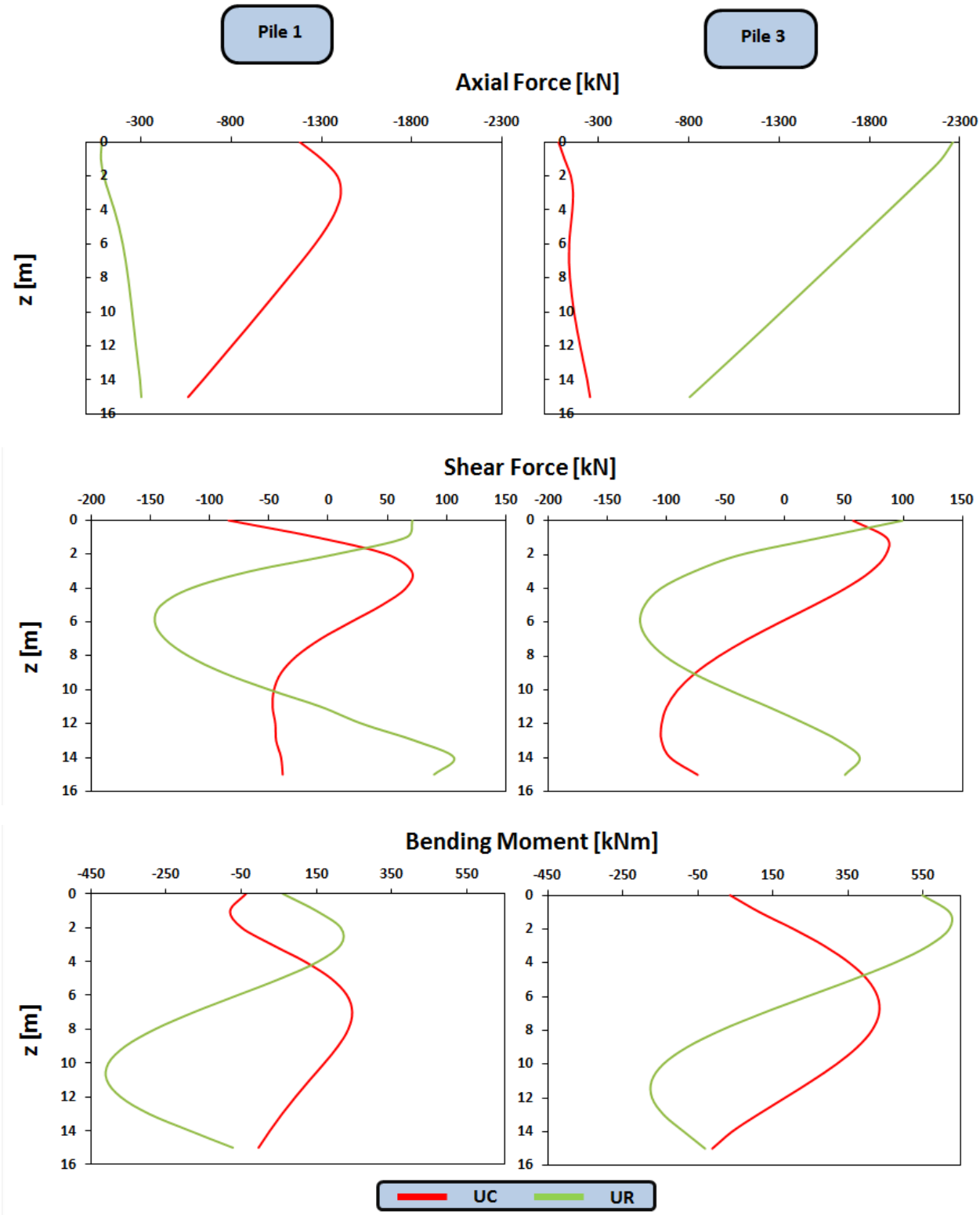

Fig. A.42: Distribution of axial forces, shear forces and bending moments along the piles when maximum moment is transmitted to the soil (Shinkobe earthquake).

APPENDIX B

Earthquake Response of Tall Piers

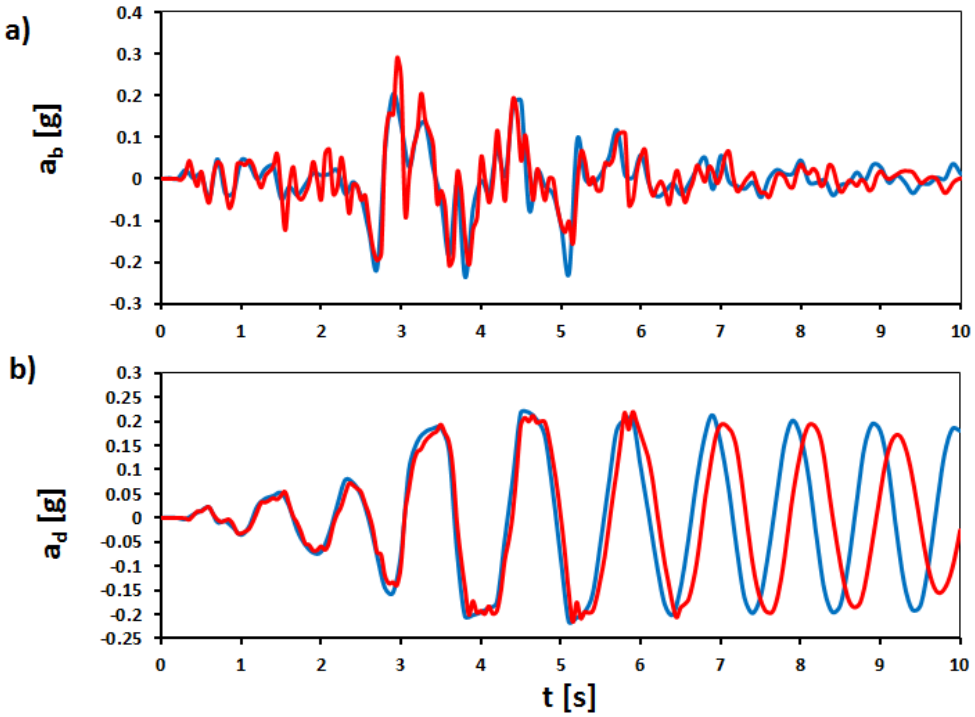

Fig. B.1: Acceleration timehistory during Aegion excitation at (a) the base of the pier (b) the deck for the case connected (blue) and unconnected (red) piles.

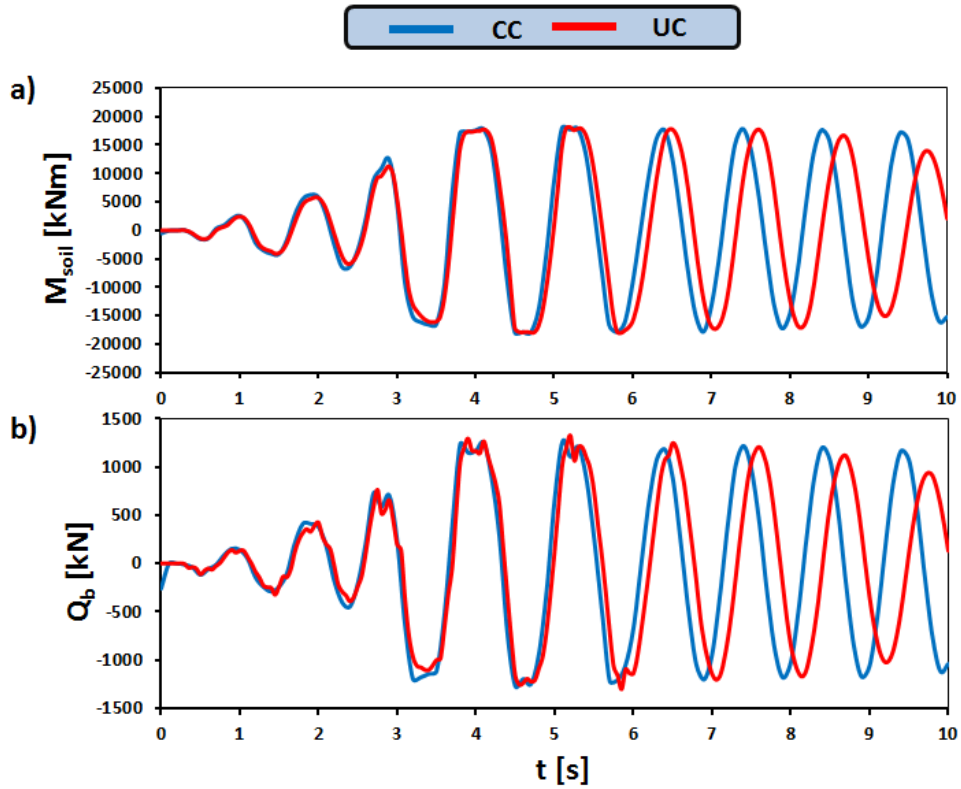

Fig. B.2: Timehistories of (a) bending moment (b) shear force at the base of the pier during Shinkobe excitation for the case of connected (blue) and unconnected (red) piles (Aegion).

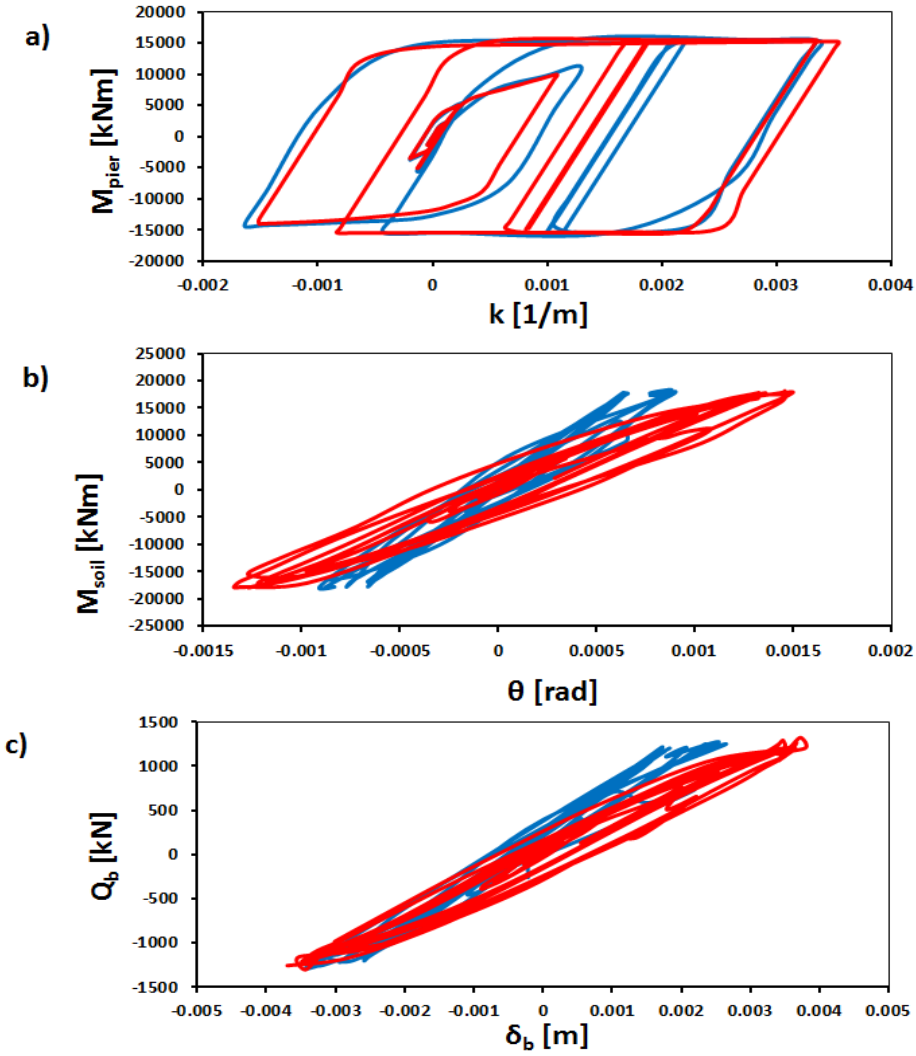

Fig. B.3: Comparison of the response of the two conventionally designed systems with connected (blue) and unconnected (red) piles in terms of (a) bending moment–curvature at the base of the pier (b) moment–rotation of the foundation level (c) base shear–displacement of the foundation. (Aegion)

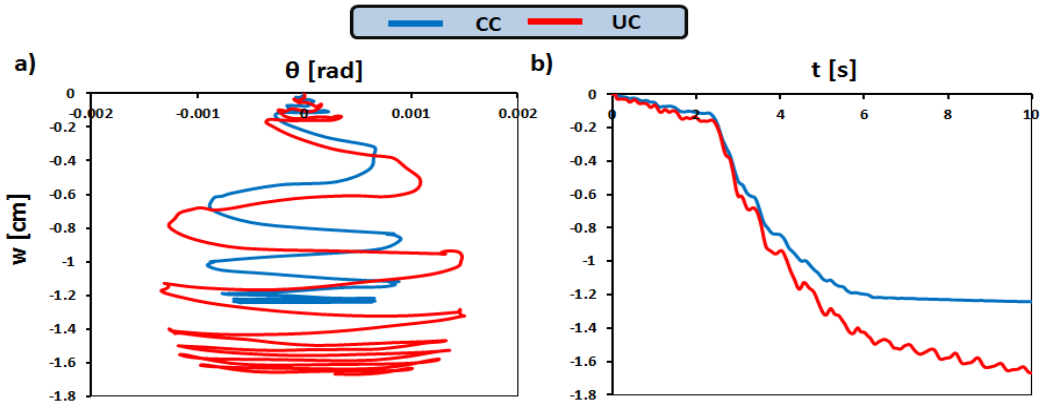

Fig. B.4: Comparison of the settlements of the two alternative conventional designs subjected to Aegion earthquake in terms of (a) settlement–rotation and (b) settlement timehistory.

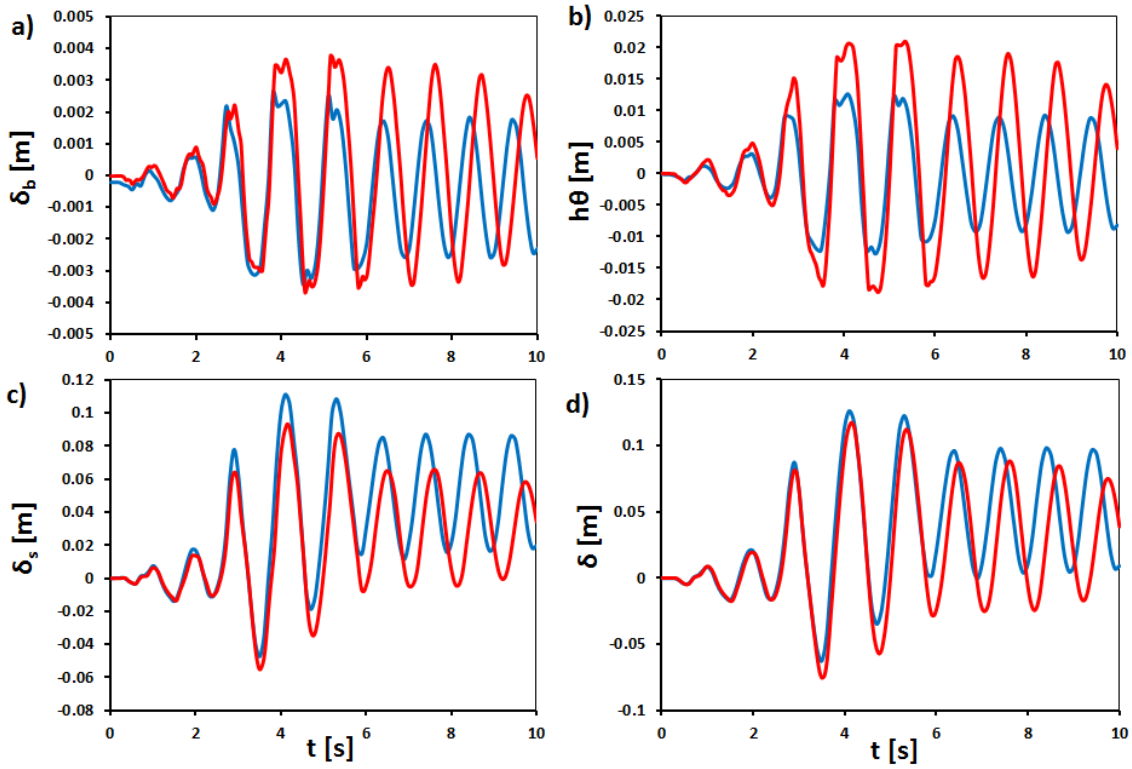

Fig. B.5: Comparison of the response of the two conventionally designed systems with connected (blue) and unconnected (red) piles in terms of (a) foundation displacement (b) displacement due to the rotation of the foundation (c) structural deformation of the pier (d) total deck displacement. (Aegion)

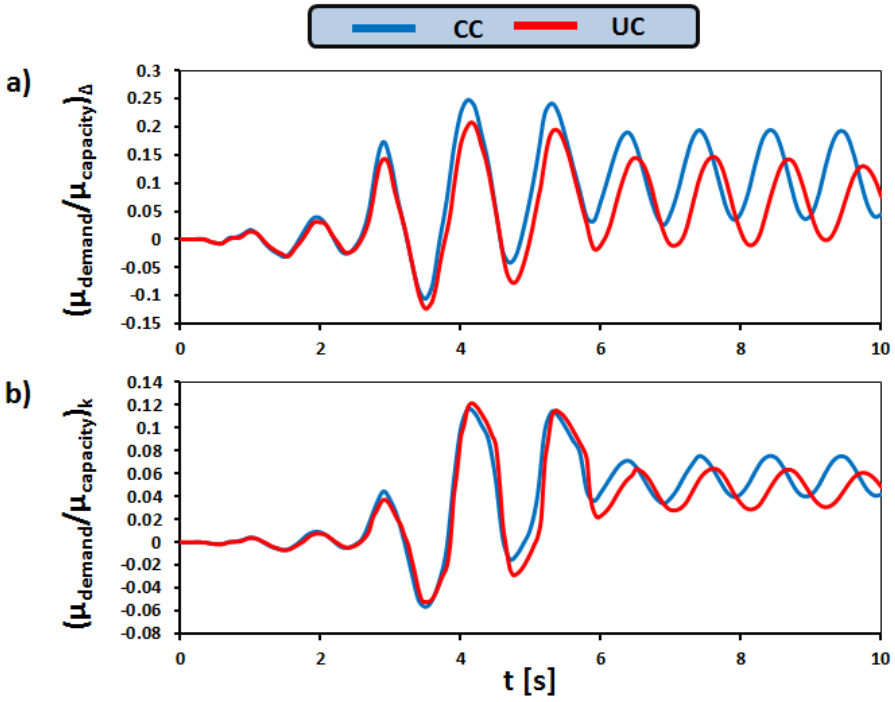

Fig. B.6: Comparison of ductility demand over ductility capacity of the two conventionally designed systems in terms of (a) displacement (b) curvature for Aegion earthquake.

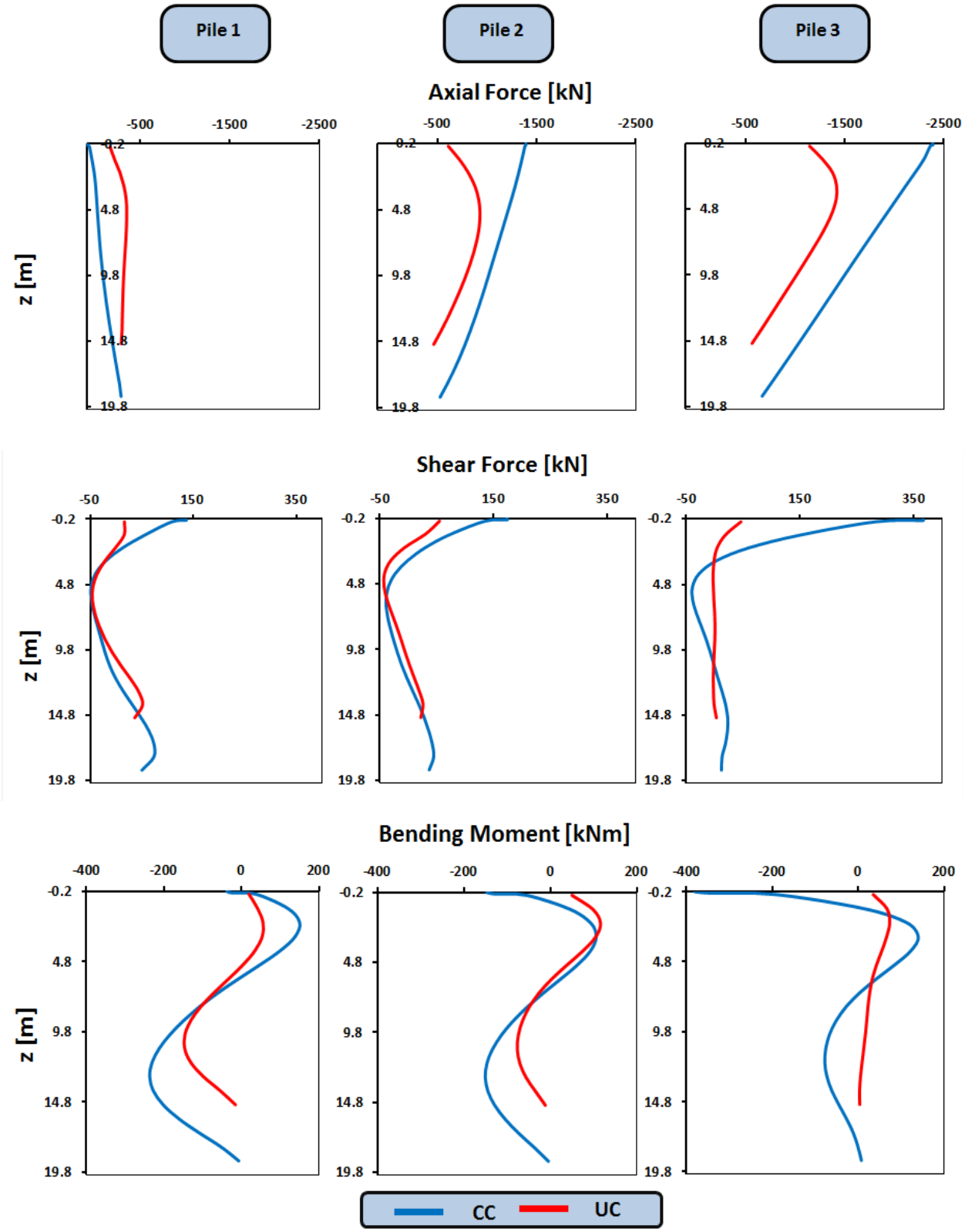

Fig. B.7: Distribution of axial forces, shear forces and bending moments along the piles when maximum moment is transmitted to the soil (Aegion).

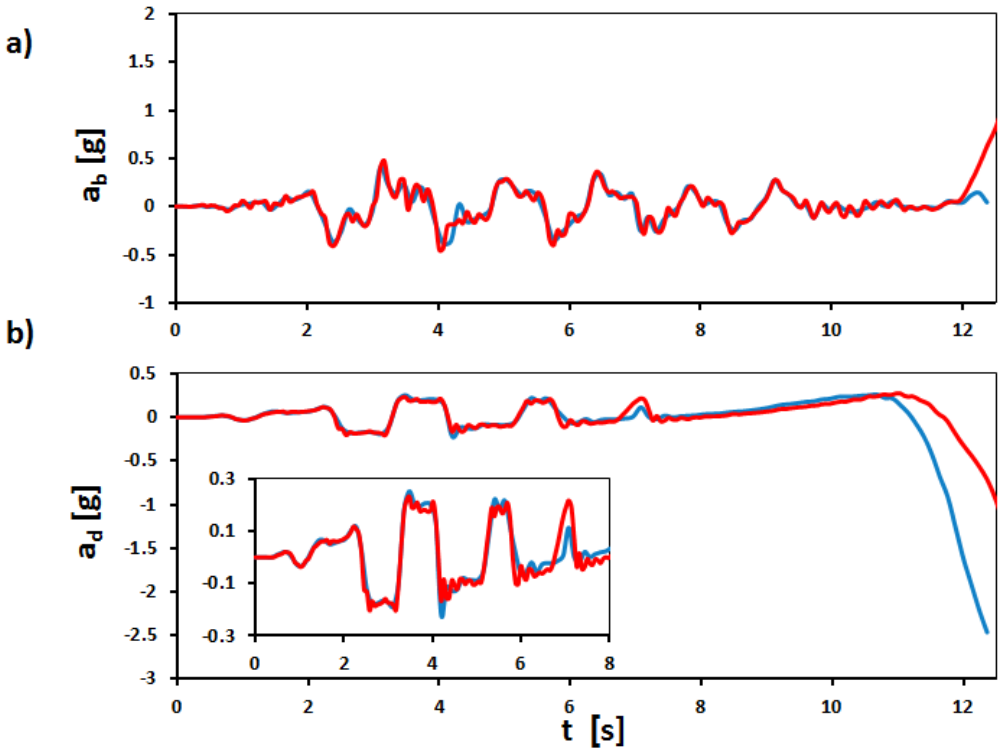

Fig. B.8: Acceleration timehistory during Lixouri excitation at (a) the base of the pier (b) the deck for the case connected (blue) and unconnected (red) piles.

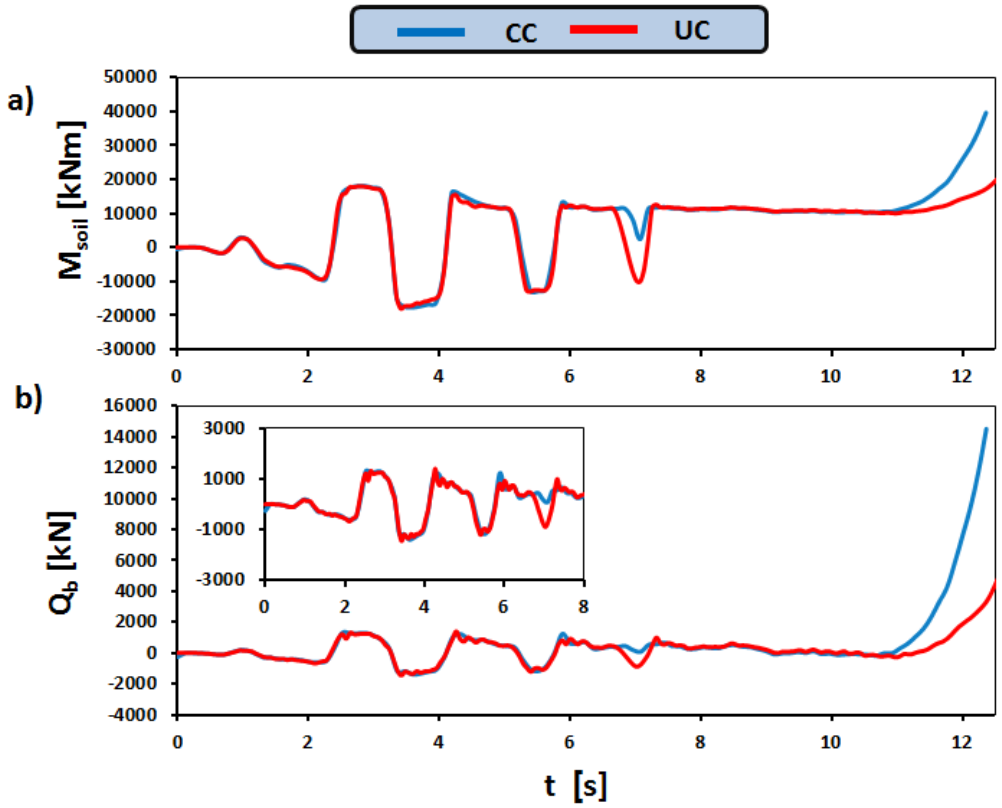

Fig. B.9: Timehistories of (a) bending moment (b) shear force at the base of the pier during Lixouri excitation for the case of connected (blue) and unconnected (red) piles.

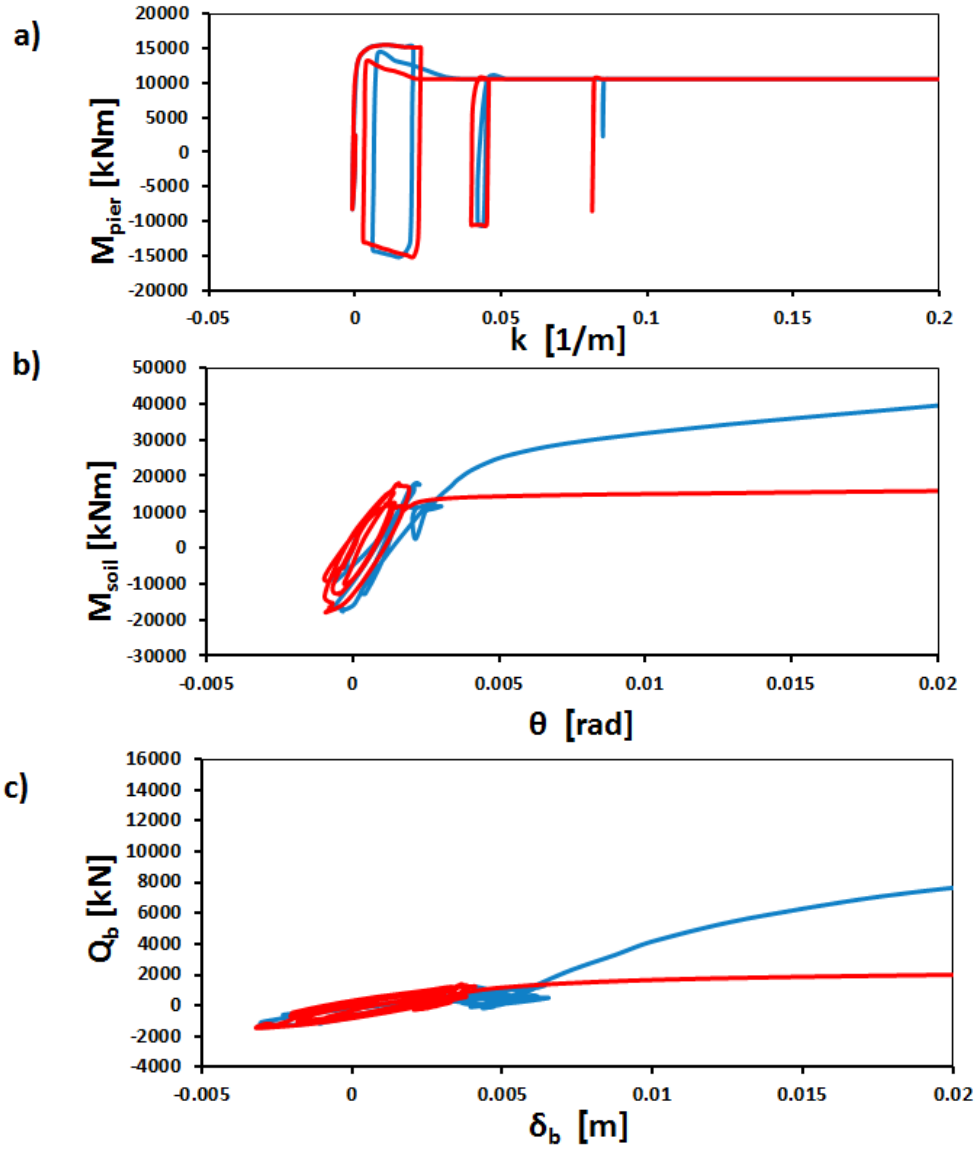

Fig. B.10: Comparison of the response of the two conventionally designed systems with connected (blue) and unconnected (red) piles in terms of (a) bending moment–curvature at the base of the pier (b) moment–rotation of the foundation level (c) base shear–displacement of the foundation. (Lixouri excitation)

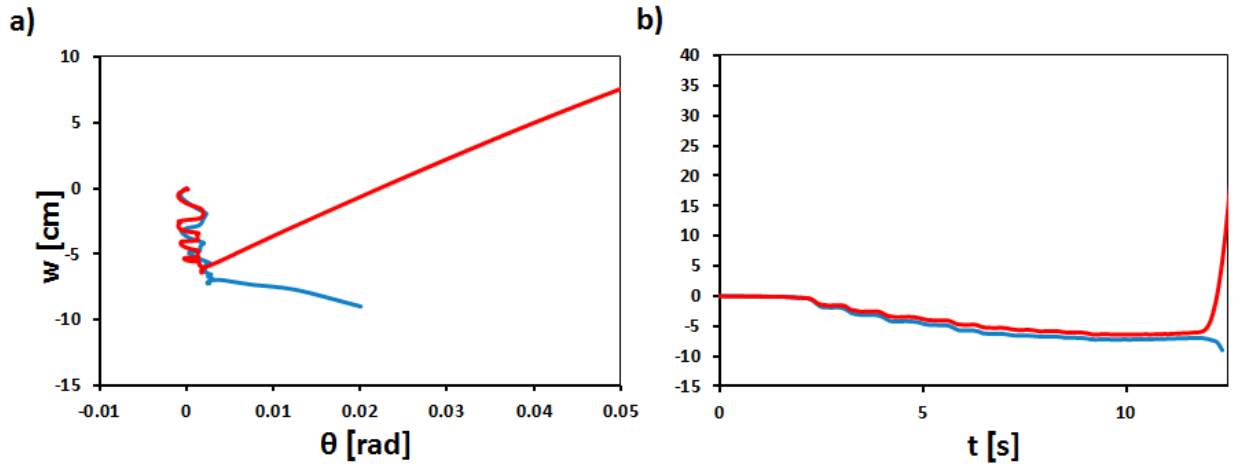

Fig. B.11: Comparison of the settlements of the two conventional aternative designs subjected to Aegion earthquake in terms of (a) settlement–rotation and (b) settlement timehistory.

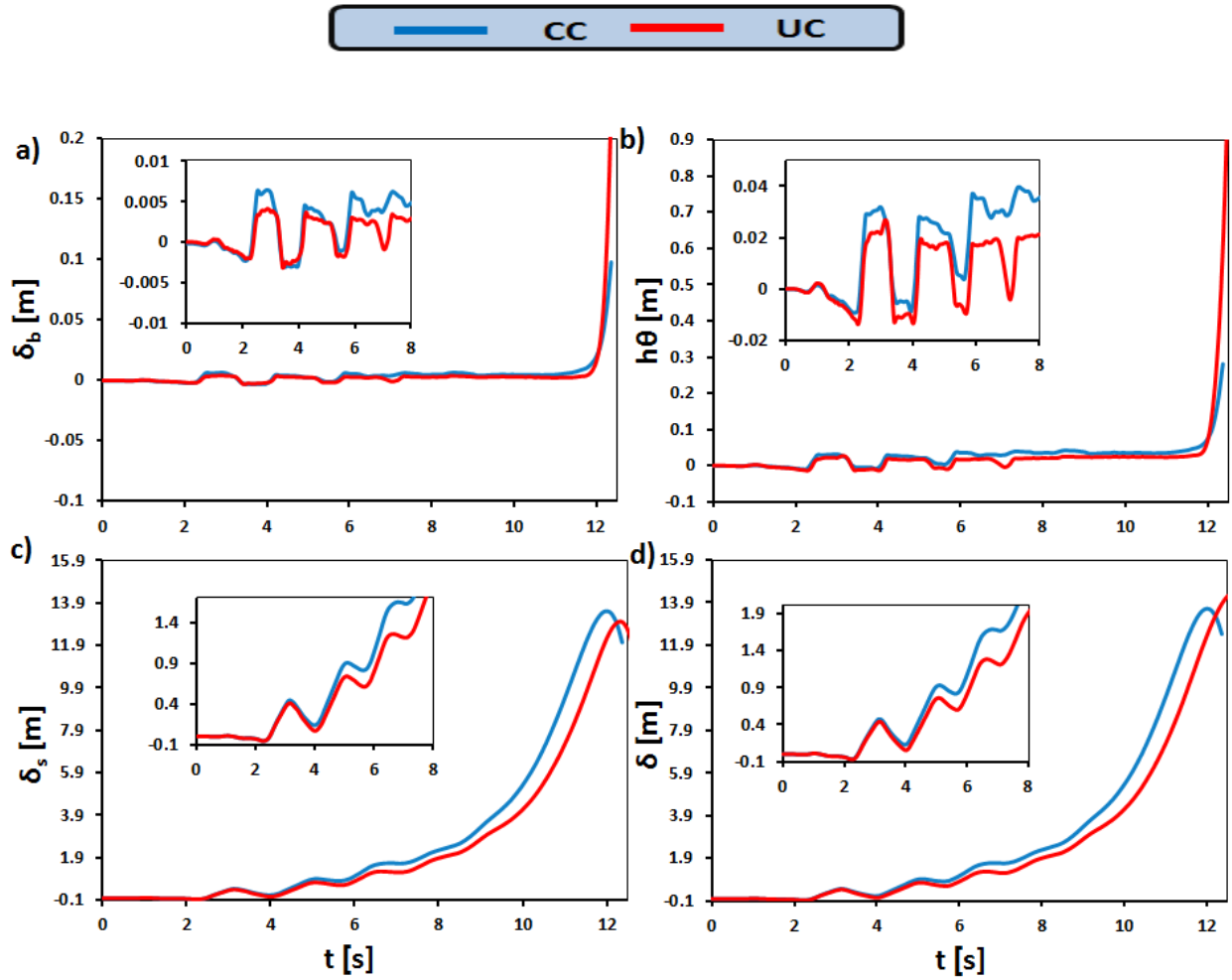

Fig. B.12: Comparison of the response of the two conventionally designed systems with connected (blue) and unconnected (red) piles in terms of (a) foundation displacement (b) displacement due to the rotation of the foundation (c) structural deformation of the pier (d) total deck displacement. (Lixouri)

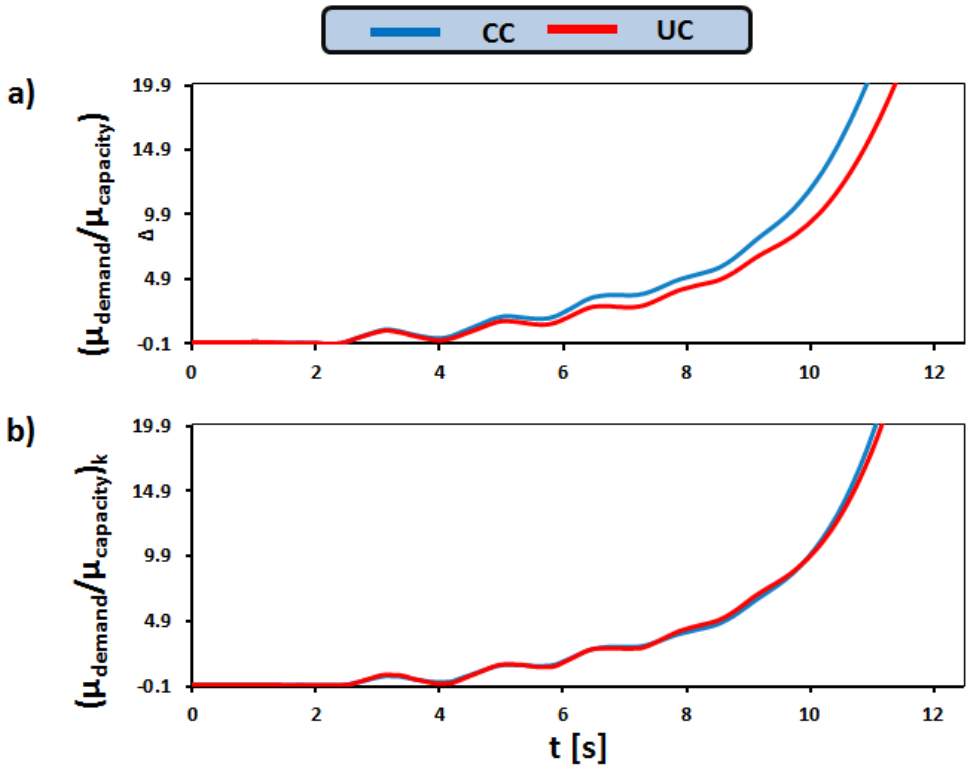

Fig. B.13: Comparison of ductility demand over ductility capacity of the two conventionally designed systems in terms of (a) displacement (b) curvature for Lixouri earthquake.

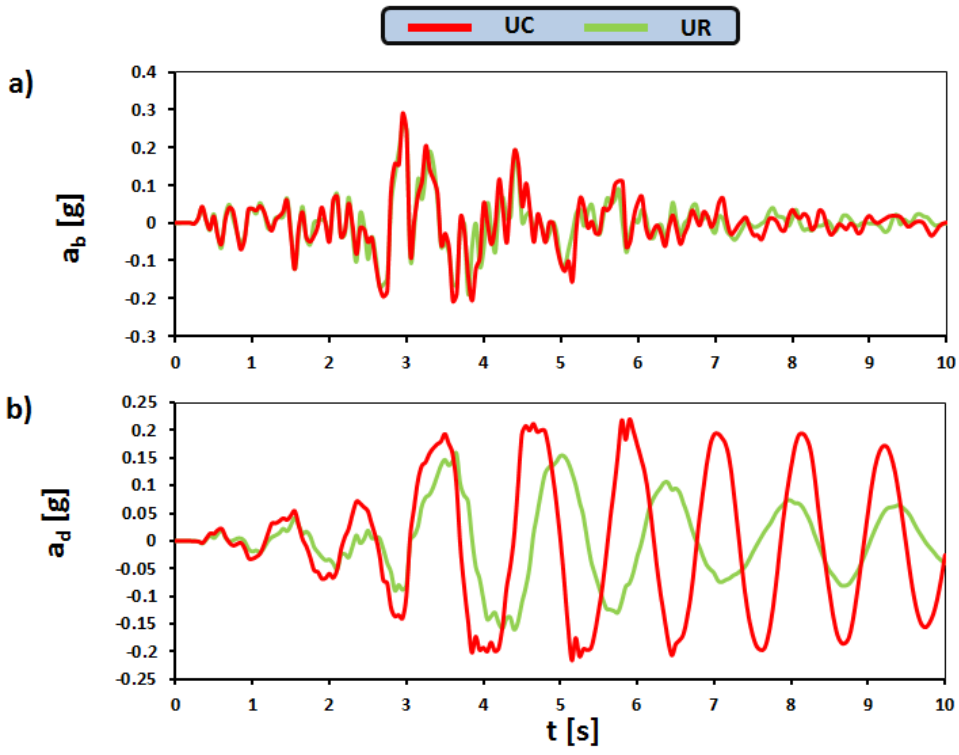

Fig. B.14: Comparison of the accelerations of the two alternative unconnected pile foundations, conventional (UC) and rocking (UR), at the (a) pier base and (b) deck for Aegion earthquake.

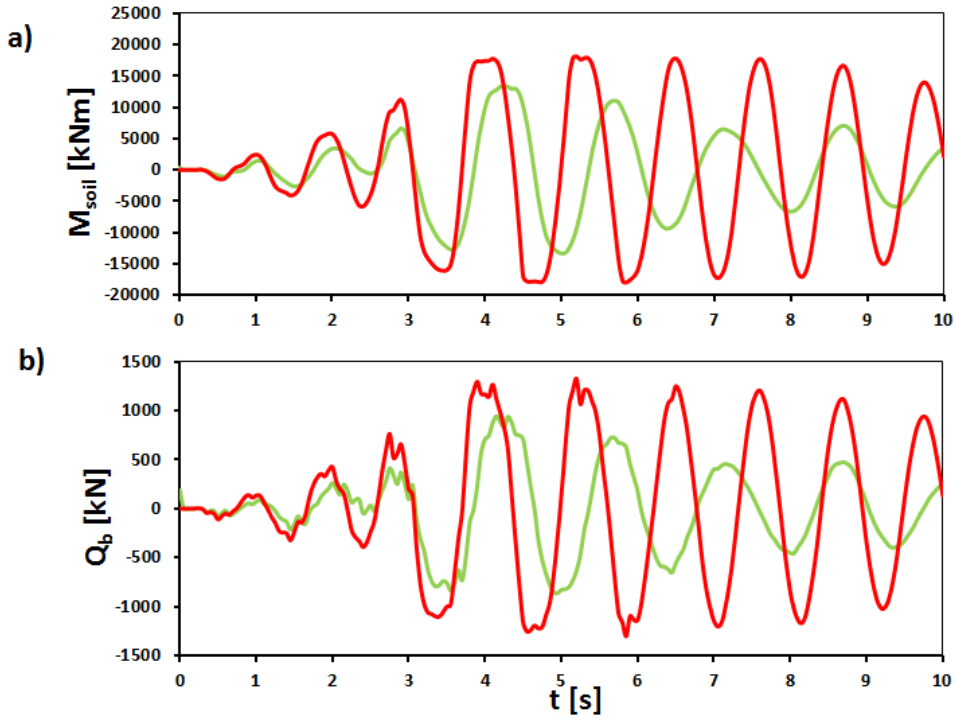

Fig. B.15: Comparison of the two alternative unconnected pile foundations, conventional (UC) and rocking (UR), in terms of (a) moment at the foundation level and (b) shear at the pier base for Aegion earthquake.

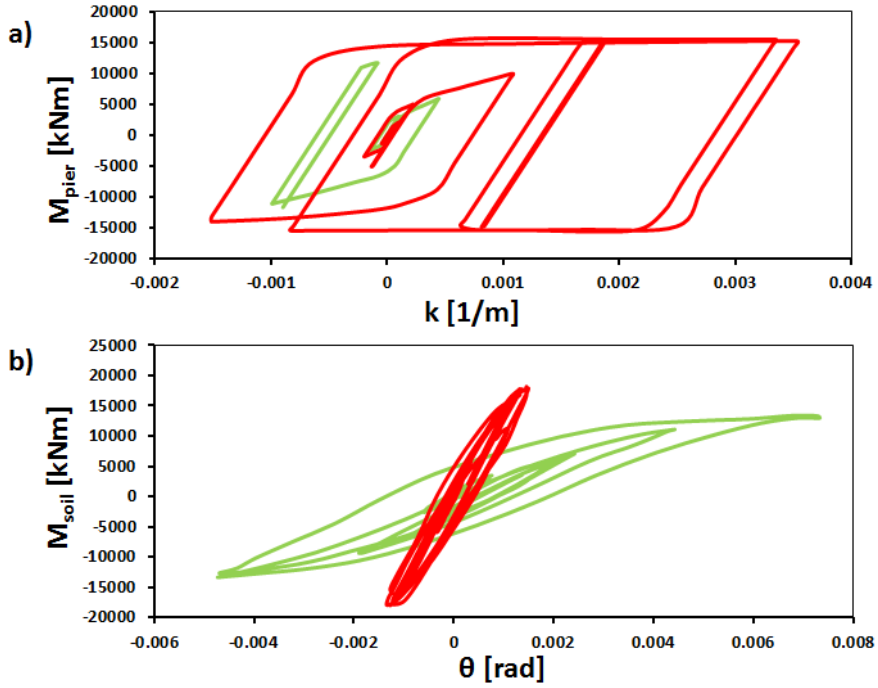

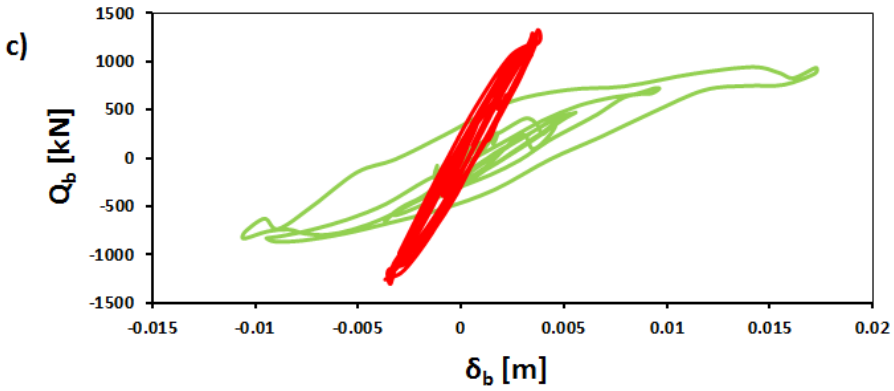

Fig. B.16: Comparison of the two alternative unconnected pile foundations, conventional (UC) and rocking (UR), in terms of (a) moment–curvature at the base of the pier (b) Moment–rotation at the foundation level (c) shear–displacement at the pier base for Aegion earthquake.

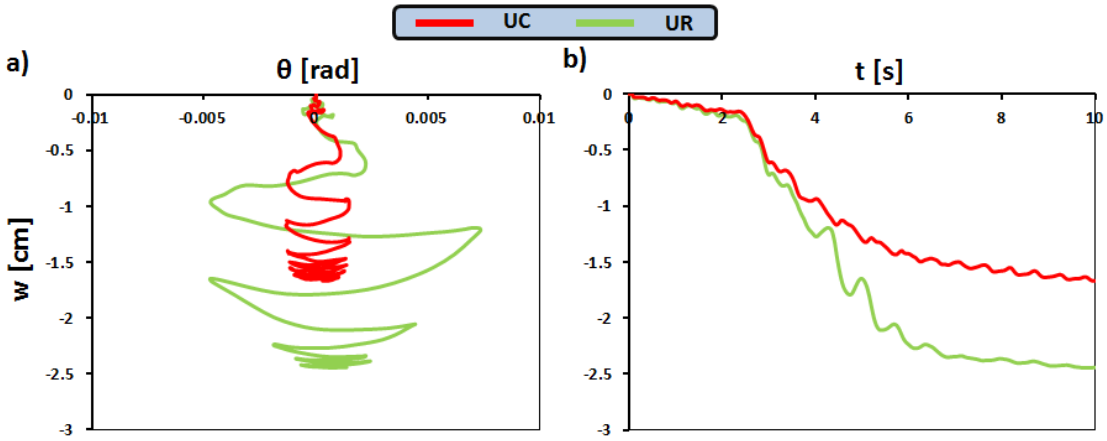

Fig. B.17: Comparison of the settlements of the two alternative conventional designs subjected to Aegion earthquake in terms of (a) settlement–rotation and (b) settlement timehistory.

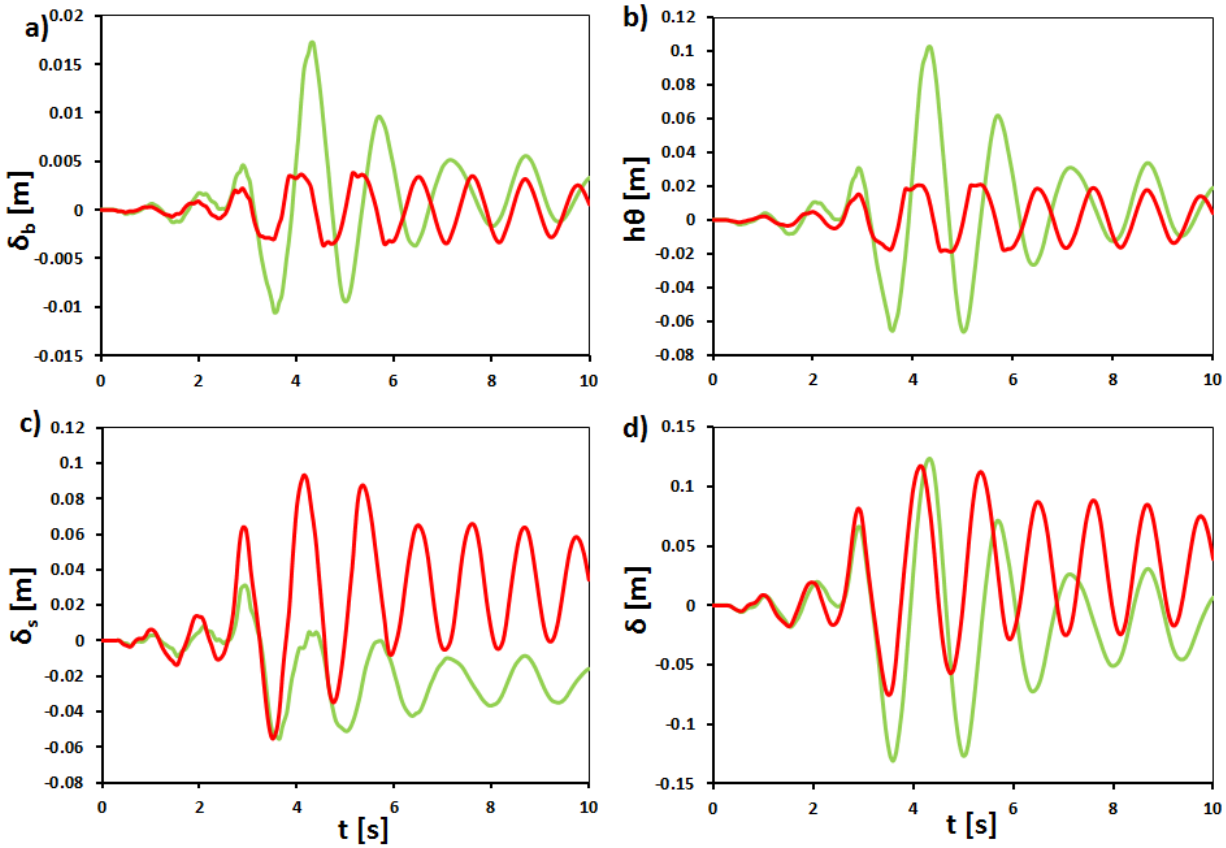

Fig. B.18: Comparison of the two alternative unconnected pile foundations, conventional (UC) and rocking (UR), in terms of (a) foundation displacement (b) displacement due to the rotation of the foundation (c) structural deformation of the pier (d) total deck displacement. (Aegion earthquake)

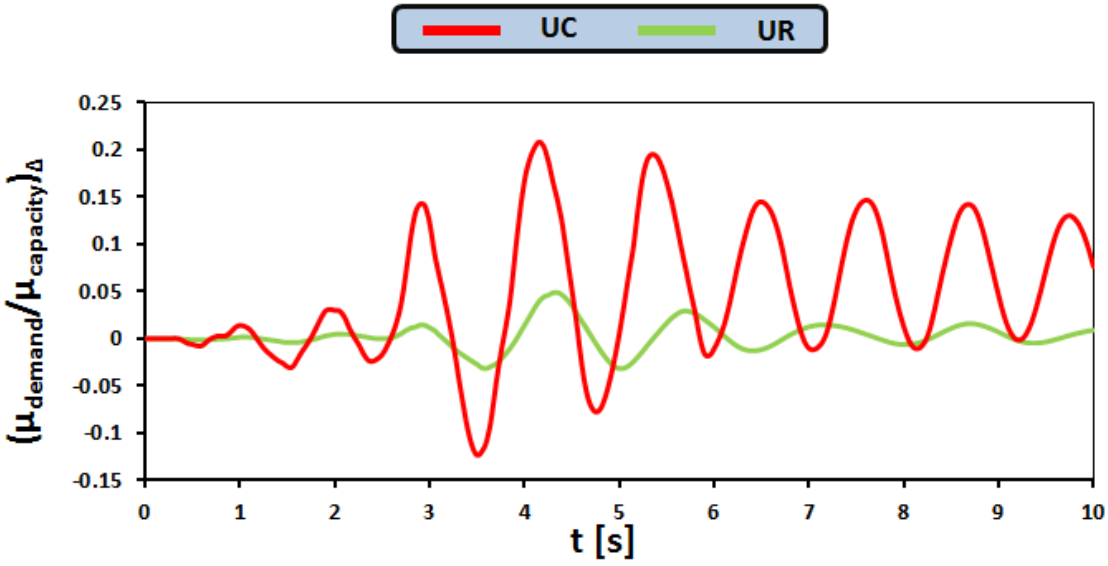

Fig. B.19: Comparison of ductility demand over ductility capacity, in terms of displacements, of the two alternative unconnected pile foundations for Aegion earthquake.

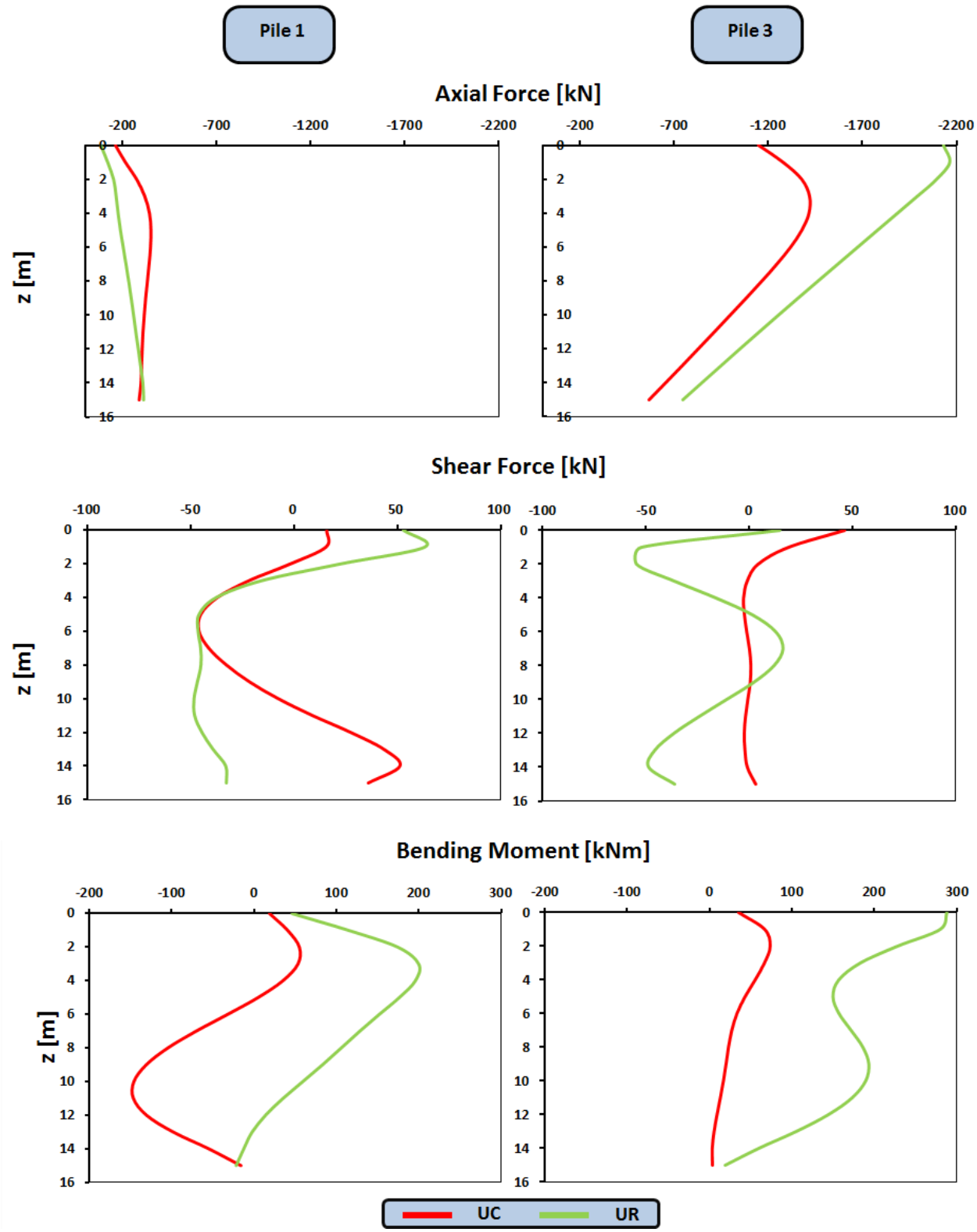

Fig. B.20: Distribution of axial forces, shear forces and bending moments along the piles when maximum moment is transmitted to the soil (Aegion earthquake).

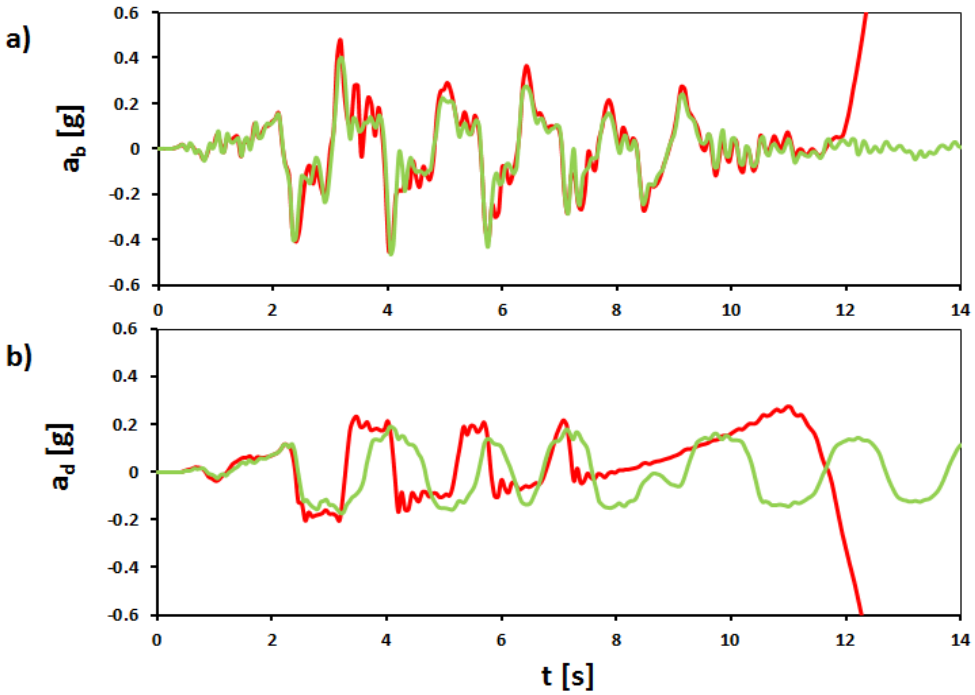

Fig. B.21: Comparison of the accelerations of the two alternative unconnected pile foundations, conventional (UC) and rocking (UR), at the (a) pier base and (b) deck for Lixouri earthquake.

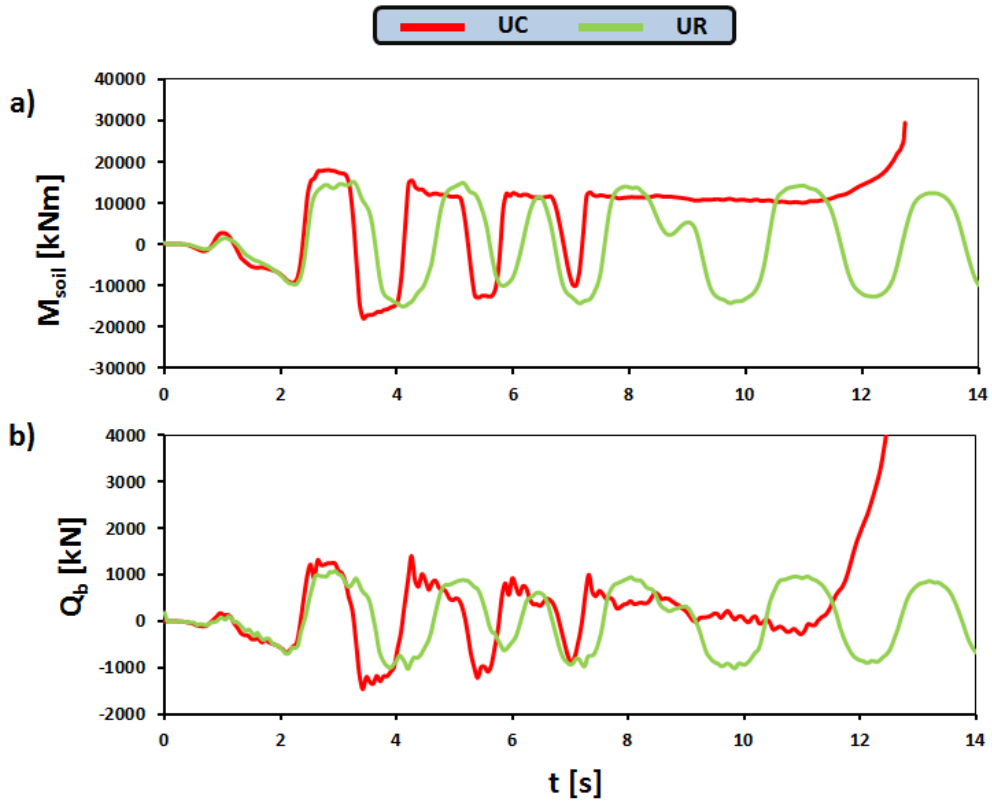

Fig. B.22: Comparison of the two alternative unconnected pile foundations, conventional (UC) and rocking (UR), in terms of (a) moment at the foundation level and (b) shear at the pier base for Lixouri earthquake.

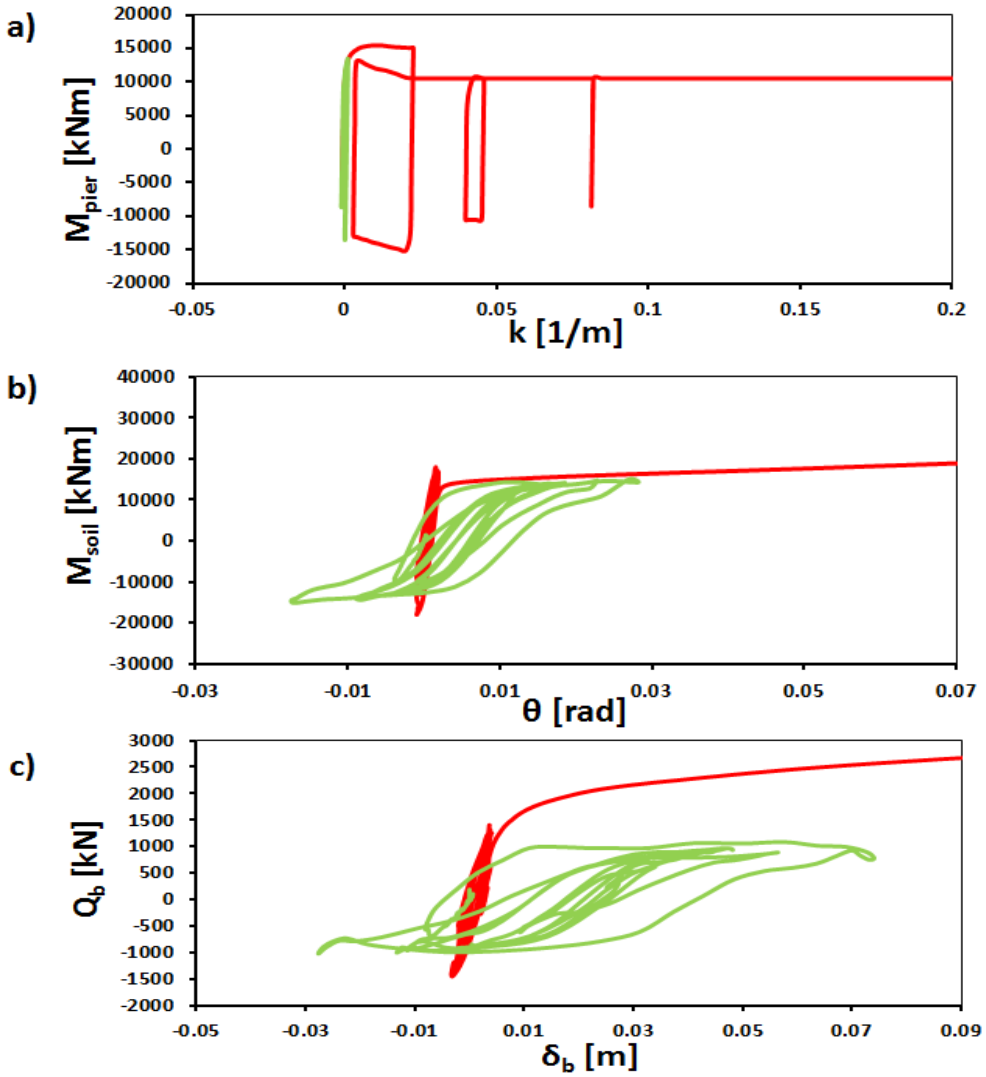

Fig. B.23: Comparison of the two alternative unconnected pile foundations, conventional (UC) and rocking (UR), in terms of (a) moment–curvature at the base of the pier (b) Moment–rotation at the foundation level (c) shear–displacement at the pier base for Lixouri earthquake.

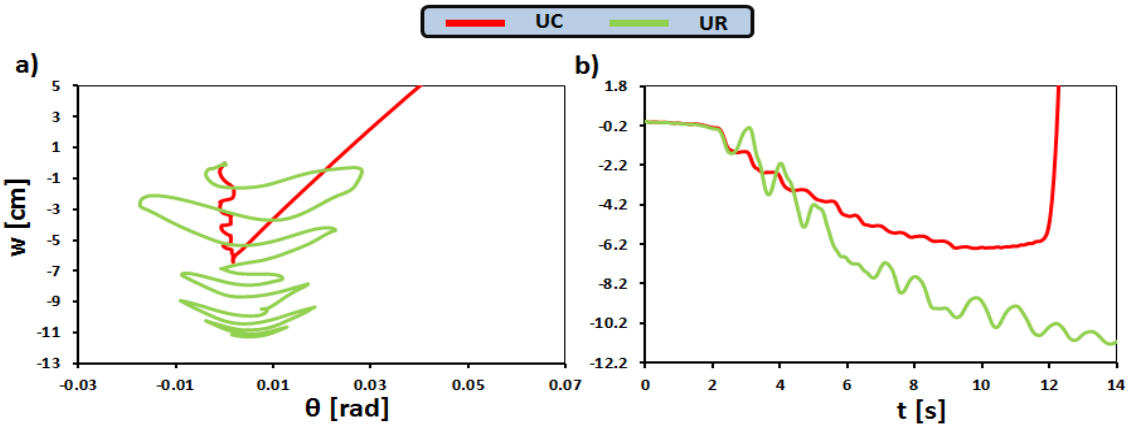

Fig. B.24: Comparison of the settlements of the two alternative conventional designs subjected to Lixouri earthquake in terms of (a) settlement–rotation and (b) settlement timehistory.

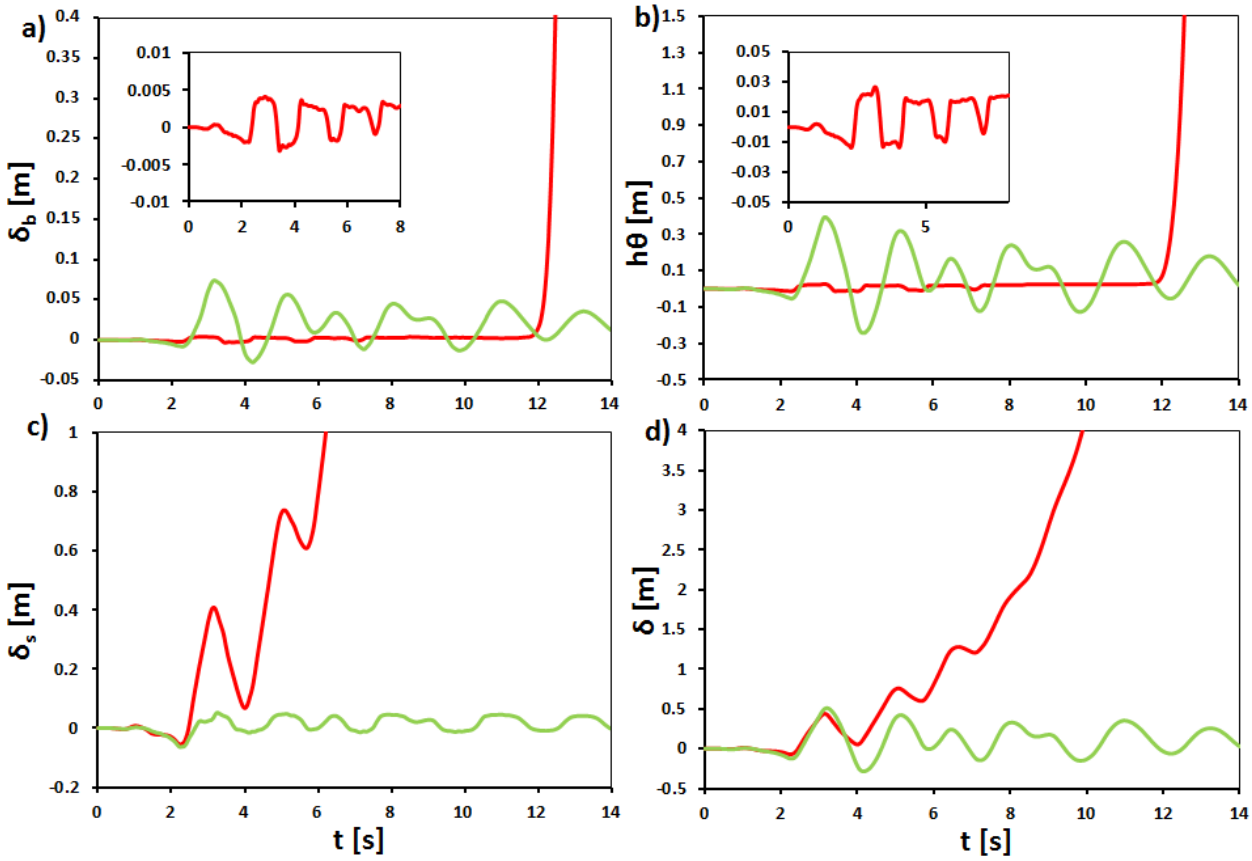

Fig. B.25: Comparison of the two alternative unconnected pile foundations, conventional (UC) and rocking (UR), in terms of (a) foundation displacement (b) displacement due to the rotation of the foundation (c) structural deformation of the pier (d) total deck displacement. (Lixouri earthquake)

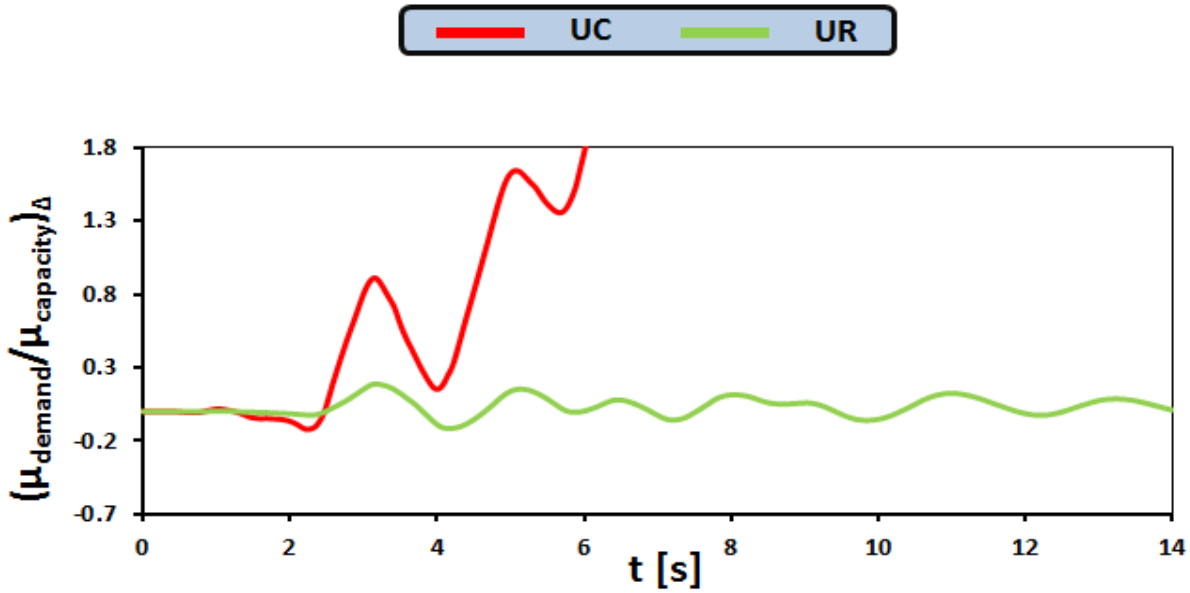

Fig. B.26: Comparison of ductility demand over ductility capacity, in terms of displacements, of the two alternative unconnected pile foundations for Lixouri earthquake.

References:

ABAQUS, Inc., *ABAQUS V.6.13 User's Manual, Providence, Rhode Island, USA.*

Allmond J. & Kutter B. L. (2012), *Centrifuge Testing of Rocking Foundations on Saturated Sand and Unconnected Piles: The Fluid Response,* GeoCongress 2012: State of the Art and Practice in Geotechnical Engineering

Anastasopoulos I., Gazetas G., Loli M., Apostolou M. & Gerolymos N. (2010), *Soil Failure Can Be Used for Seismic Protection of Structure,* Bulleting of Earthquake Engineering, Vol. 8, pp309-326

Anastasopoulos I., Kourkoulis R., Gelagoti F. & Papadopoulos E. (2012), *Rocking Response of SDOF Systems on Shallow Improved Sand: An Experimental Study*, Soil Dynamic and Earthquake Engineering, Vol. 40, pp 15-33

Antonellis G., Gavras G., Panagiotou M., Kutter B. L., Guerrini G., Sander A. C. & Fox P. J. (2015), *Shake Table Test of Large-Scale Bridge Columns on Rocking Shallow Foundations,* Journal of Geotechnical and Geoenviromental Engineering, Vol. 145

Apostolou M., Gazetas G. & Garini E. (2007), *Seismic Response of Slender Rigid Structures with Foundation Uplifting,* Soil Dynamic and Earthquake Engineering, Vol. 26, pp 642-654

Boulanger R. W., Curras C. J., Kutter B. L., Wilson D. W. & Abghari A. (1999), *Seismic Soil-Pile-Structure Interaction Experiments and Analyses,* Journal of Geotechnical And Geoenviromental Engineering, Vol. 125, pp 750-759

Cao X. D., Wong I. H. & Change M-F (2004), *Dehavior of Model Rafts Resting on Pile-Reinforced Sand,* Journal of Geotechnical and Geoenviromental Engineering, Vol. 130, pp 129-138

Curras C. J., Boulanger R. W., Kutter B. L. & Wilson D. W. (2001), *Dynamic Experiments and Analyses of a Pile-Group-Supported Structure,* Journal of Geotechnical And Geoenviromental Engineering, Vol. 127, pp 585-596

Dorby R. & Gazetas G. (1988), *Simple Method for Dynamic Stiffness and Damping of Floating Pile Groups,* Geotechnique, Vol. 38, pp 557-574

EC8 (2000), *Design Provision for Earthquake Resistance Of Structures, Part 5: Foundations, Ret. Str. And Geot. Aspects*. Brussels, 1998-5 Eur. Com. for Standard.

Fioravante V. & Giretti D. (2010), *Contact Versus Noncontact Piled Raft Foundation, Canadian Geotechnical Journal*, Vol. 47, pp. 1271–1287.

Gajan S. & Kutter B. L. (2008), *Capacity, Settlement, and Energy Dissipation of Shallow Footing Subjected to Rocking*, Journal of Geotechnical And Geoenviromental Engineering, Vol. 134, pp 1129-1141

Gajan S., Kutter B. L., Phalen J. D., Hutchinson T. C. & Martin G. R. (2004), *Centrifuge Modeling of Load-Deformation Behavior of Rocking Shallow Foundation,* Soil Dynamic and Earthquake Engineering, Vol. 25, pp 773-783

Gazetas G. (2014), *4th Ishihara Lecture: Soil-Foundation-Structure Systems Beyond Conventional Seismic Failure Thresholds*, Soil Dynamics and Earthquake Engineering, Vol. 68, pp 23-39

Gelagoti F., Kourkoulis R., Anastasopoulos I. & Gazetas G. (2012), *Rocking-Isolated Frame Structures: Margins of Safety Against Toppling Collapse and Simplified Design Approach,* Soil Dynamic and Earthquake Engineering, Vol. 32, pp 87-102

Gerolymos N., Drossou C. & Gazetas G. (2010), *Alternative Design of Rafts With Structurally Unconnected Piles,* 6th Greek Conference on Geotechnical and Environmental Engineering, 29 September – 1 October, Volos, Greece (in Greek)

Liang F.-Y., Chen L.-Z. & Shi X.-G. (2003), *Numerical Analysis of Composite Piled Raft With Cushion Subjected To Vertical Load,* Computer And Geotechnics, Vol. 30, pp 443-453

Limniati Y. S. (2012), *Unconnected Pile Foundation System: Monotonic and Seismic Response,* Diploma Thesis, National Technical University of Athens, Greece (in Greek)

Loli M. (2015), *Non-linear Seismic Interaction Between Soil and Slender Structure,* Doctoral Dissertation, National Technical University of Athens, Greece

Loli M., Gazetas G., Knappet J. A. & Anastasopoulos I. (2016), *Use of Micro-Pile Inclusions to Enhance Foundation Rocking Isolation,* 1st International Conference on Natural Hazarads & Infrastucture; Chania, Greece, 2016

Mergos P. & Kawashima K. (2005), *Rocking Isolation of a Typical Bridge Pier on Spread Foundation,* Journal of Earthquake Engineering, Vol. 09, pp 395-414

Mylonakis G. & Gazetas G. (1998), *Vertical Vibation and Additional Distress of Grouped Piles in Layered Soil,* Soils and Foundations, Vol. 38, pp 1-14

Mylonakis G. & Gazetas G. (1999), *Lateral Vibration and Internal Forces of Grouped Piles in Layer Soil,* Journal of Geotechnical and Geoenviromental Engineering, Vol. 125, pp 16-25

Nakai S., Kato H., Ishida R., Mano H. & Nagata M. (2004), *Load Bearing Mechanism of Piled Raft Foundation During Earthquake,* 3rd UJNR Workshop on Soil-Structure Interaction, March 29-30, 2004, Menlo Park, California, USA

Pecker A. (1998), *Capacity Design Principles for Shallow Foundations In Seismic Areas,* 11th European Conference on Earthquake Engineering, September 1998, Paris, France

Pecker A. (2003), *Aseismic Foundation Design Process Lessons Learned from Two Major Projects: the Vasco Da Gama and the Rion-Antrrion Bridges,* ACI International Conference on Seismic Bridge Design and Retrofit, La Jolla, California, 2003

Psycharis I. N. & Jennings P. C. (1984), *Rocking, Tipping and Upthrow of Simple Structures by Horizontal Motion,* Proceeding of the 8th World Conference on Earthquake Engineering, Vol 4, pp 291-298, San Francisco, 24-28 July, 1984

Sawwaf M. E. (2010), *Experimental Study of Eccentrically Loaded Raft with Connected and Unconnected Short Piles,* Journal of Geotechnical and Geoenviromental Engineering, Vol. 136, pp 1394-1402

Yim C.-S. & Chopra A. K. (1984), *Earthquake Response of Structures with Partial Uplift on Winkler Foundation,* Earthquake Engineering and Structural Dynamic, Vol. 12, pp 263-281